UAB

Universitat Autònoma de Barcelona

Development of novel electrochemical and optical Lab-on-a-chip platforms for contaminants and biomarkers sensing

Andrzej Chałupniak

PhD in Biotechnology

PhD Director
Prof. Arben Merkoçi
ICREA & Nanobioelectronics and Biosensors Group
Institut Català de Nanociència i Nanotecnologia (ICN2)

Department of Chemical, Biological and Environmental Engineering
Universitat Autònoma de Barcelona
2017

This work entitled "Development of novel electrochemical and optical Lab-on-a-chip platforms for contaminants and biomarkers sensing", presented by Andrzej Chałupniak to obtain the degree of doctor by Universitat Autònoma de Barcelona, was performed at the Nanobioelectronics and Biosensors Group at the Institut Catalá de Nanociencia i Nanotecnologia (ICN2), under the supervision of Prof. Arben Merkoçi, ICREA Professor and Group Leader.

Bellaterra, July 2017

Director

_____

Prof. Arben Merkoçi
ICREA Professor
Nanobioelectronics & Biosensors Group
Institut Català de Nanociència i Nanotecnologia

Tutor

_____

Dr. Jordi Joan Cairó Badillo
Autonomous University of Barcelona

_____

Andrzej Chałupniak
Nanobioelectronics & Biosensors Group
Institut Català de Nanociència i Nanotecnologia

Preface

The present PhD thesis is related with the following manuscripts and publications:

Andrzej Chałupniak and Arben Merkoçi, "Recent Trends In Nanomaterials Integration Into Simple Biosensing Platforms", *Nanotechnology in Biology and Medicine: Methods, Devices, and Applications*, Second Edition (Taylor & Francis Group, LLC), 11 October 2017. ISBN 9781439893784

Andrzej Chałupniak, Eden Morales-Narváez and Arben Merkoçi, "Micro and nanomotors in diagnostics", *Advanced Drug Delivery Reviews*, Volume 95, 1 December 2015, Pages 104-116. Impact factor: 11.764

Andrzej Chałupniak and Arben Merkoçi, "Toward integrated detection and graphene-based removal of contaminants in a lab-on-a-chip platform", *Nano Research,* 1 March 2017, doi:10.1007/s12274-016-1420-3. Impact factor: 7.354

Manuscripts in preparation:

Andrzej Chałupniak and Arben Merkoçi, "Improved electrochemical detection of heavy metals using graphene-based preconcentration platform", *In preparation* (2017),

Additional publications for annexes:

Helena Montón, Mariana Medina-Sánchez, Joan Antoni Soler, **Andrzej Chałupniak**, Carme Nogués and Arben Merkoçi, "Rapid on-chip apoptosis assay on human carcinoma cells based on annexin-V/quantum dot probes", *Biosensors and Bioelectronics*, Volume 94, 15 August 2017, Pages 408-414. Impact factor: 7.780
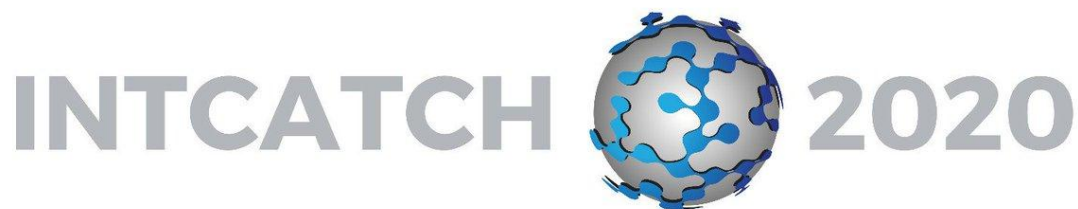
Acknowledgements for the financial support

Summary

The detection of hazardous contaminants requires special attention due to their possible toxicity, low concentration in real samples and, in most cases, an impossibility to perform detection by using such a specific approach as immunoassay. One of the approaches taking an important step towards easier detection of hazardous compounds is the use of Lab-on-a-chip platform.

In Chapter 3, a novel, miniaturized microfluidic platform for the simultaneous detection and removal of polybrominated diphenyl ethers (PBDEs) was developed. The platform consists of a polydimethylsiloxane (PDMS) microfluidic chip for the immunoreaction step, a PDMS chip with an integrated screen-printed electrode (SPCE) for detection, and a PDMS-reduced graphene oxide (rGO) chip for physical adsorption and subsequent removal of PBDE residues. The detection was based on competitive immunoassay-linked binding between PBDE and PBDE modified with horseradish peroxidase (HRP-PBDE) followed by the monitoring of enzymatic oxidation of o-aminophenol (o-AP) by using square wave anodic stripping voltammetry (SW-ASV). PBDE was detected with good sensitivity and a limit of detection similar to that obtained with a commercial colorimetric test (0.018 ppb), but with the advantage of using lower reagent volumes and a reduced analysis time. In order to design a detection system suitable for toxic compounds such as PBDEs, a reduced graphene oxide–PDMS composite has been developed and optimized to obtain increased adsorption (based on both the hydrophobicity and π–π stacking between rGO and PBDE molecules) compared to those of non-modified PDMS. This system can be easily applied to detect any analyte by using the appropriate immunoassay and it supports operation in such complex matrices as seawater.

In Chapter 4, a LOC device for the simultaneous preconcentration and detection of heavy metals was developed. This device consists of a screen-printed carbon electrode, a PDMS chip, and a GO-PDMS chip. The GO-PDMS chip was fabricated and the most crucial factors were optimized, including the concentration of GO and the concentration of the curing agent. It was found that the adsorption ability is inversely proportional to the PDMS

catalyser (curing agent) concentration in the composite and proportional to the GO concentration. The mechanism of adsorption is based on surface complexation, where oxygen active groups of negative charge can bind with such bivalent metals as Pb. The highest adsorption was obtained in pH=7.

The GO-PDMS has a relatively big large adsorption capacity, as even the samples >500 ppb are nearly fully adsorbed, taking into account that such a concentration is very high.

The desorption process was optimized as well. Thanks to this, previously adsorbed metals can be released and detected in square wave anodic stripping voltammetry. The limit of detection of this technique (using screen-printed electrodes) was 0.5 ppb for Pb. This means that by using a preconcentration GO-PDMS platform, a lower amount of Pb can be quantified because preconcentrated samples showed a current up to 30 times higher than that of non-preconcentrated one.

This platform can be used for improved heavy metal sensing and also for its removal.

Resumen

La detección de contaminantes peligrosos requiere especial atención debido a su posible toxicidad, baja concentración en muestras reales y, en la mayoría de los casos, una imposibilidad de llevar a cabo la detección a través de un metodo tan específico como el inmunoensayo. Una de las estrategias orientadas a la fácil detección de compuestos nocivos es el uso de plataformas microfluídicas llamadas Lab-on-a-chip.

En el Capítulo 3, una innovadora plataforma microfluídica en miniatura es desarrollada para la detección simultánea y extracción de polibromodifenil éteres (PBDEs). La plataforma consiste en un chip microfluídico de polidimetilosiloxano (PDMS) para el paso de la inmunoreacción, un chip de PDMS con un electrodo serigrafiado de carbono (SPCE) integrado para la detección, y un chip de PDMS-óxido de grafeno reducido (rGO) para la adsorción física y posterior eliminación de residuos de PBDE. La detección se basó en un inmunoensayo competitivo entre PBDE y PBDE modificado con Peroxidasa de Rábano Silvestre (HRP-PBDE) seguido de un monitoreo de oxidación enzimática de o-aminofenol (o-AP), utilizando voltamperometría de onda cuadrada y resolución anódica (SW-ASV). PBDE fue detectado con una buena sensibilidad y un límite de detección similar al obtenido a través de una prueba colorimétrica comercial (0.018 ppb), pero con la ventaja de utilizar volúmenes reactivos más bajos y un tiempo de análisis reducido. Con el objetivo de diseñar un sistema de detección apropiado para compuestos tóxicos como PBDEs, un compósito de óxido de grafeno reducido y PDMS ha sido desarrollado y optimizado para obtener mayor adsorción (basados en hidropobicidad e interacción π–π entre moléculas de rGO y PBDE) comparado con los PDMS sin modificación. Este sistema se puede aplicar perfectamente para detectar cualquier análito utilizando el inmunoensayo apropiado y facilitar el funcionamiento en matrices tan complejas como el agua marina.

En el Capítulo 4 se desarrolla un dispositivo LOC para la preconcentración y la detección simultánea de metales pesados. Dicho dispositivo consta de un electrodo serigrafiado de carbono, un chip de PDMS y otro de GO-PDMS. El chip de GO-PDMS fue fabricado y los

factores más esenciales fueron optimizados, incluidos la concentración de GO y aquella del curador de PDMS. Se descubrió que la habilidad de adsorción es inversamente proporcional a la concentración de curador de PDMS en el compósito y proporcional a la concentración de GO. El mecanismo de adsorción está basado en una reacción de complejación , donde grupos activos de oxígeno con cargas negativas se pueden enlazar con metales bivalentes como el Pb. La adsorción más alta fue obtenida en pH=7.

El GO-PDMS tiene una capacidad relativamente grande de adsorción, ya que incluso las muestras que contienen niveles más altas que 500 ppb (mayores a 500 ppb) son totalmente adsorbidas, teniendo en cuenta que tal concentración es muy alta.

El proceso de desorción ha sido también optimizado. Gracias a ello, metales que habían sido previamente adsorbidos se pueden liberar y detectar en voltamperometría de Onda Cuadrada y Resolución Anódica. El límite de detección de esta técnica (utilizando electrodos serigrafiados de carbono) fue de 0.5 ppb para el plomo (Pb). Esto significa que utilizando una plataforma de preconcentración GO-PDMS, se pueden cuantificar cantidades más bajas de Pb, ya que las muestras preconcentradas mostraron una corriente de hasta 30 veces más alta que las no preconcentradas.

Esta plataforma se puede utilizar para la detección mejorada de metales pesados y también para su eliminación.

List of acronyms

3-APZ	3-aminophenoxazone
AAS	Atomic absorption spectroscopy
ACSF	Artificial cerebrospinal fluid
AEC	3-amino-9-ethylcarbazole
AMP	Chronoamperometry
ApoE	Apolipoprotein E
APTES	(3-Aminopropyl)triethoxysilane
AuNP	Gold nanoparticles
Aβ	Beta-amyloid
BDD	Boron-doped diamond
BR	Britton–Robinson buffer
BSA	Bovine serum albumin
CAMPT	Camptothecin
CFU	Colony-forming unit
CNFs	Carbon nanofibers
CNTs	Carbon nanotubes
ConA	Concanavalin A
CSF	Cerebrospinal fluid
CV	Cyclic voltammetry

DAB	3,3'-Diaminobenzidine
DNA	deoxyribonucleic acid
DPV	Differential pulse voltammetry
EDXRF	Energy dispersive X-ray fluorescence
FAAS	Flame atomic absorption spectrometry
FRET	Förster Resonance Energy Transfer
GO	Graphene oxide
GQD	Graphene quantum dots
HCl	Hydrochloric acid
HER	Hydrogen evolution reaction
HNO_3	Nitric acid
HRP-PBDE	Horseradish peroxidase conjugated to PBDE
IgG	Immunoglobulin G
IrOX	Iridium oxide
IUPAC	International Union of Pure and Applied Chemistry
L-AA	L-ascorbic acid
LF	Lateral flow
LOC	Lab-on-a-chip
LOD	Limit of detection
LOQ	Limit of quantification

MB-Ab	Magnetic beads coupled to antibodies
MS	Mass spectroscopy
MWCNTs	Multi-walled carbon nanotubes
o-AP	o-aminophenol
PBDE	Polybrominated diphenyl ether
PBS	Phosphate buffer saline
PDMS	Polydimethylsiloxane
PEDOT	Poli(3,4-etyleno-1,4-dioxythiophen)
PMMA	Poly(methyl methacrylate)
QDs	Quantum dots
rGO	Reduced Graphene Oxide
RSD	Relative standard deviation
SPCE	Screen-printed carbon electrode
SU8-50	Epoxy-based negative photoresist
SW-ASV	Square wave-anodic stripping voltammetry
TBT	Tributyltin
TL	Test line
TMB	3,3',5,5'-Tetramethylbenzidine
WOR	Water oxidation reaction

Table of contents

Thesis overview

This thesis covers a broad investigation about the novel types of electrochemical Lab-on-a-chip platforms with inbuilt nanomaterials.

In **Chapter 1** (Introduction) different types of nanomaterials and their applications in simple biosensing devices is discussed comprehensively. As it can be seen, there are several roles that nanomaterials can play in biosensing devices, including signal amplification as well as analyte's capturing, transport, immobilization or removal. Besides that, general information about Lab-on-a-chip devices and the roles of nanomotors in improving sensing also are provided.

Chapter 2 (Objectives) explains the main goal to be achieved within this work, as well as discusses the detailed tasks that were performed.

Chapter 3, entitled "Lab-on-a-chip platform for detection and graphene-based removal of flame retardants" is focused on the design and development of the Lab-on-a-chip platform for the simultaneous detection and removal of the PBDE, used as flame retardant. This class of compounds belongs to persistent organic pollutants. Despite the recent advances in the field of biosensors, there is a lack of a quick and relatively easy method of the PBDE determination. Thus, we propose a modular LOC device where a competitive immunoassay is performed, followed by electrochemical detection and removal.
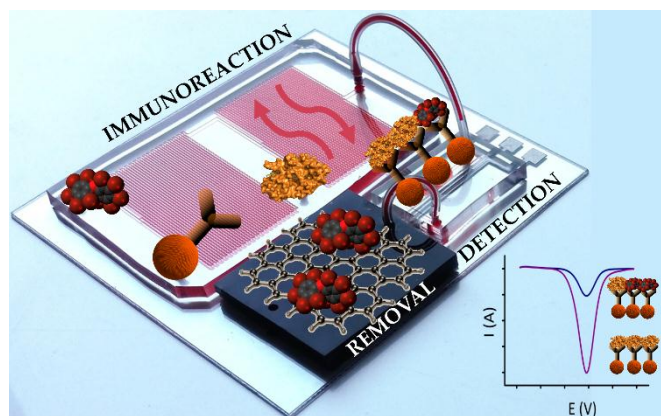
Scheme 1 Schematics of the work performed in Chapter 3.

The last step is possible due to the application of the novel rGO-PDMS composite. This material can interact with an aromatic compound, such as PBDE and bind them via π-π interaction. Electrochemical detection of PBDE, as well as the use of rGO-PDMS, was not reported so far.

Similarly, as above, **Chapter 4** entitled "Improved electrochemical detection of heavy metals using graphene-based preconcentration platform" discusses the design and fabrication of the Lab-on-a-chip platform, but this one is dedicated to the detection of heavy metals. Although heavy metals have a very known and well-reported toxicity, their detection is still challenging as they are usually present in the ppb levels as well as interact with other compounds what makes its detection difficult. We propose the use of GO-PDMS composite that is in-built in the Lab-on-a-chip platform. Oxygen active groups of GO can bind bivalent ions thanks to the surface complexation. A full optimization study was performed reliably and it was found that this platform can be used for preconcentration and electrochemical detection successfully.
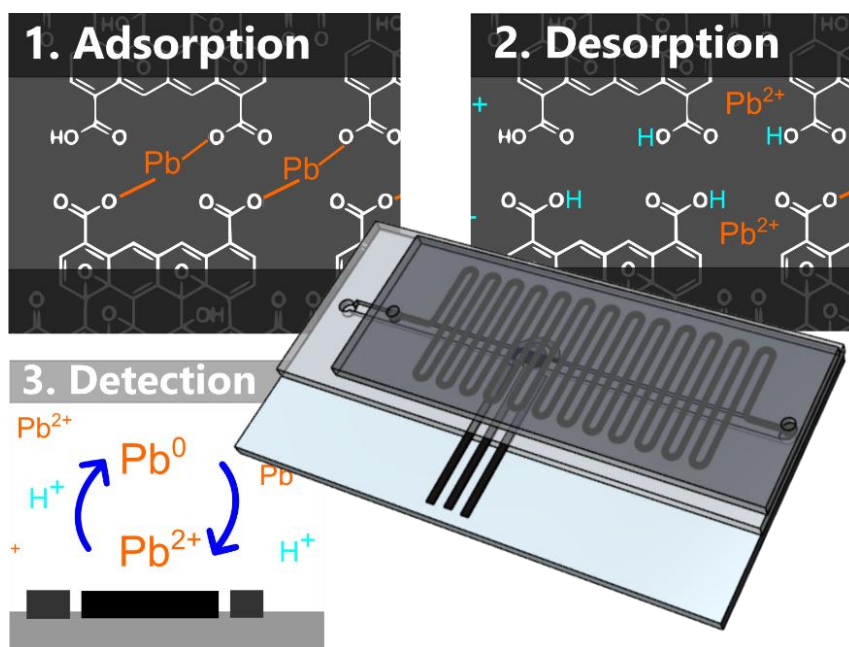
Scheme 2 Schematics of the work performed in Chapter 4.

Chapter 5 includes all the conclusions as well as the future perspectives that come to mind taking into account the work performed in the previously mentioned chapter.

Apart of the core of this thesis, several annexes are included, showing an in-depth study of some phenomena and R & D carried out in the framework of several EU projects:

- **Annex I** – discusses the use of the fully automated Lab-on-a-chip platform for the optical detection of Alzheimer disease biomarker. This work was performed in the framework of the FP7 EU Project "Nadine".

- **Annex II** – discusses the optimization and validation of the optical immunoassays for PBDE and Glyphosate. Both methods are evaluated toward compatibility with the real samples (seawater) as well as possibility to be used within commercialized flow-based detection system. This work was performed in the framework of the FP7 EU Project "SMS"

- **Annex III** – discusses the optimization of square wave anodic stripping voltammetry, an electrochemical technique used for heavy metals detection. Commercial bismuth electrodes, as well as homemade screen-printed carbon electrodes, are tested, with the special attention to the possible use in automated detection systems. This work was performed in the framework of the H2020 EU Project "INTCATCH".

CHAPTER 1

Introduction

1.1.   Introduction

For more than five decades, when the first biosensor was implemented, the research and development in this field have continuously progressed taking advantages of discoveries of new technologies and materials. Currently, due to the strategic importance of nanotechnology in modern science and industry, nanomaterials are increasingly being used in various applications with interest in various areas. There is no difference in the case of biosensors, where nanomaterials have found a versatile role as substrates for nanodevices fabrication, as signal transducers and labels.

The development of biosensors runs two ways at the same time. One of them relates to the complex and high-throughput analysis systems for certain compounds. Such biosensing systems can be used in modern analytical laboratories as clinical and industrial applications. The second group consists of biosensing devices suitable for rapid analysis, which do not require the use of sophisticated equipment or trained personnel. This group is particularly promising because it allows the creation of versatile products, available for everyone and easy to use, which are important for example in the diagnosis of disease markers, environmental monitoring out of the laboratory (in-field), in places with low resources and developing countries, where access to specialized laboratories is limited.

Access to technological innovations always affects the level of advancement of societies. For example, the widespread use of simple biosensors such as glucometers, pregnancy tests, and portable devices, can help in the further creation of awareness of health care prevention. Thus, biosensors in addition to research, development and applications can play an important role in education [1].

In this chapter, different biosensing techniques are discussed, from easy paper-based biosensors to more complex Lab-on-a-Chip devices. All of them combine the use of novel nanomaterials.

1.2.   Nanomaterials improve biosensing

Nanomaterials play a major role in biosensing, due to the versatile function that they can fulfill in biosensors. Used as labels, nanomaterials can produce an easy-to-measure signal

(for instance fluorescence emitted by QDs), as signal amplifiers, they can enhance the response of the sensor (i.e. IrOX nanoparticles with their electrocatalytic activity). The unique electrical, chemical and mechanical properties allow using nanomaterials as substrates for biosensing devices, such as electrodes covered by graphene materials. Simultaneously, some nano/microparticles, due to their porous structure, can be used as carriers for bioreceptor molecules or demonstrate the ability to adsorb selected compounds, providing the ability to use them not only for sensing but also for removal of contaminants. Most of the nanomaterials can be easily conjugated with proteins, enzymes, antibodies, and DNA, which makes it possible to obtain specific and sensitive biosensing systems. In this section, some interesting and efficient nanomaterials and their application in biosensors will be described.

1.3. Nano- and microparticles

According to IUPAC definition, nanoparticles are particles of any shape with dimensions within the range of 1 nm to 100 nm, while microparticles are larger with a size within the range of 100 nm to 100 μm [2, 3]. Because there are a lot of micro/nanoparticles already reported as useful for biosensors, only some of them, particularly those more promising, will be described.

Gold Nanoparticles (AuNP) are one of the most commonly used nanoparticles. Depending on their size, which can be controlled during the synthesis process, they show different parameters both electrochemical and optical. This makes them very versatile and useful for various detection strategies, where AuNPs can work as labels and signal transducers. The conjugation of AuNP with proteins and other biomolecules is very easy and can be obtained without using specific linkers and chemical modification. This feature encourages scientists to use gold nanoparticles in biosensing. Due to their intensive red color, AuNPs can also be used as labels in colorimetric tests like paper-based immunoassay as well as in various electrochemical techniques as explained below.

AuNPs are mainly employed as electrochemical labels in biosensors. In principle, there are two ways to detect them. The first method is Differential Pulse Voltammetry (DPV), where

the potential is applied to initiate the reaction of reducing tetrachloroaurate ions to gold metal after (prior oxidation) and measured current used as an analytical signal. This approach was reported for example for magnetoimmunoassay for *Salmonella* detection [4]. Another strategy for electrochemical detection with AuNP is taking advantage of the Hydrogen Evolution Reaction (HER). In this case, AuNP presents catalytic activity (towards hydrogen ions reduction) when they are deposited onto the electrode in the presence of acid (HCl). After applying a fixed potential, the current signal from the reducing hydrogen is measured and used as an analytical signal. This reaction is easy to be followed, making this approach very convenient and possible to be employed for various detection strategies like cancer cells [5, 6], viruses, DNA and protein detection. Another interesting example is the immobilization of casein peptides to the AuNP surface so as to obtain nanocarriers for the electrochemical study of the adhesion of casein peptides to pathogen bacteria [7].

For more specific approaches or detection improvements, AuNPs can be easily modified. For instance, when AuNPs are modified with ferrocene derivative (FcD): 1,1'-ferrocenyl bis(methylene lipoic acid ester), such complex can work as an efficient transducing system due to the shifting of the ferrocene oxidation potential. This approach was employed by Mars et al. for human IgG detection, representing a novel potential shift-based transducing system for sensitive immunosensing [8].

Another interesting example is Iridium Oxide (IrOx) nanoparticles, with a size of around 12 nm, which are synthesized from potassium hexachloroiridate (IV) (K_2IrCl_6) and sodium hydrogen citrate sesquihydrate ($Na_2C_6H_6O_7 \cdot 1.5H_2O$). Thanks to the conductivity and electronic switching properties their possible application in biosensors is diverse. IrOx nanoparticles are already reported as a conductivity enhancer for pesticides and phenol detection as well as an electrochemical label for ApoE immunoassay, where the antibodies are labeled with IrOx. They are able to enhance Water Oxidation Reaction (WOR). These nanoparticles electrocatalyze water splitting, which is followed by chronoamperometry by measurement of the current generated during the corresponding reaction [9].

One of the important expectations for the novel materials is to be environmentally friendly and biocompatible. Nanoporous calcium carbonate microparticles (CaCO₃MP) meet these demands. The work of Lopez-Marzo et al. comprehensively describes the possibility of the formation of $CaCO_3$-PEI (poly(ethyleneimine). Such complex shows high potential for biosensing applications due to the possibility of conjugating it with proteins, nucleic acids and others biomolecules [10]. These particles found applications also in microfluidic systems, working for both sensing and removal of phenol compounds. The biosensing ability was possible owing to cross-linking of $CaCO_3$MPs with tyrosinase by glutaraldehyde, while the removal ability is connected with porous structure and the capacity of microparticles to adsorb phenolic compounds [11].

1.4. Quantum Dots (QDs)

Quantum dots (QDs), fluorescent semiconductors, have recently become increasingly popular tags for molecular imaging and biosensing. Their optical properties like narrow and size-tunable emission spectra (this leads to multicolor detection), various and broad absorption profiles and chemical stability make them competitive with respect to organic fluorophores that are commonly used as fluorescent labels [12, 13]. Depending on the type of QDs, their fluorescence lifetime can be 10 times longer compared to organic fluorophores. However, QDs have some disadvantages like potential toxicity (due to the fact that it contains heavy metals), which is not well known yet, but also larger size (from 2 to 15 nm) than organic fluorophores, which can be a drawback in some approaches [14].

A major advantage is the possibility that QD is optically and electrochemically detected. The electrochemical method is related to the detection of Cd contained in CdS QD (or any other metal depending on the quantum dot). Such detection can be performed on screen-printed electrodes by using square wave anodic stripping voltammetry. While the potential is applied, in the presence of proper buffer, cadmium (Cd^{2+} ion onto the QD surface) is reduced onto the working electrode surface and oxidized again (electrochemical stripping). The specific peak at the characteristic red-ox potential of cadmium can be observed [15]. This technique is faster, less expensive and easier to be performed in comparison to optical detection. Electrochemical detection of QDs can be

implemented to high-throughput, automated detection systems. Furthermore, electrochemical detection of QD is really sensitive. In the work reported by Medina-Sánchez et al., QD detection in a microfluidic chip was possible in the range of 50 to 8000 ng mL^{-1} with a sensitivity of 0.0009 µA/(ng mL^{-1}) [16]. Since QDs contain reactive group on their surface, usually thiol (-SH) and carboxyl (-COOH), it is possible to conjugate them easily with biomolecules having sensing abilities (i.e. antibodies, aptamers) as well as with proteins like streptavidin so as to obtain QDs labels able to perform analytical signal enhancement. To make it feasible, it is necessary to use a proper biolinker like primary amines, thioglycolic acid, peptides or chitosan polymer [17]. QDs were already employed also for electrochemical screenings of apoptosis of mammalian cells. QD conjugated with Annexin-V can effectively bind to phosphatidylserine, a phospholipid expressed in the outer membrane of apoptotic cells. Electrochemical detection, comparing to optical one was characterized by shorter time and possibility to perform versatile quantified analysis [18].

1.5.   Carbon nanomaterials

Carbon is characterized by the presence in various allotropic forms. Physical and chemical properties of a given carbon allotrope depend on hybridization. Carbon materials which are found to be used in biosensing usually have sp^2 hybridization. These are for example graphite, carbon nanotubes, and graphene.

Carbon nanomaterials, due to their surface properties, conductivity and biocompatibility, are good candidates for application in electrochemical biosensors. For example, MWCNTs (multi-walled carbon nanotubes) were reported by Perez Lopez et al. as a material raising the signal intensity of tyrosinase biosensor for catechol detection by 90% [19]. This phenomenon was caused due to improved electronic transference between enzyme and MWCNTs layer. At the same time, surface properties of CNTs make them useful for enzyme and other biomolecules immobilization. The versatility of this material was also proved in the work, where MWCNTs were immobilized onto magnetic particles for catechol detection and shown to be very useful and easy to manipulate in ON-OFF response biosensing platform [20].

Carbon nanomaterials also show interesting optical properties. In the work of Morales-Narvaez et al., the Förster Resonance Energy Transfer (FRET) was measured between Quantum Dots and various carbon nanomaterials: graphite, carbon nanotubes (CNTs), carbon nanofibers (CNFs) and graphene oxide (GO). The highest quenching was observed for GO (97±1%), which makes this material very useful for future applications employing the phenomena of FRET with an? interest for biosensing approach (Fig. 1A) [21]. Moreover, Graphene Quantum Dots (GQD) can be used for small molecules detection (Fig. 1B) due to their capability of conjugating conveniently with magnetic silica beads (used as a carrier) and molecular imprinted polymer (recognition of the analyte) [22].
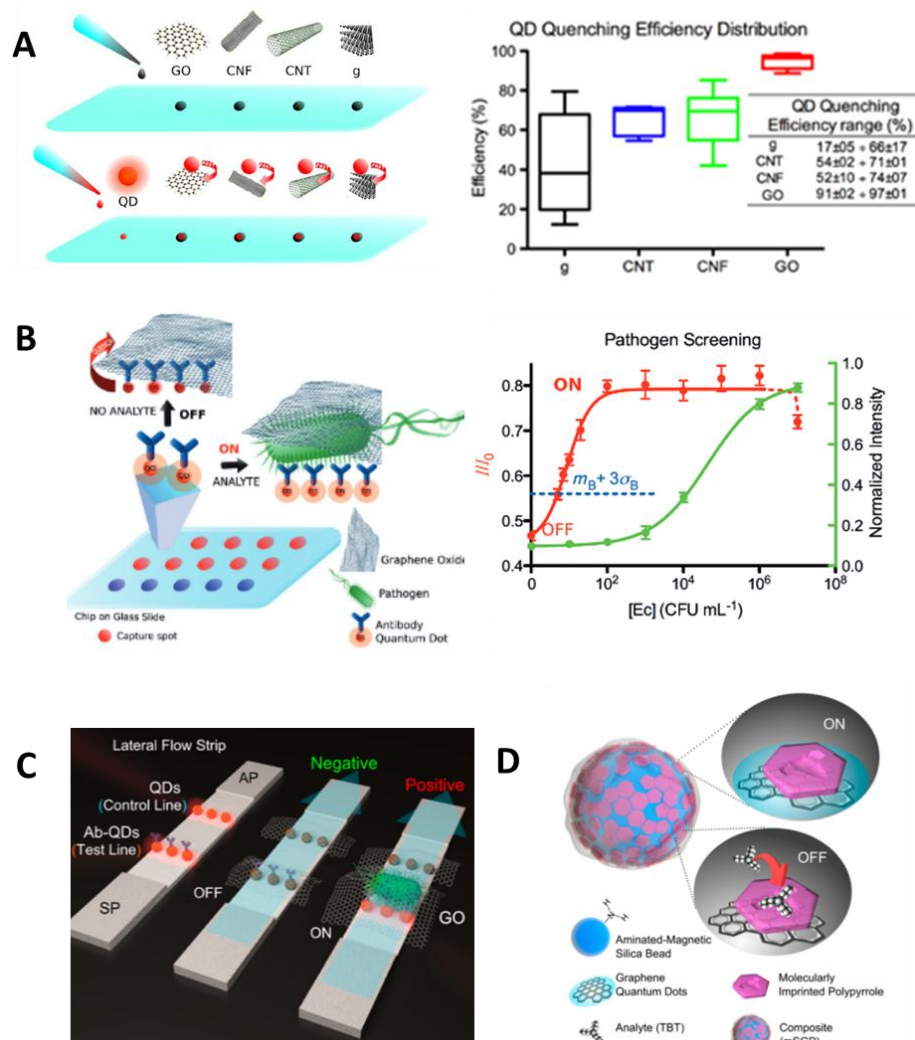
Figure 1 Carbon nanomaterials in optical biosensing. **A.** Comparison of QD quenching caused by various carbon nanomaterials (GO – Graphene Oxide, CNT – Carbon nanotubes, CNF - Carbon nanofibers, g – graphite), modified with permission from Elsevier, Copy Right (2012) [21]; **B.** Pathogen detection in microarray format using GO as a revealing agent, modified with permission from John Wiley and Sons, Copy Right (2013)[24]; **C.** Pathogen detection in lateral-flow format using GO as a revealing agent, modified with

permission from American Chemical Society, Copy Right (2015) [25]; **D.** Small-molecule detection based on molecularly imprinted polymer (MIP) and GO, modified with permission from American Chemical Society, Copy Right (2015) [26].

Carbon nanomaterials can play varied roles in biosensors. For further studies, the following reviews comprehensively describing them [13, 23] can be recommended. Some examples of the application of carbon materials in optical biosensors are presented in Fig 1.

1.6.   Micro- and nanomotors

Just as the name suggests, micro- and nanomotors are supposed to perform various mechanical movements such as shuttling, rolling, rotation or others, due to the fact that they are induced by a specific factor. We can distinguish nano/micromotors driven by light, magnetic fields, acoustic waves (physical control) as well as by energy resulting from various chemical reactions, where selected compounds act as fuels for motors [27] (Figure 2.). Nano/micromotors movement behavior opens a lot of opportunities to take as an advantage in biosensing systems. They can support mixing processes in a microscale, improving the mass transport and increasing the intensity of sensors response, like in microarray. Acting as carriers, nano/micromotors can be conjugated with biomolecules such as antibodies working as sensing or capturing probe with the ability to be applied for example in microfluidic device [28]. Nano/micromotors are promising tools not only in biodetection but also for removal. A good example is a work of Guix et al. where alkanethiol-coated Au/Ni/PEDOT/Pt shows the ability to capture, transport and remove oil droplets [29]. Another interesting example is bacteria detection performed through Concanavalin A (ConA) immobilized onto the nanomotors surface [30].
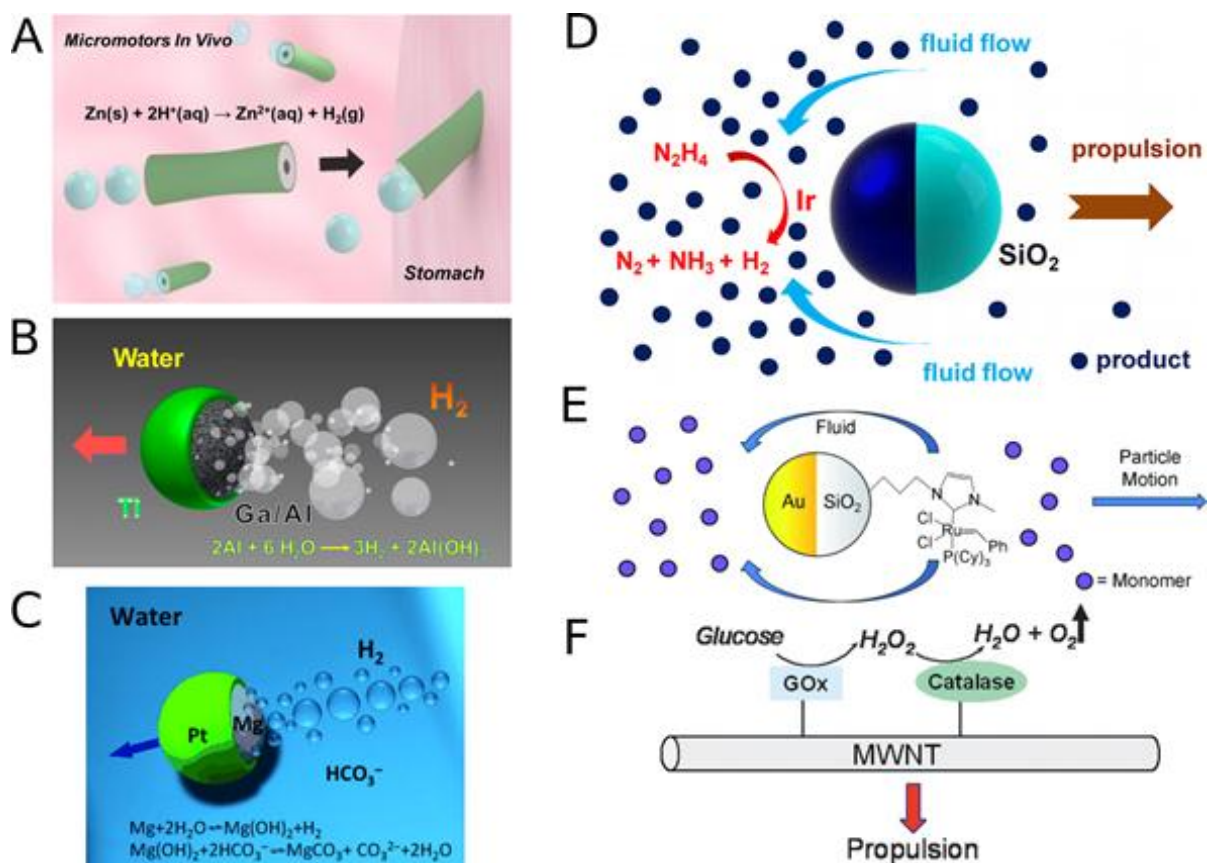
Figure 2 Different reported strategies for catalytical propulsion of micro/nanomotors. **A.** Propulsion of Zn microtubes by gastric acid (HCl) as fuel, modified with permission from American Chemical Society, Copy Right (2014) [31]. **B.** Propulsion of Al-Ga Janus micromotors based on water-Aluminium reaction, modified with permission from American Chemical Society, Copy Right (2012) [32]. **C.** Propulsion of Mg/Pt Janus micromotors by Magnesium-Water reaction, modified with permission from John Wiley and Sons, Copy Right 2013 [33]. **D.** Propulsion of Iridium-Based Janus Micromotors by Hydrazine-Iridium reaction, modified with permission from American Chemical Society, Copy Right (2014) [34]. **E.** Propulsion of Au/SiO$_2$ Janus micromotors by polymerization, modified with permission from WILEY-VCH Verlag GmbH & Co. KGaA, Copy Right (2011) [35]. **F.** Propulsion of multi-walled carbon nanotube based on catalysis of glucose, modified with permission from Royal Society of Chemistry, Copy Right (2008) [36].

1.6.1. Micromotors support mass transport and protein detection

García et al. (2013) reported the first antibody-decorated tubular microengines designed to capture and transport target proteins between microfluidic chambers. Catalytic polymer/Ni/Pt microengines were biofunctionalized with antibodies targeting IgG protein, as a model protein, in order to achieve a micromotor-based immunoassay offering "on-the-fly" capture and isolation/sorting capabilities, see Figure 3A'. The immunocomplex can

be easily visualized by optical microscopy by using an antigen/antibody labeled with a polymeric-sphere tracer. This novel assay is highly selective and eliminates time-consuming washing steps, simplifying and accelerating the overall immunoassay procedure [28]. Taking advantage of these features, Yu et al. (2014) exploited antibody-functionalized AuNP/PANI/Pt micromotors to perform rapid "on-the-fly" sandwich immunocomplexes targeting carcinoembryonic antigen. The assay takes 5 minutes and operates in a range of 1−1000 ng mL^{-1} [37]. In addition, labeling the captured proteins with microscopic particles showing different sizes and shapes facilitates multiplexed analysis of proteins, as proved by Vilela et al. (see Figure 3B') [38].

The usability and versatility of different assays performed in the liquid phase (such as immunoassays) can be limited by mass transport, which depends on chemical and physical properties of the molecules working as bioreceptors and targets. The induction of any kind of micro-mixing can be helpful for improvement the efficiency of the assay. One of the promising approaches is using self-propelling micromotors. In that work, protein detection (ApoE) based on immunoassay, with fluorophore as a label, was improved 3.5 folds (signal intensity) due to the application of Polyanyline (PANI)-platinum micromotors. Amplification of the signal at the same time can significantly reduce the limit of detection. The only potential drawback in this study is using hydrogen peroxide as a fuel for micromotors, which in some cases can be a way to degrade the proteins used in a given assay (Figure 3C') [39].
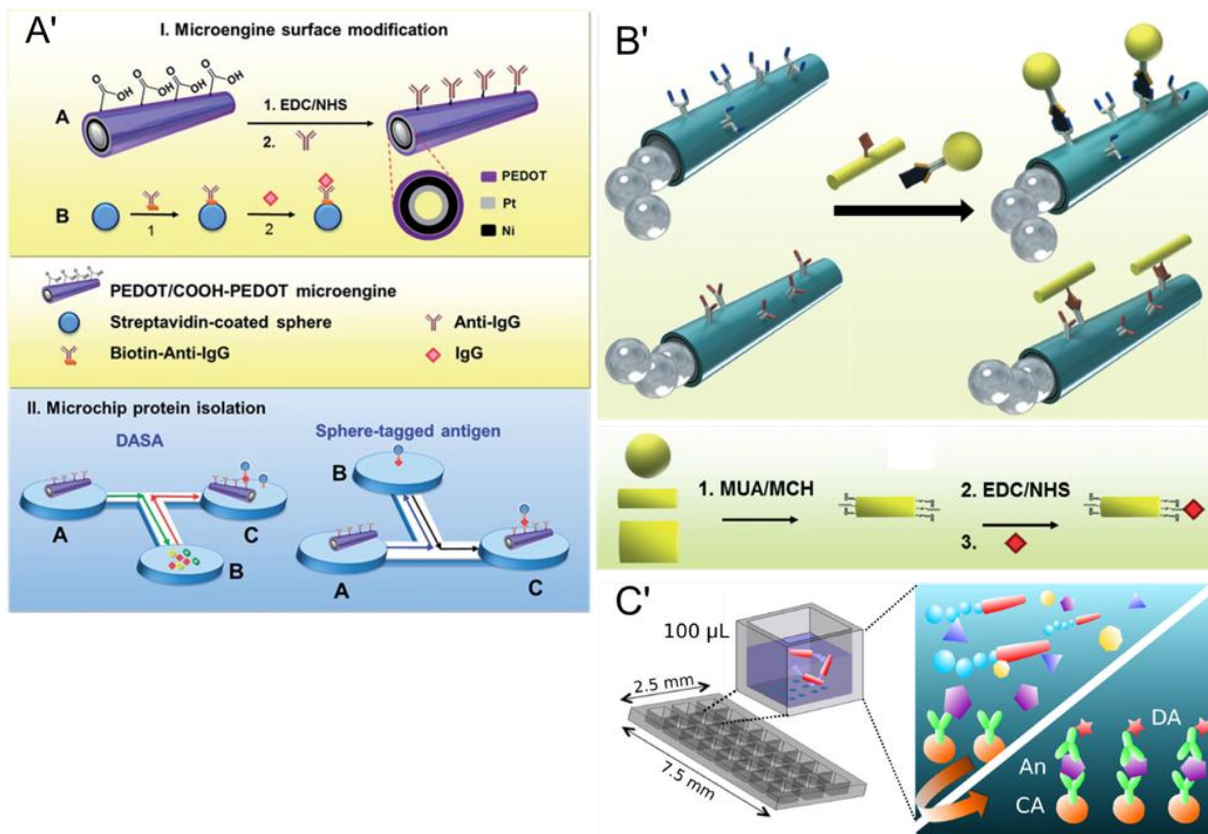
Figure 3 Micromotors for protein sensing. **A'**. Antibody-decorated micromotor for protein detection, modified with permission from Royal Society of Chemistry, Copy Right (2012) [28]. **B'**. Micromotor-based multiplexed immunoassay via different microscopic tracers. Modified with permission from Royal Society of Chemistry, Copy Right (2014) [38]. **C'**. Microarray immunoassay assisted by microengines, modified with permission from John Wiley and Sons, Copy Right (2014) [39].

1.7. Nanochannels

Another approach to the application of nanomaterials is using them as filters that selectively allow analyte (e.g. protein biomarkers) to pass through them. This is the example of the biomimetic approach because in live organisms cell metabolism is driven by proteins located in the cell membranes which are selectively permeable to various ions, nutrients and other biomolecules [40].

Nanochannels support high sensitivity and selectivity in biosensing. Due to the determined size of pores, the sample is filtered (interfering big size analytes remain on top of the channel) when it reaches the inner surface of nanochannels where the bioreception

occurs. Such behavior reduces the risk of unspecific bonding and the introduction of any interference from impurities. Nanochannels can be functionalized inside the membranes, so it is possible to stop the analyte inside them. The nanochannel blocking can be followed by electrochemical techniques [40]. One of the examples is voltammetric detection of thrombin, where anodized alumina oxide filter membrane (AOO) was used as a nanochannel, with an internal diameter of porous of 200 nm. As a bioreceptor, anti-thrombin IgG labeled with AuNP was used. When the channel is blocked due to immunocomplex formation, diffusion of $[Fe(CN)_6]^{4-}$ is decreased, such a phenomena serving (Differential Pulse Voltammetry signal decrease) as a source of the analytical signal. This system showed very low LOD (LOD 1.8 ng mL−1), even when the analysis was performed in spiked blood samples [41]. Nanochannels can be effectively used for cancer biomarkers sensing from the blood due to the nanochannel-based filtration of the whole blood. In that case, it was possible to detect 52 U mL−1 of CA15-3 breast cancer marker [42]. Another approach for cancer biomarkers was studied using Prussian blue nanoparticles (PBNPs) working as a redox indicator in immunoassay. The application of PBNPs instead of $[Fe(CN)_6]^4$ led to a lower detection limit (from 200 μg mL^{-1} to 34 pg human IgG mL^{-1}) (Fig. 4BC) [43].

Various materials can be employed for the preparation of nanochannels. One of the recently published examples is the use of carboxylated polystyrene nanospheres (PS, 500 and 200 nm-sized) coating the working area of flexible screen-printed indium tin oxide/polyethylene terephthalate (ITO/PET) electrode. Similarly, as the above-mentioned example, this platform was used for IgG detection as a model protein. Unlike AAO membranes, this approach overcomes many of the limitations in terms of integration and sensitivity, and represents a really disposable biosensing device for one-step assays (Fig. 4A) [44].
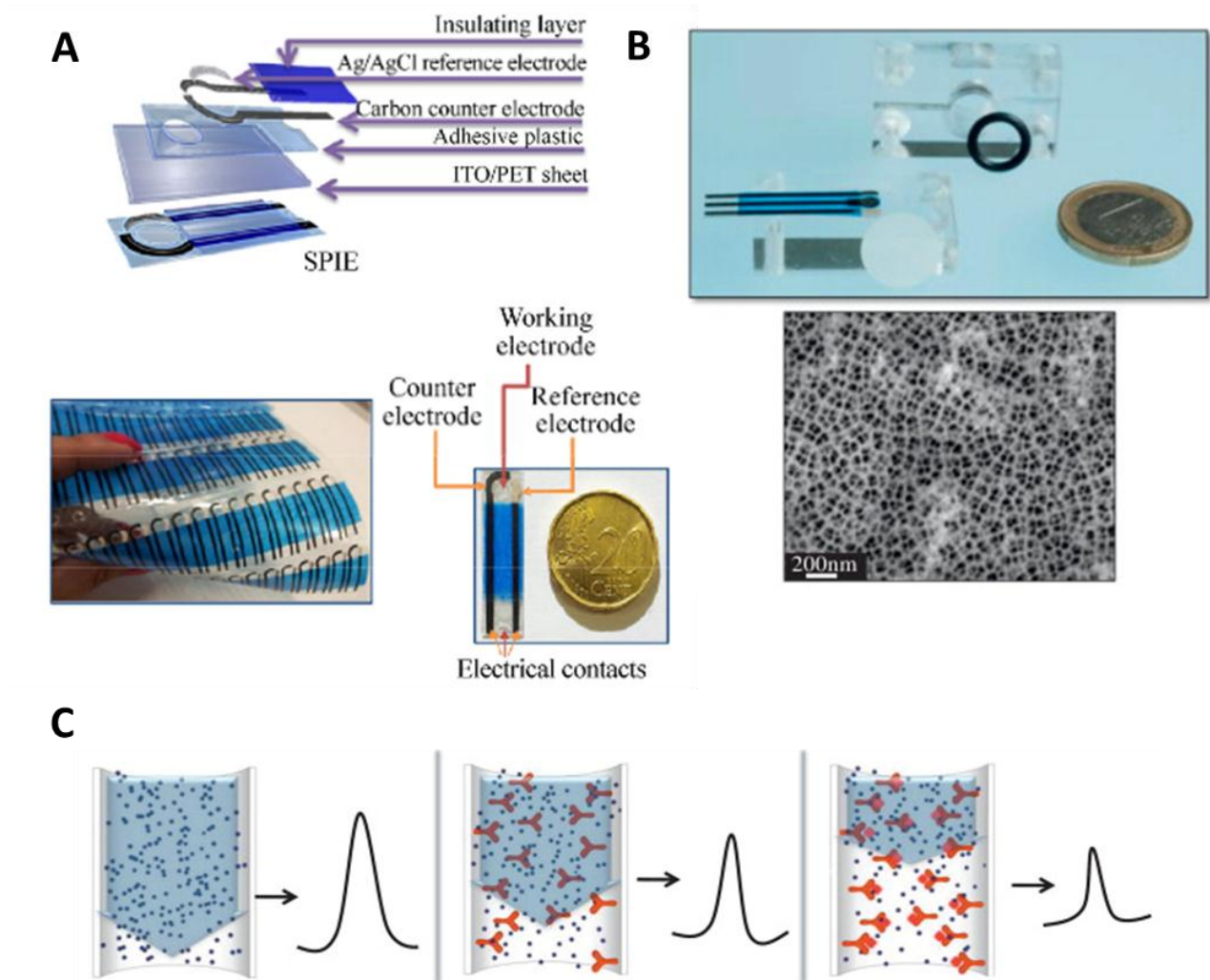
Figure 4 Application of nanochannels in biosensing. **A.** Schematic representation of the different materials and layers which form the SPIE (screen-printed ITO/PET electrodes), modified with permission from Springer, Copy Right (2015) [44]; **B.** Schematic representation of the process occurring on the nanochannels modified electrode, modified with permission from Elsevier, Copy Right (2015) [43]; **C.** Schematic representation of the sensing principle: the voltammetric signal of the PBNPs decrease with the subsequent AAO membranes modification, modified with permission from Elsevier, Copy Right (2015) [43].

1.8.   Paper nano-biosensors

The launch of the first pregnancy test in the mid-70s started the acclaim of paper-based biosensors. It was the proof that biosensors can be simple devices, possible to be used by everyone, relatively inexpensive and accessible. Nowadays, when all innovations are also assessed for their impact on the environment, paper-based biosensors positively stand out for their biodegradability and safety for the user and the environment. The portability of

paper-based biosensors allows people to use them in any place on Earth, regardless of the availability of specialized laboratories and personnel. This opens the way to improve medical diagnostics and environmental monitoring in developing countries. Paper-based biosensors can also be used for example in the food and pharmaceutical industry to perform preliminary analyses related to quality control which precedes a further in-depth test in dedicated laboratories. Furthermore, these biosensors can be both qualitative and quantitative, depending on the needs. Optical detection, possible even with the naked eye, is easy and fast [45, 46].

Paper-based biosensors are already used for proteins, DNA, and other compounds sensing. Like in most biosensors, detection is based on the affinity of the specific antibodies or DNA sequences (or aptamers) to target compounds [45] beside other receptors. Although most of the articles present paper-based biosensors for biomarkers detection, these devices also represent also an interesting solution for environmental screening. One of the examples is heavy metal detection (cadmium) in paper device reported by López-Marzo et al. [47, 48]

LFA (lateral flow assays) are one of the most popular paper-based sensors, and their main advantages is versatility and various detection possibilities (optical, electrochemical). They consist of a detection pad, a conjugation pad, a sample pad and an absorption pad. The detection pad is made of nitrocellulose and its role is to capture the analyte since capturing receptors (i.e. antibodies) are printed onto it. Glass fiber is used for the conjugation pad, where conjugate with the color label (e.g. AuNP) is stored. Sample and absorption pads are made of cellulose and those pads support the flow of the liquid and purify the sample [45, 46, 48].

Although paper-based biosensors offer many opportunities, it is still necessary to overcome some drawbacks like improving the limit of detection, sensitivity and enabling parallel detection of different targets. The application of, for example, nanoparticles working both as a carrier or label, can increase the usability of this type of biosensors.

One of the promising tools in paper-based biosensors is AuNP nanoparticles. Due to their strong red color, that facilitates optical detection and catalytic properties useful for electrochemical sensing. Applications of AuNP for the sensing of various proteins, DNA and cancer cells in paper biosensors are already reported. In order to improve detection, different types of particles can be used i. e. QDs or magnetic particles [45].

A very interesting solution to enhance the signal for optical detection in paper-based biosensors is the use of enzymes able to produce a reaction resulting in the appearance of color. Such an approach was proposed by Parolo C. et al. where AuNPs were conjugated with antibodies previously labeled with HRP. The increase of the colour on the strip (by the use of various HRP substrates; in that case TMB, AEC and DAB) results in an increase of the sensitivity of the assay up to 1 order of magnitude in comparison to non-modified AuNPs [49].

Seeing that paper-based biosensor operation is based on liquid flow, optimization of this parameter can provide interesting results. Changing the geometry characteristics of the pads like width, shape or length affects the flow speed and the distribution of the liquid (Fig. 5). In the work of Parolo et al. the increase of the sensitivity was up to 8-fold due to an enlargement the size of the conjugation and sample pad (Fig. 5B) [50]. Referring to the idea of liquid flow manipulation to enhance the sensitivity of paper-based devices, Rivas et al. proposed the use of delay hydrophobic barriers fabricated by wax printing. For this purpose, wax pillar patterns were printed onto the nitrocellulose membrane to generate delays as well as pseudoturbulence in the microcapillary flow. Biosensing performed for model proteins (HIgG) showed 3-folds improvement of the sensitivity (Fig. 5C) [51].

Another approach increasing sensitivity is the triple line lateral flow sensor reported by L. Rivas et al. for *Leishmania infantum* DNA detection. Besides a control line, two test lines are printed onto the LF strip in order to detect: double labelled (FITC/biotin) amplified *Leishmania* DNA (TL1) and 18S rRNA gene (endogenous control) (TL2) [52].

All of the examples mentioned above were focused on colorimetric detection of analytes. However, it is also possible to design photoluminescent LF biosensors, where the QD-Ab

complex in printed on the substrate and Graphene Oxide is used as a quenching agent. Morales-Narvaez et al. reported photoluminescent detection of *E. Coli* and *S. Typhimurium* with a limit of detection of 10 CFU mL^{-1} in standard buffer and 100 CFU mL^{-1} in bottled water and milk [25].

Mechanical strength and chemical non-interference allow the fabrication of electrochemical paper-based biosensors, where electrodes are printed directly on the various paper materials in the same way as the commonly used screen-printed electrodes. An example of this approach was shown by Parolo C. et al. The nitrocellulose membrane HF240 was used to fabricate screen-printed carbon electrodes (SPCE) furtherly tested for AuNP and QD electrochemical detection. Such electrodes, compared to SPCE based on the polyester show significantly higher hydrophilicity of the surface and a better electrochemical response. Such properties are linked to 3D structure of the membrane, which enhances the performance of the device [53].

The future development for paper-based devices seems to be so potent because of the need for readily available and inexpensive biosensors. The main challenge is to increase the level of specificity, sensitivity and improve the fabrication process, which would help attain a better reproducibility of the assays performed in paper-based biosensors.

One of the critical points in the development of paper-based nanobiosensors is finding the novel types of paper substrates which are easy to fabricate, biocompatible and suitable for performing various chemical/biological reactions. One of the most promising materials is nanopaper. Bacterial cellulose nanopaper is a multifunctional material known for its numerous properties such as biocompatibility, optical transparency, sustainability, biodegradability, thermal properties, high mechanical strength, flexibility, hydrophilicity, broad chemical-modification capabilities, high porosity and high surface area. Its interactions with QD, GO, AuNP, AgNP were already studied by Morales-Narvaez et al. showing a very good suitability of nanopaper for further biosensing applications (Fig. 5A) [54].
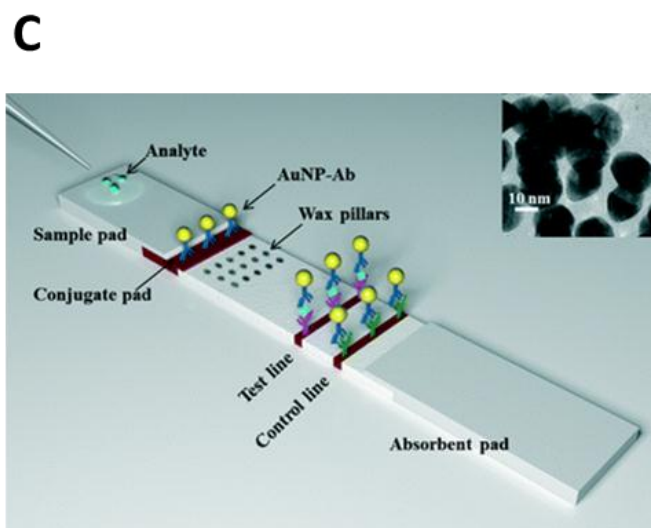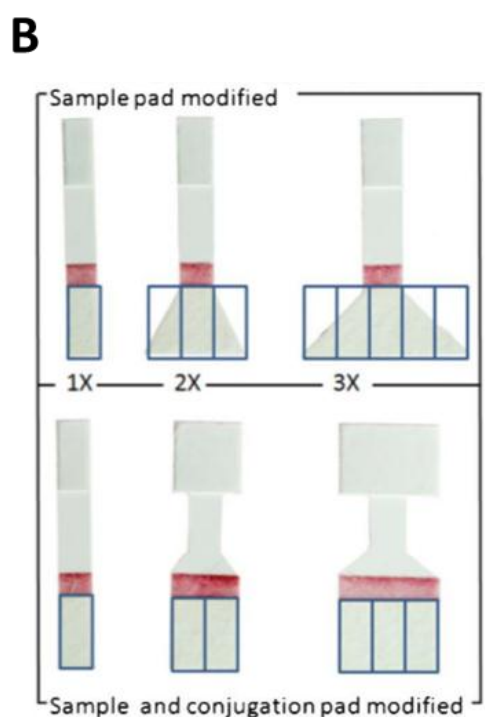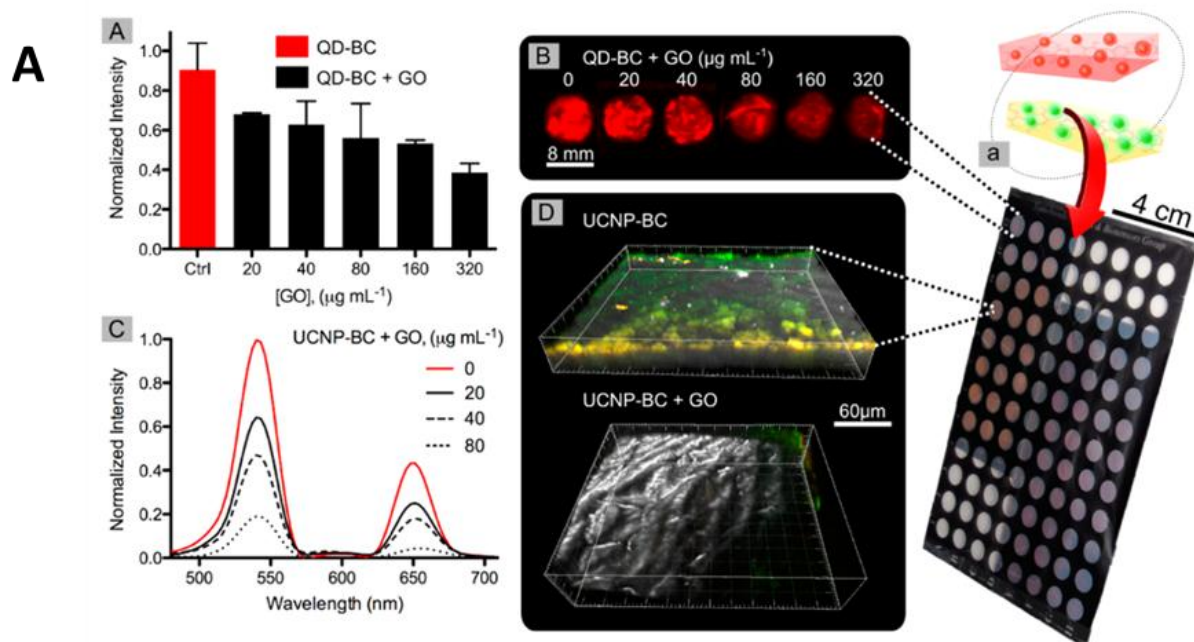
Figure 5 Novelties in the field of paper biosensors. **A.** Nanopaper (BC) multiwell plate for photoluminescent tests, modified with permission from American Chemical Society, Copy Right (2015) [54]; **B.** Modification of lateral flow test geometry in order to improve sensitivity, modified with permission from Royal Society of Chemistry, Copy Right (2013) [50]; **C.** Application of Wax pillars as a hydrophobic barriers in the lateral flow test, modified with permission from Royal Society of Chemistry (2014) [51].

1.9.   Microarray technology

High-throughput technologies are of interest to both scientists and entrepreneurs. Microarrays, due to their versatility, are currently used for sensing of the different compounds and molecules like DNA, RNA, peptides, proteins (including antibodies) as well as cells and tissues. Microarray revolutionized genomic studies due to its capability of measuring an expression of various genes in a short time or performing genotyping. Nowadays, microarrays gain recognition as a promising tool for biosensing [55]. These platforms are truly flexible. As a substrate for spotting, different types of glass (or other materials) with various chemical modifications like silanization can be used, so as to fit it to the type of spotted molecule. Depending on the willingness of the user/researcher, targets or capture agents can be spotted (i. e. antibodies). In this case, microarray sensing can act as a direct, indirect or competitive assay – similarly to ELISA. In this section the main lines of the development of this biosensing technology, including another way to improve their versatility, are described [56-57].

1.9.1. Quantum Dots as a fluorescence enhancer

Many researchers are looking for new compounds that will be successfully used as fluorescence markers in biodetection systems. Quantum Dots can effectively replace organic fluorophores in microarray biosensing. It is worth mentioning that QDs, compared to organic fluorophores, have a broader and stronger absorption spectra and their emission is characterized by narrow and symmetric spectrum [14]. Depending on the type of QDs, their fluorescence lifetime can be 10 times longer in comparison to organic fluorophores. In the work of Morales Narvaez et al., Cadmium-Selenide/Zinc Sulphide QDs (CdSe@ZnS) were tested versus fluorescent dye Alexa 647 as reporters in protein immunoassay (ApoE was used as a model protein). Authors observed that QDs are highly effective reporters in a microarray, but their properties depend largely on the excitation wavelength. For 532 nm excitation wavelength, the use of QDs provides five times lower limit of detection (LOD). These studies open the way for further use of QDs in microarray [14].

1.9.2. Graphene Oxide as a fluorescence quenching factor in microarray

Due to the ability of GO to quench the fluorescence that was described before, it is possible to take advantage of this phenomenon in biosensing strategy. The properties of fluorescence quenching depend on the distance between the donor and acceptor (according to FRET phenomena). Therefore it can be assumed that by increasing the distance between QDs (donor) and GO (acceptor), measurable changes in fluorescence can be observed [12, 58]. This approach has been used for bacteria detection (*E. coli* O157:H7). QDs conjugated with antibodies against bacteria were spotted on the glass slide. Then, slides were incubated with samples with or without (blank) bacteria and after that, GO was added. The biggest quenching was observed in blanks while spots with bacteria showed lower quenching (Fig. 1B). However, this response was found to be like a digital-like test that is very versatile and efficient for bacteria detection (LOD: 5 CFU mL^{-1}). This cannot be used for sensing proteins or small molecules, due to their size, which is not sufficient to affect the level of quenching [24, 59].

1.10.   Lab-on-a-chip (LOC)

Microfluidic Lab-on-a-Chip devices are characterized by the small size of sensing platforms, a small volume of reagents (µL, nL, pL, fL) used for performing the assay and low energy consumption. Microfluidic systems can be well automated and used either for preconcentration, isolation, and detection of interesting analytes. One of the most interesting applications is microfluidic chips for electrochemical and optical biosensing that can be applied for detection of various biomarkers, organic compounds etc. The versatility of LOC devices makes it possible to integrate various sensing materials and strategies [60].

LOC microfluidic devices usually consist of microfluidic chips and driving units. The samples and reagents are introduced into the channel. The flow can be driven by different kinds of syringe pumps or dedicated flow control systems. The newest solutions also allow the manipulation of liquids by surface acoustic wave and micropumps. The small diameter of the microfluidic channel causes relatively low usage of reagents. Thanks to the external driving units, parameters of reaction can be well controlled. The environment of the microfluidic channel is permanently isolated from the outside (unlike most assays

performed in microplates, test-tubes etc.), which protects reactions and facilitates reproducible results. Depending on the purpose, different designs of microfluidic chips can be used for mixing, incubation, or preconcentration of the sample. Channels can also work as incubators for cell culturing and carry out specific chemical reactions. An example of the modular platform for rapid on-chip apoptosis assay on human carcinoma cells is shown in Fig. 6. For biosensing applications, chips with incorporated electrodes are particularly interesting to obtain electrochemical sensors. The surface of the channel can be treated by different reagents for further modification by biomolecules (for example proteins). In addition, devices equipped with magnets are useful for performing magneto-immunoassay utilizing magnetic particles [60, 61]. Researchers are focused on miniaturized detection platforms, as well as all driving units which assist them. Recently LOC devices with all integrated electronic driving units were obtained using PCB (printed circuit board) as a substrate for microfluidic chip [62, 63].
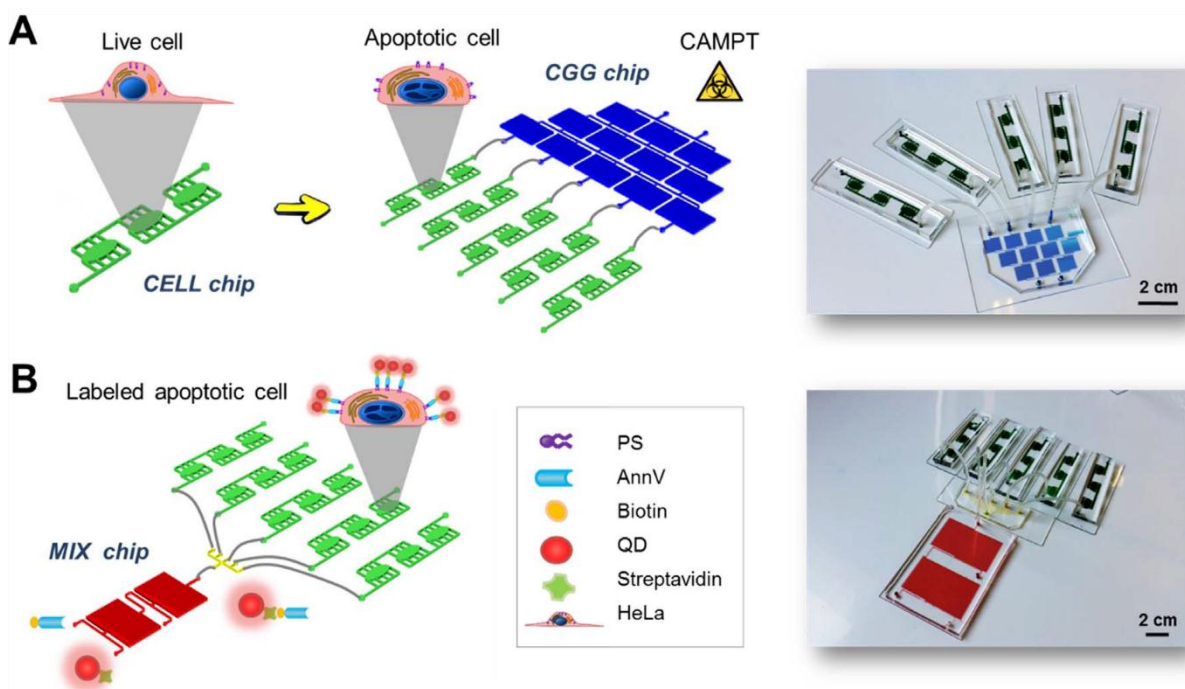
Figure 6 Modular microfluidic platform for apoptosis monitoring. A. Human carcinoma cells (HeLa) are cultured in the CELL chip composed of three identical chambers. Cells growing in the CELL chip are exposed to different CAMPT doses obtained through the concentration gradient generator chip (CGG). In this stage, cells will start translocation the PS to the outer leaflet of the plasma membrane. B. In a second step, a mixer chip (MIX) with two identical areas is in charge, first, of the conjugation of biotinylated AnnV with streptavidin-QD and, second, the mixture of AnnV-QD conjugates with the binding buffer containing the Ca2+ required for the specific binding with the translocated PS. The MIX chip is then connected to the CELL

chip in order to incubate cells with the probe and to label the apoptotic cells. Modified with permission from Elsevier, Copy Right (2017)[64].

1.10.1. Unlimited possibilities of microfluidic devices designs

One of the common techniques for efficient prototyping of microfluidic devices is soft-photolithography, where the polydimethylsiloxane (PDMS) chip is fabricated with a hollowed microfluidic channel and substrate capable of keeping a permanent bonding with PDMS [63]. Apart from glass, one of the most widespread materials used for this purpose is polycarbonate (PC). PC is especially interesting as a substrate in electrochemical microfluidic devices due to its possibility of using electrodes directly printed on its surface. This is possible thanks to well-developed screen-printed technology, although it can be fabricated using different techniques like ink-jet printing and photolithography. The flexibility of screen-printing technology allows their application in microfluidic platforms obtaining various platforms with customized electrodes. On the other hand, transparency of PDMS enables visual control of the process either in macro- and microscale (using optical microscopes). More sophisticated microfluidic chips can consist of a channel layer where all reaction occurs and a control layer, also made of PDMS but responsible for controlling the flow of liquid by operating the valves built in the chip and driven by air pressure. This strategy can be used for increasing the sensitivity of assay by recirculating the compounds that can be detected [16]. Another important feature of PDMS is oxygen permeability, thanks to this, PDMS chips are widely used for cell culturing [60]. An example of the full fabrication process of PDMS-glass microfluidic chip is shown in Fig.7.
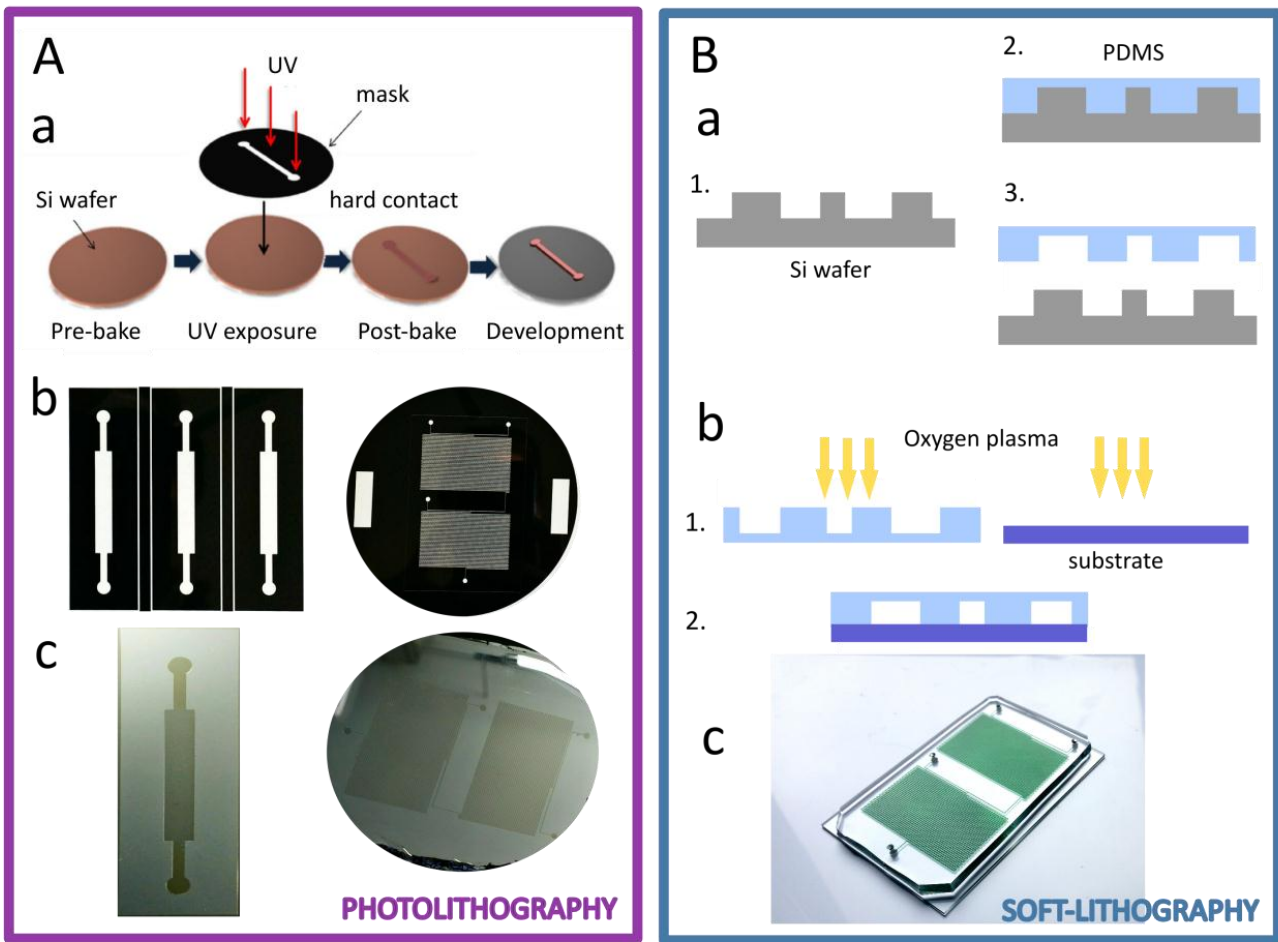
Figure 7 Fabrication of the PDMS-based Lab-on-a-chip device. **A.** Photolithography; (a) master fabrication using Si wafer as a substrate and negative photoresist; (b) examples of flexible masks used for UV treatment; (c) Silicon wafers with the developed patter of the channels; **B.** Soft-lithography; (a) PDMS is poured into a? Si wafer (2.) and afterwards, polymerization is peeled off (3.); (b) PDMS and substrate are washed and treated with oxygen plasma (1.) afterwards, both parts are assembled in order to create a permanent bonding; (c) Fully fabricated PDMS-glass chip with color ink inside.

1.10.2.   Detection and removal of hazardous compounds in microfluidic systems

A large number of dangerous compounds such as toxins, pesticides, chemicals and biocidal compounds require continuous and rapid monitoring of their concentrations. Microfluidic systems, due to their automation and a small volume of samples needed for analysis, can be a promising approach, especially for analysis of such kind of compounds. Microfluidic platforms can combine in one device all analysis steps like cleaning, preconcentration, detection and further removal of a given analyte. This also leads to the possibility of creating portable devices which could work without having to use

sophisticated professional laboratory equipment. Smart systems for different pollutants detection, where the sensing strategy is based on the inhibition of enzymatic reactions, are already reported. For example, a simple lab-on-a-chip (LOC) device is based on biocompatible and biodegradable $CaCO_3$- poly(ethyleneimine) (PEI) nanostructured microparticles (MPs) used to detect and remove phenolic wastes. The detection of phenol by using a hybrid polydimethylsiloxane (PDMS)/glass chronoimpedimetric microchip and its removal in the same LOC system through the use of an extra $CaCO_3$-PEI MPs microcolumn was achieved (with the limit of detection 4.64 nM)[11, 65].

Due to the easy fabrication process and flexibility, Lab-on-a-chip devices can integrate novel material for electrochemical detection. One of the examples is the work reported by Medina-Sanchez et al., where boron-doped diamond (BDD) electrodes are employed for electrochemical detection and degradation of the atrazine, a herbicide of the triazine class. Chronoamperometry revealed a very low limit of detection (LOD) of 3.5 pM for atrazine [66].

1.10.3.   Effective sensing of biomarkers

Common biological interactions usually used for biomarkers detection like antigen-antibody (immunoassays), enzyme-substrate, aptamer-target can be easily implemented in microfluidic platforms. Thanks to this, it is possible to obtain a better limit of detection, a faster response of the sensor and, moreover, prototyping of multifunctional devices able to analyze a number of biomarkers from one sample in one device. As is the case with microfluidic systems for environment monitoring, it is possible to perform in one chip all necessary steps for sample pretreatment. This is of paramount importance taking into account that clinical samples usually consist of blood, serum etc. In our group we already proposed microfluidic devices for different biomarkers (such as IgG [67], ApoE) working as electrochemical sensors. Most of the solutions obtained are based on sandwich immunoassay, where specific antibodies against a given target are used. Furthermore, secondary antibodies were employed and functionalized with QDs which allowed for sensitive electrochemical detection (square wave anodic stripping voltammetry) of interesting biomarkers [61] (Fig.8).
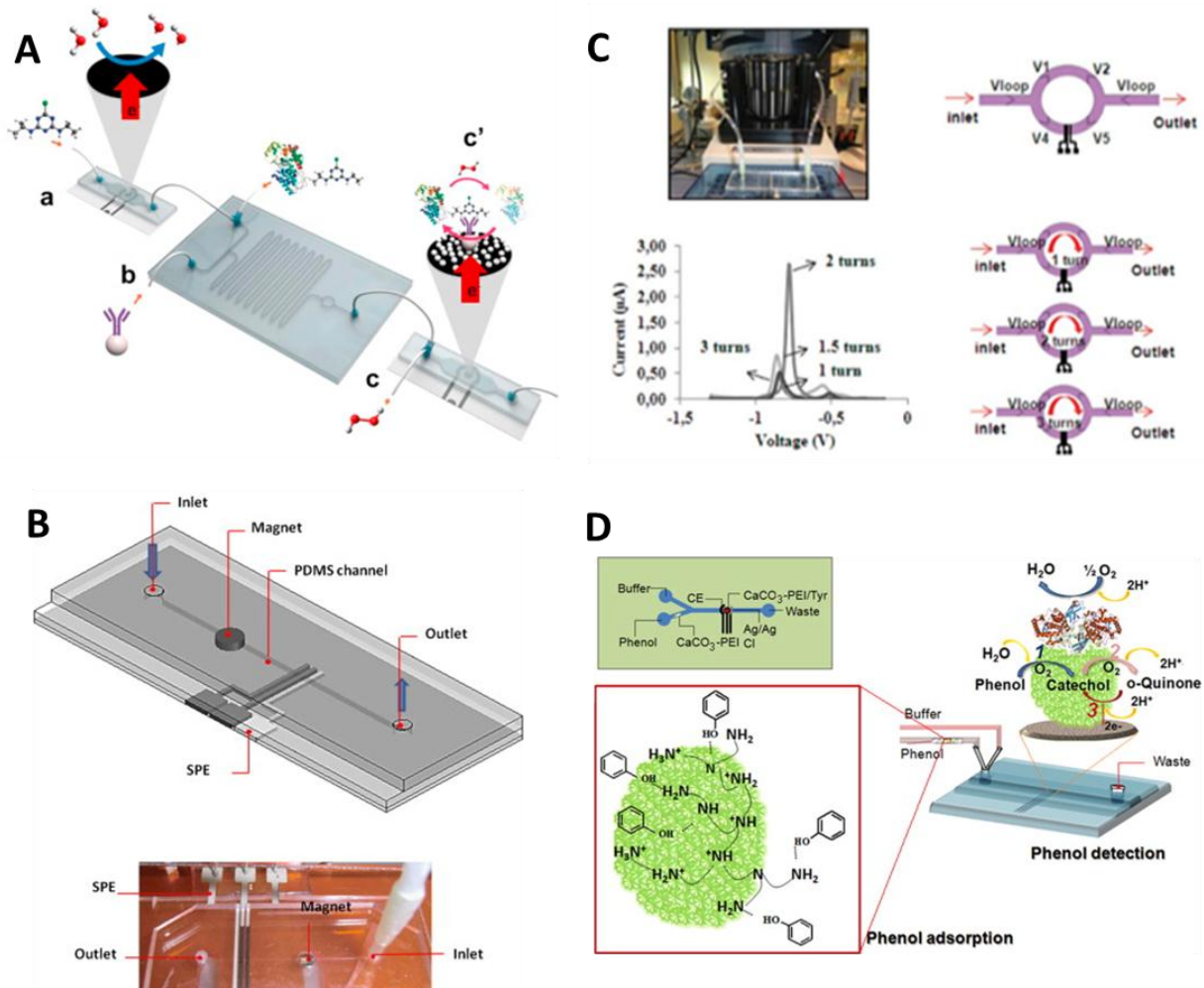
Figure 8 Lab-on-a-chip platforms for biosensing application. **A.** Atrazine detection and degradation in LOC device modified with permission from Elsevier, Copy Right (2015) [66]; **B.** Electrochemical detection of ApoE in LOC device using QDs as labels, modified with permission from Elsevier, Copy Right (2014) [61]; **C.** Improved electrochemical QDs detection in recycling flow through mode LOC device, modified with permission from Royal Society of Chemistry, Copy Right (2012) [16]; **D.** Phenol detection and removal in LOC device with CaCO3 microparticles as an adsorbent, modified with permission from Elsevier, Copy Right (2014) [65].

1.11.   Conclusions

In this chapter, nanomaterials as flexible building blocks of biosensing devices have been presented. We can observe a progressive change in the field of biosensing devices thanks to the use of them.

Electrochemical biosensors achieved increased sensitivity and limit of detection due to the application of various nanoparticles such as AuNP, IrOxNPs, QD as well as carbon materials. All these materials play a role of an effective label, as the chemical reaction they catalyze/perform is related to the quantity of a given analyte. In a similar way, optical biosensing became more potent by using QDs in microarray assays compared to well-known organic fluorophores. Most of the nanomaterials are suitable to be used in various conditions. Thanks to this, they can be employed for paper-based nanobiosensors as well as lab-on-a-chip devices. The latter is especially interesting taking into account the topic of this thesis.

Another possible function of nanomaterials is intermediation in (bio)chemical reactions, a good example of which being nanomotors which motion support the mass transport of biomolecules by improving the sensitivity of immunoassays performed in the microarray format. Moreover, nanomaterials can be used as a substrate for a biosensing platform and/or environment of reaction. Nanopaper (bacterial cellulose) is a very promising material in various optical sensing techniques due to its physical and chemical properties. Nanochannels made of different materials can work as effective filters and separate analyte from the solution.

One of the factors facilitating popularization of nanomaterials is its ease of synthesis. Another crucial issue is that even though nanomaterials themselves may be expensive, the quantity used for biosensing assay is low enough (this is especially seen in microfluidic biosensors) to make the final biosensing device relatively cost-effective, which is essential from the point of view of possible commercialization of such novelties.

However, although nanomaterials present interesting chemical and physical properties their interaction with humans, animals, and the environment is not completely/deeply

known yet. For this reason, the implementation of any new nanomaterial in biosensors should be always preceded by a thorough risk analysis.

1.12. References

1.   Naik, P.P., et al., *Android integrated urea biosensor for public health awareness.* Sensing and Bio-Sensing Research, 2015. **3**: p. 12-17.

2.   Aleman, J., et al., *Definitions of terms relating to the structure and processing of sols, gels, networks, and inorganic-organic hybrid materials (IUPAC Recommendations 2007).* Pure and Applied Chemistry, 2007. **79**(10): p. 1801-1827.

3.   Vert, M., et al., *Terminology for biorelated polymers and applications (IUPAC Recommendations 2012).* Pure and Applied Chemistry, 2012. **84**(2): p. 377-408.

4.   Afonso, A.S., et al., *Electrochemical detection of Salmonella using gold nanoparticles.* Biosensors & Bioelectronics, 2013. **40**(1): p. 121-126.

5.   de la Escosura-Muniz, A., et al., *Rapid Identification and Quantification of Tumor Cells Using an Electrocatalytic Method Based on Gold Nanoparticles (vol 81, 10268, 2009).* Analytical Chemistry, 2012. **84**(8): p. 3855-3855.

6.   Maltez-da Costa, M., et al., *Detection of Circulating Cancer Cells Using Electrocatalytic Gold Nanoparticles.* Small, 2012. **8**(23): p. 3605-3612.

7.   Espinoza-Castaneda, M., et al., *Casein modified gold nanoparticles for future theranostic applications.* Biosensors & Bioelectronics, 2013. **40**(1): p. 271-276.

8.   Mars, A., et al., *Gold nanoparticles decorated with a ferrocene derivative as a potential shift-based transducing system of interest for sensitive immunosensing.* Journal of Materials Chemistry B, 2013. **1**(23): p. 2951-2955.

9.   Mayorga-Martinez, C.C., et al., *Iridium oxide nanoparticle induced dual catalytic/inhibition based detection of phenol and pesticide compounds.* Journal of Materials Chemistry B, 2014. **2**(16): p. 2233-2239.

10.   Lopez-Marzo, A., J. Pons, and A. Merkoci, *Controlled formation of nanostructured CaCO3-PEI microparticles with high biofunctionalizing capacity.* Journal of Materials Chemistry, 2012. **22**(30): p. 15326-15335.

11.   Mayorga-Martinez, C.C., et al., *Nanostructured CaCO3-poly(ethyleneimine) microparticles for phenol sensing in fluidic microsystem.* Electrophoresis, 2013. **34**(14): p. 2011-2016.

12.   Marin, S., et al., *Electrochemical Investigation of Cellular Uptake of Quantum Dots Decorated with a Proline-Rich Cell Penetrating Peptide.* Bioconjugate Chemistry, 2011. **22**(2): p. 180-185.

13.   Marin, S. and A. Merkoci, *Nanomaterials Based Electrochemical Sensing Applications for Safety and Security.* Electroanalysis, 2012. **24**(3): p. 459-469.

14.   Morales-Narvaez, E., et al., *Signal Enhancement in Antibody Microarrays Using Quantum Dots Nanocrystals: Application to Potential Alzheimer's Disease Biomarker Screening.* Analytical Chemistry, 2012. **84**(15): p. 6821-6827.

15.   Marin, S. and A. Merkoci, *Direct electrochemical stripping detection of cystic-fibrosis-related DNA linked through cadmium sulfide quantum dots.* Nanotechnology, 2009. **20**(5).

16.   Medina-Sanchez, M., et al., *On-chip electrochemical detection of CdS quantum dots using normal and multiple recycling flow through modes.* Lab on a Chip, 2012. **12**(11): p. 2000-2005.

17.   Mazumder, S., et al., *Review: Biofunctionalized Quantum Dots in Biology and Medicine.* Journal of Nanomaterials, 2009, doi:10.1155/2009/815734

18.   Monton, H., et al., *Annexin-V/quantum dot probes for multimodal apoptosis monitoring in living cells: improving bioanalysis using electrochemistry.* Nanoscale, 2015. **7**(9): p. 4097-4104.

19.   Perez Lopez, B. and A. Merkoci, *Improvement of the electrochemical detection of catechol by the use of a carbon nanotube based biosensor.* The Analyst, 2009. **134**(1): p. 60-4.

20.   Perez-Lopez, B. and A. Merkoci, *Magnetic Nanoparticles Modified with Carbon Nanotubes for Electrocatalytic Magnetoswitchable Biosensing Applications.* Advanced Functional Materials, 2011. **21**(2): p. 255-260.

21.   Morales-Narvaez, E., et al., *Simple Forster resonance energy transfer evidence for the ultrahigh quantum dot quenching efficiency by graphene oxide compared to other carbon structures.* Carbon, 2012. **50**(8): p. 2987-2993.

22.   Zor, E., et al., *Graphene Quantum Dots-based Photoluminescent Sensor: A Multifunctional Composite for Pesticide Detection.* Acs Applied Materials & Interfaces, 2015. **7**(36): p. 20272-20279.

23.   Perez-Lopez, B. and A. Merkoci, *Carbon nanotubes and graphene in analytical sciences.* Microchimica Acta, 2012. **179**(1-2): p. 1-16.

24.   Morales-Narvaez, E., A.-R. Hassan, and A. Merkoci, *Graphene Oxide as a Pathogen-Revealing Agent: Sensing with a Digital-Like Response.* Angewandte Chemie-International Edition, 2013. **52**(51): p. 13779-13783.

25.   Morales-Narvaez, E., et al., *Photoluminescent Lateral-Flow Immunoassay Revealed by Graphene Oxide: Highly Sensitive Paper-Based Pathogen Detection.* Analytical chemistry, 2015. **87**(16): p. 8573-7.

26.   Zor, E., et al., *Graphene Quantum Dots-based Photoluminescent Sensor: A Multifunctional Composite for Pesticide Detection.* - ACS Applied Materials & Interfaces, 2015.

27.   Guix, M., C.C. Mayorga-Martinez, and A. Merkoci, *Nano/Micromotors in (Bio)chemical Science Applications.* Chemical Reviews, 2014. **114**(12): p. 6285-6322.

28.   Garcia, M., et al., *Micromotor-based lab-on-chip immunoassays.* Nanoscale, 2013. **5**(4): p. 1325-1331.

29.   Guix, M., et al., *Superhydrophobic Alkanethiol-Coated Microsubmarines for Effective Removal of Oil.* Acs Nano, 2012. **6**(5): p. 4445-4451.

30.   Campuzano, S., et al., *Bacterial Isolation by Lectin-Modified Microengines.* Nano Letters, 2012. **12**(1): p. 396-401.

31.   Gao, W., et al., *Artificial Micromotors in the Mouse's Stomach: A Step toward in Vivo Use of Synthetic Motors.* Acs Nano, 2015. **9**(1): p. 117-123.

32.   Gao, W., A. Pei, and J. Wang, *Water-Driven Micromotors.* Acs Nano, 2012. **6**(9): p. 8432-8438.

33.   Mou, F., et al., *Self-Propelled Micromotors Driven by the Magnesium-Water Reaction and Their Hemolytic Properties.* Angewandte Chemie-International Edition, 2013. **52**(28): p. 7208-7212.

34.   Gao, W., et al., *Catalytic Iridium-Based Janus Micromotors Powered by Ultralow Levels of Chemical Fuels.* Journal of the American Chemical Society, 2014. **136**(6): p. 2276-2279.

35.   Pavlick, R.A., et al., *A Polymerization-Powered Motor.* Angewandte Chemie-International Edition, 2011. **50**(40): p. 9374-9377.

36.   Pantarotto, D., W.R. Browne, and B.L. Feringa, *Autonomous propulsion of carbon nanotubes powered by a multienzyme ensemble.* Chemical Communications, 2008(13): p. 1533-1535.

37.   Yu, X., et al., *Motor-Based Autonomous Microsensor for Motion and Counting Immunoassay of Cancer Biomarker.* Analytical Chemistry, 2014. **86**(9): p. 4501-4507.

38.   Vilela, D., et al., *Multiplexed immunoassay based on micromotors and microscale tags.* Lab on a Chip, 2014. **14**(18): p. 3505-3509.

39.   Morales-Narvaez, E., et al., *Micromotor Enhanced Microarray Technology for Protein Detection.* Small, 2014. **10**(13): p. 2542-2548.

40.   de la Escosura-Muniz, A. and A. Merkoci, *Nanochannels Preparation and Application in Biosensing.* Acs Nano, 2012. **6**(9): p. 7556-7583.

41. de la Escosura-Muniz, A., et al., *Nanochannels for diagnostic of thrombin-related diseases in human blood.* Biosensors & Bioelectronics, 2013. **40**(1): p. 24-31.

42. de la Escosura-Muniz, A. and A. Merkoci, *A Nanochannel/Nanoparticle-Based Filtering and Sensing Platform for Direct Detection of a Cancer Biomarker in Blood.* Small, 2011. **7**(5): p. 675-682.

43. Espinoza-Castaneda, M., et al., *Nanochannel array device operating through Prussian blue nanoparticles for sensitive label-free immunodetection of a cancer biomarker.* Biosensors & Bioelectronics, 2015. **67**: p. 107-114.

44. de la Escosura-Muniz, A., et al., *Nanoparticles-based nanochannels assembled on a plastic flexible substrate for label-free immunosensing.* Nano Research, 2015. **8**(4): p. 1180-1188.

45. Parolo, C. and A. Merkoci, *Paper-based nanobiosensors for diagnostics.* Chemical Society Reviews, 2013. **42**(2): p. 450-457.

46. Quesada-Gonzalez, D. and A. Merkoci, *Nanoparticle-based lateral flow biosensors.* Biosensors & Bioelectronics, 2015. **73**: p. 47-63.

47. Lopez Marzo, A.M., et al., *All-Integrated and Highly Sensitive Paper Based Device with Sample Treatment Platform for Cd2+ Immunodetection in Drinking/Tap Waters.* Analytical Chemistry, 2013. **85**(7): p. 3532-3538.

48. Lopez-Marzo, A.M., et al., *High sensitive gold-nanoparticle based lateral flow Immunodevice for Cd2+ detection in drinking waters.* Biosensors & Bioelectronics, 2013. **47**: p. 190-198.

49. Parolo, C., A. de la Escosura-Muniz, and A. Merkoci, *Enhanced lateral flow immunoassay using gold nanoparticles loaded with enzymes.* Biosensors & Bioelectronics, 2013. **40**(1): p. 412-416.

50.   Parolo, C., et al., *Simple paper architecture modifications lead to enhanced sensitivity in nanoparticle based lateral flow immunoassays.* Lab on a Chip, 2013. **13**(3): p. 386-390.

51.   Rivas, L., et al., *Improving sensitivity of gold nanoparticle-based lateral flow assays by using wax-printed pillars as delay barriers of microfluidics.* Lab on a Chip, 2014. **14**(22): p. 4406-4414.

52.   Rivas, L., et al., *Triple lines gold nanoparticle-based lateral flow assay for enhanced and simultaneous detection of Leishmania DNA and endogenous control.* Nano Research, 2015. **8**(11): p. 3704-3714.

53.   Parolo, C., et al., *Paper-Based Electrodes for Nanoparticle Detection.* Particle & Particle Systems Characterization, 2013. **30**(8): p. 662-666.

54.   Morales-Narvaez, E., et al., *Nanopaper as an Optical Sensing Platform.* Acs Nano, 2015. **9**(7): p. 7296-7305.

55.   Goldsmith, Z.G. and N. Dhanasekaran, *The microrevolution: Applications and impacts of microarray technology on molecular biology and medicine (Review).* International Journal of Molecular Medicine, 2004. **13**(4): p. 483-495.

56.   Tu, S., et al., *Protein Microarrays for Studies of Drug Mechanisms and Biomarker Discovery in the Era of Systems Biology.* Current Pharmaceutical Design, 2014. **20**(1): p. 49-55.

57.   Dufva, M., *Fabrication of high quality microarrays.* Biomolecular Engineering, 2005. **22**(5-6): p. 173-184.

58.   Monton, H., et al., *The use of quantum dots for immunochemistry applications.* Methods in molecular biology (Clifton, N.J.), 2012. **906**: p. 185-92.

59.   Morales-Narvaez, E. and A. Merkoci, *Graphene Oxide as an Optical Biosensing Platform.* Advanced Materials, 2012. **24**(25): p. 3298-3308.

60.   Medina-Sanchez, M., S. Miserere, and A. Merkoci, *Nanomaterials and lab-on-a-chip technologies.* Lab on a Chip, 2012. **12**(11): p. 1932-1943.

61.   Medina-Sanchez, M., et al., *On-chip magneto-immunoassay for Alzheimer's biomarker electrochemical detection by using quantum dots as labels.* Biosensors & Bioelectronics, 2014. **54**: p. 279-284.

62.   Chee, P.S., et al., *Micropump Pattern Replication Using Printed Circuit Board (PCB) Technology.* Materials and Manufacturing Processes, 2013. **28**(6): p. 702-706.

63.   Duffy, D.C., et al., *Rapid prototyping of microfluidic systems in poly(dimethylsiloxane).* Analytical Chemistry, 1998. **70**(23): p. 4974-4984.

64.   Montón, H., et al., *Rapid on-chip apoptosis assay on human carcinoma cells based on annexin-V/quantum dot probes.* Biosensors and Bioelectronics, 2017. **94**: p. 408-414.

65.   Mayorga-Martinez, C.C., et al., *An integrated phenol 'sensoremoval' microfluidic nanostructured platform.* Biosensors & Bioelectronics, 2014. **55**: p. 355-359.

66.   Medina-Sanchez, M., et al., *Microfluidic platform for environmental contaminants sensing and degradation based on boron-doped diamond electrodes.* Biosensors & Bioelectronics, 2016. **75**: p. 365-374.

67.   Ambrosi, A., M. Guix, and A. Merkoci, *Magnetic and electrokinetic manipulations on a microchip device for bead-based immunosensing applications.* Electrophoresis, 2011. **32**(8):   p.   861-869.

CHAPTER 2

Objectives

Objectives

The main goal of this thesis is to design, develop/fabricate and integrate different types of Lab-on-a-chip platforms for contaminants detection (flame retardants, heavy metals). In order to fulfil this objective, graphene materials are used in order to obtain novel composites: rGO-PDMS as well as GO-PDMS. These nanomaterial-based composites are used for the first time in a Lab-on-a-chip platform.

Specifying, the following tasks were performed in order to reach the objective of this thesis:

- Fabrication of various PDMS-based chips to be employed as electrochemical cells, incubators, and mixers;
- Optimization of the electrochemical detection of PBDE;
- Transfer of the PBDE electrochemical detection approach from tube test to microfluidic chip ;
- Development of the rGO-PDMS composite and study of its interaction with PBDE;
- Design and fabrication of the complete Lab-on-a-chip platform for the detection and removal of PBDE;
- Optimization of the heavy metals electrochemical detection;
- Development of the GO-PDMS composite and study of its interaction with heavy metal ions in various conditions;
- Design and fabrication of the complete Lab-on-a-chip platform for the preconcentration and detection of heavy metals;
- Comparison of the developed approaches with the state-of-the-art in the field of Lab-on-a-chip platforms and nanomaterials.

CHAPTER 3

Electrochemical detection and graphene-based removal of the flame retardants in a LOC device

3.1.   Introduction

Lab-on-a-chip (LOC) platforms have been intensively developed since the last decade due to their versatility, ease of fabrication, and a multitude of applications in biosensing and analysis. So far, LOC devices have been reported for the detection of protein [1], nucleic acids [2, 3], drugs [4, 5], hormones [6, 7], and many different organic compounds. Thus, LOC devices are very promising for health diagnostics, environmental screening, and ensuring safety and security.

Various methodologies of LOC fabrication have recently been developed involving materials such as paper [8], glass [9, 10], polymers [11, 12], or even proteins (e.g., gelatin [13, 14]). The use of a certain material depends on the desired application, physicochemical properties of the analyte to be detected, the need for biocompatibility, and, possibly, its integration with other devices and materials [11].

One of the most common approaches in LOC development is polydimethylsiloxane-based (PDMS) technology (soft-lithography), where a polymeric elastomer is used to fabricate chips of different shapes, patterns, and properties [15].

The development of low-volume (in the range of micro- and nano-liters) and portable devices is especially interesting for the environmental screening of potentially hazardous compounds. The monitoring of various pollutants present in air, soil, or water requires regular monitoring, and the use of an LOC device can allow efficient in-field detection since access to sophisticated laboratories is limited, expensive, and time-consuming.

LOC devices have been reported for electrochemical detection of phenolic compounds [16, 17] and atrazine [18], optical platforms for pesticides [19], and heavy metal detection [20]. An LOC can be applied not only for the analysis of pollutants derived from industry and urban areas but also for toxins originating from the natural environment such as those produced from marine microalgae [21–23].

The detection of polybrominated diphenyl ethers (PBDEs), a class of halogenated compounds similar to polychlorinated diphenyls (PCBs) and commonly used as flame

retardants, needs to be improved. PBDEs were introduced into the market in the 1960s and used for many years in domestic electronics, toys, furniture, polyurethane foams, and building materials [24, 25]. Over time, however, the negative effects of long-term exposure to PBDEs have been demonstrated, although many cases are not well investigated. As a result, commercial mixtures of PBDEs were banned from all applications in 2004 (penta-brominated diphenyl ether (BDE) and octa-BDE) and in 2013 (deca-BDE) in the United Stated, European Union, and elsewhere [26, 27].

Due to their hydrophobicity, PBDEs can accumulate in various tissues and organs, especially in adipose tissue and their exposure is correlated with liver dysfunction [28]. PBDEs can also be found in breast milk, and many investigations have demonstrated dependence between the persisting contact with materials containing PBDE (by dermal absorption, consumption of contaminated food or inhalation) and their further accumulation in the body. Besides the small size and hydrophobicity, the biphenyl chemical structure of PBDEs is similar to that of the thyroid hormones (3,5-diiodothyronine (T2), 3,3,5-triiodothyronine (T3), and 3,3,5,5-tetraiodothyronine (T4)), and it has been confirmed that PBDEs bind with alpha- and beta-thyroid hormone receptors. PBDEs are also linked to neurodevelopment toxicity and various types of tumors [28, 29].

Despite the need for monitoring PBDE levels, only a few methods have been reported so far for their detection. Standard determination of PBDE is based on gas chromatography (GC) separation combined with electrode capture detection (GC-ECD) or mass spectrometry (GC-MS). The use of these methods is still limited by their high equipment cost, the need for a qualified workforce, and high time consumption [30–32]. One of the alternatives is a competitive immunoassay for PBDE detection that is based on competition between PBDE molecules and PBDE modified with horseradish peroxidase (HRP-PBDE) in binding to anti-PBDE antibodies that are coupled to magnetic beads (MB-Ab). The signal is revealed using a well-known enzymatic reaction that catalyzes 3,3',5,5'-tetramethylbenzidine (TMB) oxidation, resulting in a colored product that can be easily measured by spectrophotometry. This method is relatively simple and offers an attractive

range of detection (0.025–1.0 ppb of PBDE), both in standard solutions and environmental samples like soil or seawater.

Figure 1 Lab-on-a-chip system for detection and removal of PBDEs **A.** components of the LOC device with visualisation of the microfluidic structures (10x magnification objective); **B.** side and top view of assembled LOC device on polycarbonate substrate with screen-printed electrode (SPCE); **C.** assay procedure: (1) on-chip mixing and incubation of magnetic beads coupled to anti-PBDE antibodies (MB-Ab) with samples containing PBDE, (2) on-chip mixing and incubation of MB-Ab with HRP-PBDE, (3) immobilization of immunocomplex in chip using external magnet and washing of unbound molecules, (4) incubation with substrate solution (o-AP + H_2O_2), (5) electrochemical detection of the product of enzymatic reaction (3-APZ, 3-aminophenoxazone).

Taking advantage of well-developed antibodies and a competitive reaction, we modified the colorimetric kit by performing electrochemical detection of HRP-PBDE and replacing TMB with o-aminophenol (o-AP) as a substrate for the electrochemical reaction. We believe that the electrochemical reaction will provide an opportunity to assay PBDEs with better sensitivity and may lead to improved automation by integration into an LOC device. The LOC system and the detection approach are shown in Fig. 1.

The role of nanomaterials in LOC and other devices has grown significantly in recent years for both sensing and environmental removal of contaminants. In this context, we take advantage of the adsorption and removal capabilities of reduced graphene oxide (rGO) toward certain contaminants. As a proof of concept, a composite of PDMS and rGO (PDMS-rGO) was developed and used to fabricate a microfluidic chip, where post-measurement samples are injected and organic traces, including excess PBDE, are immobilized and adsorbed onto the channel walls to improve the safety of the whole system. Such non-covalent interactions between PBDEs and carbon materials (based on π–π stacking) were previously used for novel extraction methods [33, 34] and micromotor-based removal of PBDEs [35]. Various composites of PDMS with carbon materials have also been developed, but most of them are based on sophisticated protocols that have been optimized to obtain conductive rather than highly adsorptive materials [36, 37].

To the best of our knowledge, this is the first approach showing an LOC device with an electrochemical approach for PBDE detection. Herein, a novel rGO-PDMS composite is used for the first time in an LOC device for biosensing and removal purposes.

3.2. Experimental section

3.2.1. Reagents

The PBDE colorimetric immunoassay kit was purchased from Abraxis (Pennsylvania, USA). The PBDE stock solution was purchased from AccuStandard Inc. The screen-printed inks (carbon sensor paste C2030519P4 and silver–silver chloride paste C2130809D5) were purchased from Gwent Group, UK. The polycarbonate sheets were purchased from Vink

Plastics S.L.U., Spain. The PDMS (Sylgard® 184 Elastomer kit) was purchased from Ellsworth Adhesives Iberica, Spain. The graphene oxide stock solution (5 mg/mL) was purchased from Angstron Materials (Dayton, USA). A negative photoresist (SU8-50) and an appropriate developer were purchased from Microchem, USA). The flexible photolithography masks were provided by Microlitho, UK. The four-inch silicon wafers were purchased from NOVA Electronic Materials. The hydrogen peroxide, o-aminophenol, HPLC grade methanol, phosphate buffered saline (PBS), 3-aminopropyltriethoxylane (APTES), L-ascorbic acid (L-AA), and microscopic glass slides were purchased from Sigma. The Britton–Robinson (BR) buffer (0.04 M, pH 5.7) was prepared as described elsewhere [39]. All the commercial reagents were of analytical grade and handled according to the material safety data sheets suggested by the suppliers.

3.2.2. Instruments

Screen-printed carbon electrodes (SPCE) were fabricated by screen-printing technology using a screen-printer (DEK 248, UK). Electrochemical measurements were carried out using computer-controlled Autolab PGSTAT-12 (302 N-High performance) (potentiostat/galvanostat) with a general-purposes electrochemical software operating system (GPES version 4.9.007, from Eco Chemie B.V., Utrecht, The Netherlands). The microfluidic chips with integrated SPCE electrode were connected to the Autolab PGSTAT-12 with a specially adapted electrical edge connector. A syringe pump (Pump 11 Elite; Harvard Apparatus, USA) was used as a driving unit for the microfluidic system. The syringe pump was equipped with 0.5 mL glass syringes (Gastight®, Hamilton, USA). A centrifuge SIGMA 2-16PK was used for rGO purification and the magnetic stirrer (IKA lab disc white) during the reduction process. Plasma cleaner PDC-002 was used as a source of oxygen plasma for the fabrication of the chip. The optimization of microfluidic chips operation was performed by an optical microscope (Olympus IX71, Germany) coupled with a CCD camera (Olympus DP72, Germany) with the bright field mode, 10 x magnifications.

3.2.3. Experimental methodology

Unless otherwise stated, all the optimization experiments regarding microfluidic chips were carried out on 5 independent chips. The optimization of electrochemical measurements was based on the use of 5 independent screen-printed electrodes. The final calibration curves were obtained based on 3 repetitions. When the colorimetric method was used, each sample was run in duplicate according to the manufacturer´s procedure (see Annex II). All the errors of the results obtained were expressed as a relative standard deviation (RSD).

3.2.4. Fabrication and operation of Lab-on-a-Chip (LOC) devices

The fabrication of screen-printed electrodes based on already reported design and procedures, using polycarbonate sheets as a substrate [43]. The microfluidic mold was prepared by using a previously reported methodology of the photolithography process [15, 43], where a 4-inch silicon wafer was spin coated with a negative photoresist SU8-50 and patterned by photolithography using a flexible mask.

PDMS was mixed with its curing agent in the mass ratio 10:1. After intensive stirring for 5 minutes, an excess of air bubbles was removed using a vacuum. Afterward, PDMS was poured onto the silicon wafer with a given design of the microfluidic chip and kept on the hotplate at 70 °C for 4-5 hours until completely polymerized. After polymerization, proper shapes of PDMS were cut out from the template, washed in miliQ water, followed by isopropanol and dried on the hotplate at 70 °C for 10 minutes. In order to modify the surface, an oxygen plasma treatment was performed. Meanwhile, the polycarbonate sheets (either with or without screen-printed electrodes) were washed with miliQ water, followed by an isopropanol, ethanol, plasma treatment and incubated in 2% APTES solution in order to silanize the surface (1h). Afterward, both parts (PDMS and polycarbonate) are simply attached to each other forming a permanent bonding that is strengthened by incubation on the hotplate at 70 °C for 1 hour. Prior to the assay, the chips were connected with each other using polymeric tubes.

The general scheme of the system, as well as dimensions of microfluidic channels, are shown in Fig. 1. The system consists of 3 microfluidic chips: IMMU-CHIP, DET-CHIP, and GO-CHIP.

The IMMU-CHIP consists of channels with repeatable curvatures and 3 inlets (MB-Ab, PBDE, PBDE-HRP). The role of the curvatures is to support the diffusion between mixed reagents. In this chip, an immunoreaction between PBDE/PBDE-HRP and MB-Ab occurs. The PDMS layer is attached either to glass or polycarbonate.

The DET-CHIP consists of a single channel and a chamber (10 mm length, 3 mm width and approximate volume of 15 µL) where immunocomplex (MB-Ab-PBDE/PBDE-HRP) is immobilized as an external magnet is placed underneath the chip. This chip is bonded to polycarbonate with SPCE. The DET-CHIP can be employed as a part of the LOCs system as well as a separate chip simply for various electrochemical measurements.

The GO-CHIP is fabricated by using rGO-PDMS composite. The design used to fabricate this chip is based on a broad channel with pillars along its surface so as to increase the surface-area-to-volume ratio and improve the adsorption performance through the microfluidic channel. The fabrication process is based on the patterning of the SU-8 photoresist.

3.2.5. Optical evaluation of on-chip immunoreaction performance

The motivation of using a microfluidic chip for mixing (IMMU-CHIP) is the possibility of the process automation as samples passing through the channel will be mixed with each other supporting a (1) PBDE binding to MB-Ab as well as a (2) PBDE-HRP binding. The design of the IMMU-CHIP was previously used and its effectiveness (not reported here) in biochemical reactions was confirmed.

By using an optical microscope, the process of mixing was under observation, so as to match the best parameters and make sure that all the chemicals used in the assay are compatible with the materials used for the LOC device. As all the reagents seem to be transparent under the microscope, Trypan blue (10%) was used to facilitate the distinction of two different solutions mixed with each other. Besides the mixing process, the washing

step was assessed in order to find an optimum flow rate and buffer volume (data not shown).

3.2.6. Optimization of the on-chip magneto-immunoassay

The IMMU-CHIP was fabricated as in (2.4) and washed by priming 1 mL of washing buffer (water + 0,05% Tween-20) prior to use. A dedicate inlet was connected to the syringe containing reagents of magneto-immunoassay for PBDE detection.

Two types of optimization experiments were performed. The first one checked the occurrence of non-specific adsorption of PBDE to PDMS and how it is changing with respect to the flow rate. A solution of 1.0 ppb PBDE was flushed through the whole chip and collected in the Eppendorf tube at the outlet. Afterward, a colorimetric test was performed following the standard procedure (see Annex II). Results were expressed as a % of a signal related to the control sample of 1.0 ppb of PBDE.

The second experiment checked the possible adsorption of magnetic beads and HRP-PBDE onto the microchannel. The first inlet was connected to PBDE blank solution (0.0 ppb), the second to MB-Ab and the third one to HRP-PBDE. The solutions were injected and mixed with each other in the chip by using different flow rates, collected in the Eppendorf tube and preceded as in the standard procedure for colorimetric detection of PBDE. Results were expressed as a % of a signal obtained by a control sample containing MB-Ab, HRP-PBDE and 0.0 ppb of PBDE.

3.2.7. Preparation of rGO-PDMS composite

An already reported approach of GO reduction via L-Ascorbic Acid (L-AA) was employed [44]. L-AA was added to 200 mL GO solution to reach a concentration of 50 mg/mL. Samples were adjusted to the desired pH by using a NaOH solution and incubated for 48 hours with continuous magnetic stirring (600 rpm). After reduction, the solution was transferred to 15 mL centrifugal tubes and centrifuged for 1 hour, 12000 rpm, at 4 °C. The supernatant was discarded, while the pellet washed with miliQ water. This step was repeated twice using miliQ and twice using 96% (v/v) ethanol. The purified solution of rGO was used for further experiments promptly.

Two components of the PDMS kit (elastomer and curing agent) were mixed in volume ratio 10:2. After stirring, a desired amount of rGO was added and vigorous stirring was continued for approximately 10 minutes. Afterward, rGO-PDMS was poured onto a silicon wafer with the design of a given chip. The wafer with rGO-PDMS was kept for 1h in RT in order to remove air bubbles entrapped within polymer before its polymerization. Then, the wafer was kept on the hotplate and incubated for 4-5 hours, at 70 ºC until the rGO-PDMS is completely polymerized. Microfluidic chips were fabricated using exactly the same procedure as mentioned above.

An analysis of rGO-PDMS composite (the effect of pH, flow rate, rGO concentration) was performed regarding the ability of adsorption of a standard solution of PBDE (1.0 ppb). All parameters had been chosen in such way to maximize the adsorption yield. Experiments based on passing PBDE sample through the rGO-PDMS chip (single channel of 5 cm length, 500 µm width and 100 µm depth) and afterward determining the concentration of PBDE using the colorimetric kit. As this kit is a competitive assay, the relative adsorption was counted by using the following formula (Eq. 1):

$$ADS = A_1(1.0ppb) - A_0(1.0ppb)/B_0(0.0ppb) \quad (1)$$

where $A_1(1.0ppb)$ is the absorbance of the sample used in the chip, with an initial concentration of 1.0ppb; $A_0(1.0ppb)$ is the absorbance of the control sample with an initial concentration of 1.0 ppb and $B_0(0.0ppb)$ is the absorbance of the control sample where a 0.0 ppb solution was used as a blank.

3.2.8. Electrochemical detection

Electrochemical detection of HRP is inspired by already reported works [39, 45]. According to the competitive immunoassay, the level of HRP is inversely proportional to the level of PBDE. HRP catalyzes the redox reaction, where hydrogen peroxide is converted to water molecules, while a given substrate is oxidized. In this approach (Fig. 1C) o-AP was chosen as a substrate of enzymatic reaction due to its compatibility with other reagents used in this assay as well as electrochemical properties. Oxidation of o-AP leads to the formation of 3-aminophenoxazone (3-APZ) that can be reduced onto the SPCE surface and

detected in several electrochemical techniques such as Cyclic Voltammetry (CV), Differential Pulse Voltammetry (DPV), Chronoamperometry (AMP) and Square Wave Anodic Stripping Voltammetry (SW-ASV). As the PBDE detection kit based on HRP-PBDE molecule is optimized for a relatively narrow range of PBDE concentration, SW-ASV was chosen, since this technique is reported as much more sensitive than others. Nevertheless, some examples of PBDE detection using CV and DPV are shown in Figure 2. For SW-ASV the following parameters were applied: deposition potential (-0.6 V); deposition time 20 s; equilibration time 15 s; potential range from 0,0 to -0.6 V; step potential 4 mV; amplitude 25 mV; frequency 25 Hz.
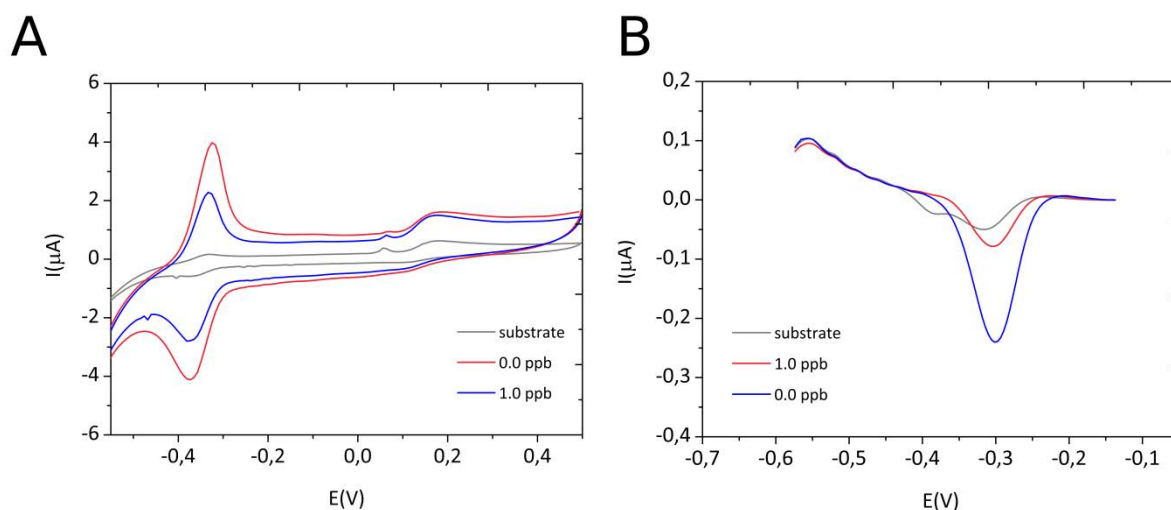
Figure 2. Alternative techniques for PBDE detection: **A.** Cyclic Voltammetry, **B.** Differential Pulse Voltammetry. All curves obtained in static measurements according to the same protocol as in 3.2.8.

Detection in microfluidic chip was preceded by measurements based on bare SPCE so as to find the optimal detection protocol. Briefly, an immunoassay was performed as usual, after washing an immunocomplex, samples were reconstituted in 10 µL of PBS buffer and 100 µL of substrate solution (o-AP + H_2O_2 in BR buffer) and incubated for 30 min. After incubation, 50 µL of sample was pipetted onto the SPCE surface and electrochemical measurements were performed. Following this procedure, incubation time, o-AP concentration, H_2O_2 concentration and deposition time in SW-ASV were optimized.

Afterward, electrochemical detection was performed by using DET-CHIP. Parameters of detection were chosen based on optimization in static measurements. In this case, when a substrate solution is injected into the microfluidic channel, it passes through the chamber

where magnetic beads with immunocomplex are immobilized, so the enzymatic reaction is performed in flow and the product is passing further along the channel up to the electrode surface, where it is electrochemically deposited and detected. Besides that, an optimum flow rate was analyzed in order to find the best sensitivity and limit of detection.

3.3. Results and discussion

3.3.1. rGO-PDMS composite

Graphene oxide and other derivative carbon materials are already reported as effective adsorbents of different types of molecules. In this work, we tried to combine the ability of rGO to adsorb PBDE with convenient properties of PDMS chips by obtaining an LOC device with increased adsorption performance (Fig. 3). There are already reported similar approaches where graphene materials and PDMS are used as a composite but they are devoted to its electrical properties and none of them were applied for adsorption/removal applications in LOCs [36, 38]. Moreover, as the presented rGO-PDMS composite does not need to be conductive, a much simpler protocol of fabrication could be applied, where the effect of rGO adsorption is still maintained/visible and attractive for Lab-on-a-Chip applications.

Furthermore, as the adsorption mechanism is based on π-π stacking, the rGO-PDMS composite can be employed for various biomolecules such as DNA or proteins as both of them are rich in structures containing aromatic rings. As a proof of concept, we performed an analogical test, as we did for PBDE, but measuring the adsorption of a model protein (HRP) and the effect of rGO adsorption can be clearly observed (data not shown).

We found pH to be an important factor facilitating rGO reduction, thus the efficiency of PDMS adsorption. Experiments based on PBDE adsorption onto the rGO-PDMS channel (Fig. 3E) showed that an increase of pH leads to an increase of adsorption; however, this effect is well visible until the pH value reaches 7. When it is higher, there is no significant improvement anymore.

It is not surprising that an increase of rGO content (concentration) in PDMS will make adsorption stronger as more rGO will be exposed at the channel surface. However, any compound added to PDMS may affect its ability to polymerize. We found (Fig. 3D) that when rGO concentration is lower than 1% (w/w), it not only has no effect on adsorption improvement but also causes adsorption to decrease slightly (comparing to bare PDMS). A Concentration of about 4.5% (w/w) seems to be optimal, as it brings the highest adsorption of PBDE (around 70%). When the concentration is higher than 4.5% but lower than 10%, the adsorption capacity significantly decreases, although the composite keeps its physical properties, such as durability, hardness etc. If the concentration of rGO is higher than 10% (v/v), polymerization is hardly affected by the presence of many air bubbles (always appearing during the polymerization of PDMS but are released over time), what makes it impossible obtaining a homogenous and flat layer of rGO-PDMS. Such a high concentration of rGO-PDMS also changes some physical properties - the polymer is too flexible and spongy. This effect may be related to the presence of rGO but, in our opinion, is mainly related to the presence of an excessive solvent (from rGO suspension) in PDMS whose evaporation affects the structure of polymer during polymerization. Taking into account these observations, we decided to perform the last steps of rGO purification in ethanol solution, as it is compatible with PDMS and can evaporate very quickly without affecting the polymerization itself.
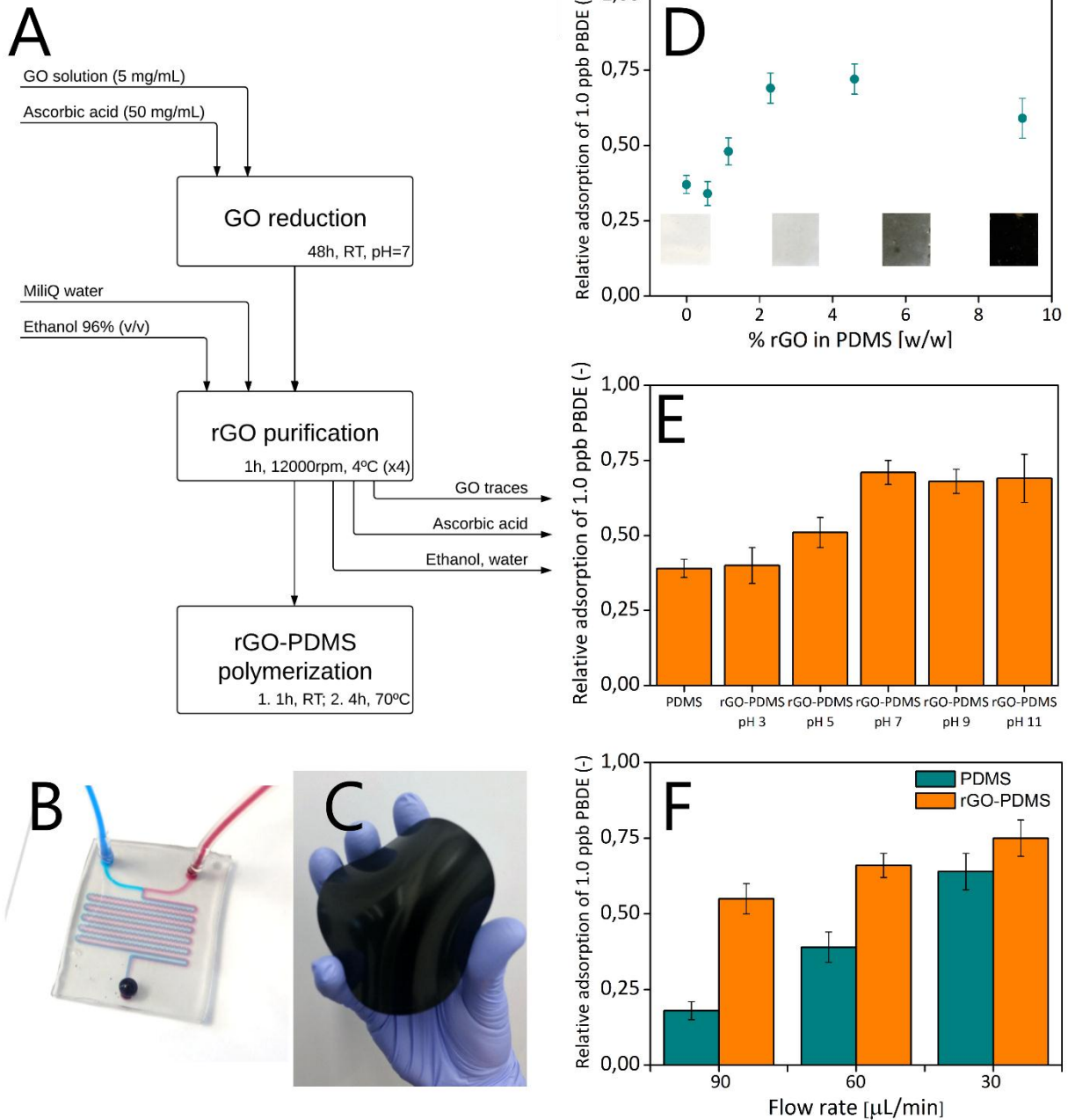
Figure 3 rGO-PDMS composite A. fabrication process; B. example of rGO-PDMS-glass chip filled with colour inks; C. example of flexible solid piece of rGO-PDMS; D. the effect of rGO concentration (w/w) on PBDE adsorption; E. the effect of pH during reduction process on PBDE adsorption; F. the effect of flow rate on PBDE adsorption using rGO-PDMS and bare PDMS.

The flow rate is a major factor that influences microfluidic processes. We proved (Fig. 3F) that an increase of the flow rate will decrease the adsorption yield. However, a comparison of PDMS with rGO-PDMS shows that in a higher flow rate (90 µL/min) the effect of rGO is well observed (significant increase of adsorption) compared to lower flow rates (30 µL/min).

The final measurements in LOCs system were equipped with the rGO-PDMS chip fabricated using the design showed in Fig. 1 (GO-CHIP) and following the optimal conditions mentioned above. Due to the significantly much larger contact surface area between the liquid and the rGO-PDMS channel, its adsorption capacity is higher compared to the single-channel chip.

We tested PBDE in the range of concentration 1-1000 ppb and found the total adsorption capacity between 100 and 1000 ppb, both in the standard buffer solution and seawater (Fig. 4). We believe that this is sufficient for real sample treatment as the usual level of PBDE in seawater is rather lower than 10 ppb [40-42]. Moreover, a decrease of the flow rate may bring further improvements regarding adsorption capability. in this work, however, the flow rate value is chosen based on the demands for other steps performed in the IMMU-CHIP and DET-CHIP, as all the operations are performed simultaneously.
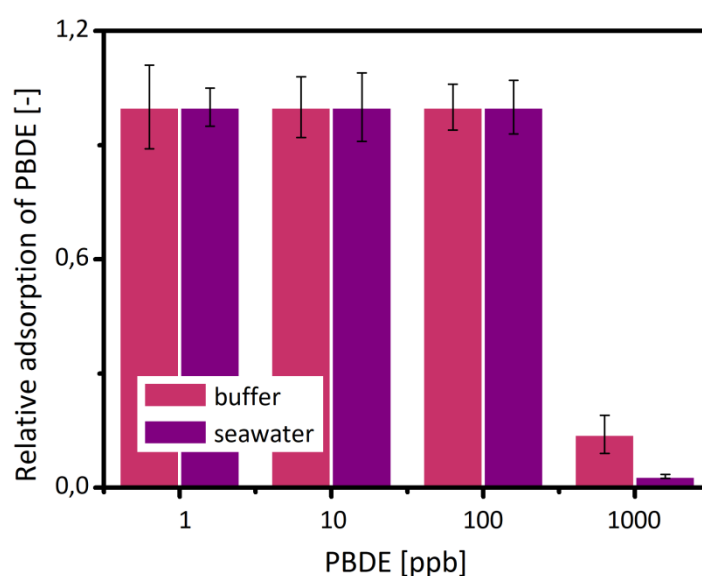
Figure 4 Adsorption of PBDE (1, 10, 100, 1000 ppb) to GO-CHIP in buffer and seawater. Results obtained from 3 repetitions using a new GO-CHIP in each case.

Apart from adsorption capability, a possible reusability of the platform was tested. We found that solvents introduced to the GO-CHIP channel can extract a previously adsorbed PBDE. Acetone showed the best performance, as with the use of this solvent it was possible to perform desorption of PBDE in 4 subsequent cycles and recover nearly 100% of PBDE (Fig. 5). Nevertheless, the ease of fabrication suggests that this platform is more feasible when considered as disposable, rather than reusable.
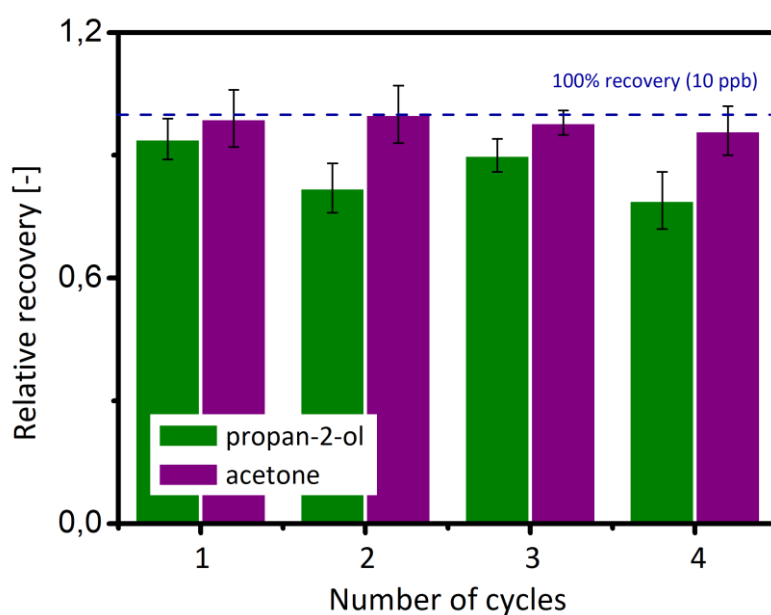
Figure 5 Recovery of PBDE (10 ppb) adsorbed by GO-CHIP using propan-2-ol and acetone as solvents for extraction. Results obtained from 3 repetitions using a new GO-CHIP in each case.

3.3.2. Electrochemical detection of PBDE (bare SPE)

The development of the Lab-on-a-chip platform for electrochemical detection was preceded by experiments involving only screen-printed electrodes. Fig. 6 shows parameters that were optimized in order to find the best conditions for PBDE determination. One of the most crucial ones is the concentration of o-AP (Fig. 6A). If it is higher than 0.12 mM, it contributes to non-enzymatic oxidation and reduces signal-to-noise ratio, similarly as reported elsewhere [39]. For this reason, 0.6 mM o-AP was chosen for further experiments providing satisfactory sensitivity. The effect of the other component, the substrate solution (hydrogen peroxide) upon reaction sensitivity (Fig. 6B), was also studied, thus the concentration of $2*10^{-4}$ M was used, as in [39].

Incubation time is the time when redox reaction is catalyzed by HRP. 30 min was found as the time providing the highest SNR (Fig. 6c) and it is quite similar to the time of reaction in a commercial colorimetric method (20 min). Further time extension does not lead to sensitivity improvement.

An increase of deposition time (Fig. 6D) leads to a proportional increase of SNR; however, if the deposition time exceeds 60 s, an enormous decrease of SNR is observed due to the electrochemical oxidation of the substrate (o-AP) which prevails over the effect of enzymatic reaction (HRP catalysis). Thus, 20 s was chosen as an optimum deposition time providing good sensitivity and reducing the risk of false-positive results.
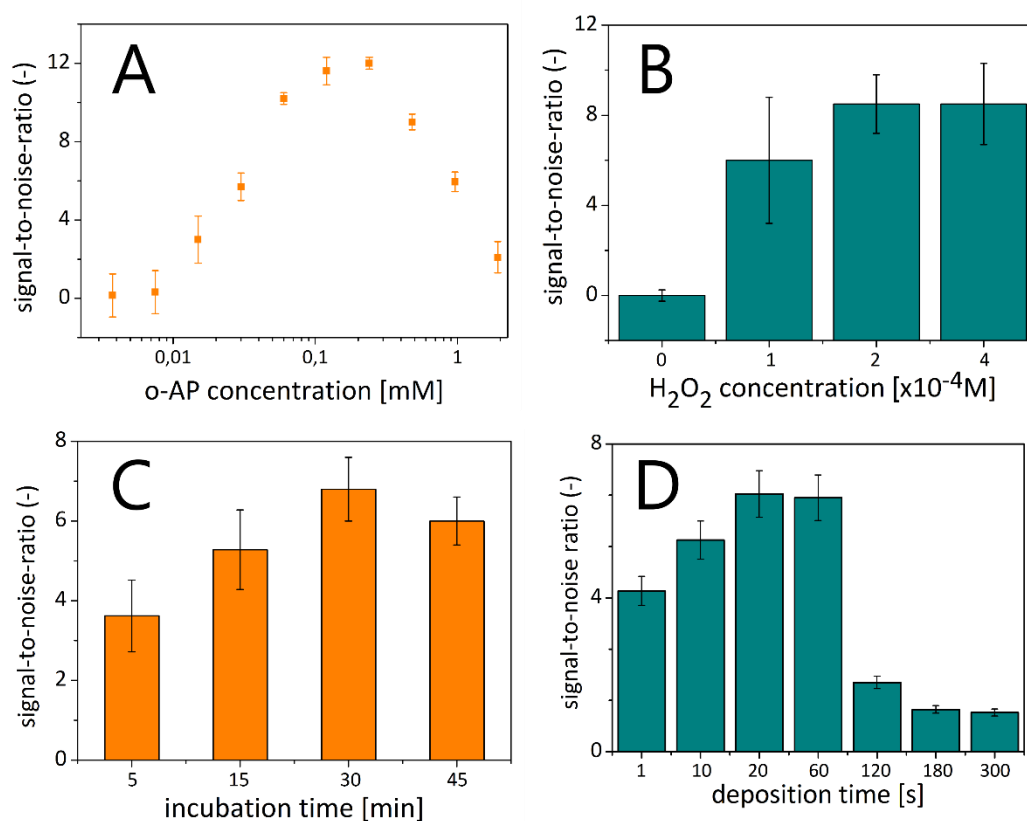
Figure 6 Optimization of electrochemical detection in static conditions using bare SPCE **A.** optimization of substrate (o-AP) concentration, **B.** optimization of hydrogen peroxide concentration, **C.** optimization of incubation time (enzymatic reaction), **D.** optimization of deposition time in square wave anodic stripping voltammetry. All results expressed as signal-to-noise ratio calculated as a ratio between signal represented by control sample 0,0 ppb of PBDE and substrate solution.

3.3.3. Lab-on-a-chip optimization

The next step of the LOC platform development was an evaluation of the IMMU-CHIP performance. Fig. 6A shows the process of mixing between the solution of PBDE and MB-

Ab suspension. It can be seen that when the solutions meet each other in the microfluidic channel, they do not penetrate themselves and flow separately. However, due to the curvature of the channel, a solution is further conveyed from laminar into the turbulent flow so the diffusion between them occurs quite efficiently, facilitating immunoreaction.

Fig. 7A-3 shows the ending section of the mixer chip where the color of the solution is already uniform, hence, a reaction between PBDE and MB-Ab may be occurring.

Fig. 7B presents the results of the flow rate optimization, where the colorimetric kit was used as a reference technique. Regarding PBDE adsorption, an increase of the flow rate is linked with an increase of the PBDE recovery, which means that no analyte is lost during the assay. For the flow rate equal or higher than 100 μL/min, PBDE adsorption is no longer observed. Regarding the on-chip immunoreaction, the efficiency of the reaction is not so high when the low flow rate is applied (60% of a control signal for the flow rate of 5 μL/min), which is probably related to protein adsorption or the physical loss of magnetic beads. On the other hand, when very high flow rates are applied, the efficiency of the reaction is not satisfactory either, probably due to the reduced time that limits the occurrence of the immunoreaction. Thus, when analyzing both curves, it can be seen that the flow rate of about 100 μL/min offers the compromise, as PBDE adsorption is not observed and the reaction between HRP-PBDE and MB-Ab works with the maximum efficiency.

Compared to electrochemical measurements performed just by drop casting (batch/static measurements), in chip detection (DET-CHIP) requires close attention to the flow rate, as the main factor affecting sensitivity and the limit of detection. The flow of the sample supports particularly the enzymatic reaction, where substrate solution is mixed with immunocomplex and 3-APZ is obtained as well as a deposition process, where 3-APZ is accumulated onto the electrode surface. In the case of electrochemical stripping (detection step) the flow is stopped and this step is performed in static conditions.
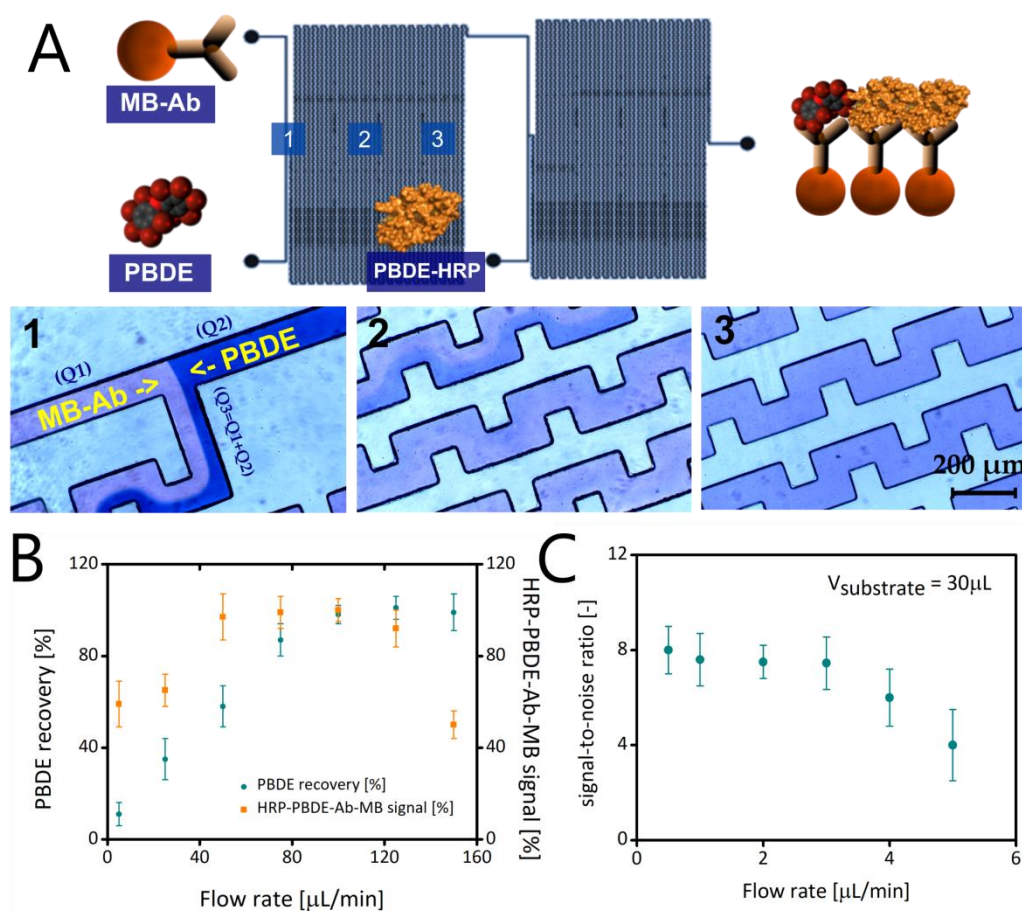
Figure 7 Optimization of LOC operation. **A.** Visualisation of mixing in IMMU-CHIP between reagents in (1) intersection where magnetic beads with antibody (MB-Ab) meet PBDE, (2) middle part of the chip where mixing process partially occurred, (3) terminal section of the channel where samples are fully mixed. Trypan-blue (10%) was used to visualize PBDE solution, pictures taken using optical microscope with 20x magnification; **B.** Optimization of the flow rate in IMMU-CHIP based on colorimetric test as regards PBDE recovery and immunocomplex (HRP-PBDE-Ab-MB) signal when passing the microfluidic channel; **C.** optimization of the flow rate during enzymatic reaction in electrochemical detection of HRP-PBDE (DET-CHIP). All results expressed as signal-to-noise ratio calculated as a ratio between signal represented by substrate solution without PBDE as control sample.

In order to find the optimal conditions, some measurements of different flow rates (defined taking into account the constant volume of injected o-AP/H_2O_2/PBS solution, 30 µL), as well as the desired time of enzymatic reaction were carried out. Fig. 7C shows that an increase of the flow rate is generally related to a decrease of signal-to-noise ratio. This is obviously caused by the reduced time, which is a key factor in enzymatic reactions. Flow rates between 0.5-3 µL/min allowed the occurrence of the reaction with the relatively high signal-to-noise ratio, similar to that in the optimal condition (30 minutes) of static measurements. The final experiments were performed by using the flow rate of 2 µL/min, where the reaction time is only 15 minutes.

Regarding deposition step, similarly to that in static measurements, the time of 20 sec was found to be the optimal time (data not shown). The process of the deposition was performed with the flow rate of 90 µL/min in order to transfer all the solution from the chip, where an enzymatic reaction occurred. We have observed that such a relatively high flow rate supports the sensitivity of the assay, as the background current is much lower than in static measurements. This results from the quantity of molecules adsorbed onto electrodes during the deposition step that is lower in a higher flow rate.

3.3.4. Complete detection of PBDE using Lab-on-a-chip platform

Fig. 8 presents the final results of all the methods compared. As it can be seen in Fig. 8A, the signal of SW-ASV is represented by the curves whose negative current is inversely proportional to the PBDE concentration. Each peak is characterized by a specific potential of about -0.35 V that shifts slightly towards -0.3 V when the concentration of HRP-PBDE increases. We have also observed that the presence of salts (PBS) influences the potential value by shifting it towards -0.4 V. However, it does not affect the signal intensity (data not shown). All the measurements were performed in the presence of PBS (o-AP + H_2O_2 and PBS in a ratio 10:1) so as to keep a reproducible value of potential. In order to validate the developed technique, we performed, at the same time, the commercial colorimetric test (Fig. 8B). The limit of detection of this technique is about 0.019 ppb PBDE, what is in accordance with the results obtained in the electrochemical measurements, where the limit of detection is about 0.018 ppb, both for the whole assay performed on the chip as well as

only detection step performed in the chip. This is not surprising, since the LOD of this method is limited by the immunoassay performance, rather than the HRP detection, as the concentration of the labeling protein is large enough, both in samples with a high and low concentration of PBDE. Such a limit of detection seems to be sufficient for all the possible applications taking into consideration the level of PBDEs found in different places for instance seawater in Jiaozhou Bay in China (6.59 ppb)[40], the coastal waters of the Aegean Sea (0.03-0.05 ppb)[41] or in various indoor environments in Barcelona, Spain (7.3-13.9 ppb)[42].

PBDE spiked (ppb)	Relative signal (buffer) (%)	Relative signal (seawater) (%)	Recovery (%)	RSD (%)
1	12,01	11,30	94,09	9,60
0,5	20,20	19,10	94,55	8,10
0	100,00	103,00	103,00	5,12
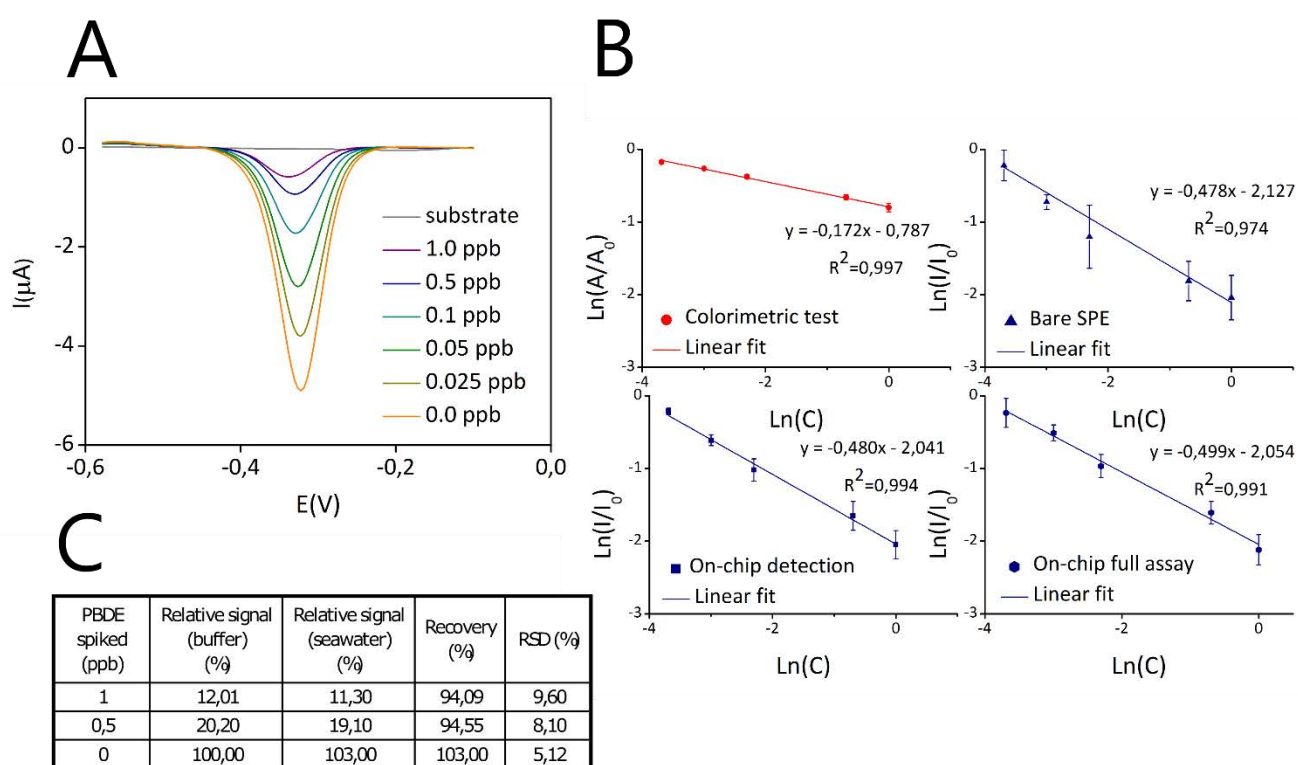
Figure 8 Comparison of optical and electrochemical detection of PBDE A. Example of SW-ASV measurements of different concentrations of PBDE (0.0-1.0 ppb) using Lab-on-a-chip system; B. Calibration curves showing detection of PBDE using colorimetric test as well as different modes of electrochemical approach; C. electrochemical detection in seawater samples spiked with PBDE standard solutions.

The electrochemical approach, compared to the optical one, brings higher sensitivity of the method, which is clearly seen by the slope of the calibration curves (Fig. 7B). Furthermore, a major difference regarding linearity and reproducibility can be observed in comparison with the measurements performed only on bare electrodes and those in the

microfluidic chip (either simply detection or the whole assay). Detection based only on bare electrodes was linked to a much worse coefficient of determination (R^2=0.974 compared to R^2=0.994) and to higher errors among all repetitions of the experiment as regards measurements in the microfluidic. This is probably related to the nature of the square wave anodic stripping voltammetry as a good performance of this technique depends on the diffusion and contact between the electrode's surface and the sample. Apparently, this works better in microfluidics, where the deposition process is performed in flow and the presence of microfluidic channels keeps constant the volume of the liquid being in contact with the working electrode and also prevents the evaporation of the sample by limiting any influences from the external environment. This confirms already reported statements on the improved performance of SW-ASV in microfluidics, compared to bare screen-printed electrodes. It is especially meaningful taking into account the use of home-made electrodes fabricated using more eco-friendly materials (carbon, silver/silver-chloride) than electrodes containing, for example, toxic mercury [43].

3.3.5. Validation of Lab-on-a-chip in seawater samples

In order to justify the practical application of the presented LOCs device, we evaluated seawater samples spiked with PBDE standard solution as described in (Annex II). Results are shown in Fig. 8C and there is a clear evidence of good recovery yield between 94.1% and 103%. It can, therefore, be assumed that the presented method is fully compatible with seawater samples. This is possible due to the washing steps, where all the traces are removed so that there is no influence on electrochemical detection. On the other hand, as mentioned before, the presence of salts (ionic strength) does not affect the signal intensity. As the system based on magneto-immunoassay, the use of magnetic beads in the chip also supports an efficient capturing of analyte from such a complex matrix as seawater.

3.3.6. Comparison with other methods and future perspectives

The comparison between the colorimetric and electrochemical method regarding the use of reagents is shown in Table 1. As can be seen, thanks to microfluidics, fewer reagents are spent as well as significant amount of time is saved. Just by using a syringe pump as a driving unit, automation of the system is provided. Moreover, instead of a syringe pump,

programmable microfluidic flow controllers may be applied for this platform, providing full automation of the process and eliminating the need for the qualified workforce (see Annex I). This is crucial since PBDE, as a small molecule, can be detected mainly in competitive immunoassay format. This kind of assays is generally more sophisticated than, for example, label-free methods; thus, more time and attention is usually required to perform the analysis. However, simple and sensitive label-free methods for PBDE detection based on pattern recognition are reported, the risk of cross-reactivity and the need for data separation limit their practical application [46]. Another example of label-free detection of PBDE is Electrochemical Impedance Spectroscopy, which, although specific, provides much higher LOD (1.3 ppb) compared to that in our work [47].

Table 1 Comparison of reagents usage (in µL) in different systems.

	Colorimetric	Electrochemical (SPE)	Electrochemical (LOC)
MB-Ab		500	250
PBDE/sample		250	125
PBDE-HRP		250	125
Washing buffer		1000	400
Colour Solution	500	-	-
Stopping Solution	500	-	-
o-AP+H_2O_2	-	100	27
PBS		10	3

Another possible future improvement of the presented platform is its high-throughput performance. By miniaturizing all of the chips and multiplying them, it would be possible to run several assays in parallel without an extension of the total size of the sensing system.

3.4.   Conclusions

This work describes the synthesis of a novel, integrated microfluidic platform for simultaneous capture, detection, and removal of polybrominated diphenyl ethers. The presented system consists of three microfluidic chips: the IMMU-CHIP, where the analyte is captured and immunoreaction occurred; the DET-CHIP, where the level of HRP-PBDE is quantified using SW-ASV; and the GO-CHIP, which is responsible for the removal of potentially toxic PBDEs.

The LOD achieved was 0.018 ppb, which is in accordance with that of the currently available methods for PBDE detection. Electrochemical detection performed in the microfluidic chip showed better sensitivity compared to that of the commercial colorimetric method and better reproducibility and linearity than those of electrochemical measurements performed simply using a bare screen-printed electrode.

The practical impact of this work is twofold: firstly, the proof that electrochemical detection of PBDEs can be performed, and secondly, that the rGO-PDMS composite in microfluidic devices can be employed as an efficient adsorbent of various compounds. To the best of our knowledge, both of the issues mentioned above are not yet reported.

Furthermore, the small size, durability, and suitability for operation with seawater samples suggest that the presented platform can be employed in marine environmental analysis; for example, as an integrated component of buoys. Combining this with commercially available miniaturized potentiostats (electrochemical detection) and microfluidic driving units will result in a small and fully automated detection platform.

3.5.   References

1.   Medina-Sanchez, M., et al., *On-chip Magneto-immunoassay for Alzheimer's Biomarker Electrochemical Detection by Using Quantum Dots as Labels*. Biosensors & Bioelectronics 2014, **54**, 279-284.

2.   Marasso, S. L., et al., *A Multilevel Lab on chip Platform for DNA Analysis*. Biomedical Microdevices 2011, **13**, 19-27.

3.   Lee, H., et al., *Microfluidic lab-on-a-chip for microbial identification on a DNA microarray*. Biotechnology and Bioprocess Engineering 2007, **12** (6), 634-639.

4.   Kurbanoglu, S., et al., *Antithyroid Drug Detection Using an Enzyme Cascade Blocking In a Nanoparticle-based lab-on-a-chip System*. Biosensors & Bioelectronics 2015, **67**, 670-676.

5.   Kimura, H., et al., *An On-Chip Small Intestine-Liver Model for Pharmacokinetic Studies*. Jala 2015, **20**, 265-273.

6.   Ozhikandathil, J., et al., *Detection of Bovine Growth Hormone Using Conventional and Lab-on-a-chip Technologies: a Review*. International Journal of Advances in Engineering Sciences and Applied Mathematics 2015, **7** (4), 177-190.

7.   Ozhikandathil, J., et al., *Nano-islands Integrated Evanescence-based Lab-on-a-chip on Silica-on-silicon and Polydimethylsiloxane Hybrid Platform for Detection of Recombinant Growth Hormone*. Biomicrofluidics 2012, **6**, doi: http://dx.doi.org/10.1063/1.4757968.

8.   Medina-Sanchez, M., et al., *Eco-friendly Electrochemical Lab-on-paper for Heavy Metal Detection*. Analytical and Bioanalytical Chemistry 2015, **407**, 8445-8449.

9.   da Costa, E., et al., *Fast Production of Microfluidic Devices by CO2 Laser Engraving of Wax-coated Glass Slides*. Electrophoresis 2016, **37**, 1691-1695.

10.   Ambrosi, A., et al., *Magnetic and Electrokinetic Manipulations On a Microchip Device for Bead-based Immunosensing Applications*. Electrophoresis 2011, **32**, 861-869.

11.   Medina-Sanchez, M., et al., *Nanomaterials and Lab-on-a-chip Technologies*. Lab on a Chip 2012, **12**, 1932-1943.

12. Li, S. G., et al., *In Review of Production of Microfluidic Devices: Material, Manufacturing and Metrology*, Conference on MEMS, MOEMS and Micromachining III, Strasbourg, France, Apr 09-10; Strasbourg, France, 2008.

13. Bhise, N. S., et al., *A liver-on-a-chip platform with bioprinted hepatic spheroids*. Biofabrication 2016, **8**, 12, doi: 10.1088/1758-5090/8/1/014101.

14. He, J. K., et al., *Fabrication of Circular Microfluidic Network in Enzymatically-crosslinked Gelatin Hydrogel*. Materials Science & Engineering C-Materials for Biological Applications 2016, **59**, 53-60.

15. Xia, Y. N., et al., *Soft Lithography*. Annual Review of Materials Science 1998, **28**, 153-184.

16. Mayorga-Martinez, C. C., et al., *An Integrated Phenol 'Sensoremoval' Microfluidic Nanostructured Platform*. Biosensors & Bioelectronics 2014, **55**, 355-359.

17. Mayorga-Martinez, C. C., et al., *Nanostructured CaCO3-poly(ethyleneimine) Microparticles for Phenol Sensing in Fluidic Microsystem*. Electrophoresis 2013, **34**, 2011-2016.

18. Medina-Sanchez, M., et al., *Microfluidic Platform for Environmental Contaminants Sensing and Degradation Based on Boron-doped Diamond Electrodes*. Biosensors and Bioelectronics 2015, **75**, 365-364.

19. Tan, H. Y., et al., *Lab-on-a-chip For Rapid Electrochemical Detection of Nerve Agent Sarin*. Biomedical Microdevices 2014, **16**, 269-275.

20. Ibarlucea, B., et al., *PDMS Based Photonic Lab-on-a-chip For The Selective Optical Detection of Heavy Metal Ions*. Analyst 2013, **138**, 839-844.

21. Feng, C. Y., et al., *An On-chip Pollutant Toxicity Determination Based on Marine Microalgal Swimming Inhibition*. Analyst 2016, **14**, 1761-1771.

22. Zheng, G. X., et al., *Marine Phytoplankton Motility Sensor Integrated Into A Microfluidic Chip for High-throughput Pollutant Toxicity Assessment*. Marine Pollution Bulletin 2014, **84** (1-2), 147-154.

23. Zheng, G. X., et al., *An Integrated Microfluidic Device In Marine Microalgae Screening Application*. Marine Pollution Bulletin 2013, **72**, 231-243.

24. Hooper, K., et al., *The PBDEs: An Emerging Environmental Challenge and Another Reason for Breast-milk Monitoring Programs*. Environmental Health Perspectives 2000, **108**, 387-392.

25. Andrade, N. A., et al., *Persistence of Polybrominated Diphenyl Ethers in Agricultural Soils after Biosolids Applications*. Journal of Agricultural and Food Chemistry 2010, **58**, 3077-3084.

26. Guo, W. H. et al., *PBDE Levels in Breast Milk are Decreasing in California*. Chemosphere 2016, **150**, 505-513.

27. Ward, J., et al., *An Overview of Policies for Managing Polybrominated Diphenyl Ethers (PBDEs) in The Great Lakes Basin*. Environment International 2008, **34**, 1148-1156.

28. Darnerud, P. O., et al., *Polybrominated Diphenyl Ethers: Occurrence, Dietary Exposure, and Toxicology*. Environmental Health Perspectives 2001, **109**, 49-68.

29. Porterfield, S. P., et al., *Vulnerability Of The Developing Brain To Thyroid Abnormalities - Environmental Insults To The Thyroid System*. Environmental Health Perspectives 1994, **102**, 125-130.

30. Ahn, K. C., et al., *Immunoassay for Monitoring Environmental and Human Exposure to the Polybrominated Diphenyl Ether BDE-47*. Environmental Science & Technology 2009, **43**, 7784-7790.

31. Butryn, D. M., et al., *"One-Shot" Analysis Of Polybrominated Diphenyl Ethers and Their Hydroxylated and Methoxylated Analogs In Human Breast Milk and Serum Using Gas Chromatography-Tandem Mass Spectrometry*. Analytica Chimica Acta 2015, **892**, 140-147.

32. Li, Z., et al., *Analysis of Polybrominated Diphenyl Ethers in Vegetables Collected from Shanghai, China*. Proceedings of the 2013 International Conference on Material Science and Environmental Engineering (Msee 2013) 2013, 292-296.

33. Liu, Q., et al., *Graphene-Assisted Matrix Solid-Phase Dispersion for Extraction of Polybrominated Diphenyl Ethers and Their Methoxylated and Hydroxylated Analogs From Environmental Samples*. Analytica Chimica Acta 2011, **708**, 61-68.

34. Zhang, H., et al., *Plunger-In-Needle Solid-Phase Microextraction with Graphene-Based Sol-Gel Coating as Sorbent for Determination of Polybrominated Diphenyl Ethers*. Journal of Chromatography A 2011, **1218**, 4509-4516.

35. Orozco, J., et al., *Graphene-based Janus Micromotors for the Dynamic Removal of Pollutants*. Journal of Materials Chemistry A 2016, **4**, 3371-3378.

36. Chen, M. T., et al., *Highly Conductive and Stretchable Polymer Composites Based on Graphene/MWCNT network*. Chemical Communications 2013, **49**, 1612-1614.

37. Shahzad, M. I., et al., *In Study of carbon nanotubes based Polydimethylsiloxane composite films*, 6th Vacuum and Surface Sciences Conference of Asia and Australia (VASSCAA), Islamabad, Pakistan, Oct 09-13; Islamabad, Pakistan, 2012.

38. Xu, R. Q., et al., *Facile Fabrication of Three-Dimensional Graphene Foam/Poly(dimethylsiloxane) Composites and Their Potential Application as Strain Sensor*. ACS Applied Materials & Interfaces 2014, **6**, 13455-13460.

39. Lee, A. C., et al., *Sensitive Electrochemical Detection of Horseradish Peroxidase at Disposable Screen-printed Carbon Electrode*. Electroanalysis 2008, 20 (**18**), 2040-2046.

40. Ju, T. et al., *Polybrominated Diphenyl Ethers in Dissolved and Suspended Phases of Seawater and in Surface Sediment from Jiaozhou Bay, North China*. Science of the Total Environment 2016, **557**, 571-578.

41. Lammel, G., et al., *Air and Seawater Pollution and Air-Sea Gas Exchange Of Persistent Toxic Substances in The Aegean Sea: Spatial Trends of PAHs, PCBs, OCPs and PBDEs*. Environmental Science and Pollution Research 2015, **22**, 11301-11313.

42. Cristale, J. et al., *Occurrence and Sources of Brominated and Organophosphorus Flame Retardants in Dust From Different Indoor Environments in Barcelona, Spain*. Environmental Research 2016, **149**, 66-76.

43. Medina-Sanchez, M., et al., *On-Chip Electrochemical Detection of Cds Quantum Dots Using Normal and Multiple Recycling Flow Through Modes*. Lab on a Chip 2012, **12**, 2000-2005.

44. Zhang, J., et al., *Reduction of Graphene Oxide via L-ascorbic acid*. Chemical Communications 2010, **46**, 1112-1114.

45. Nourani, S., et al., *Magnetic Nanoparticle-based Immunosensor for Electrochemical Detection of Hepatitis B Surface Antigen*. Analytical Biochemistry 2013, **441**, 1-7.

46. Xu D., et al., *Label-free detection and discrimination of poly-brominated diphenylethers using molecularly imprinted photonic cross-reactive sensor arrays*. Chemical Communications 2014, **50**, 14133-14136

47. Radhakrishnan, R., et al., *Impedance Biosensors: Applications to Sustainability and Remaining Technical Challenges*. ACS Sustainable Chemistry & Engineering 2014, **2**, 1649–1655.

CHAPTER 4. IMPROVED ELECTROCHEMICAL DETECTION OF HEAVY METALS USING GRAPHENE-BASED LAB-ON-A-CHIP PLATFORM 82

CHAPTER 4

Improved electrochemical detection of heavy metals using graphene-based Lab-on-a-chip platform

Related Publications

Andrzej Chałupniak and Arben Merkoçi, "Improved electrochemical detection of heavy metals using graphene-based Lab-on-a-chip platform". (In preparation, 2017).

4.1.   Introduction

Recent decades brought an incredible progress in the field of analytical chemistry allowing researchers to detect more compounds in a shorter time with a significantly lower limit of detection than ever before. Unfortunately, many of the hazardous compounds are present in nature in a very low concentration and as they interact with other compounds, their separation and detection are still challenging. One of the examples is heavy metals, considered as hazardous as they accumulate easily in live organisms, including animals and plants, as well as due to their (bio)degradation which occurs to a very low extent. For example, cadmium can be accumulated in liver and kidney for more than 10 years seriously affecting human's health [1, 2]. In the case of lead, its toxicity carries a risk of irreversible health effects. It can interfere with a number of body functions particularly the central nervous, hepatic, renal system and hematopoietic [3].

The presence of heavy metals in natural environments is caused both due to anthropogenic activities (rapid industrialization) as well as natural process (i.e. aeolian process). Obviously, the main impact of current heavy metals contamination is linked to industrial wastes leading to water and soil pollution including inland and coastal ecosystems[4, 5]. For example, some common sources of lead contamination are leaded gasoline, industrial processes like coal combustion and lead smelting, lead-containing pipes, paints, solders and bearings [3, 6].

Analytical laboratories usually use atomic absorption spectroscopy (AAS) [7], flame atomic absorption spectrometry (FAAS) [8], energy dispersive X-ray fluorescence (EDXRF) [9] or mass spectroscopy (MS) [10] for heavy metals determination. Those techniques provide very good sensitivity and accuracy but on the other hand, generate a high single cost of analysis and require sophisticated equipment that can be used only by very well trained personnel. For this reason, there is a strong need of simple sensors development that can perform sensitive and accurate measurements but are cheaper and easier to use in the laboratory as well as in-field. Various classes of sensors are already reported such as optical, electrochemical, ion-selective and piezoelectric. Most of them are based on

electrochemistry either using (bio)sensing approach for example, interaction of HM with nucleic acids, proteins or enzymes [4, 11-16].

Electrochemical detection can be also performed directly, using Anodic Stripping Voltammetry, as certain metals are oxidized at specific voltage what can be used for their determination. square wave anodic stripping voltammetry is very sensitive, as the accumulation step is performed so metals are reduced onto the working electrode surface (see Annex III) [17, 18]. This method is also compatible with screen-printed electrodes which are the most promising tools (transducers) in novel sensors due to the low cost, easy fabrication process and possibility to perform a surface modification, as well as integration with various devices and platforms. Although stripping voltammetry is one of the best electrochemical techniques for HM measurements, its sensitivity means that many compounds may affect the final performance. Thus, detection of heavy metals in complex samples such as seawater (due to high salt content and therefore matrix interference) might be more complicated and requires sample pretreatment or some preconcentration method included [4, 11, 19-21].

Various materials have been reported recently as effective adsorbents of heavy metals. One of the most common is activated carbon which is well known for its adsorption properties and can be obtained from cheap and abundant materials. For example, heavy metals adsorption using activated carbon made of palm shell [22], coir pitch [23], saffron leaves [24] or nut shell [25] is already reported. Activated carbon is suitable for further modification such as sulfurization. Tajar et al. used SO_2 for activated carbon sulfurization and observed an increased adsorption capacity towards Cd(II) comparing to unmodified activated carbon [25].

Simultaneously, graphene and its derivatives are especially attractive for scientists recently. Sitko et al. investigated the adsorptive properties of graphene oxide (GO) towards divalent metal ions. It was found that a strong adsorption occurs in a wide range of pH: 3–7 for Cu(II), 5–8 for Zn(II), 4–8 for Cd(II), 3–7 for Pb(II). All of the studied metals compete with each other to bind onto GO surface, with Pb(II) having the highest and Zn(II) the lowest

affinity. The mechanism of the adsorption involves surface complexation of metal ions with the oxygen-containing groups on the surface of GO [26]. Same research group used GO/cellulose membranes to evaluate heavy metals adsorption in a more convenient way. The platform showed good adsorption performance as well as reusability up to more than 10 cycles of adsorption and desorption [27].

Another interesting approach reported by Wu et al. used 3D sulfonated reduced graphene oxide (3D-SRGO) with very high adsorption capacity of 234.8 mg/g towards Cu(II) [28] Hallaj et al. used exfoliated graphene nanosheets for Cd(II) adsorption performed in ultrasonic bath [29].

As can be seen, there are many materials with excellent adsorption properties but unfortunately, in most cases, the use of them requires membrane-based systems or centrifugal separation of the adsorbent from the solution. In some cases, such approaches are quite impractical, especially taking into account the need of special equipment and additional work. In this case, the use of Graphene/Polymer composites might be more promising, as polymeric composites are more flexible and can be used for microdevices fabrication such as Lab-on-a-chip.

Polymer composites consist of two components: nanofiller – a nanomaterial which is in-built in polymer structure; polymer – which defines the main physicochemical properties of the composite [30]. So far, various polymers were employed as matrices to fabricate graphene-based composite. Poly(vinyl alcohol) [31], epoxy [32], Polystyrene [33], Polypropylene [34], Poly(methyl metacrylate) [35], Polyimide [36] and Polycarbonate [37] are some of them.

The main advantage of graphene comparing with other carbon nanomaterials (such as Carbon Nanotubes) is a high surface-to-volume ratio. Graphene can tune many properties of polymers as well as enrich these with the new ones. This opens an access to many applications in the field of novel materials, electronics, biosensors and medicine [38, 39]. For instance, many graphene-based polymers are under development due to their unique electrical behaviour. An addition of conductive filler increases composite conductivity. In

this application, rGO is especially interesting as it is more conductive than pure GO due to surface defects and different C/O ratio [40, 41]. In case of mechanical properties, there are many reports of using GO as a nanofiller as it influences Young's modulus and composite's stiffness. The presence of reactive hydroxyl and epoxy group on its surface facilitate solubility and reactivity with the polymer matrix, unlike pure Graphene which tends to stack due to Van der Waals interactions [41-43]. Another motivation for graphene-based composite can be related to its optical properties. Graphene is the most transparent material that can be used for electrodes and photovoltaic devices fabrication[44]. Moreover, fluorescence quenching ability can be employed [45, 46]. The use of nanofillers is not indifferent to composites thermal properties. Graphene is reported to increase thermal stability as well as thermal conductivity. In presence of graphene or GO, the glass transition temperature (Tg) might be also shifted [43, 47, 48]. Last but not least, the poor solubility of graphene in gases (due to high aspect ratio) affects polymers permeability. This property can be used for intentional design of nanoscalled pores working as a separation membranes for gases [49, 50].

There are several ways of Graphene/Polymer composite preparation. The most common are based on the use of GO that is simply blended with a polymer matrix and let for curing/polymerization afterward. Alternatively, blending step can be combined with the thermal reduction so finally, an rGO/polymer composite will be obtained. In a case of more sophisticated modification, a proper graphene derivative is prepared first and then blended with polymer matrix [39, 51].

The relative simplicity of Graphene/Polymer composite preparation is the main motivation of using it instead of particle- or membrane-based adsorption materials for heavy metals preconcentration. In this work, a GO-PDMS composite was developed with the purpose of Lab-on-a-Chip device fabrication. The use of Lab-on-a-chip platforms due to their small size and flexibility might be a solution to provide a preconcentration system of heavy metals combined with simultaneous detection.

In the previous work (Chapter 3) an rGO-PDMS composite was used for effective removal of polybrominated diphenyl ethers. The mechanism was based on π-π stacking between rGO aromatic rings and PBDE [52]. In a case of heavy metals (or any bivalent metals) interaction with graphene is due to surface complexation, as metals have an affinity to oxygen groups richly present on GO surface, unlike rGO [53].

The developed device consist of three layers: GO-PDMS channel, where preconcentration is performed, PDMS channel, where detection is performed and screen-printed electrode where heavy metals are deposited and detected using anodic stripping voltammetry. As a proof of concept, we used Pb(II) as an example of the heavy metal that due to its toxicity there is a high demand to ensure its sensitive detection.

4.2. Experimental section

4.2.1. Reagents

Isopropyl alcohol, tetrahydrofuran, ethanol, acetone, 3-aminopropyltriethoxylane (APTES) and Heavy metals standard solution TraceCERT® was purchased from Sigma. The screen-printed inks (carbon sensor paste C2030519P4 and silver-silver chloride paste C2130809D5) were purchased from Gwent Group, United Kingdom. Polycarbonate sheets were purchased from Vink Plastics S.L.U., Spain. PDMS (Sylgard® 184 Elastomer kit) was purchased from Ellsworth Adhesives Iberica, Spain. Graphene Oxide stock solution (5 mg/mL) was purchased from Angstron Materials (Dayton, USA). All commercial reagents were of analytical grade and handled according to the material safety data sheets suggested by the suppliers.

4.2.2. System operation

Presented approach is based on a multilayer Lab-on-a-chip platform (LOC) that consists of a) screen-printed carbon electrode printed on polycarbonate sheet; b) PDMS microfluidic chip bonded with an electrode; c) GO-PDMS chips containing a network of serpentine channels, connected vertically with PDMS layer. Samples are passing through the LOC starting in GO-PDMS layer where heavy metals are adsorbed to graphene oxide molecules via surface complexation. This allows performing a preconcentration of the

heavy metals using the sample of desired volumes and pump (peristaltic or syringe) as a driving unit of the given flow rate. After this step, desorption buffer is introduced (0.1 M HCl), so previously adsorbed heavy metals are released from the surface and move to the detection chip where the process of electrochemical deposition is already going on. As the same buffer is used for desorption and detection, those steps occur subsequently. As a result, sensitive electrochemical detection with inbuilt preconcentrated platform can be performed (Fig.1.).

4.2.3. Fabrication and assembling of Lab-on-a-Chip platform

4.2.3.1.   Fabrication of the microfluidic mold

The microfluidic mold was fabricated following the same procedure as in Chapter 3 as well as in other works reported [52, 54]. The design of the LOC platform is shown in Figure 1 and the dimensions of the microfluidic channels of GO-PDMS in Figure 2. GO-PDMS chips contain channels with extra curvatures in the initial part. This support the diffusion as the laminar flow is rendered impossible.

4.2.3.2.   Fabrication of the GO-PDMS composite

Various approaches to GO-PDMS preparation have been studying and some of the parameters are discussed in Results section. For the final application, the following protocol was employed: 40 mL of 5 mg/mL GO solution was mixed with 15 mL of THF and sonicated (QSonica sonicator) for 20 minutes. Meanwhile, 20 g PDMS monomer was mixed with 10 mL of THF. Both parts were stirred together and sonicated another 1 hour (90% amplitude, pulse mode). After that, a composite was placed on the hotplate with magnetic stirring and stirred for 24 hours at 70 °C until the whole solvent evaporates. This can be visually inspected as the composite containing solvent is brownish-opaque while the well-prepared one is glossy and translucent. After cooling down, a containing catalysers PDMS curing agent is added, following the mass ratio 10:1 (PDMS:curing agent). The material is stirred vigorously for about 10 minutes and air bubbles are removed using a vacuum. Afterwards, the GO-PDMS is poured onto Si mold with the shape of serpentine channels (50 cm total length, 530 µm width, 100 µm height, 27 cm^2 active surface) and

kept at room temperature for 1 hour, protected in a plastic petri dish. Then the composite is transferred onto 70 ºC hotplate for about 3-4 hours until completely polymerized.

4.2.3.3. PDMS preparation

A PDMS was mixed with its curing agent in the mass ratio 10:1. After intensive stirring for 5 minutes, an excess of air bubbles was removed using a vacuum. Afterward, PDMS was poured onto Si wafer mold with a given design of microfluidic chip and kept on the hotplate, 70 ºC, for 3 hours until completely polymerized.

4.2.3.4. LOC device fabrication

Chips of GO-PDMS and PDMS were cut out from the mold and inlet/outlet was made using biopsy puncher (1.5 mm diameter). In order to get rid of impurities, samples were washed in miliQ water, followed by isopropanol and dried on the hotplate 70 ºC for 10 minutes. So as to modify the surface, oxygen plasma treatment (Harrick Plasma) was performed. The same treatment was performed on screen-printed electrodes which surface was previously modified using APTES and commonly known protocol [55].

Assembling was performed by placing PDMS layer onto electrode and GO-PDMS onto PDMS. The outlet of the GO-PDMS layer was centered in the same position as the inlet of PDMS layer. Bonded device was kept in 70 °C on the hotplate for another 30 min so as to strengthen the bonding. Polymeric tubes were connected to the inlet and outlet of LOC platform as well as to the pump.
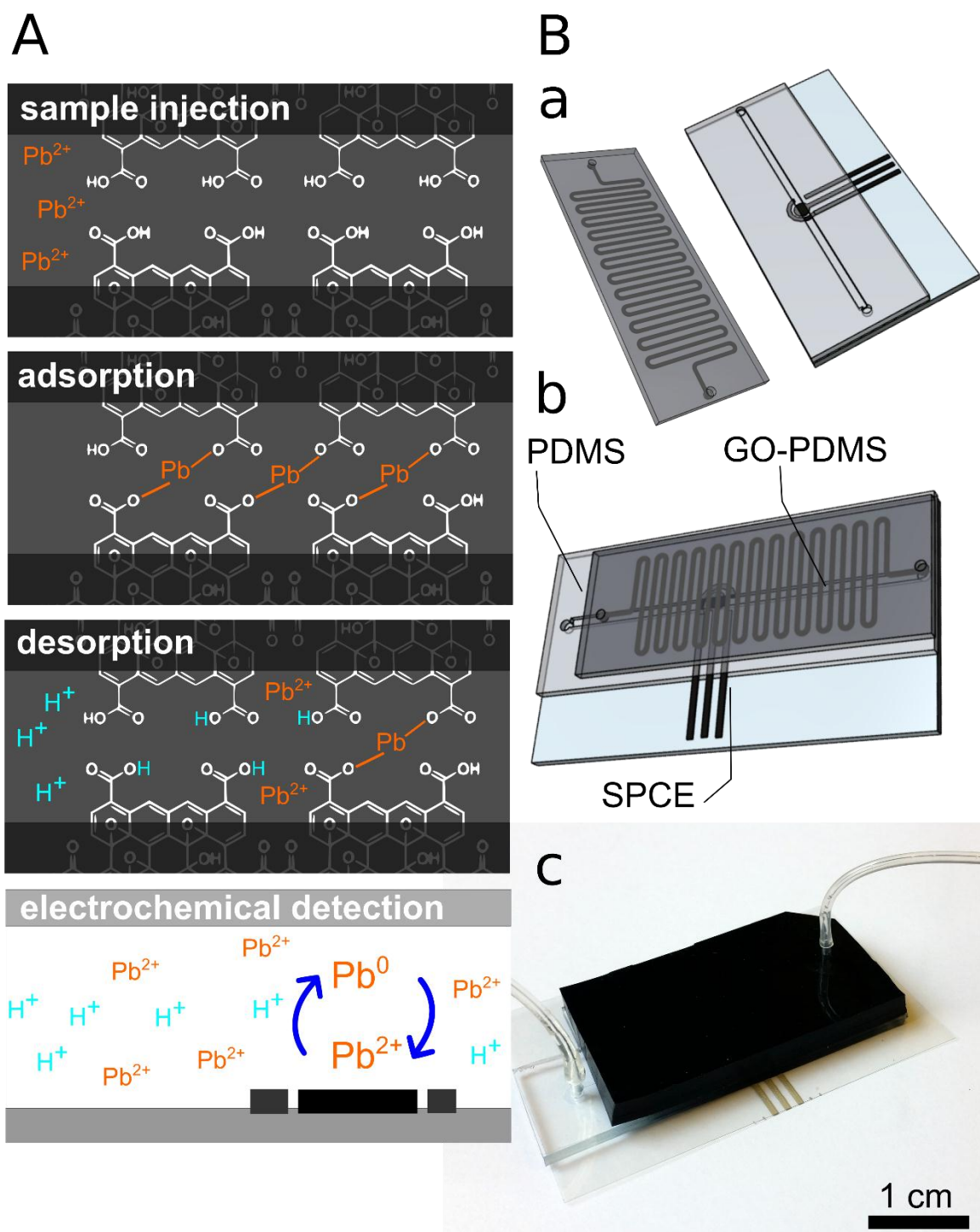
Figure 1 LOC system for heavy metals preconcentration. **A.** Reactions occurring in the chip: Pb(II) is adsorbed to GO-PDMS; 0.1 M HCl is injected in order to perform desorption and detection. A sample is passing from GO-PDMS chip to PDMS electrochemical chip, where the SW-ASV is performed; **B.** Design of the platform; the scheme of the GO-PDMS chip and PDMS chip separately (**a.**) and bonded (**b.**); image of the full LOC device with polymeric tubes connected to the inlet and outlet (**c.**).

4.2.4. Electrochemical detection of heavy metals

Screen-printed carbon electrodes (SPCE) were fabricated by screen-printing technology using a screen-printer (DEK 248, UK). Electrochemical measurements were carried out using computer-controlled Autolab PGSTAT-12 (302 N-High performance) (potentiostat/galvanostat) with general-purposes electrochemical software operating system (GPES version 4.9.007, from Eco Chemie B.V., Utrecht, The Netherlands).

During preliminary experiments, commercial Bismuth electrodes were used for the sensitive detection of heavy metals (Annex III). Measurements were performed by dropping 150 µL of the sample onto the electrode surface. As a detection technique, square wave anodic stripping voltammetry (SWASV) was used. Parameters were as follows: deposition potential -1.2 V, deposition time 230 s, equilibration time 10, Frequency 25 Hz, step potential 0.006 V, amplitude 0.03 V, potential range from -1.4 V to 0.0V. 0.1 M HCl was used for detection. Each measurement was repeated 3 times.

In the final approach, microfluidic chips with integrated home-made SPCE electrodes were connected to the Autolab PGSTAT-12 with a specially adapted electrical edge connector. The same electrochemical technique was used with slightly different parameters: deposition potential -1.2 V, deposition time 120 s, equilibration time 30 s, Frequency –25 Hz, step potential 0.006 V, amplitude 0.03 V, potential range from -1.4V to 0.0V. Unless otherwise indicated, 0.1 M HCl was used for detection and the flow rate was 0.5 mL/min. Each measurement was repeated 3 times.

4.2.5. Adsorption studies

All the parameters regarding GO-PDMS composition, as well as the influence of the external factors were optimized toward an adsorption ability of the standard solution containing 250 ppb of Pb^{2+} in water. A sample of this concentration has a pH=7 so further adjustments were not performed. In selected tests where the effect of pH was tested 1 M HCl or 1 M $NH_3 \cdot H_2O$ was used for adjustment.

As a proof of concept, using a biopsy puncher, a cylindrical shape GO-PDMS pieces were cut out. Their surface area was about 0.5 cm^2. Depending on the experiment, a different

number of GO-PDMS pieces were immersed in 1 mL of Pb^{2+} standard solution in 2 mL Eppendorf tubes and shake for 2h (unless otherwise stated) with 500 rpm on thermoshaker in a constant temperature of 25 °C.

After the incubation, 100 µL of the sample was collected and mixed with 900 µL of HCl so as to obtain a final concentration of 0.1 M HCl. In a case of the highly concentrated Pb^{2+} samples which are out of the linear detection range, further dilutions were applied accordingly.

In each case, a control experiment was run, using the same type of Eppendorf, same initial concentration, but no GO-PDMS placed in it. This was used for the relative adsorption calculation.

Adsorption was expressed as a relative decrease of the concentration in comparison to the control samples. Concentration was calculated using a calibration curve obtained previously. A general formula was as follows:

$A_{Pb2+} = [(C_0-C_1)/C_0]*100\%$

Where C_0 is the initial concentration of the Pb^{2+} (250 ppb usually), C_1 is the concentration of Pb^{2+} measured after the experiment.

In order to study the recovery of the GO-PDMS composite, desorption experiments were performed. Samples after standard adsorption assay were washed 3-times with miliQ water in order to remove an unbound and excessive Pb^{2+} solution. After drying, a given desorption buffer was added (usually 0.1 M HCl). Standard desorption experiments took 2 hours, using shaker similarly as for the adsorption studies. Measurements were performed analogically providing adequate dilutions. A relative desorption was calculated using the following formula:

$D_{Pb2+} = [C_D/(C_0-C_1)]*100\%$

Where C_D is the concentration of the Pb^{2+} found in a sample after recovery experiment. As it can be seen, desorption is calculated as regards of previously adsorbed metal. This means, that a % of desorption can be higher than % of adsorption.
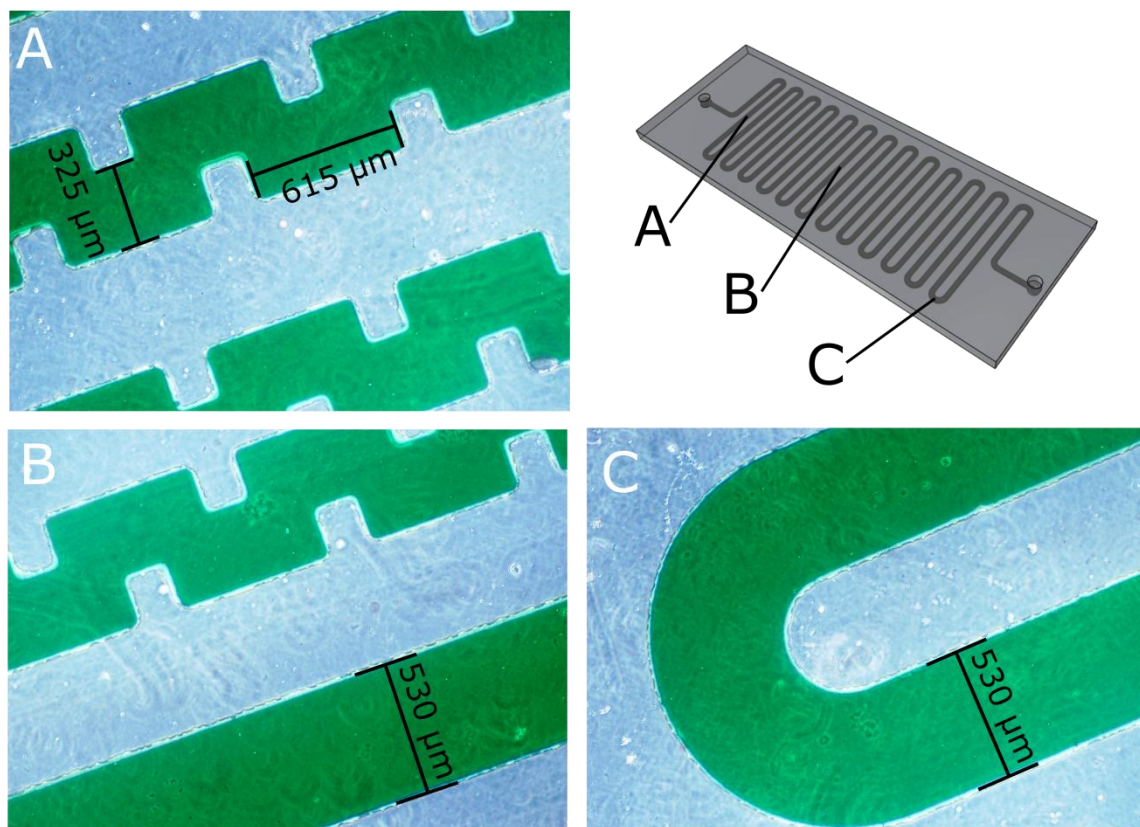
Figure 2 Microfluidic channels of the GO-PDMS chip. Using a mold dedicated to GO-PDMS chip, a PDMS chip was fabricated to ensure transparency. A green ink was introduced to visualize the geometry of the channels which dimensions were measured using optical microscope (4x magnification).

4.2.6. On-chip preconcentration of heavy metals

Experiments with LOC device were performed using peristaltic pump as a driving unit. A LOC device consists of screen-printed electrode, PDMS chip and GO-PDMS chip. All elements are connected through the microfluidic channels. Sample containing metals to be adsorbed is passing through GO-PDMS. The direction of the flow (1 mL/min) is changed every 30 s so as to ensure the best catchment of the metals from a given sample. Unless otherwise stated, a dynamic incubation with the metal-containing solution took 30 minutes. Afterwards, a sample is withdrawn from the chip and 0.1 M HCl is introduced with

the flow rate of 1 mL/min. Similarly as during preconcentration, the flow is moved back and forward. Once desorption is finished, the flow rate is slowed down to 0.5 mL/min and moved towards electrode. At this moment an electrochemical deposition is already going on. After 120 s, an electrochemical stripping is performed.

4.3. Results and discussion

4.3.1. Optimization of the GO-PDMS performance

4.3.1.1. GO-PDMS composition

GO-PDMS is made of Graphene Oxide solution and PDMS followed by curing agent addition. Obviously, an increase of GO concentration leads to higher adsorption yield. PDMS itself is neutral and does not have a negative charge that could attract bivalent metals to its surface. But an important factor is a curing agent, playing a role of catalyser, allowing PDMS to polymerize. We evaluated the influence of the composite composition on adsorption. As it shows in Figure 3A, the more curing agent added, the lower adsorption is observed.

As mentioned before, in this approach dependence between adsorbent mass and adsorption yield is not relevant. Thus, an effect of the total adsorptive surface was studied. It can be seen the increase of adsorption proportional to the increase of GO-PDMS surface (proportional to the number of cylindrical GO-PDMS pieces immersed in the tested solution). In this proof of concept test (Figure 3B) a maximum adsorption was achieved for the GO-PDMS surface 15 cm^2.

Another crucial factor is the concentration of GO in PDMS. It can be seen (Figure 3C) that if the concentration of GO is lower than 2 mg/g PDMS an adsorption actually does not occur. Most probably at this point, all the GO react with PDMS so there are no free oxygen groups that could interact with bivalent metals. For higher concentration, there is a significant increase of adsorption ability having the maximum for GO=10 mg/g PDMS. Further increase of the GO content does not improve adsorption performance as probably the inhibition of the polymerization is more likely to occur. We have observed very

inconsistent results for highly concentrated GO-PDMS. For this reason, a 10 mg/g PDMS was maintained as the best concentration to be used.

During the composite preparation, PDMS and GO are dissolved in THF and stirred on the hotplate until the solvent is evaporated. This process has a strategic influence on the GO-PDMS performance. If there is no full evaporation, a GO, as hydrophilic, is more likely to agglomerate within water droplets. Such composite is not homogenous, neither translucent and its surface shows an irregular distribution of GO as well as air bubbles. It was found that a mandatory time for an efficient adsorption is at least 24h on the hotplate (Figure 3D). A shorter amount of time, but with the increased temperature (>100 °C) led to possibly partial reduction of the GO (a significant blacking of the composite is observed; data not shown), thus this approach was not furtherly considered.
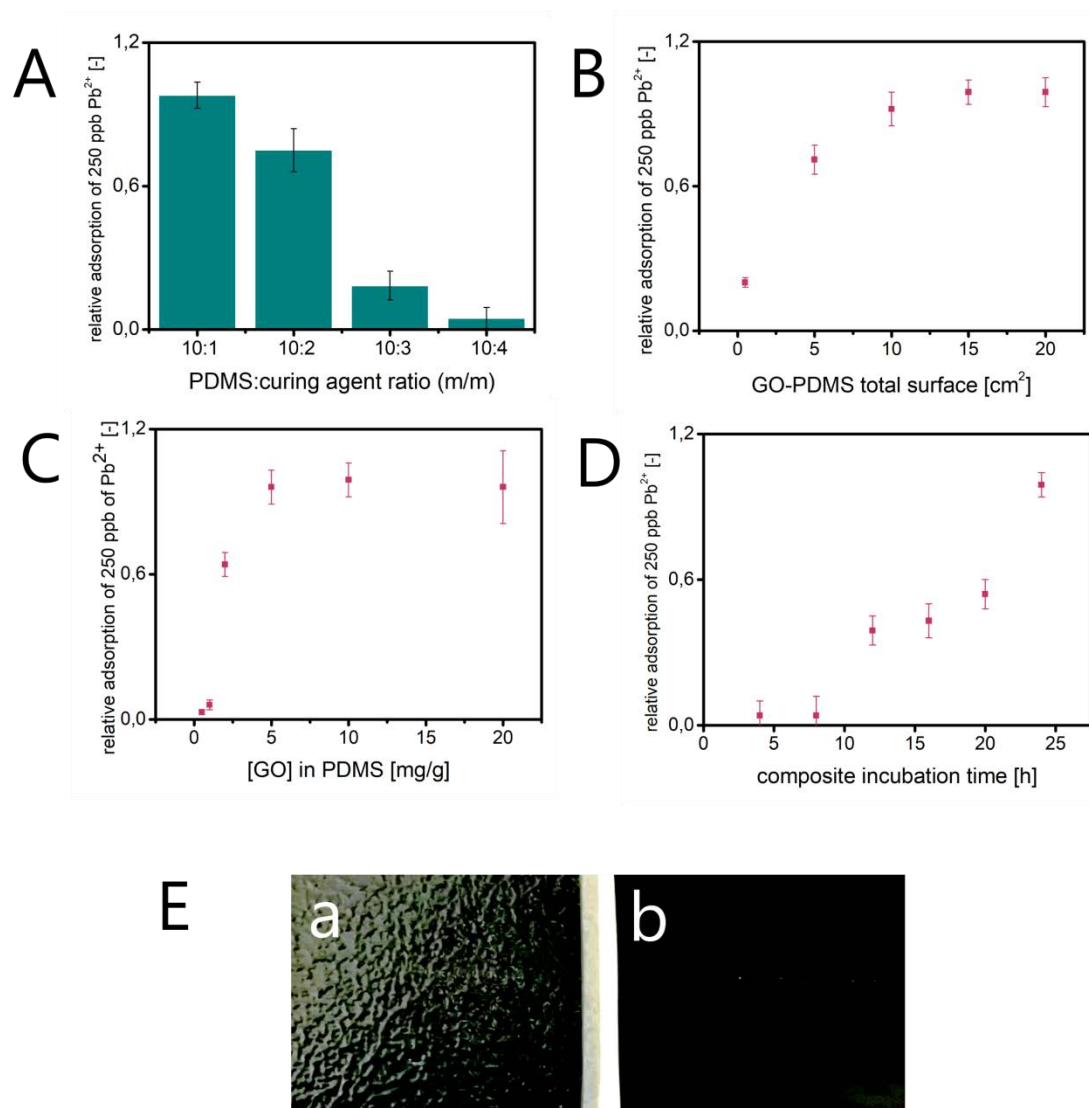
Figure 3 GO-PDMS parameters affecting adsorption ability. **A.** Mass ratio of PDMS:curing agent; **B.** Total surface of GO-PDMS in contact with sample; **C.** GO concentration in PDMS; **D.** Effect on composite incubation time (solvent evaporation); **E.** Composite quality **a.** example of 12 h evaporation with visible inhomogeneity, **b.** example of 24 h evaporation with visible, homogenous GO-PDMS.

4.3.1. Optimization of external factors affecting adsorption

4.3.1.1. Initial pretreatment

Although the process of GO-PDMS composite synthesis is quite simple and does not involve many chemicals, it is important to perform an initial treatment of the material before running an adsorption experiment, so as to ensure the lack of contamination possibly affecting adsorption ability.

We found alkaline-treatment as the most efficient, allowing reaching nearly double adsorption yield comparing to acid or isopropanol treatment. If the GO-PDMS is contaminated with acid residues, in presence of base a neutralization reaction occurs. On the other hand any cations possibly blocking the active surface of GO will be released as reacts with negatively charged OH^-. Moreover, it was observed that the oxygen plasma treatment does not cause any change in the adsorption ability (Figure 4A).

4.3.1.2. Initial concentration

As it can be predicted, lower initial concentration results in higher adsorption yield at a certain point of time. We evaluated the adsorption performance of GO-PDMS in the range 62.5-2000 ppb (Figure 4B). It can be seen that a full adsorption is observed for the concentrations ≤250 ppb, while for the 2000 ppb nearly does not occur. This can be explained mainly by the adsorbent surface capacity insufficient for such amount of metal. Moreover, highly concentrated Pb^{2+} samples were adjusted to the neutral pH=7 (so as to not introduce another variable in the experiment). This means the presence of some extra NH_4^+ ions that may interact with Pb creating an ammonia complex $Pb(NH_3)^{2+}$, $Pb(NH_3)_2^{2+}$, $Pb(NH_3)_3^{2+}$, as suggested in [56]. On the other hand, from the practical approach, such a big concentration is never present in real conditions.

4.3.1.3. Contact time

A general assumption that an increase of contact/incubation time causes an increase of heavy metals adsorption was confirmed. As it shows in Figure 4C, during the first 15 minutes of the process, adsorption occurs very quickly. After that, the process significantly slows down and the maximum occurs after less than 3 hours so the further adsorption is

no longer observed. It is important to take into account that the contact time depends on the amount of adsorbent, volume of the sample as well as initial concentration. Thus, in different conditions, other values can be obtained. Nevertheless, it does not affect the kinetic profile of the adsorption process, where most of the lead present in the sample is adsorbed at the beginning of the process

4.3.1.4.   pH

The major mechanism of metals adsorption to GO is surface complexation. Thus, ionic composition and metals present in the solution affect the adsorption efficiency, kinetics as well as affinity. We have analyzed the effect of pH on Pb^{2+} adsorption in the range 2-12 (Figure 4D). It can be observed that adsorption grows gradually together with the increase of the pH reaching maximum at pH=7. At pH 11-12 a significant decrease of adsorption is observed. This is in accordance with the works of Dowlatshahi et al. [24] and Gaya et al. [22] where the highest adsorption of Pb^{2+} was observed in pH=7. On the other hand, Sitko et al. reported pH=4 as the optimal for Pb^{2+} [26] and pH=5 when GO is immobilized onto cellulose membrane [27]. This may suggest that in our case, the presence of PDMS in composite affect the adsorption performance and shifts its maximum toward higher pH. That may result from the number of oxygen functional groups that is lower where GO is entrapped within PDMS.

Such behaviour can be explained taking into account two issues: protonation of the oxygen functional group of GO and the form in which metal is present in the solution. In highly alkaline solution metals precipitate as $Me(OH)_m^{n-}$ hydroxides which have no longer affinity to GO surface due to a negative charge. Lower pH maintains metals predominantly in cationic form (Me^{2+}) thus, they are chemically active. Highly acidic pH, on the other hand, means that oxygen groups of GO are protonated so metals compete with hydrogen ions to be adsorbed. According to literature, for the pH <3.9 GO has a low negative charge, while for the pH>3.9 the charge is getting highly negative and from this point, the best conditions for metal adsorption shall have occurred [27, 53].
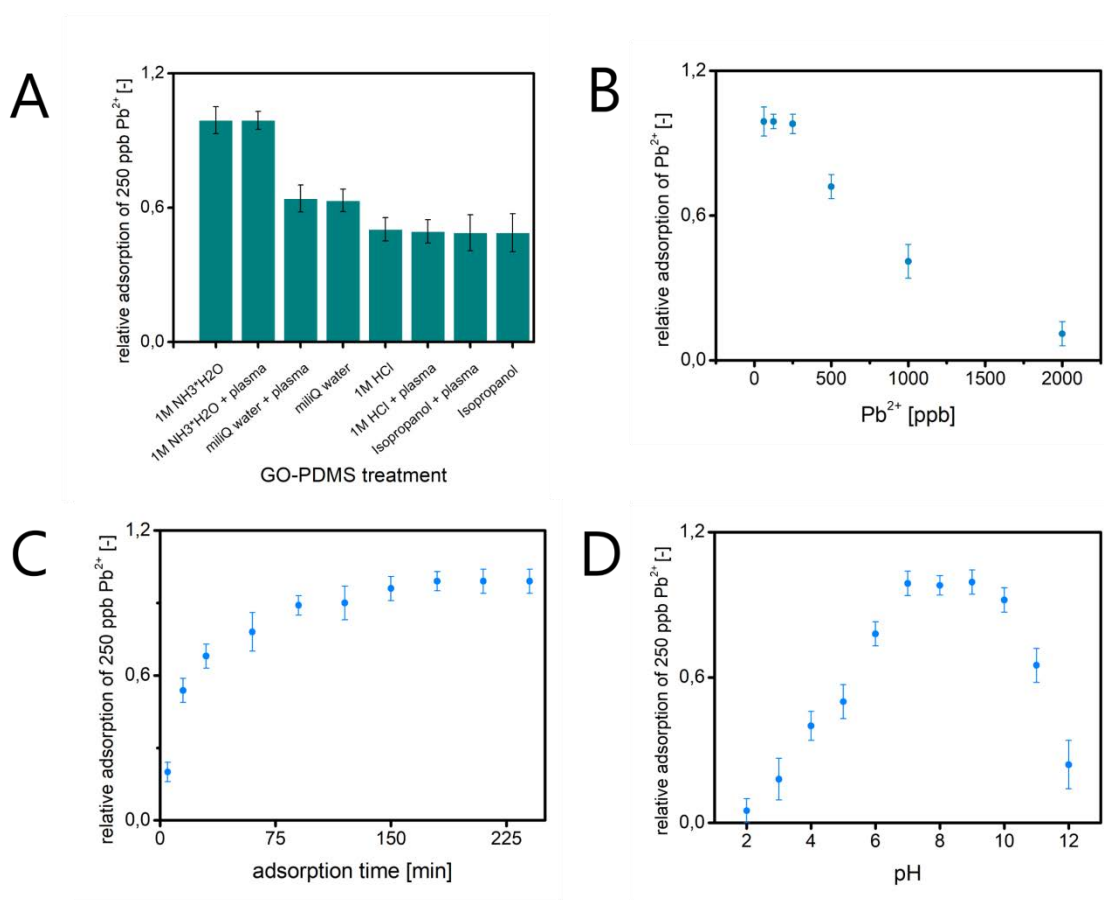
Figure 4 Selected parameters affecting adsorption ability. **A.** Initial treatment of the GO-PDMS surface; **B.** Initial concentration of Pb^{2+}; **C.** Contact time between GO-PDMS and Pb^{2+}; **D.** pH of the Pb^{2+} solution.

4.3.2. Desorption

The ability of GO-PDMS to reversibly adsorb and desorb metals is very crucial from the point of practical application of this material (preconcentration and detection). In principle, any acidic solution should cause metal's desorption as H^+ ions compete with bivalent metals, such as Pb^{2+} to be bonded with GO surface so the metal displacement reaction can be observed. For the desorption of bivalent ions from carbon materials, various chemicals were reported until now. For 3D-SRGO HNO_3 pH<1 was found as the most efficient leaching solutions [28]. 0.1 M HNO_3 was used by Sitko et al. for Pb desorption from Graphene oxide/cellulose membranes [27]. Hallaj et al. studied the desorption of Cd^{2+} from exfoliated graphene nanosheets and found 0.1 M HCl as more efficient (99.12% of recovery) comparing with 0.1 M HNO3 (78.7% of recovery) [29]. HCl had also the best

desorption performance (comparing with H_2SO_4 and HNO_3) in the case of Cd^{2+} desorption from the sulfurized activated carbon [25]. In our case, HCl in different concentrations was tested (Figure 5A). We found that 1 M HCl desorbs Pb^{2+} more effectively than 0.1 M. However, adjusting the proper time of desorption allow to match an appropriate reagent for the desorption. The maximum recovery for 1 M HCl was 98.96% while for 0.1 M HCl 98.58%. In our case 0.1 M HCl is more attractive as it can be used directly for electrochemical detection of heavy metals in LOC platform. This means that within one step a desorption and subsequent detection might be performed.

4.3.3. GO-PDMS reusability

One of the most important requirements for the adsorbent is the reusability. We performed several cycles of adsorption and desorption within different days (Figure 5B). To highlight the importance of surface pretreatment we compared GO-PDMS pre-treated with $NH_3.H_2O$ with GO-PDMS rinsed only with miliQ water (after the desorption process). It can be clearly seen that the pre-treated surface shows a full adsorption capacity and can be re-used at least several times without the loss of performance. Same happens in the case of desorption ability. In the case of non-treated GO-PDMS after the first adsorption-desorption cycle, the material loose nearly 50% of adsorption capacity and it cannot be well recovered.

It is worthy to mention that the important advantage of this composite is a big resistance toward chemical and physical factors. PDMS provided mechanical strength and durability (Figure 6), as well as it is not affected by concentrated acid or bases treatment. This supports an opportunity to use this device for multiple times rather than single.

Although a good approach to surface recovery was showed, to extend the viability of GO-PDMS it should be stored under protected atmosphere, like i.e. vacuum bags. This will protect the surface from the macroscopic impurities that are easily attracted due to the hydrophobicity of the PDMS.
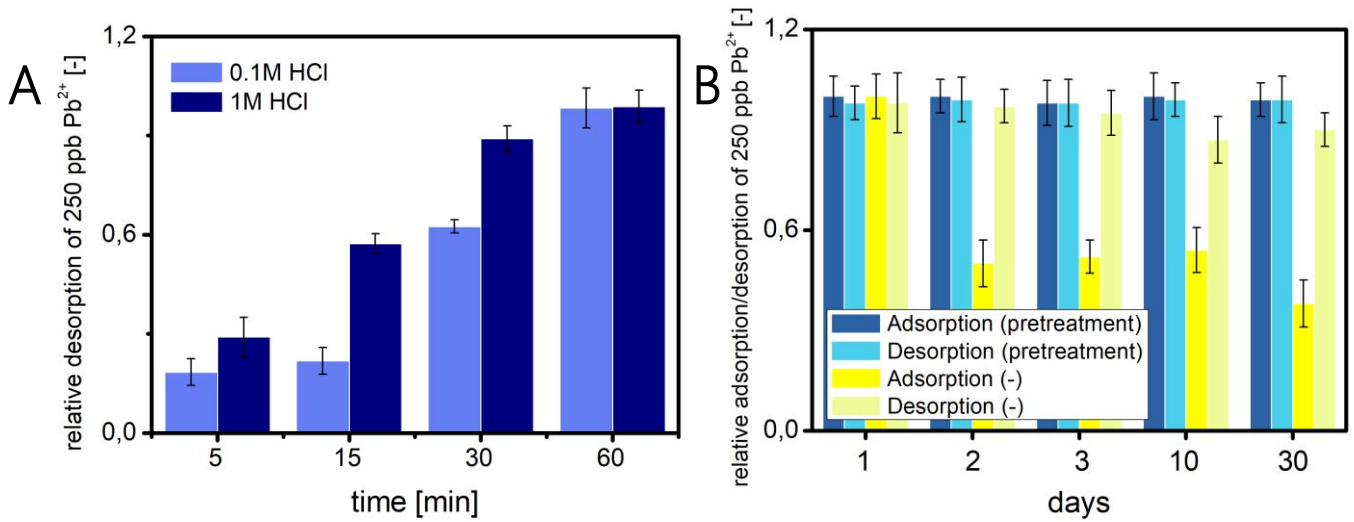
Figure 6 A. Desorption of Pb^{2+} from GO-PDMS Surface using 0.1 M and 1 M HCl; **B.** Adsorption/desorption cycles performed in different days using non-treated and pre-treated ($NH_3 \cdot H_2O$) GO-PDMS.
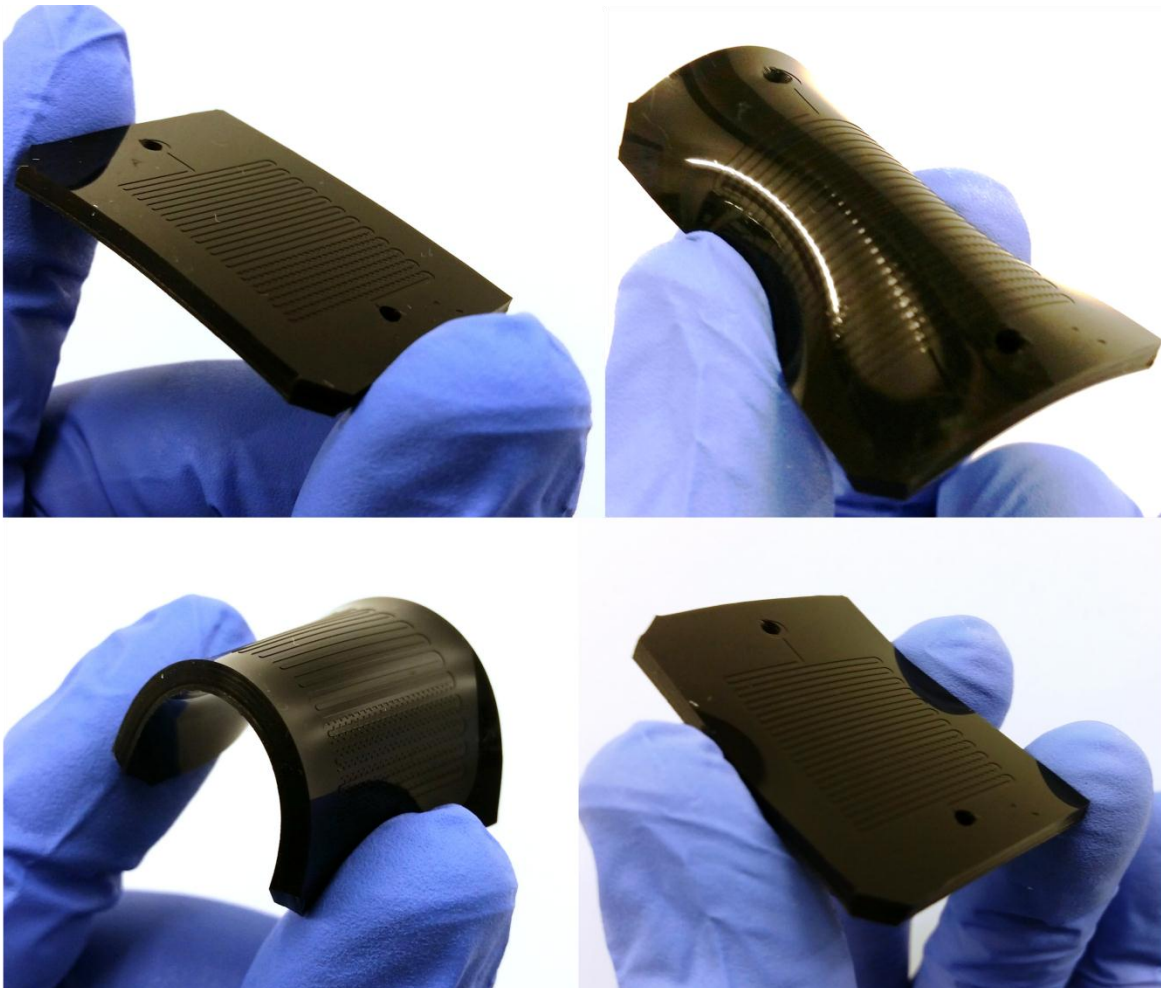
Figure 7 GO-PDMS chip. Despite the high content of GO, the composite maintains typical physical properties of PDMS like mechanical durability and elasticity.

4.3.4. Lead preconcentration in LOC device

4.3.4.1. The effect of the flow rate

The flow rate is one of the most important factors affecting any process in a microfluidic chip. However in the range of the flow rates that we evaluated (0.2-2 mL/min) the differences were not that significant (data not shown), thus we used 1 mL/min as a standard flow rate for the experiments. The use of higher flow rate was impossible as the generated pressure was too high leading to the disruption of the bonding between chips layers.

Inherently the crucial factor is the contact time and this depends on the flow rate. In the case of 1 mL samples and the flow rate of 1 mL/min within 1 minute, the whole sample will pass through the chip. This is not sufficient to ensure 100% adsorption, thus we decided to perform the back and forward operation, where the direction of the flow rate is changed every 60 s. This means that the same sample is in a dynamic contact with the GO-PDMS chip for a longer time. Thanks to this, a significant improvement on adsorption ability was achieved (Figure 8A). The volume of the sample to be introduced can be tuned, so as to achieve the best preconcentration performance. In that case, the flow direction was changed in the proportional interval of the time, so as to ensure that all the volume will be in contact with a chip (for example, for 2 mL of the sample, a flow direction is changed every 120 s.

4.3.4.2. Desorption

Similarly, like in preliminary experiments, a 0.1 M HCl was chosen for the desorption as well as for the subsequent electrochemical detection. As low concentrated HCl need more time to desorb ions from GO-PDMS surface than 1 M HCl, a dynamic incubation was performed and the time of 30 minutes was applied.

4.3.4.3. Justification of the approach

Square wave anodic stripping voltammetry is a technique used for the detection of heavy metals. This technique includes the preconcentration step itself, as during the deposition step, ions are reduced onto the electrode surface and due to the flow rate, a sample being

in contact with an electrode is consistently renewed. This allows to significantly improve the sensitivity and the limit of the detection but this approach has some limitations. In the case of our electrodes, if the deposition time is longer than 600 s further increase of the signal is not observed anymore. This can result from the electrodes properties and other phenomena, as the level of current is still below the saturation. On the other hand, the use of very long deposition time may reduce the electrodes viability, especially taking into account samples of the increased ionic strength. Due to that, the use of GO-PDMS might be an interesting way to perform preconcentration, as the only limitation is the adsorption capacity, while the other parameters can be tuned (time, flow rate, initial concentration). Both approaches were compared in Figure 8B.
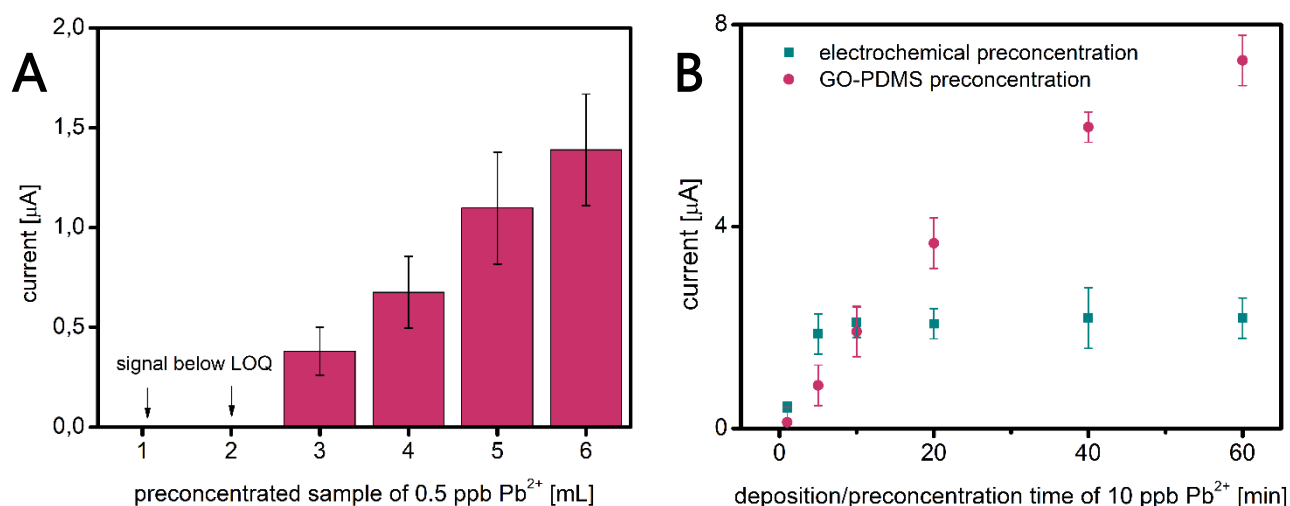
Figure 8 On-chip preconcentration and detection of the Pb(II). A. The effect of the volume to be adsorbed (0.5 ppb Pb^{2+}) using the constant flow rate 1 mL/min and t=30 min; B. Comparison of the electrochemical and GO-based preconcentration of 10 ppb Pb(II). Samples for electrochemical measurement were directly diluted in 0.1 M HCl and measurement was performed with different deposition time (1-60 min) using only a PDMS chip and the flow rate of 1 mL/min. In the case of GO-PDMS experiment in flow was performed as described before using different incubation time in GO-PDMS chip (1-60 min). Afterwards, a desorption and subsequent detection were performed using a standard protocol (1 mL of 0.1 M HCl for 30 min at 1 mL/min).

4.4.   Conclusions

In this work, a versatile LOC platform for heavy metals preconcentration and detection was designed and developed. This is the first report of the application of GO-PDMS composite toward metals adsorption. This composite can be characterized by physical and mechanical properties of PDMS having simultaneously exposed oxygen functional groups originated from GO. This allows performing adsorption of bivalent metals through the mechanism of surface complexation. An opposite process – desorption – occurs in presence of 0.1 M HCl. The same reagent is used for the electrochemical detection, as the device has screen-printed electrodes inbuilt. Thanks to the use of this platform, samples containing Pb^{2+} in the level below the limit of detection (0.5 ppb), can be preconcentrated and detected successfully reaching a current value nearly 30 times higher. Moreover, the platform can be reused for a multiple time and subsequent cycles of adsorption/desorption can be performed without the loss of capacity. PDMS, as well as GO-PDMS, can be very easily adapted to any kind of design of the microfluidic device. This increase the applicability of the presented work in the field of Lab-on-a-chip devices.

Future work should include exhaustive studies about the use of real samples, such as sea or river water, in this device.

4.5.   References

1.   Lopez-Marzo, A.M., et al., *High sensitive gold-nanoparticle based lateral flow Immunodevice for Cd2+ detection in drinking waters*. Biosensors & Bioelectronics, 2013. **47**: p. 190-198.

2.   Lin, Y., et al., *Detection of heavy metal by paper-based microfluidics*. Biosensors & Bioelectronics, 2016. **83**: p. 256-266.

3.   Kalia, K. and S.J.S. Flora, *Strategies for safe and effective therapeutic measures for chronic arsenic and lead poisoning*. Journal of Occupational Health, 2005. **47**(1): p. 1-21.

4.   Barton, J., et al., *Screen-printed electrodes for environmental monitoring of heavy metal ions: a review*. Microchimica Acta, 2016. **183**(2): p. 503-517.

5.   Jiang, X., et al., *Distribution and pollution assessment of heavy metals in surface sediments in the Yellow Sea*. Marine Pollution Bulletin, 2014. **83**(1): p. 366-375.

6.   Gaur, N., et al., *A review with recent advancements on bioremediation-based abolition of heavy metals*. Environmental Science-Processes & Impacts, 2014. **16**(2): p. 180-193.

7.   Bagheri, H., et al., *Preparation and characterization of magnetic nanocomposite of Schiff base/silica/magnetite as a preconcentration phase for the trace determination of heavy metal ions in water, food and biological samples using atomic absorption spectrometry*. Talanta, 2012. **97**: p. 87-95.

8.   Sohrabi, M.R., et al., *Solid phase extraction of Cd(II) and Pb(II) using a magnetic metal-organic framework, and their determination by FAAS*. Microchimica Acta, 2013. **180**(7-8): p. 589-597.

9.   Obiajunwa, E.I., et al., *Characterisation of heavy metal pollutants of soils and sediments around a crude-oil production terminal using EDXRF*. Nuclear Instruments & Methods in Physics Research Section B-Beam Interactions with Materials and Atoms, 2002. **194**(1): p. 61-64.

10.   Djedjibegovic, J., et al., *Contents of cadmium, copper, mercury and lead in fish from the Neretva river (Bosnia and Herzegovina) determined by inductively coupled plasma mass spectrometry (ICP-MS)*. Food Chemistry, 2012. **131**(2): p. 469-476.

11.   Mehta, J., et al., *Progress in the biosensing techniques for trace-level heavy metals*. Biotechnology Advances, 2016. **34**(1): p. 47-60.

12.   Chang, J.B., et al., *Graphene-based sensors for detection of heavy metals in water: a review*. Analytical and Bioanalytical Chemistry, 2014. **406**(16): p. 3957-3975.

13.   Serradell, M., et al., *Mercury-free PSA of heavy metals using graphite-epoxy composite electrodes*. Electroanalysis, 2002. **14**(18): p. 1281-1287.

14.   Aragay, G., et al., *Medium Dependent Dual Turn-On/Turn-Off Fluorescence System for Heavy Metal Ions Sensing*. Journal of Physical Chemistry C, 2012. **116**(2): p. 1987-1994.

15.   Aragay, G. and A. Merkoci, *Nanomaterials application in electrochemical detection of heavy metals*. Electrochimica Acta, 2012. **84**: p. 49-61.

16.   Aragay, G., et al., *Aminopyrazole-Based Ligand Induces Gold Nanoparticle Formation and Remains Available for Heavy Metal Ions Sensing. A Simple "Mix and Detect" Approach*. Langmuir, 2010. **26**(12): p. 10165-10170.

17.   Castaneda, M.T., et al., *Sensitive stripping voltammetry of heavy metals by using a composite sensor based on a built-in bismuth precursor*. Analyst, 2005. **130**(6): p. 971-976.

18.   Carregalo, S., A. Merkoci, and S. Alegret, *Application of graphite-epoxy composite electrodes in differential pulse anodic stripping voltammetry of heavy metals*. Microchimica Acta, 2004. **147**(4): p. 245-251.

19.   Wei, Y., et al., *Application of Nanomaterials Modified Electrode in Detection of Heavy Metal Ions*. Progress in Chemistry, 2012. **24**(1): p. 110-121.

20.   Cadevall, M., J. Ros, and A. Merkoci, *Bismuth nanoparticles integration into heavy metal electrochemical stripping sensor*. Electrophoresis, 2015. **36**(16): p. 1872-1879.

21.   Medina-Sanchez, M., et al., *Eco-friendly electrochemical lab-on-paper for heavy metal detection*. Analytical and Bioanalytical Chemistry, 2015. **407**(28): p. 8445-8449.

22.   Gaya, U.I., E. Otene, and A.H. Abdullah*, Adsorption of aqueous Cd(II) and Pb(II) on activated carbon nanopores prepared by chemical activation of doum palm shell*. Springerplus, 2015. **4**.

23.   Kadirvelu, K., K. Thamaraiselvi, and C. Namasivayam, *Removal of heavy metals from industrial wastewaters by adsorption onto activated carbon prepared from an agricultural solid waste*. Bioresource Technology, 2001. **76**(1): p. 63-65.

24.   Dowlatshahi, S., A.R. Haratinezhad Torbati, and M. Loloei, *Adsorption of copper, lead and cadmium from aqueous solutions by activated carbon prepared from saffron leaves*. Environmental Health Engineering and Management Journal, 2014. **1**(1): p. 37-44.

25.   Tajar, A.F., T. Kaghazchi, and M. Soleimani, *Adsorption of cadmium from aqueous solutions on sulfurized activated carbon prepared from nut shells*. Journal of Hazardous Materials, 2009. **165**(1-3): p. 1159-1164.

26.   Sitko, R., et al., *Adsorption of divalent metal ions from aqueous solutions using graphene oxide*. Dalton Transactions, 2013. **42**(16): p. 5682-5689.

27.   Sitko, R., et al., *Graphene oxide/cellulose membranes in adsorption of divalent metal ions*. Rsc Advances, 2016. **6**(99): p. 96595-96605.

28.   Wu, S.B., et al., *Enhanced adsorption of cadmium ions by 3D sulfonated reduced graphene oxide*. Chemical Engineering Journal, 2015. **262**: p. 1292-1302.

29.   Hallaj, R., et al., *Adsorption of cadmium(II) ions from aqueous solution on exfoliated graphene nanosheets and its determination by flame atomic absorption spectrometry*. Canadian Journal of Chemistry-Revue Canadienne De Chimie, 2014. **92**(1): p. 62-67.

30.   Terrones, M., et al., *Interphases in Graphene Polymer-based Nanocomposites: Achievements and Challenges*. Advanced Materials, 2011. **23**(44): p. 5302-5310.

31.   Zhao, X., et al., *Enhanced Mechanical Properties of Graphene-Based Poly(vinyl alcohol) Composites*. Macromolecules, 2010. **43**(5): p. 2357-2363.

32.   Teng, C.C., et al., *Thermal conductivity and structure of non-covalent functionalized graphene/epoxy composites*. Carbon, 2011. **49**(15): p. 5107-5116.

33.   Shen, B., et al., *Melt Blending In situ Enhances the Interaction between Polystyrene and Graphene through pi-pi Stacking*. Acs Applied Materials & Interfaces, 2011. **3**(8): p. 3103-3109.

34.   Yun, Y.S., et al., *Reinforcing effects of adding alkylated graphene oxide to polypropylene*. Carbon, 2011. **49**(11): p. 3553-3559.

35.   Wang, J.C., et al., *Preparation and Mechanical and Electrical Properties of Graphene Nanosheets-Poly(methyl methacrylate) Nanocomposites via In Situ Suspension Polymerization*. Journal of Applied Polymer Science, 2011. **122**(3): p. 1866-1871.

36.   Koo, M., et al., *Thermo-dependent characteristics of polyimide-graphene composites*. Colloid and Polymer Science, 2011. **289**(13): p. 1503-1509.

37.   Yoonessi, M. and J.R. Gaier, Highly *Conductive Multifunctional Graphene Polycarbonate Nanocomposites*. Acs Nano, 2010. **4**(12): p. 7211-7220.

38.   Sobolewski, P., M. Piwowarczyk, and M. El Fray, *Polymer-Graphene Nanocomposite Materials for Electrochemical Biosensing*. Macromolecular Bioscience, 2016. **16**(7): p. 944-957.

39.   Du, J.H. and H.M. Cheng, *The Fabrication, Properties, and Uses of Graphene/Polymer Composites*. Macromolecular Chemistry and Physics, 2012. **213**(10-11): p. 1060-1077.

40.   Foygel, M., et al., *Theoretical and computational studies of carbon nanotube composites and suspensions: Electrical and thermal conductivity*. Physical Review B, 2005. **71**(10).

41.   Moon, I.K., et al., *Reduced graphene oxide by chemical graphitization*. Nature Communications, 2010. **1**.

42.   Kuilla, T., et al., *Recent advances in graphene based polymer composites*. Progress in Polymer Science, 2010. **35**(11): p. 1350-1375.

43.   Cao, L.L., et al., *Interphase Induced Dynamic Self-Stiffening in Graphene-Based Polydimethylsiloxane Nanocomposites*. Small, 2016. **12**(27): p. 3723-3731.

44.   Yin, Z.Y., et al., *Organic Photovoltaic Devices Using Highly Flexible Reduced Graphene Oxide Films as Transparent Electrodes*. Acs Nano, 2010. **4**(9): p. 5263-5268.

45.   Xu, Y.F., et al., *A Graphene Hybrid Material Covalently Functionalized with Porphyrin: Synthesis and Optical Limiting Property*. Advanced Materials, 2009. **21**(12): p. 1275-+.

46.   Morales-Narvaez, E., et al., *Simple Forster resonance energy transfer evidence for the ultrahigh quantum dot quenching efficiency by graphene oxide compared to other carbon structures*. Carbon, 2012. **50**(8): p. 2987-2993.

47.   Liu, N., et al., *One-step ionic-liquid-assisted electrochemical synthesis of ionic-liquid-functionalized graphene sheets directly from graphite*. Advanced Functional Materials, 2008. **18**(10): p. 1518-1525.

48.   Flory, A.L., T. Ramanathan, and L.C. Brinson, *Physical Aging of Single Wall Carbon Nanotube Polymer Nanocomposites: Effect of Functionalization of the Nanotube on the Enthalpy Relaxation*. Macromolecules, 2010. **43**(9): p. 4247-4252.

49.   Bunch, J.S., et al., *Impermeable atomic membranes from graphene sheets*. Nano Letters, 2008. **8**(8): p. 2458-2462.

50.   Jiang, D.E., V.R. Cooper, and S. Dai, *Porous Graphene as the Ultimate Membrane for Gas Separation*. Nano Letters, 2009. **9**(12): p. 4019-4024.

51.   Arzac, A., et al., *Water-Borne Polymer/Graphene Nanocomposites.* Macromolecular Materials and Engineering, 2017. **302**(1).

52.   Chałupniak, A. and A. Merkoçi, *Toward integrated detection and graphene-based removal of contaminants in a lab-on-a-chip platform*. Nano Research, 2017: p. 1-15.

53.   Zhao, G.X., et al., *Removal of Pb(II) ions from aqueous solutions on few-layered graphene oxide nanosheets*. Dalton Transactions, 2011. **40**(41): p. 10945-10952.

54.   Montón, H., et al., *Rapid on-chip apoptosis assay on human carcinoma cells based on annexin-V/quantum dot probes*. Biosensors and Bioelectronics, 2017. **94**: p. 408-414.

55.   Medina-Sanchez, M., et al., *On-chip electrochemical detection of CdS quantum dots using normal and multiple recycling flow through modes*. Lab on a Chip, 2012. **12**(11): p. 2000-2005.

56.   Fuerstenau, D.W. and K. Osseoasare, *Adsorption of copper, nickel, and cobalt by oxide adsorbents from aqueous ammoniacal solutions*. Journal of Colloid and Interface Science, 1987. **118**(2): p. 524-542.

CHAPTER 5

Concluding remarks

The goal of this PhD thesis was to develop a novel Lab-on-a-chip platform for the detection of hazardous compounds. In Chapter 3 the modular LOC device was developed. The device consists of immunoassay chip, detection chip with the screen-printed electrode and rGO-PDMS chip dedicated for the removal of the hazardous compounds. As a model analyte, polybrominated diphenyl ethers were detected with the low detection limit of 0.018 ppb. Moreover, it was proved that rGO-PDMS can interact with PBDEs molecules via π- π stacking and this can be applied for the removal well as preconcentration. Chapter 4 presents also an electrochemical platform but dedicated to heavy metals. As electrochemical detection of heavy metals is quite challenging, a novel GO-PDMS chip was proposed as a preconcentration platform. In this case, heavy metal ions can be attached to the GO-PDMS thanks to the surface complexation. In presence of the desorption agent, like HCl, a metal displacement occurs, so the process is reversible. Thanks to this approach, it was possible to detect Pb(II) samples of 0.5 ppb, being below the limit of detection of the stripping voltammetry.

As this work is very multidisciplinary, several conclusions and future issues are discussed below.

Lab-on-a-chip allows miniaturization

One of the advantages of the LOCs devices usually pointed out by researchers is miniaturization. Small dimensions of the LOCs devices allow saving reagents that sometimes may be very expensive. On the other hand, the miniaturization of the whole system affects its behavior. One of the common examples is the change of Reynolds number in a microfluidic channel, where the laminar flow is predominant over turbulent flow. Due to that, the occurrence of various (bio)chemical reactions is limited as they depend on diffusion and mass transport. This can be solved playing with the design of the chip, as we proved in Chapter 3 (immunoassay chip) and Chapter 4 (GO-PDMS chip).

Lab-on-a-chip as a simple device as well as professional laboratory equipment

(Bio)sensing devices can be divided into two main groups: the first one is dedicated to in-field applications and usually qualitative measurements, while the second is based on sophisticated and bulky approaches for the fully standardized qualitative analysis. LOCs devices belong to both groups in parallel. Due to miniaturization and automation, they can be employed in the field. For example, the use of portable potentiostat allows performing electrochemical measurements in LOCs device using just Bluetooth connection. Miniaturized pumps and other driving units are also available, so the whole platform (LOC + driving units) do not need to be bulky, as it usually happens in research laboratories so in this case there is no reason for criticism toward Lab-on-a-chips (by calling it "Chips in the lab").

Lab-on-a-chip platforms can be fully automated

An automation of the processes performed in LOCs devices is one of the most promising advantages. Fully automated LOCs are more accurate, well controlled and do not require well-trained personnel to perform an analysis. One of the examples of the full LOC automation is discussed in Annex I. In this approach, a microfluidic system for optical detection of Alzheimer biomarkers is employed. Due to the use of pressure controlling system and a dedicated script, the process is fully automated and a single analysis time is only 10 minutes.

Lab-on-a-chip platforms can benefit from nanomaterials

There are many approaches where nanomaterials are used in LOCs devices, usually as signal transducers, such as QD or AuNP. However, there are a lot of perspectives regarding the use of nanomaterials as the platforms itself. In this work, two novel composites were successfully developed: rGO-PDMS and GO-PDMS. In both cases the role of the microfluidic channel has changed, making it an active environment where the reaction occurs its function is not just that of a channel for reagents passing through. Moreover, the use of nanomaterials can bring novel mechanical, thermal and chemical

properties to LOCs platform. The new properties of LOCs devices enriched with nanomaterials may be of interest to both scientific community and industry.

Lab-on-a-chip for the detection of hazardous compounds

The detection of various hazardous compounds is usually challenging not only due to limited analytical techniques but also due to the toxicity of these analytes itself. Samples handling during the process of the analysis may be dangerous even for a well-trained personnel. PBDEs and heavy metals, analytes evaluated in this work, are able to accumulate in human's body easily and their biodegradation practically does not occur. The use of LOCs devices, where the process involving hazardous compounds is automated and isolated from the environment, significantly reduces the risk of exposure. This also allows working with analytes that require very specific conditions such as temperature, humidity or atmosphere control.

ANNEXES

ANNEX I

Integration and prototyping of Lab-on-a-chip platform for Alzheimer disease biomarkers

6.1.　Introduction

The aim of the Nadine project was to develop various nanotechnology-based systems for the diagnosis of neurodegenerative diseases. This project consisted of two essential parts: the development of the novel nanotechnology-based sensing approaches and development of the prototype devices employing novel sensing approaches (Fig. 1).

The main target analytes of the project were ApoE and Aβ. Apolipoprotein E (ApoE) is encoded by three different alleles: *APOE2*, *APOE3*, *APOE4*. Although ApoE4 is routinely involved in cholesterol metabolism, the level of this protein is also linked to a potential risk of Alzheimer's disease as well as other central nervous system disorders. A significantly different level of ApoE in cerebrospinal fluid (CSF) of Alzheimer patients comparing with the control group is already reported [1, 2].

β-amyloid(1–42) (Aβ-42) is a well-established Alzheimer biomarker. For patients suffering from Alzheimer, a reduced level of Aβ-42 in CSF is observed. Another protein, Aβ(1–40) in a case of Alzheimer's disease is maintained on the same or increased level in CSF. Therefore, some researchers suggest analyzing the ratio between both proteins Aβ42/Aβ40 as a relevant Alzheimer's disease indicator [3, 4].

During the first stage of the project, several approaches of Alzheimer's disease biomarkers were developed including electrochemical Lab-on-a-chip platform, as well as a microarray-based optical platform. Medina-Sánchez developed an electrochemical microfluidic platform for ApoE detection using CdSe@ZnS quantum dots. The limit of detection was estimated at 12.5 ng/mL of ApoE [5]. A novel approach of porous magnetic microspheres for ApoE and Aβ detection was developed by A. de la Escosura-Muñiz et al. Due to a preconcentration effect as well as sensitive detection with AuNP as labels, a very low limit of detection 80 pg/mL and 19 pg/mL for ApoE and Aβ respectively was obtained[6]. Electrochemical detection of Alzheimer's disease biomarkers was also evaluated by L. Rivas et al. who employed Iridium Oxide nanoparticles (IrOX NP) as labels in electrochemical immunoassay. In this case, ApoE was detected with the LOD of 68 ng/mL [7].

Regarding optical detection, Morales-Narvaez et al. presented a versatile microarray platform for ApoE detection using Quantum Dots as labels instead of conventional organic fluorophores. The LOD of ApoE varied from 62-247 pg/mL depending on the condition of the experiments (excitation wavelength)[8]. Another microarray platform was developed by Gagni et al. but using Aß-42 as a target analyte and Si/SiO2 slides as a substrate. In this case, both immunoassay and label-free (Interferometric Reflectance Imaging Sensor) detection were performed obtaining a LOD of 73 pg/mL [9].

For the final prototype device development, the microarray approach was selected as optical detection is well established and high-throughput – this allows to get a significant number of output data by performing just one single test. That is especially important as the device is expected to work mainly with clinical samples, whose volume is always limited and the time of analysis is crucial for having a quick feedback about the patient's situation.
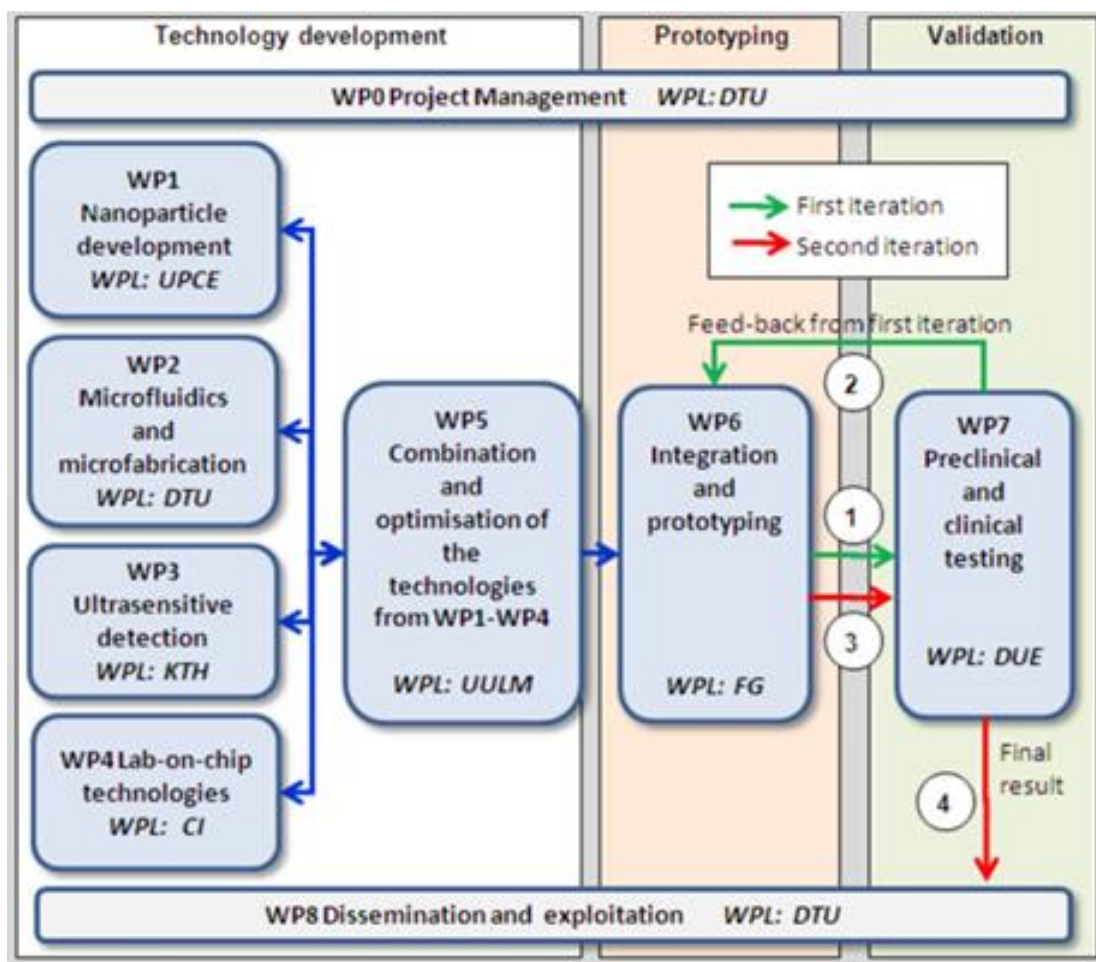
Figure 1 An overview of the Nadine project tasks and work packages.

6.2.   Experimental section

6.2.1. Microarray-based biomarker detection

The method of microarray spotting was previously described and optimized by ICRM [9]. Si/SiO2 slides were coated with copoly(GMA-DMA-MAPS). Afterward, the surface was blocked with ethanolamine (1h) and spotted with antibodies using a non-contact microarray spotter. Slides were incubated overnight in a desiccated atmosphere and afterward directly used in a given experiment. After the assay, slides were detached from the PDMS chip, rinsed twice with miliQ water, dried with nitrogen and scanned using a fluorescence scanner (90% PMT, 90% laser power).

The detection of ApoE is based on a dedicated immunoassay kit (Mabtech). A Monoclonal capture antibody (0.5 mg/mL, E276) is directly spotted on the Silicon slide. A Biotinylated monoclonal detection antibody (E887) is used for target molecule recognition and Cy3-Streptavidin for microarray spots visualization (labeling).

The detection of Aβ-40/Aβ-42 was similarly performed but using Covance antibodies. In order to simulate the environment of a real sample, Aβ standards were dissolved in artificial cerebrospinal fluid (ACSF).

6.2.2. Fabrication of microfluidic chip

The microfluidic chip was fabricated by simple alignment of the spotted Si/SiO$_2$ slide with the PDMS chip (without permanent bonding) obtained using a standard soft-lithography method [10]. A chip was placed within the screw-based holder in order to prevent detachment or any leakage. Microfluidic mold, chip holders, and assisting elements were made of PMMA and fabricated using micro-machining by DTU. Two different designs of the chip were fabricated (Figure 2) and according to that, a different distribution of microarray spots was applied. Using tissue puncher (Unicore, 0.5 mm diameter) holes in the PDMS chip were made providing an inlet and outlet for tubing (Cole-Parmer). Prior to the assay, the PDMS was blocked with 5% BSA solution (Sigma), rinsed in miliQ water and dried with nitrogen.

127

Figure 2 Microfluidic chips for optical detection of biomarkers **A.** The design of 7x7 mm, 200 μm (100 μm) depth, 10 μL volume (a) general scheme of the chip and PMMA mold, (b) PDMS chip (c) distribution of the spotted samples (+) positive control Cy3-Streptavidin, (-) negative control BSA, A – analyte, (d) example of the assayed chip; **B.** The design of 9x3 mm, 100 μm depth, 8 μL volume (a) general scheme of the chip design, (b) example of the assayed chip, (c) microfluidic chip, (d) cross section illustration of the microfluidic chip and silicon slide.

6.2.3. Automation of the method

The aim of this work was to perform a fully automated detection of Alzheimer biomarker using a pressure-control system provided by Fluigent. The system dedicated for this project was combined with commercial units as well as customized solution. The general idea of the operation is based on the application of pressure into reservoirs with liquid, leading to the generation of flow. The use of specific valves and switches allows changing a sample that is injected into the system in a certain moment. Using a microfluidic tubing, the PDMS chip is connected with other parts of the system, so the conditions applied (such as flow rate, sample volume, time) are reproduced in the microfluidic chamber. Due to precise pressure controls, all possible issues such as leakage, and/or pressure loss can be automatically detected. The system consists of the following parts (Fig.3.):

MFCS flow control system – this part is connected to the source of air (pump) and can apply a given pressure. This component directly communicates with the dedicated software MAESFLO.

Reservoirs – samples and buffers are stored in microtubes placed in a special holder where the pressure is applied. The higher pressure applied, the higher flow rate is generated so the sample is passing through the further components of the system.

M-switch – is a bidirectional valve that allows to connect up to 10 different reservoirs. This facilitates the performance of fully automated assays with the use of various samples and buffers, without the need of changing tubes etc.

Flow rate platform – this unit is placed after the M-switch and before the inlet of the microfluidic chip. Thanks to the use of this component an exact flow rate can be measured. This ensures that the pressure applied realizes the flow rate that we want.

MAESFLO – is the dedicated software for the pressure control. Allows to define all the conditions of experiments as well as executing a previously written script so the full assay can be performed automatically.

The M-switch, reservoirs, flow-rate platform are placed onto the one platform where the holder for the microfluidic chip is placed as well. This facilitates the system operation as everything is integrated into one place.
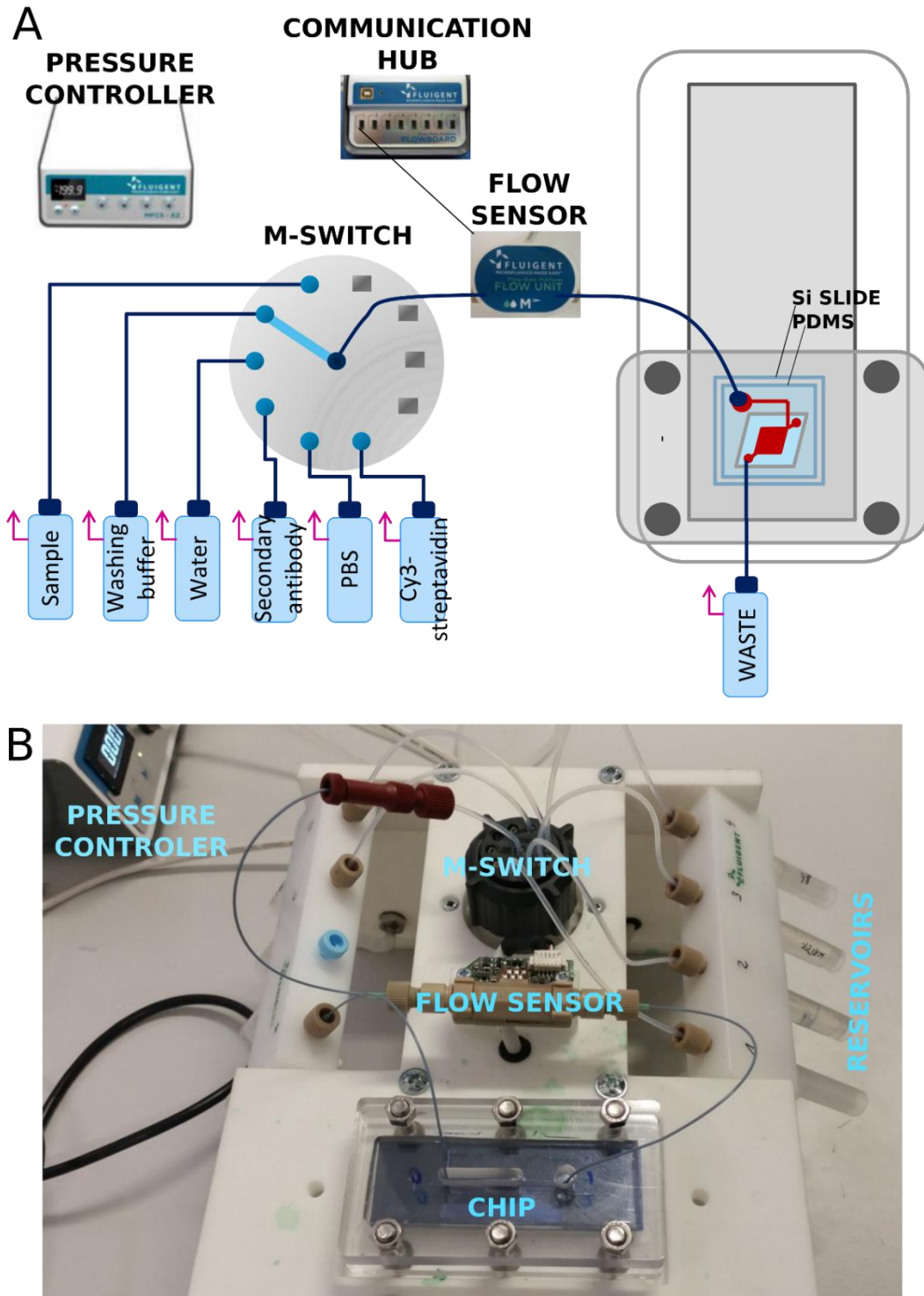

Figure 3 Flow-control system **A**. a general scheme of the system components **B**. final integrated platform.

Preliminary experiments were performed manually – a given pressure (flow rate) was applied with the determined time of the operation as reservoirs were changed manually (refilling or changing samples). The final experiments were performed using a fully automated mode thanks to the script (AutoIt v3 is a freeware BASIC-like scripting language).

```
#include <Group.au3>

Init()

;========================================================================
==
; The Script must start with #include <Group.au3>
; directly followed by Init() sequence
; Do not change this initialization
; Do not change the file Group.au3
; The user scripts start after this commentary sequence
; Case insensitive
;========================================================================
==

;Initialisation

MSw("A",8)
Pressure(); Set all pressures to zero
wait(2); Wait 2 seconds

; Introduction of the sample PORT NUMBER 1

Load("MF_320_FRCM_0351814805934")
;This function loads an identification file that must exist. Note: You must start
with a load function before using any other
;Flow-rate command
MSw("A",9)
wait(2)


Q(1,60);Set the flow-rate channel 1 to 60 µl/min.
V(1,100); until a volume of 100 µL/min

Q(1,10);Set the flow-rate channel 1 to 10 µl/min.
V(1,100); until a volume of 100 µL/min



;Washing step PORT NUMBER 2 with washing buffer

MSw("A",2)
Q(1,60);Set the flow-rate channel 1 to 60 µl/min.
V(1,100); until a volume of 100 µL/min

;Washing step PORT NUMBER 3 with water

MSw("A",3)
Q(1,60);Set the flow-rate channel 1 to 60 µl/min.
V(1,100) ; until a volume of 100 µL/min

;Introduction of the secondary antibody PORT NUMBER 4 with antibody solution

MSw("A",4)
Q(1,60);Set the flow-rate channel 1 to 60 µl/min.
V(1,100); until a volume of 100 µL/min
```

131

```
Q(1,10);Set the flow-rate channel 1 to 10 µl/min.
V(1,100); until a volume of 100 µL/min

;Washing step PORT NUMBER 5 with PBS

MSw("A",5)
Q(1,60);Set the flow-rate channel 1 to 60 µl/min.
V(1,100); until a volume of 100 µL/min

MSw("A",3)
Q(1,60);Set the flow-rate channel 1 to 60 µl/min.
V(1,100); until a volume of 100 µL/min

;LABELING WITH CY3 PORT NUMBER 6

MSw("A",6)
Q(1, 60);Set the flow-rate channel 1 to -60 µl/min.
V(1, 100); until a volume of -50 µL/min

Q(1, 10);Set the flow-rate channel 1 to -60 µl/min.
V(1, 100); until a volume of -50 µL/min

;Washing step PORT NUMBER 5 with PBS

MSw("A",5)
Q(1,60);Set the flow-rate channel 1 to 60 µl/min.
V(1,100); until a volume of 100 µL/min

MSw("A",3)
Q(1,60);Set the flow-rate channel 1 to 60 µl/min.
V(1,100); until a volume of 100 µL/min

P(1,0) ;Set the pressure to zero
P(2,0)
```

The optimization of the assay was performed on several factors such as optimal flow rate, samples volume as well as pressure direction (negative or positive).

6.3.   Results and discussion

6.3.1. Microfluidic chip

Two different designs of microfluidic chips were compared. In both cases, it was observed that the flow rate is a major factor affecting the operation in the microfluidic chip. When the flow rate was relatively low, the chamber was not fully filled with sample and the liquid was just passing through the outer walls of the chip. That means the majority of the microarray spots were not immersed in the solution containing a given reagents. The use of higher flow rate, such as >50 µL/min allows the chamber to be filled properly and cover all the spots in liquid. As a compromise, we found that the optimal solution is to run the process with the high flow rate in order to fill in the chamber and then decrease it so as to

132

slow down the reaction and support the mass transport. An example of the effect of the flow rate is shown in Fig. 4.
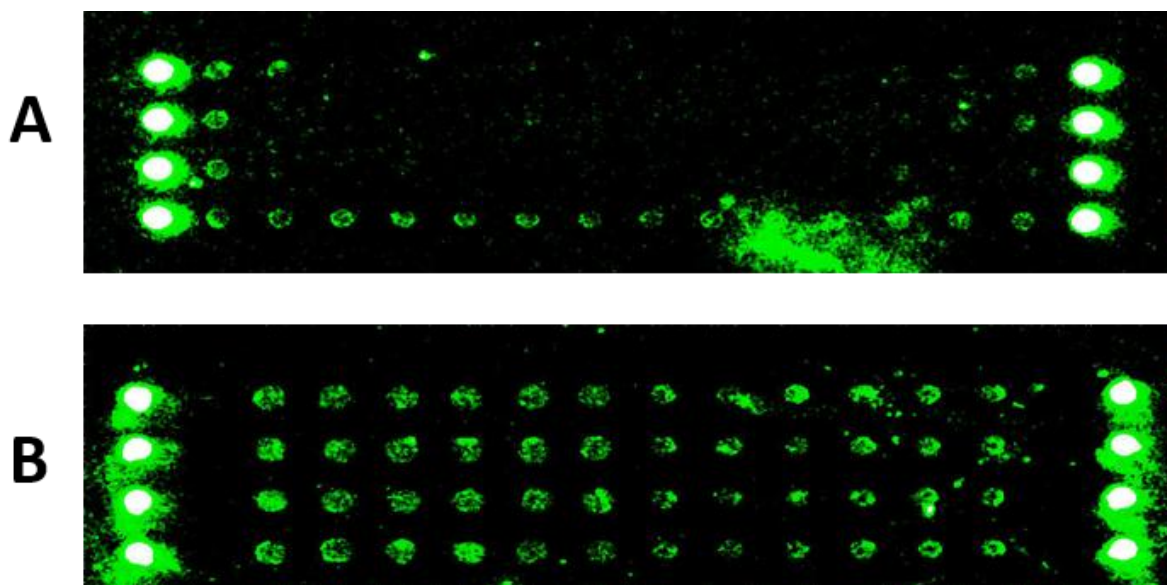
Figure 4 The effect of flow rate on signal intensity **A.** 10 μL/min during incubation with 100 ng/mL Aß-42 (100 μL volume); **B.** 50 μL Aß-42 with the flow rate 60 μL/min and 50 μL with 10 μL/min.

Design A (Fig.2A) was fabricated in two variants: with 100 μm and 200 μm depth respectively. In the case of 200 μm, some problems with chamber collapsing as well as a homogenous distribution of the liquid flow were observed. The problem of the collapse was solved thanks to the use of the thinner chip of 100 μm but in this case, a very low sensitivity was observed. Probably due to the problems with mass transport all the molecules are either adsorbed to PDMS layer or just pass through the chamber without interacting.

Regarding design B (Fig.2B), where the chamber depth is 100 μm and the volume is 8 μL, the general performance is much better, although the PDMS need to be prepared with care in order to ensure the good alignment of the chip to the Si slide. Thus, this design was selected for upcoming experiments.

6.3.2. Microarray detection of ApoE

ApoE was considered a main reference target molecule in a device development process due to a well-established immunoassay as well as the stability of the analyte. However, the Aβ-42 is considered the most relevant Alzheimer biomarker, we focused our experiments on Aβ-40 due to the variable quality of antibodies for Aβ-42.
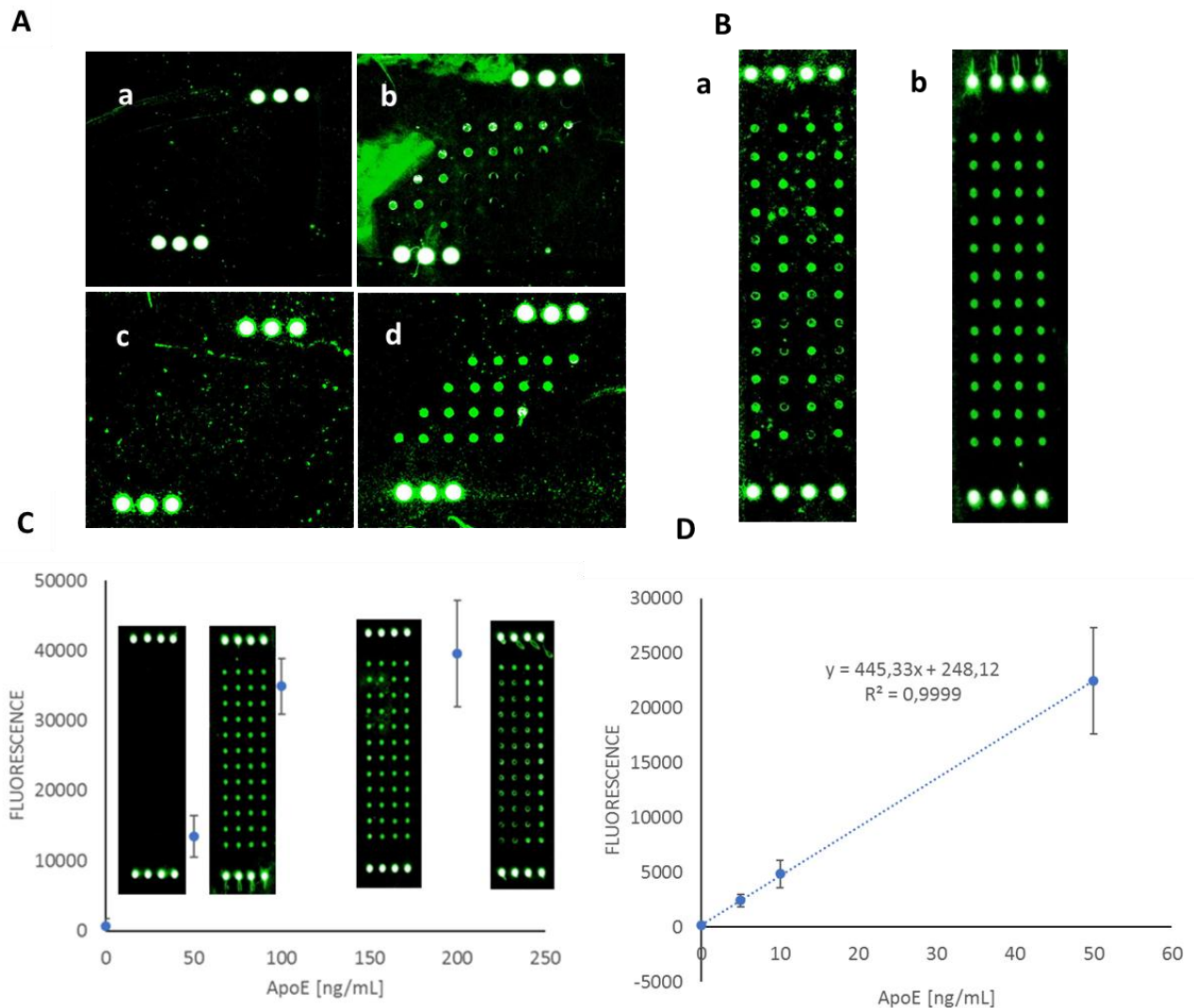
Figure 5 Selected results of ApoE detecion A. preliminary comparison between (a) 0 ng/ml, (b) 100 ng/ml in dynamic conditions (microfluidic chip) and (c) 0 ng/ml, (d) 100 ng/ml in static conditions; B. 50 ng/ml incubated in (a) 60 μL/min standard flow, (b) 60 μL/min back and flow; C. ApoE detection in the range of 0-200 ng/ml; D. ApoE detection in the range of 0-50 ng/ml.

During the preliminary experiments it was shown that despite the use of a highly concentrated analyte, the detection in the microfluidic chip was unsuccessful (Fig.5A). Due to that, the microfluidic chip was re-designed but the results were still not satisfactory. Taking advantage of the flexible microfluidic system, where the flow can operate in

different directions, a protocol including back and forward incubation was applied (Fig.5B). This means that the sample containing analyte is introduced from the inlet to the outlet but then the direction of the pressure is changing so the flow is reversed. This cycle is respectively repeated, allowing the mass transport to increase as the same amount of sample is in dynamic contact with microarray spots for a relatively longer time. The other steps such as incubation with antibodies are performed following the standard protocol.

The final protocol of ApoE detection was as follows: sample 100 μL is injected and 80 μL is moved back and forward (60 μL/min, -60 μL/min); washing buffer: 100 μL (60 μL/min); water: 100 μL (60 μL/min); m-Ab-Biotin to ApoE E887: 100 μL (60 μL/min); PBS 100 μL (60 μL/min); water: 100 μL (60 μL/min); Cy3-SA: 100 μL (60 μL/min); PBS: 100 μL (60 μL/min); water: 100 μL (60 μL/min); drying and detection.

The detection performance depends largely on the range of concentration. As can be seen in Fig.5C, ApoE range from 0-200 ng/mL shows a non-linear response as for the concentration higher than 100 ng/mL the saturation of the signal is observed. The assay performed following the same protocol but within the range 0-50 ng/ml shows good linearity (R^2=0,999) and the limit of detection as low as 1.67 ng/ml.

6.3.3. Microarray detection of beta-amyloid (Aβ-40 and Aβ-42)

Aβ-40 was successfully detected using an automated microfluidic system in the range 1-150 ng/mL with the limit of detection (LOD) of 9.23 ng/mL. Moreover, measurements performed with the use of real CSF (provided by UULM) showed a good recovery of the sample spiked with 25 ng/mL Aβ-40.

During the optimization different parameters were investigated including the flow rate, the direction of the pressure as well as incubation time. Unlike ApoE, Aβ-40 could not be detected using "back and forward" mode as instead of signal increase an aggregation of the protein is observed (data not shown). Taking into account the fragility of Aβ protein, the goal was to obtain as quick an assay as possible. The final detection protocol was as follows:

135

Introduction of the sample: a) 50 µl, 60 µl/min b) 50 µl, 10 µl/min; Washing buffer: 100 µl, 50 µl/min; Water: 100 µl, 50 µl/min; Antibodies: 100 µl, 50 µl/min; Washing PBS: 100 µl, 50 µl/min; Water: 100 µl, 50 µl/min; Cy3-Streptavidin: 100 µl, 50 µl/min; Washing PBS: 100 µl, 50 µl/min; Water: 100 µl, 50 µl/min. That means the total analysis time is less than 10 minutes, making a microfluidic approach very competitive compared to the static incubation method, where 1-2 hours of microarray slide incubation with a sample is necessary to obtain similar signal intensity. The short time of the analysis facilitates working with sensitive analytes and antibodies, as they are not affected by external factors such as temperature.

The presented microfluidic system is based on a closed circuit of the flow, where the samples are passed through the system by applying pressure. This allows the assay performance to be fully automated (like in our case by executing a script) as well as protecting the reagents and analytes from possible contaminations and interaction with the environment (dust, particles, bacteria etc.).
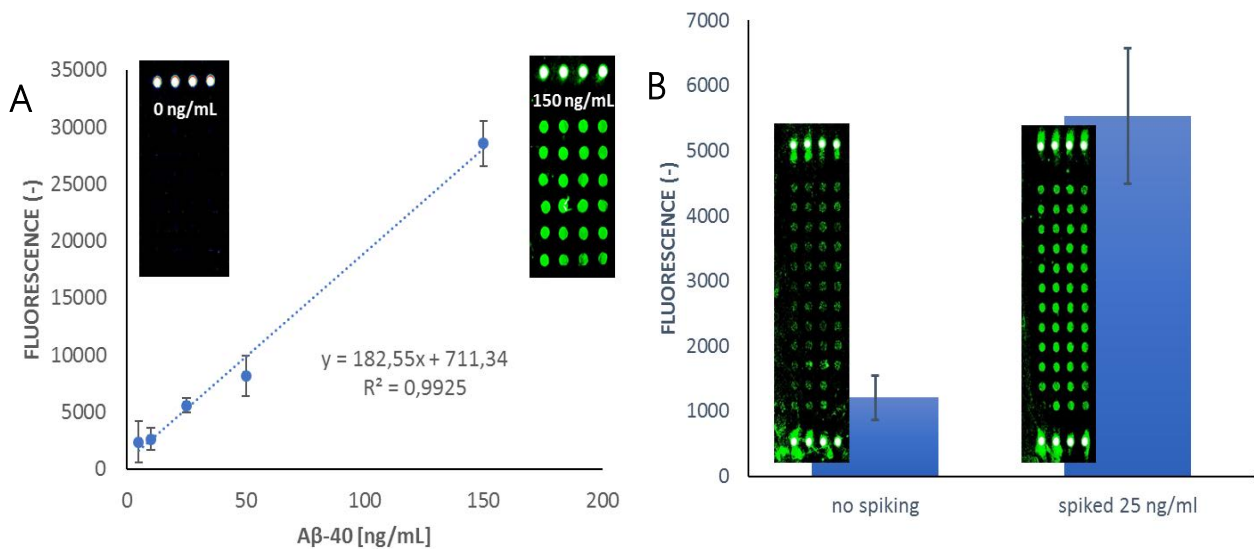
Figure 6 Aβ-40 detection in automated microfluidic system **A.** calibration curve **B.** example of clinical CSF sample spiked with 25 ng/mL Aβ-40.

6.4.   Conclusions

The aim of this work was to develop an automated Lab-on-a-Chip platform for the detection of Alzheimer's disease biomarkers, such as ApoE (Apolipoprotein E) and Aβ (beta-amyloid).

The major requirements for this kind of devices are high automation level, reproducibility, sensitivity as well as ability to operate with the use of real clinical samples. The Optimization of the microfluidic chip design, as well as assay's condition, allowed detecting ApoE and Aβ with the LOD of 1.67 ng/mL and 9.23 ng/mL respectively.

Even though the LOD obtained is not significantly lower than already reported, the use of presented systems brings/offers some significant advantages. Compared to detection performed in batch, only 10 minutes is necessary to perform a single test (2h in static detection). The use of microfluidics cause much lower reagents use. This is especially important taking into account the clinical application of the device, where samples from patients are available in very limited quantities and the detection of low-concentrated biomarkers requires expensive antibodies.

We also proved that the analysis can be fully automated, substantially reducing the need for a qualified protocol. An automated script is able to drive the whole process starting from the incubation with analyte up to labeling with the fluorophore.

Although such results are promising, further work would be necessary for the complete validation of the presented system and its possible application in the clinical area.

6.5.   References

1.   Kim, J., H. Yoon, and J. Basak, *Apolipoprotein E in Synaptic Plasticity and Alzheimer's Disease: Potential Cellular and Molecular Mechanisms.* Molecules and Cells, 2014. **37**(11): p. 767-776.

2.   Takeda, M., et al., *Apolipoprotein E and central nervous system disorders: Reviews of clinical findings.* Psychiatry and Clinical Neurosciences, 2010. **64**(6): p. 592-607.

3.   Humpel, C., *Identifying and validating biomarkers for Alzheimer's disease.* Trends in Biotechnology, 2011. **29**(1): p. 26-32.

4.   Lui, J.K., et al., *Plasma Amyloid-beta as a Biomarker in Alzheimer's Disease: The AIBL Study of Aging.* Journal of Alzheimers Disease, 2010. **20**(4): p. 1233-1242.

5.   Medina-Sanchez, M., et al., *On-chip magneto-immunoassay for Alzheimer's biomarker electrochemical detection by using quantum dots as labels.* Biosensors & Bioelectronics, 2014. **54**: p. 279-284.

6.   de la Escosura-Muniz, A., et al., *Alzheimer's disease biomarkers detection in human samples by efficient capturing through porous magnetic microspheres and labelling with electrocatalytic gold nanoparticles.* Biosensors & Bioelectronics, 2015. **67**: p. 162-169.

7.   Rivas, L., et al., *Alzheimer Disease Biomarker Detection Through Electrocatalytic Water Oxidation Induced by Iridium Oxide Nanoparticles.* Electroanalysis, 2014. **26**(6): p. 1287-1294.

8.   Morales-Narvaez, E., et al., *Signal Enhancement in Antibody Microarrays Using Quantum Dots Nanocrystals: Application to Potential Alzheimer's Disease Biomarker Screening.* Analytical Chemistry, 2012. **84**(15): p. 6821-6827.

9.   Gagni, P., et al., *Development of a high-sensitivity immunoassay for amyloid-beta 1-42 using a silicon microarray platform.* Biosensors & Bioelectronics, 2013. **47**: p. 490-495.

10.	Xia, Y.N. and G.M. Whitesides, *Soft lithography*. Annual Review of Materials Science, 1998. **28**: p. 153-184.

ANNEX II. EVALUATION OF THE DETECTION STRATEGIES FOR PBDE AND GLYPHOSATE..

ANNEX II

Evaluation of the detection strategies for PBDE and Glyphosate

7.1. Introduction

The quality of the coastal water is a good indicator of the environment condition in general. Coastal water poses a unique ecosystem in which chronic or acute pollution caused by anthropogenic factors affect the local fauna as well as flora. In order to respond to xenobiotics, organisms living at the bottom of the ocean can burrow or develop physiological strategies to cope with their sublethal effects. Therefore, pollution of coastal water has a negative impact on the environment, human health, and economy [1, 2].

For instance, The Mediterranean can be considered as one of the richest regions of Europe, in terms of the diversity of marine species, predominant by algae and magnoliophyte. They play a key role in a primary production, a source of food and oxygen, sediment stabilization and habitats. Unfortunately, an advanced regression or functional change of these coastal ecosystems can be observed. The Mediterranean area, as a relatively small and closed one, cannot perform self-counterbalance, as it usually happens for instance in oceans. That means that the relatively low level of contamination can already cause major problems [3-6].

Despite the having know-how of different hazardous substances monitoring, coastal waters remain poorly assessed comparing to terrestrial areas. There are several factors making coastal water monitoring more demanding. Checkpoints of water monitoring are located far from urbanized zones, due to which a handmade analysis and sample collection is practically impossible. Thus, water monitoring requires full automation regarding analysis performance, as well as data transmission. Taking into account the water currents, the area of interest may change from time to time, therefore being repositioned [7, 8]. This means that the most promising solutions are based on in-situ detection. The main advantage of this approach is the reduced time of analysis, without the need for special bottles or sample transportation. Moreover, there is a lower risk of contamination or degradation [7, 8].

The main goal of the SMS project is to deliver a novel automated networked system able to perform real-time in situ monitoring of marine water chemicals and ecological status in

coastal areas. In order to fulfill these requirements, a modular apparatus will be developed.

This device will integrate several functions such as water sampling, preconcentration, target analyte detection and data acquisition. Thus, the project is divided into 3 main sections: sensor development; sensor integration; laboratory and in-field validation (Figure 1.).

Among analytes to be detected, there are several groups of compounds both of natural and anthropogenic origin (Figure 2.). As regards algal toxins, TBT, Diuron and PBDE the required limit of detection is in the range of ng/L (0.001 ppb). Regarding Sulphonamides it is about 5 ng/L (0.005 ppb).

Out target analytes were PBDE, Diuron, TBT, and Glyphosate. Although each of them belongs to different classes of chemical, they can be characterized as small molecules. This significantly affects the possible strategies of the sensor's development. For example, it is impossible to develop a sandwich immunoassay, one of the most popular formats of a biosensor. This is because such molecules are too small to let both capture and detection antibody bind to them. This will lead to steric conflict[9]. Similar challenges need to be taken into account when gene-based, aptamer sensors are developed.

Although some chemical compounds cannot be detected by means of immunoassays or any direct assays, they can be measured by using some specific reaction like enzymatic activity etc. Neither of those analytes has this ability. Some of them are reported to work as enzyme inhibitors [10] but such types of sensors are not specific enough, also its performance depends largely on the type of sample, pH, ionic strength and the presence of certain ions.

144
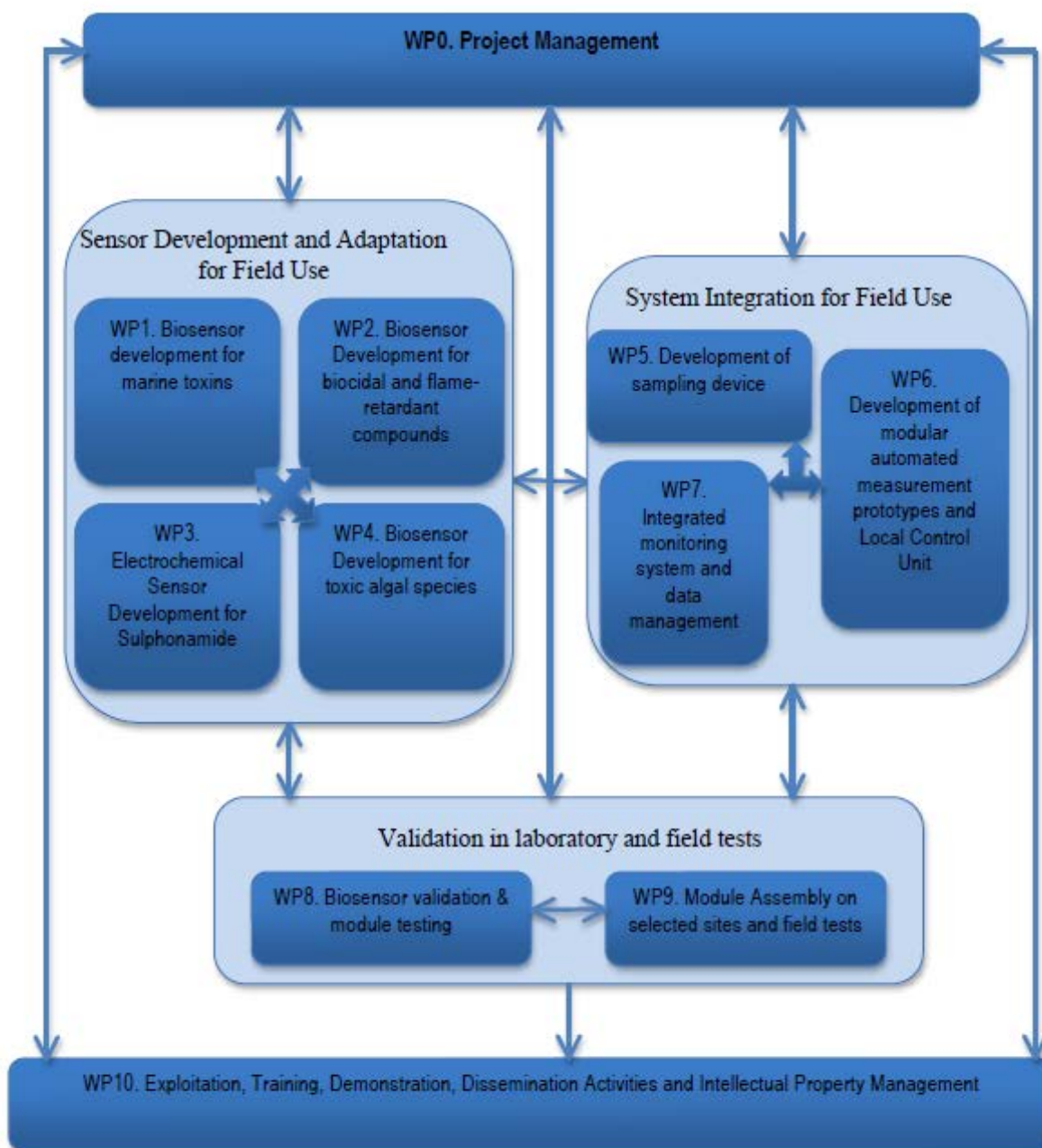
Figure 1 PERT diagram of the SMS project.
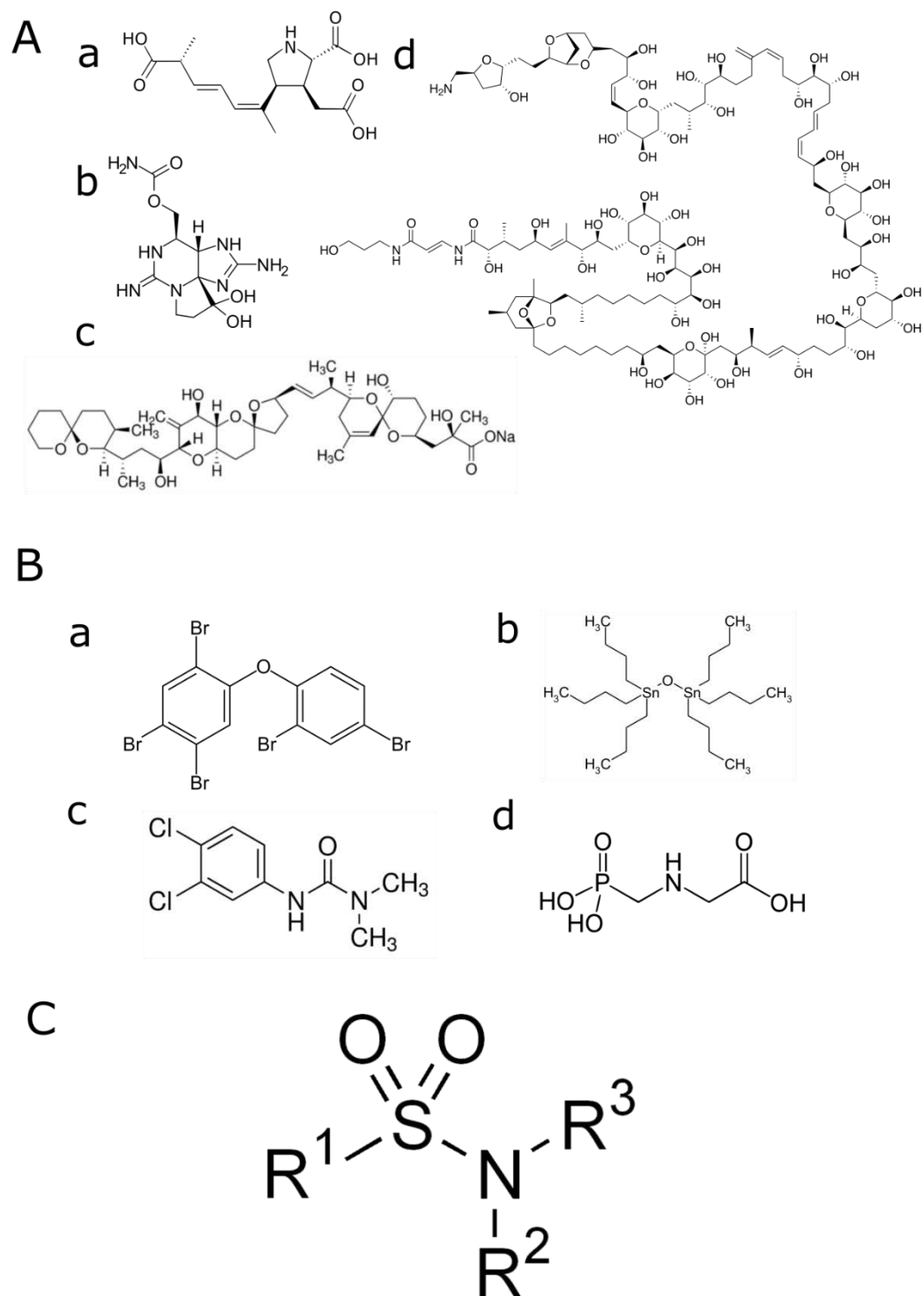
Figure 2 Target analytes for SMS project. **A.** Algal toxin (a) Domoic acid; (b) Saxitoxin; (c) Okadaic acid; (d) Palytoxin; **B.** Pesticides, herbicides and flame retardants (a) Pentabromodiphenyl ether; (b) Tributyltin; (c) Diuron; (d) Glyphosate; **C.** Sulphonamides.

Another common approach is the electrochemical detection, either by using an electroactive label [11] or taking into account electroactive properties itself. Unfortunately, none of those compounds are electroactive. They are also too small to be applied in Label-free impedance biosensors (where the change of mass represents the presence of the analyte). [12].

Due to the above-mentioned reasons, it was impossible to develop a fully novel approach for target analytes recognition. Thus, we based ourselves on commercial immunoassays kits for such analytes like PBDE and Glyphosate. Those kits, based on competitive immunoassay, consist of antibody against target molecule that can bind either to analyte or detection probe that is HRP conjugated with the analyte analog.

In this work a full evaluation of those kits was performed, including analysis of real samples (seawater). Taking into account that the final application of this detection method occurs in the flow, additional experiments regarding compatibility with various materials were performed.

7.2.   PBDE competitive immunoassay

The polybrominated diphenyl ether (PBDE) kit (PN 500090) provided by Abraxis is an immunoassay based on anti-PBDE antibodies coupled to magnetic beads. As in the competitive assay, magnetic beads are incubated both with a sample containing PBDE (or blank) and HRP-PBDE (Fig.3). Enzyme conjugate (HRP-PBDE) is used as a probe due to its ability to bind PBDE-specific antibodies as well as producing a reporting signals (catalysis of reaction leading to the synthesis of a colorful product, Fig.4). The intensity of the color can be measured by using any spectrophotometer device capable of reading the wavelength of 450 nm. The signal intensity is proportional to the concentration of HRP-PBDE and inversely proportional to the PBDE concentration.
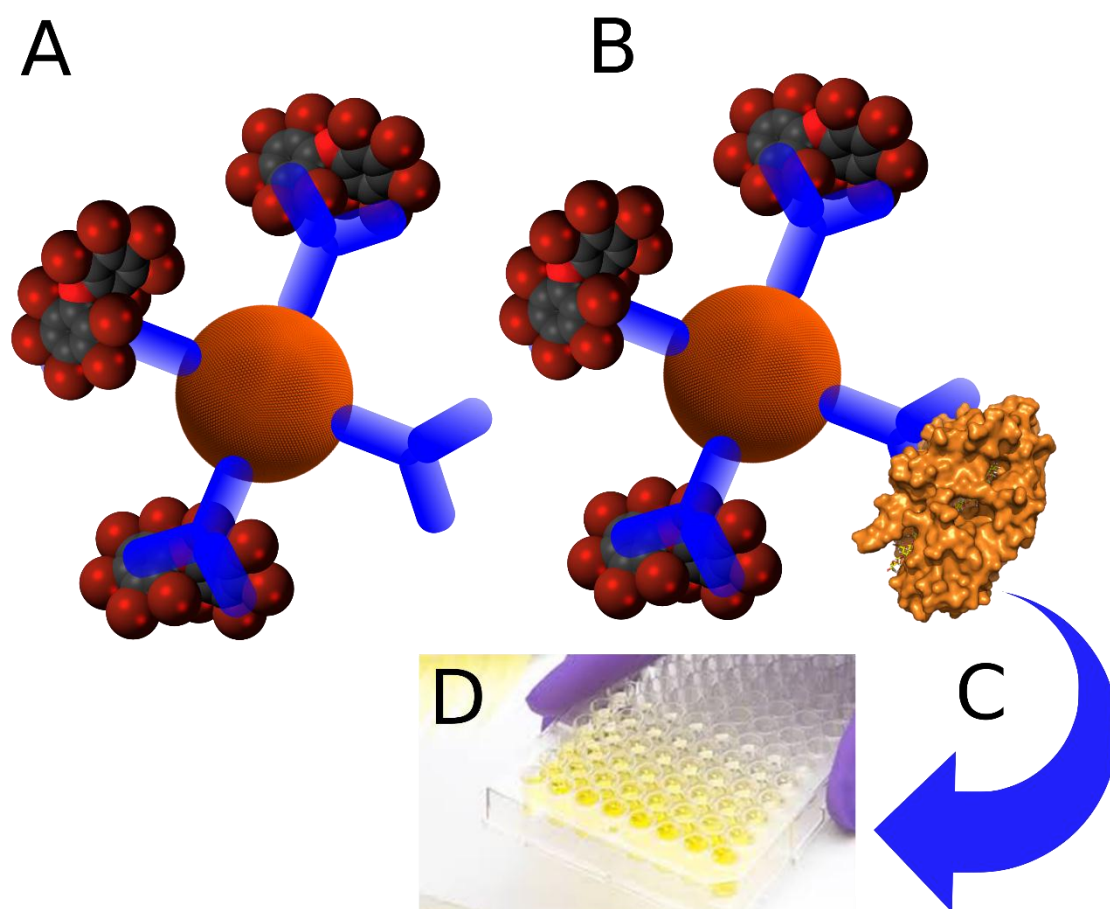
Figure 3 Sensing principle of Abraxis colorimetric test for PBDE detection. **A.** PBDE molecules bind to anti-PBDE antibody coupled to magnetic beads; **B.** HRP-PBDE molecules bind to available anti-PBDE anitbody; **C.** HRP catalyzes enzymatic reaction leading to the formation of (**D.**) yellow product which absorbance is inversely proportional to the PBDE concentration.

The detection kit can be used for samples diluted in various buffers, is the best one being a miliQ water supplemented with 10% of methanol. The presence of methanol facilitates solubility of PBDE but is still low enough so as to not affect immunoassay, stability of proteins etc.

$$\text{TMB}_{red} + \text{H}_2\text{O}_2 \xrightarrow{\text{Horseradish peroxidase}} \text{TMB}_{ox} + 2\,\text{H}_2\text{O}_2$$

(colourless)   (blue)
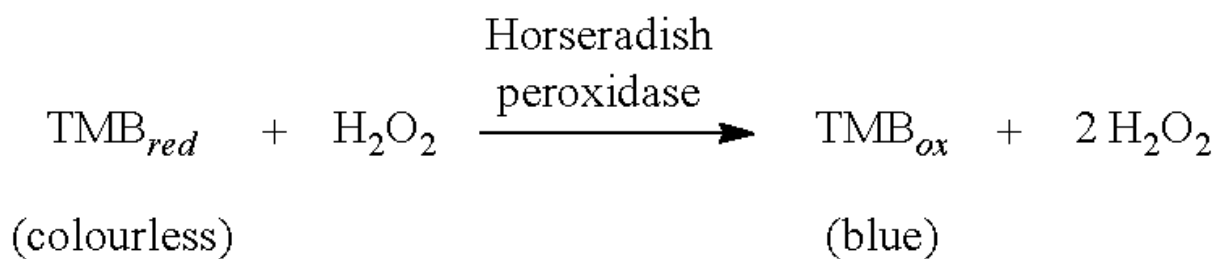
Figure 4 Colorimetric reaction where HRP-PBDE catalyses the oxidation of TMB (3,3',5,5'-Tetramethylbenzidine).

7.2.1. Materials and reagents

The kit contains the following materials:

1. PBDE Antibody Coupled with Paramagnetic Particles - The PBDE antibody (rabbit anti-PBDE) is covalently bound to paramagnetic particles, which are suspended in buffered saline containing preservative and stabilizers. 100 test kit: one 60 mL vial

2. PBDE Enzyme Conjugate - The horseradish peroxidase (HRP) labelled PBDE analog is diluted

in buffered saline containing preservative and stabilizers. 100 test kit: one 30 mL vial

3. PBDE Standards - Five concentrations (0.025, 0.05, 0.1, 0.5, 1.0 ppb) of PBDE Congener 47 in a methanolic solution with preservative and stabilizers. Each vial contains 2.0 mL.

4. Control - A concentration (approximately 0.25 ppb) of PBDE in a methanolic solution containing preservative and stabilizers. A 2.0 mL volume is supplied in one vial.

5. Diluent/Zero Standard - A methanolic solution containing preservative and stabilizers without any detectable PBDE. 100 test kit: one 35 mL vial.

6. Color Solution - A solution of hydrogen peroxide and 3,3',5,5'-tetramethylbenzidine in an organic base. 100 test kit: one 65 mL vial.

7. Stopping Solution - A solution of diluted sulphuric acid (0.5%). 100 test kit: one 60 mL vial

8. Washing Solution T - Preserved deionized water with surfactants. 100 test kit: one 250 mL vial.

9. Test Tubes - Glass tubes (36) are packed in a box. 100 test kit: three 36 tube boxes.

It is worthy to mention that the magnetic particles can be freely preconcentrated/diluted and used in the desired ratio after optimization. PBDE standards can be replaced with any other standards of PBDE congener 47, but they should be validated in comparison to

those provided with the kit. The stopping solution can be replaced with any other sulphuric acid (0.5%).

The colour solution can be replaced with any other TMB/H2O2 reagent used for HRP-based ELISA and similar tests.

The test tubes can be replaced by any other tubes/eppendorf of the desired volume. However, there are some limitations related to the absorption of PBDE by the tubes' walls.

7.2.2. Detection procedure

1. Add 250 μL of the appropriate standard, control, or sample.

2. Mix the PBDE Antibody Coupled Paramagnetic Particles thoroughly and add 500 μL to each tube.

3. Vortex for 1 to 2 seconds minimizing foaming.

4. Incubate for 20 minutes at room temperature.

5. Add 250 μL of PBDE Enzyme Conjugate to each tube.

6. Vortex for 1 to 2 seconds minimizing foaming.

7. Incubate for 20 minutes at room temperature

8. Separate in the Magnetic Separation Rack for two (2) minutes.

9. Decant and gently blot all the tubes briefly in a consistent

manner.

10. Add 1 mL of Washing Solution T to each tube and vortex tubes for 1-2 seconds. Return the tubes and allow them to remain in the magnetic separation unit for two (2) minutes.

11. Decant and gently blot all tubes briefly in a consistent manner.

12. Repeat Steps 10 and 11.

13. Remove the rack from the separator and add 500 µL of Color Solution to each tube.

14. Vortex for 1 to 2 seconds minimizing foaming.

15. Incubate for 20 minutes at room temperature.

16. Add 500 µL of Stopping Solution to each tube.

17. Add 1 mL Washing Solution to a clean test tube. Use as blank in Step 17.

18. Read results at 450 nm within 15 minutes after adding the Stopping Solution.

7.2.3. Remarks

Depending on the type of reader used, absorbance measurements can be performed in cuvette or microplates. 96-well microplate is the simplest and easiest approach. From the final sample of 1000 µL, 300 µL is transferred to a well (3 repetitions) and measured all together.

We have observed, that the volumes of each reagents can be tuned but the volume ratio between them must be kept as follows

Reagents	Volume ratio (-)
Magnetics beads	2
PBDE standard/sample	1
HRP-PBDE	1
Colour solution	2
Stopping solution	2
Washing buffer	4

From our observation, the limit of scaling down the assay is 100 µL of Magnetic beads/PBDE sample (instead of 250 µL). Below this volume we have observed that

sensitivity of the assay is slightly reduced, however, it still works. Moreover, if this assay is adjusted to be used in the flow system, different volumes and different ratios can probably be applied.

7.2.4. Selected results

Examples of calibration curves obtained by means of standards provided with the kit are shown below (Fig.6). Values obtained from spectrophotometer are normalized by dividing them by the absorbance of blank (0 ppb solution). Then, the logarithm, both of the concentration and normalized absorbance, is calculated in order to plot the calibration curve ($\log 10(A/A0)$ and $\log 10$(concentration)). This operation is necessary because the dependence between absorbance change and concentration is not linear. The kit includes several sheets of calibration curve templates with a logarithmic scale, but they are not as useful as they need to be filled in manually. A detailed description of data analysis can be found in the manual of this kit.

We performed several tests comparing standard solutions provided by Abraxis and standards prepared by ourselves from concentrated stock solution (1000 ppm, Accustandard, diluted in ethanol). We have observed that Accustandard samples show slightly better reproducibility and sensitivity in comparison to Abraxis standards. As Abraxis standards are provided as ready-to-use solutions, they may lose some activity with time, while samples from Accustandard of the desired concentration are prepared prior to use.
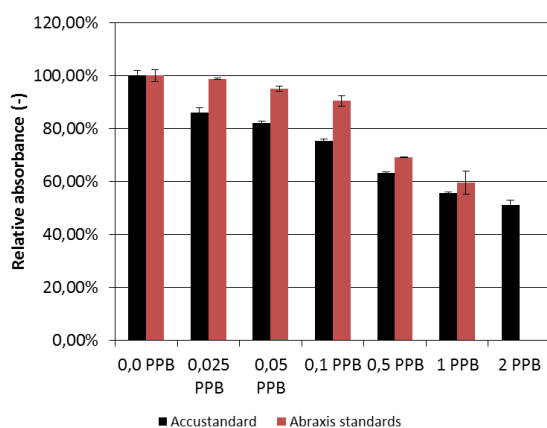
Figure 5 Absorbance (450 nm) of samples (3 repetitions each) containing different amounts of PBDE. Standards from Abraxis and Accustandard were compared. Both experiments were performed in the same conditions.
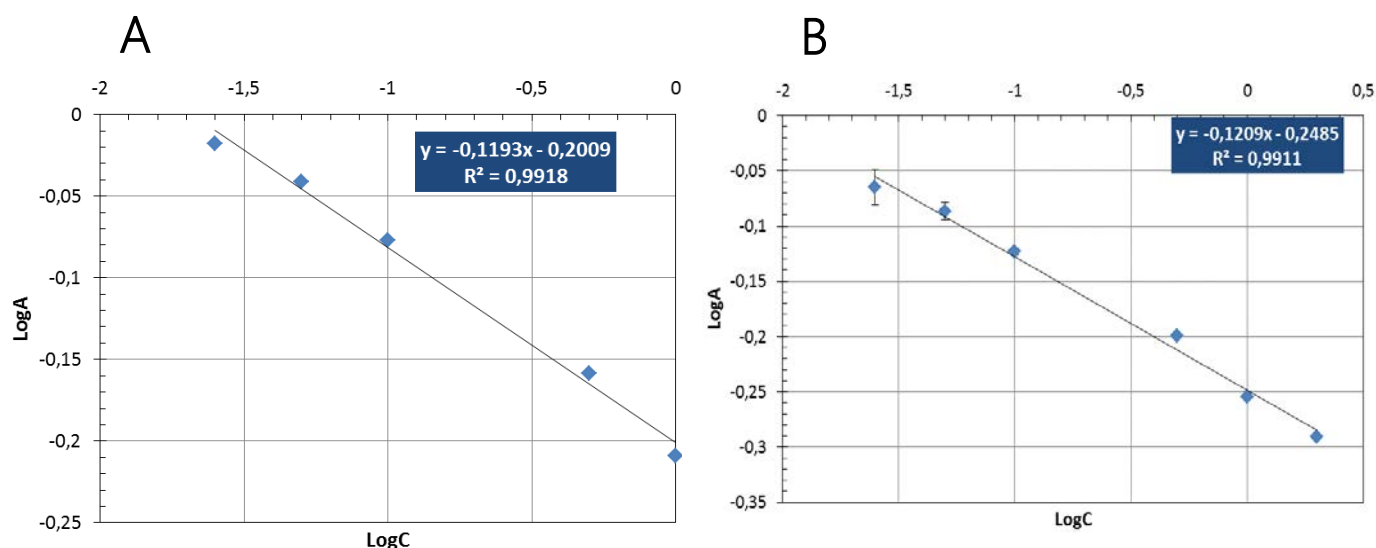
Figure 6 Calibration curves for PBDE obtained using **A.** Abraxis standard solution; **B.** Accustandard standard solution.

According to our experience, this kit shows good reproducibility and a relatively low standard deviation between each repetition. The critical point of the assay is the magnetic beads separation, as due to the lack of accuracy, some particles can be accidentally removed, leading to a decrease of the final signal. Probably, in the automated flow system, this risk can be significantly reduced.

The Limit of detection (LOD) is expressed as a concentration assigned to a relative absorbance (A/A0) of 90%. Abraxis claims that the LOD should be around 0.017 ppb. In our case, LOD is slightly higher and equal to 0.021 ppb.

LOD was obtained from the calibration curve as follows:

$y = ax + b$

$\log(A/A0) = a\log C + b$

$\log C = [\log(A/A0) - b]/a$

$\log C = [\log(90\%) + 0.2485]/-0.1209$

$\log C = -1.67694$

$C = 0.021$ ppb

7.2.5. Detection of PBDE in seawater

This kit is dedicated to various types of samples. Thus, the detection of PBDE in seawater is also possible. We performed several measurements in order to examine it (Figure 7).

Seawater samples were collected from the Barcelona coast. The pH of the collected seawater was around 6.5-7.0. The Seawater was immediately mixed with HPLC grade methanol (1:1 vol. ratio). To avoid the presence of particles, the samples were filtrated through a 0.2 µm syringe filter. An immunoassay was performed promptly after samples preparation. The seawater was spiked with PBDE samples so as to have the following expected concentrations: 0.0, 0.5, 1.0 ppb.

The recovery of PBDE was calculated as a ratio of mean absorbance of spiked samples to standard samples of the same desired concentration (all measurements performed in parallel). We can observe that there is an increase in the recovery with the concentration of the spiked PBDE. This can be related to the presence of some low-concentrated PBDE traces (or other compounds that interact) in those samples.

Conc.	standard solution		seawater		Recovery
	Abs. (mean)	RSD%	Abs. (mean)	RSD%	
0,0 ppb	0,20553333	1,86%	0,19566667	2,27%	95,20%
0,5 ppb	0,12991833	0,31%	0,12908333	4,98%	99,36%
1,0 ppb	0,11436667	0,33%	0,11601667	2,73%	101,44%
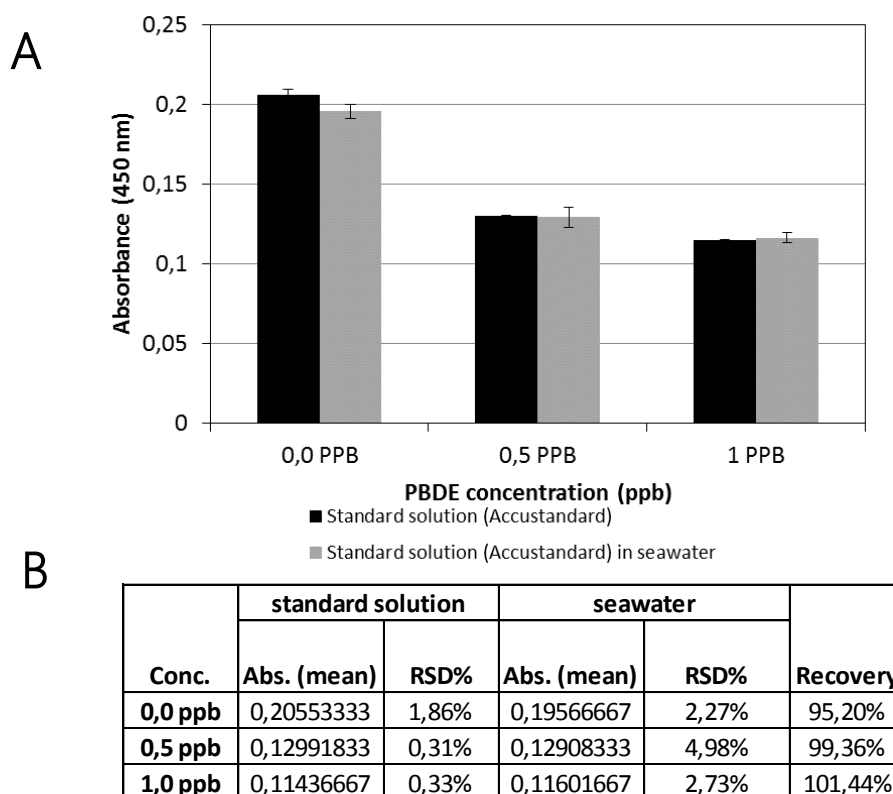
Figure 7 Signal recovery from spiked seawater. A. Absorbance of PBDE in buffer and seawater; B. Full data.

7.2.6. Perspectives and issues regarding application of the kit

7.2.6.1. Absorption of PBDE to various materials

PBDE as a hydrophobic compound attached strongly to many materials such as plastics, polymers etc. For this reason, in this kit, glass tubes are provided in order to reduce the risk of PBDE absorption that may significantly affect the reliability and sensitivity of the assay.

Nevertheless, we have decided to use standard plastic eppendorfs of 1.5 mL volume for this assay. This is possible to be performed without the loss of sensitivity if the protocol of the assay is followed strictly – the incubation time for PBDE (20 min) is too short to let molecules be strongly adsorbed. We performed several tests showing that the storage of PBDE samples in a plastic eppendorf tube for more than 3-4 hours lead to the loss of PBDE. Thus, the assay can be performed in plastic eppendorf tubes but standard solutions cannot be stored in any plastic tubes for a longer time.

Other materials that we found adsorbing PBDE while incubated for several hours are PDMS (Polydimethylsiloxane), COC (cyclic olefin copolymer) and Polycarbonate (Figure 8).
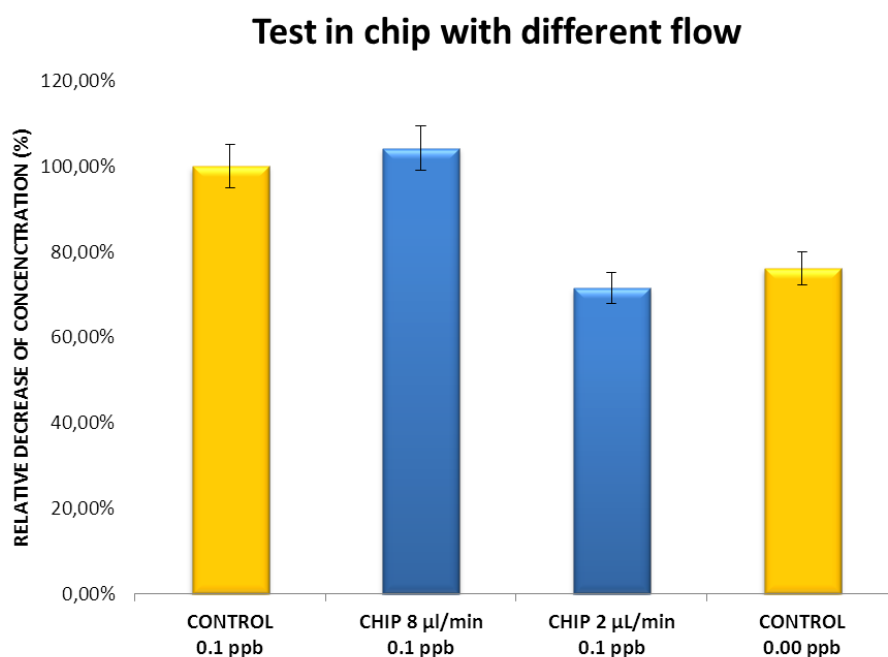
Figure 8 Absorption of PBDE by PDMS in microfluidic chip. This phenomenon strongly depends on the flow rate.

We also evaluated the absorption phenomena for different materials commonly used in microfluidic devices. As we can see, the level of absorption is quite large and the main factor that helps to reduce it is a flow rate. Once the flow rate increases, the absorption yield decrease. Thus, if this kit is going to be applied in SMS prototype, it is necessary to check if the absorption of PBDE occurs.

The effect of absorption depends largely on the flow rate. In these experiments an increase from 2μL/mL up to 8 μL/mL totally reduced the phenomena of PBDE absorption.

7.2.7. Proposal for PBDE detection in an automatic flow mode

A possible approach of flow-based PBDE detection using the kit presented above is shown in Figure 9. This idea can be transferred to a μMAC device – a prototype developed by Systea (partner in SMS project) able to perform ELIMO assays (Enzyme Linked Immuno-Magnetic Optical). An example of prototype for other compounds is shown in Figure 10.
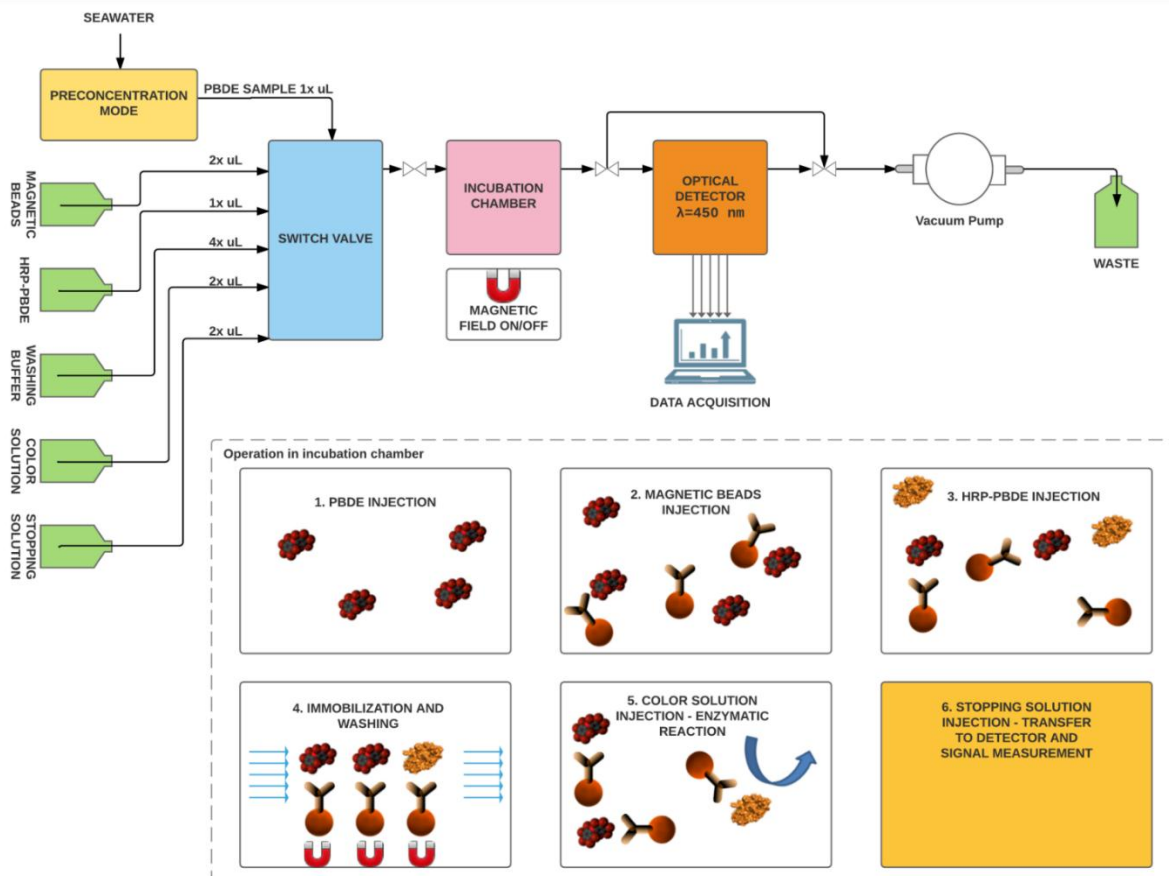
Figure 9 A general scheme of the possible automated detection of PBDE in seawater.
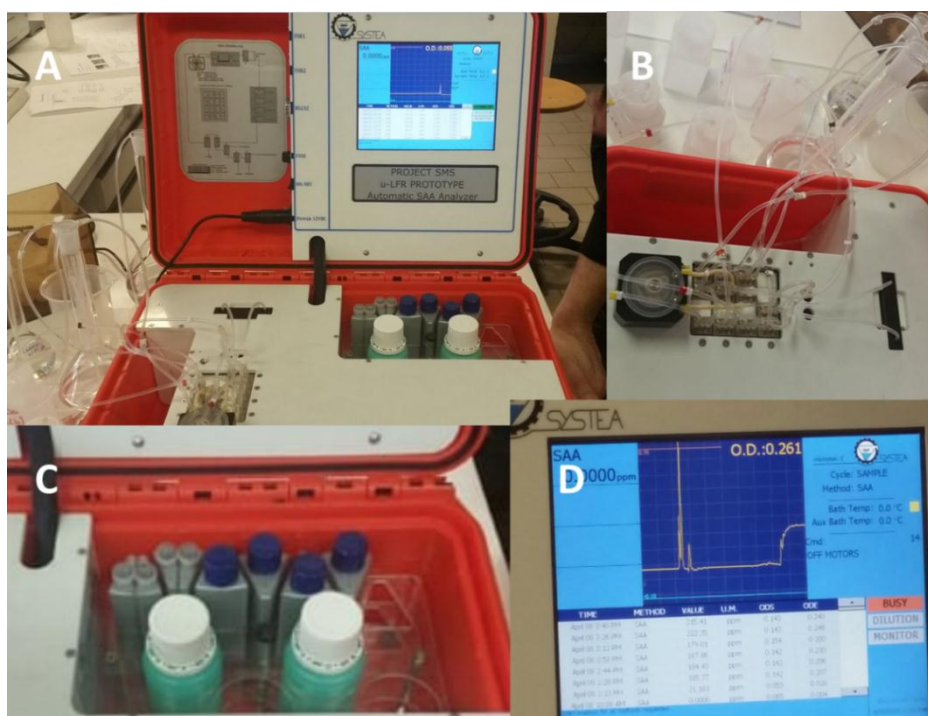
Figure 10 µMAC-Smart water analyzer **A.** a general view on portable analyser; **B.** fluidic system with in-built peristaltic pump and optical reader; **C.** Reservoirs for reagents and samples storage; **D.** integrated touch screen for parameters control and results analysis.

7.3.   Glyphosate detection
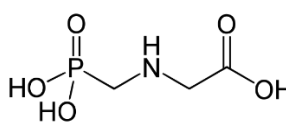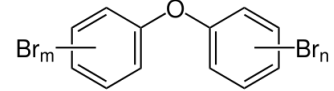
The glyphosate kit, provided by Abraxis (PN 500081), is an immunoassay based on anti-Glyphosate antibodies coupled to magnetic beads. As in the competitive assay, magnetic beads are incubated both with a sample containing Glyphosate (or blank) and HRP-Glyphosate. The Enzyme conjugate is used as a probe due to its ability to bind Glyphosate-specific antibodies as well as producing a reporting signal (a catalysis of reaction leading to a synthesis of a colorful product). The intensity of the color can be measured by using any spectrophotometer device able to read the wavelength of 450 nm. The signal intensity is proportional to the concentration of HRP-Glyphosate and inversely proportional to the glyphosate concentration.

The detection kit can be used for samples diluted in various buffers. In this kit, as a diluent, distilled water with preservatives and stabilizers is used.

7.3.1. Comparison with the PBDE kit

Both kits are based on competitive immunoassay, the strategy of signal detection is the same. However, some differences come from chemical properties of analyte – Glyphosate requires its derivatization before it can be detected in the colorimetric test. All reagents necessary for the derivatization are provided with the kit. The other issues are shown in Table   1:

Table 1 Brief comparison of PBDE and Glyphosate detection method using Abraxis kit.

	Glyphosate Abraxis Kit	PBDE Abraxis kit
Kit components		
Antibody coupled Paramagnetic Particles	65 mL	60 mL
Enzyme Conjugate (HRP)	35 mL	30 mL
Standard solutions	0-4000 PPT, 2 mL vial, in distilled water with preservatives and stabilizers	0-1 PPB, 2 mL vial in methanolic solution with preservatives and stabilizers
Diluent	distilled water with preservatives and stabilizers, 65 mL	methanolic solution containing preservative and stabilizers, 35 mL
Color solution	A solution of hydrogen peroxide and 3,3',5,5'-tetramethylbenzidine in an organic base, 65 mL	
Stopping solution	A solution of diluted sulfuric acid (0.5%), 65 mL	
Washing solution	Preserved deionized water, 250 mL	Preserved deionized water with surfactants, 250 mL
Assay buffer	Dissolved buffer salts, 125 mL	n/a
Derivatization reagent	3 x 80 µL vials	n/a
Derivatization reagent diluent	DMSO, 3 x 4 mL vials	n/a
Detection procedure		
Sample pretreatment	Derivatization: 3,5 mL of derivatization diluent is mixed with 80 µL of derivatization reagent 1 mL of assay buffer is mixed with 250 µL of standard/sample 100 µL diluted derivatization	n/a

159

	reagent is added Incubation 10 minutes	
Sample/standard incubation with Antibody coupled Paramagnetic Particles	300 µL **derivatized** standard solution is incubated with 500 µL of paramagnetic particles, 30 minutes	250 µL standard solution is incubated with 500 µL of paramagnetic particles, 20 minutes
Competitive reaction	250 µL of HRP-Glyphosate is added and incubated for 30 minutes	250 µL of HRP-PBDE is added and incubated for 20 minutes
Separation and washing	Using magnetic rack, immunocomplex is separated and washed (2x) with 1 mL of washing buffer	
Enzymatic reaction	Color solution (500 µL) is added and samples are incubated for 20 minutes	
Detection	Stopping solution is added (500 µL) and absorbance (450 nm) is measured within 15 minutes	

As it also occurs with PBDE, magnetic particles can be freely preconcentrated/diluted and used in the desired ratio after optimization. Regarding DMSO, any can be used, not only the one provided in kit. The stopping solution can be replaced by any other sulphuric acid (0.5%). The color solution can be replaced by any other TMB/H_2O_2 reagent used for HRP-based ELISA and similar tests. The test tubes can be replaced by any other tubes/eppendorf of the desired volume.

7.3.2. Detailed protocol

Derivatization of Standards, Control, and Samples

Dilute Derivatization Reagent with 3.5 mL of Derivatization Reagent Diluent (the Diluted Reagent needs to be used within the same day). Mix thoroughly.

Label single test tubes for standards, control, and samples.

Pipette 250 µL of standard, control, sample(s) into separate disposable tubes.

Add 1.0 mL Assay buffer, vortex to mix.

Add 100 μL the diluted derivatization reagent, vortex each tube immediately after addition of reagent.

Incubate at room temperature for 10 minutes.

Perform the ELISA like in the assay procedure, start with step 1 of the assay procedure.

Alternative Derivatization Procedure

Performing the alternative derivatization procedure allows the user to use the same derivatization tubes in the performance of the assay, therefore eliminating the use of additional assay tubes.

Dilute Derivatization Reagent with 3.5 mL of Derivatization Reagent Diluent (Diluted Reagent needs to be used within the same day). Mix thoroughly.

Label the test tubes in duplicate for standards, control, and samples.

Pipette in duplicate, 50 μL of standard, control, sample(s) into disposable assay tubes.

Add 200 μL Assay buffer, vortex to mix.

Add 20 μL the diluted derivatization reagent, vortex each tube immediately after addition of reagent.

Incubate at room temperature for 10 minutes.

Perform the ELISA as in the assay procedure, starting with step 3 of the Assay Procedure.

Assay procedure

Label the test tubes for standards, control, and samples.

Add 300 μL of the appropriate derivatized standard, control, or sample.

Mix the Glyphosate Antibody Coupled Paramagnetic Particles thoroughly and add 500 μL to each tube.

Vortex for 1 to 2 seconds minimizing foaming.

161

Incubate for 30 minutes at room temperature.

Add 250 µL of Glyphosate Enzyme Conjugate to each tube.

Vortex for 1 to 2 seconds minimizing foaming.

Incubate for 30 minutes at room temperature.

Separate in the Magnetic Separation System for two (2) minutes.

Decant and gently blot all the tubes briefly in a consistent manner.

Add 1 mL Washing Solution to each tube and allow them to remain in the magnetic separation unit for two (2) minutes.

Decant and gently blot all the tubes briefly in a consistent manner.

Repeat Steps 11 and 12 two (2) additional times.

Remove the rack from the separator and add 500 µL Color Solution to each tube.

Vortex for 1 to 2 seconds minimizing foaming.

Incubate for 20 minutes at room temperature.

Add 500 µL Stopping Solution to each tube.

Add 1 mL Washing Solution to a clean test tube. Use as blank in Step 19.

Read results at 450 nm within 15 minutes after adding the Stopping Solution.

7.3.3. Selected results

Examples of the calibration curve obtained by using standards provided with the kit are shown below. The values obtained from spectrophotometer are normalized by dividing them by the absorbance of blank (0 ppt solution) (A/A0). Then, the logarithm of the concentration is calculated in order to plot calibration curve (log10(concentration) vs. A/A0). This operation is necessary because the dependence between absorbance change and concentration is not linear. The kit includes several sheets of calibration curve

templates with a logarithmic scale, but they are not as useful as they need to be filled in manually. A detailed description of data analysis can be found in the manual of this kit.

Different calibration curves were obtained taking into account different derivatization procedures and derivatization reagent stability.

Table 2 Glyphosate detection using various approaches.

Assay performed with simplified derivatization method										
Conc. (PPT)	Abs_1	Abs_2	Abs_3	Abs_4	$Abs_{av.}$	$Abs_{st.dv.}$	Abs_1/Abs_0	Log_C	Log_{Abs}	LOD (PPT)
0	1.395	1.391	1.364	1.429	**1.395**	*0.023*	100.00%			
75	1.150	1.146	1.144	1.149	**1.147**	*0.004*	82.25%	1.875	-0.085	
200	1.050	1.095	1.080	1.083	**1.077**	*0.066*	77.22%	2.301	-0.112	<75
750	0.943	0.933	0.773	0.765	**0.854**	*0.085*	61.19%	2.875	-0.213	
4000	0.541	0.540	0.556	0.555	**0.548**	*0.008*	39.29%	3.602	-0.406	

Assay performed with full derivatization method

Conc. (PPT)	Abs_1	Abs_2	Abs_3	Abs_4	$Abs_{av.}$	$Abs_{st.dv.}$	Abs_1/Abs_0	Log_C	Log_{Abs}	LOD (PPT)
0 (no der.)	1.540	1.556	1.389	1.378	**1.466**	*0.083*				
0	1.162	1.135	1.126	1.129	**1.138**	*0.014*	100.00%			
75	1.089	1.085	1.018	0.999	**1.048**	*0.040*	92.07%	1.875	-0.036	>75
200	0.865	0.870	0.877	0.879	**0.873**	*0.006*	76.69%	2.301	-0.115	
750	0.665	0.666	0.645	0.648	**0.656**	*0.010*	57.64%	2.875	-0.239	
4000	0.389	0.391	0.375	0.381	**0.384**	*0.006*	33.74%	3.602	-0.472	
Assay performed with simplified derivatization method (2)										
Conc. (PPT)	Abs_1	Abs_2	Abs_3	Abs_4	$Abs_{av.}$	$Abs_{st.dv.}$	Abs_1/Abs_0	Log_C	Log_{Abs}	OD (PPT)
0	1.067	1.103	1.129	1.130	**1.100**	*0.026*	100.00%			>75

75	1.040	1.056	1.037	1.030	**1.044**	*0.010*	94.97%	1.875	-0.022	
200	0.925	0.934	0.934	0.934	**0.931**	*0.004*	84.66%	2.301	-0.072	
750	0.686	0.687	0.610	0.614	**0.661**	*0.037*	60.11%	2.875	-0.221	
4000	0.426	0.427	0.375	0.370	**0.409**	*0.027*	37.22%	3.602	-0.429	

Assay performed with full derivatization method (standard derivitized 24 hours before)

Conc. (PPT)	Abs_1	Abs_2	Abs_3	Abs_4	$Abs_{av.}$	$Abs_{st.dv.}$	Abs_1/Abs_0	Log_C	Log_{Abs}	LOD (PPT)
0 (no der.)	1.385	1.387	1.443	1.430	**1.411**	*0.026*				
0	1.060	1.055	1.259	1.254	**1.157**	*0..100*	100.00%			
75	0.939	0.934	0.962	0.964	**0.950**	*0.013*	82.09%	1.875	-0.086	<75
200	0.830	0.828	0.803	0.803	**0.816**	*0.013*	70.53%	2.301	-0.152	
750	0.546	0.546	0.561	0.557	**0.553**	*0.007*	47.75%	2.875	-0.321	
4000	0.374	0.380	0.343	0.349	**0.362**	*0.016*	31.24%	3.602	-0.505	

Assay performed with the full derivatization method (fresh standards + derivatization reagent diluted 24h before)

Conc. (PPT)	Abs_1	Abs_2	Abs_3	Abs_4	$Abs_{av.}$	$Abs_{st.dv.}$	Abs_1/Abs_0	Log_C	Log_{Abs}	LOD (PPT)
0 (no der.)	1.395	1.448	1.405	1.444	**1.423**	*0.023*				
0	1.107	1.107	1.238	1.239	**1.173**	*0.066*	100.00%			
75	0.988	1.002	1.000	1.007	**0.999**	*0.007*	85.21%	1.875	-0.070	<75
200	0.850	0.853	0.847	0.852	**0.851**	*0.002*	72.52%	2.301	-0.140	
750	0.624	0.629	0.728	0.730	**0.678**	*0.051*	57.79%	2.875	-0.238	
4000	0.421	0.411	0.430	0.432	**0.424**	*0.008*	36.11%	3.602	-0.442	

Assay performed with the full derivatization method (fresh standards + derivatization reagent diluted 48h before)

Conc. (PPT)	Abs_1	Abs_2	Abs_3	Abs_4	$Abs_{av.}$	$Abs_{st.dv.}$	Abs_1/Abs_0	Log_C	Log_{Abs}	LOD (PPT)

0 (no der.)	1.543	1.392	1.584	1.465	**1.496**	*0.074*			
0	1.150	1.090	1.214	1.154	**1.152**	*0.044*	100.00%		
75	1.037	0.998	1.148	1.140	**1.081**	*0.065*	93.82%	1.875	-0.028
200	0.898	0.892	0.873	0.870	**0.883**	*0.012*	76.67%	2.301	-0.115
750	0.651	0.658	0.700	0.697	**0.677**	*0.022*	58.72%	2.875	-0.231
4000	0.505	0.510	0.413	0.420	**0.462**	*0.046*	40.10%	3.602	-0.397

It seems that the kit works well and provides acceptable sensitivity. There are, however some issues that need to be taken into account when the flow system is designed.

Derivatization method - there are two methods of derivatization: the first one is based on preparing a separate tube where diluted derivatization reagent is mixed with buffer and standard/sample, derivatized and used in a proper immunoassay. The second one uses reduced volumes of reagents, thus immunoassay is performed in the same test tubes. According to the results obtained, where the simplified method (low volumes in a single tube) of derivatization is used, the correlation and limit of detection are slightly worse; probably this is due to the pipetting errors. Even the repetitions of the same standard solution are prepared separately, not using any stock solution of derivatized sample as it happens in the full derivatization method.

Derivatization time – according to the manual, derivatization should take 10 minutes. We have observed that extending this time does not affect results in some cases but even improves them. The samples derivatized for 24 hours showed a very good limit of detection. On the other hand, in some cases where derivatization took the minimum time of 10 minutes the reproducibility was slightly worse. Thus, an extended time of 20 minutes for derivatization step should be the optimal one.

Derivatization Reagent – derivatization reagent is prepared by adding 3.5 mL DMSO to a vial containing 80 µL stock of derivatization reagent. The exact composition of the reagent

is confidential so we do not know if we are able to replicate it and prepare our own. The stability of diluted derivatization reagent is recognized by the manufacturer as 24 hours. In our case, fresh, 24h- and 48 h diluted derivatization reagent were tested. In all cases, quite satisfactory results were obtained. After 48 hours, however, the limit of detection is slightly worse and the specific odor can be detected. That means that probably some conversion processes of the derivatization reagents are already occurring. The practical problem of this issue is that the amount of the derivatization reagent provided with the kit is not so large (3x80 µL vials, each valid for 24 hours when diluted), so in order to use reagents optimally, a lot of measurements should be performed within 24 hours.

Limit of detection – like in PBDE kit, in this test LOD is understood as a concentration (PPT) that is related to A/A0=90% and it is estimated by a manufacturer at 50 PPT. All results where A/A0>90% are considered as below the limit of detection. In our case, some of the measurements were below the limit of detection, probably due to too short derivatization time (mentioned above) or too old and partially degraded derivatization reagent (also discussed above).

Immunoassay – in this case, everything works properly and in a similar way as to the PBDE test. It can be noticed that this test, compared to PBDE works in a broader range of absorbance (the highest Abs for 0.0 PPT is about 1.2 while the lowest for 4000 PPT shows an absorbance of about 0.4).

Compatibility with the flow system –unlike PBDE, Glyphosate is hydrophilic and very easy to dissolve in water, thus we do not expect that it might be adsorbed by different materials used in the prototype.

7.3.4. Glyphosate in seawater

This kit is dedicated to various types of samples. Thus, detection of Glyphosate in seawater is also possible. We performed several measurements in order to examine it. The procedure of seawater collection and pretreatment was the same as that for the PBDE. The following results were obtained:

Table 3 Glyphosate recovery from the seawater.

Concentration (PPT)	Recovery (%)
75	99
200	104.5
700	101.7

It can be seen that this kit is compatible with seawater samples and there is no significant amount of Glyphosate in tested water.

7.3.5. Proposal for Glyphosate detection in an automated flow mode

In-flow measurements of Glyphosate using Abraxis kit are supposed to be almost identical to the one of PBDE. However, the step of derivatization needs to performed:

-Dilution of derivatization reagent with DMSO (dilution factor 44.75, ≈45 times)

-Mixing of diluted derivatization reagent with sample/standard solution. Incubation for >10 minutes or different amount of time (to be optimized)

-Mixing with magnetic beads coupled to antibodies

The rest of steps are the same as for PBDE.

What needs to be taken into account:

DMSO cannot be stored at 4 °C as the rest of reagent (due to the melting point around 19 °C). Incubation at the temperature >30 °C makes DMSO liquid again but arranging this within the system may be too sophisticated. It is, consequently, better to store it without any special cooling.

Low volumes of derivatization reagent stock need a special solution regarding tubing, container used etc. so that they do not loose significant amounts of reagent and generate some dead volumes in the flow system.
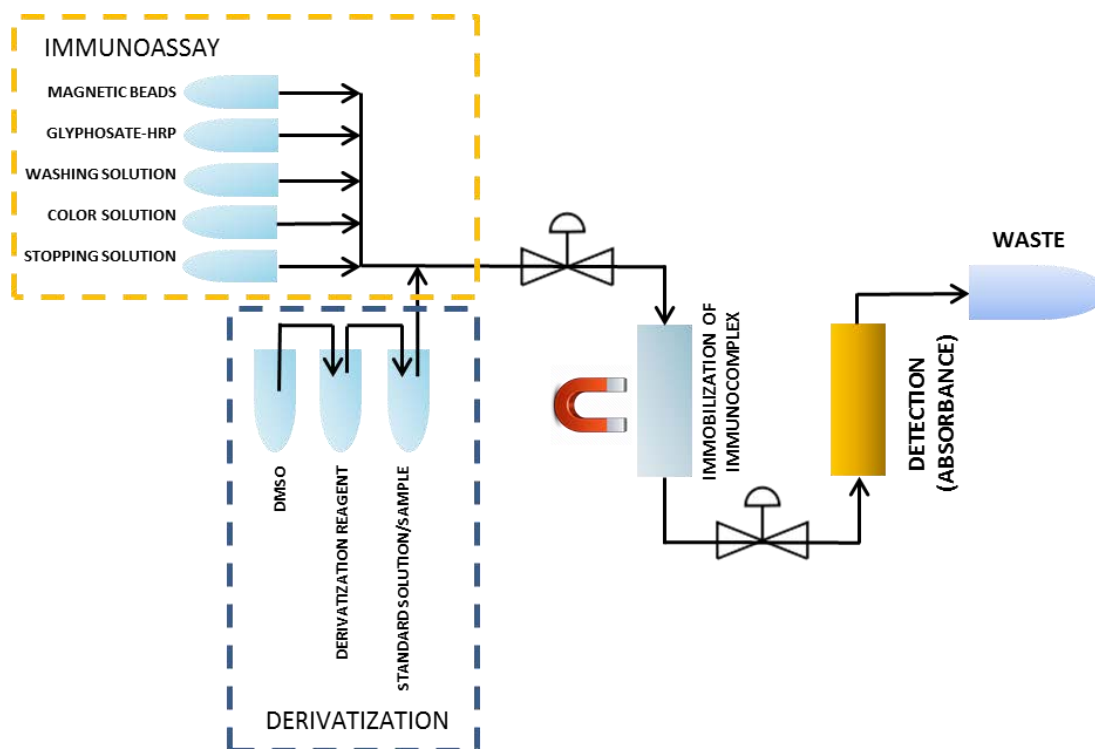
Figure 11 A general scheme of possible automated detection of Glyphosate including derivatization and immunoassay steps.

7.4.   References

1.   Wake, H., *Oil refineries: a review of their ecological impacts on the aquatic environment.* Estuarine Coastal and Shelf Science, 2005. **62**(1-2): p. 131-140.

2.   Croquer, A., et al., *Monitoring coastal pollution associated with the largest oil refinery complex of Venezuela.* Peerj, 2016. **4**. doi: 10.7717/peerj.2171

3.   Bianchi, C.N. and C. Morri, *Marine biodiversity of the Mediterranean Sea: Situation, problems and prospects for future research.* Marine Pollution Bulletin, 2000. **40**(5): p. 367-376.

4.   Levin, L.A., et al., *The function of marine critical transition zones and the importance of sediment biodiversity.* Ecosystems, 2001. **4**(5): p. 430-451.

5.   Occhipinti-Ambrogi, A. and D. Savini, *Biological invasions as a component of global change in stressed marine ecosystems.* Marine Pollution Bulletin, 2003. **46**(5): p. 542-551.

6.   Richir, J. and S. Gobert, *Trace Elements in Marine Environments: Occurrence, Threats and Monitoring with Special Focus on the Coastal Mediterranean.* J Environ Anal Toxicol, 2016. **6**(349).

7.   Azzaro, F., *Automated nutrients analysis for buoys in sea-water and intercalibration.* International Journal of Environmental Monitoring and Analysis, 2013. **1**(6): p. 315-322.

8.   Vuillemin, R., et al., *CHEMINI: A new in situ CHEmical MINIaturized analyzer.* Deep-Sea Research Part I-Oceanographic Research Papers, 2009. **56**(8): p. 1391-1399.

9.   Cheng, S.Y., et al., *Sensitive Detection of Small Molecules by Competitive Immunomagnetic-Proximity Ligation Assay.* Analytical Chemistry, 2012. **84**(5): p. 2129-2132.

10.   Mayorga-Martinez, C.C., et al., *Iridium oxide nanoparticle induced dual catalytic/inhibition based detection of phenol and pesticide compounds.* Journal of Materials Chemistry B, 2014. **2**(16): p. 2233-2239.

11.   Mayorga-Martinez, C.C., et al., *Bismuth nanoparticles for phenolic compounds biosensing application*. Biosensors & Bioelectronics, 2013. **40**(1): p. 57-62.

12.   Barreiros dos Santos, M., et al., *Highly sensitive detection of pathogen Escherichia coli O157:H7 by electrochemical impedance spectroscopy*. Biosensors and Bioelectronics, 2013. **45**(0): p. 174-180.

ANNEX III

Heavy metals detection using screen-printed electrodes

8.1.   Introduction

Electrochemical detection of heavy metals was performed using square wave anodic stripping voltammetry (SW-ASV). The main advantage of this technique is the possibility to directly detect selected metals without the need of electrodes' surface modification or sophisticated pretreatment. This method consists of the several subsequent steps:

- Conditioning step – a positive (or at least 0.0 V) potential is applied to the working electrode. If they are any traces of the reduced metal ions from the previous measurement of other reason, it can be removed from its surface. Thanks to this, the whole surface of the electrode will be engaged in actual measurements as well as the risk of false-positive response is lowered.

- Deposition step – the most important step of SW-ASV detection. It is characterized by a deposition potential (ex. at -1.2 V) that is applied in order to reduce metal ions onto the working electrode surface. Depending on the exact value of the deposition potential, certain compounds may or may not be reduced, thus this step ensures a kind of semi-selectivity. Deposition of the metals onto an electrode is a mass transport based process. Usually, only a very thin interface between a sample and electrode participate in the reaction, so by applying a flow, stirring etc. an increase of the signal can be observed.

- Equilibration step – the role of this step is to stabilize the recently formed metal (reduced) deposited layer. None of the stirring or flow is maintained as this could create interference and noises during read out.

- Stripping step – metals that were reduced onto electrode during the deposition step are now released (oxidized) as a square-wave is applied within the specific potential range (ex. from -1.4 to 0.0 V). Oxidation for each metal occurs under the specific potential value, so the final voltammogram represents various peaks of different potential and different current proportional to the metal's concentration.

All the steps described above are shown in Fig. 1.
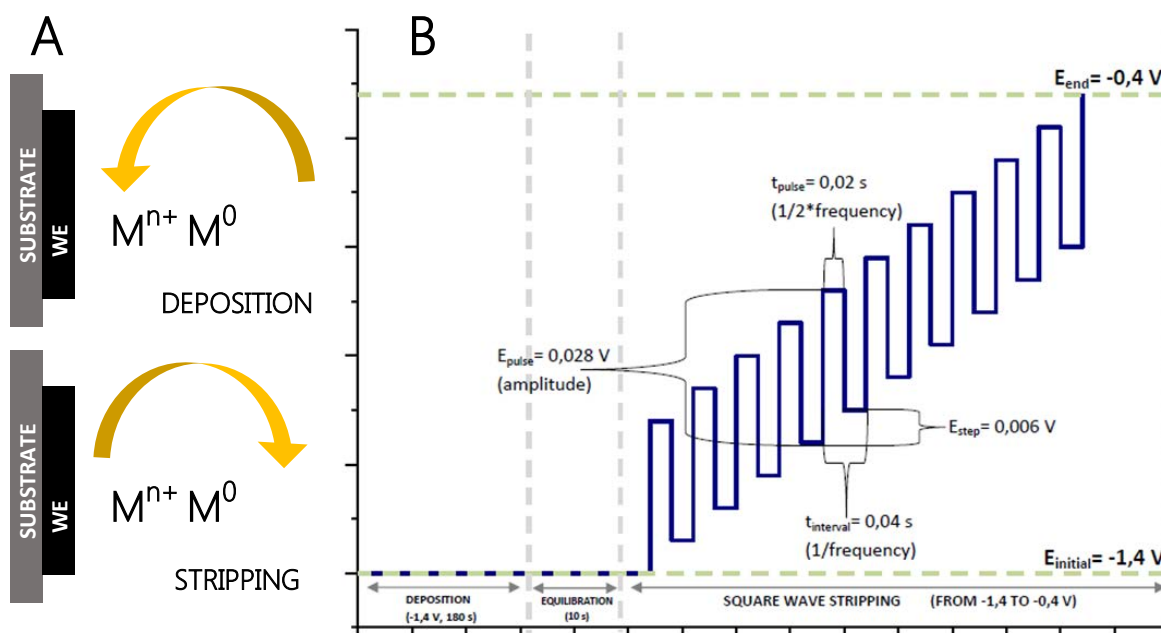
Figure 1 General concept of SW-ASV detection. **A.** Deposition and Stripping steps, WE – working electrode; **B.** Change of the voltage in a function of time using -1.4 V as a deposition potential.

SW-ASV is considered as a very sensitive technique, suitable for traces detection. On the other hand, heavy metals are usually present in ppb range and their availability is affected by various compounds present in real samples. This means that special strategies need to be applied in order to maximize the efficiency of this electrochemical technique.

As mentioned above, working with the stirring or with the flow is the most relevant approach. This allows to improve the detection performance as the overall amount of sample in contact with working electrode is much higher. Simultaneously, the dynamic flow of the liquid ensures sample renewal and lowers the risk of impurities accidentally adsorbing onto the electrode. A very useful approach is the use of Lab-on-a-chip platforms where screen-printed electrodes can be integrated within a microfluidic chip (usually made of PDMS). This approach allows increasing the sensitivity of the detection as well as miniaturized the detection set-up. Several examples of electrochemical LOC platforms for heavy metal detection are already reported [1, 2].

Another approach already applied in a commercial area is the use of metals improving an electrochemical performance. One of the most common used to be mercury, but its high

toxicity has a legitimate objection to the further use [3]. That is why an interesting alternative is the use of bismuth, which can interact with metals (forming alloys) of interest and increase their response. Moreover, its toxicity is negligible [3]. There are several approaches to use Bi in heavy metal detection. The in-situ approach is based on spiking a given sample with Bi(III) solution in acidic pH that leads to co-deposition of Bi and target metals onto the electrode. If Bismuth is electroplated onto the electrode before immersing it in a target sample that is an ex-situ method.

Bi, as other heavy metals, will be participating in the deposition and stripping process but thanks to the phenomena of co-deposition, the presence of Bismuth in the sample cause an increase of the specific signal of other metals. The last, bulk method, required an addition a Bi_2O_3 to the carbon ink. This means that a printed electrode is already modified with Bismuth. The main advantage of the last approach is the possibility to precisely control the quality of the ink and thus, the influence of Bi presence in it [4, 5]. Besides the use of Bismuth salts or oxides, Bismuth nanoparticles (BiNP) are reported as well [8].

Apart from the strategies mentioned above, detection of heavy metals can be improved using novel electroactive materials. However, they are not discussed here, as those solutions are not commercialized yet and need further improvements regarding reproducibility etc.[4]

In this annex, an optimization of electrochemical detection of heavy metals is presented. The goal was to obtain a reference method of Pb(II) detection using Bi-modified electrodes as well as to develop a flow-based method of heavy metals detection using the home-made screen-printed electrodes. The second approach is dedicated to the application within H2020 EU project "INTCATCH" where automated sensors will be employed to monitor the water quality in various Europeans catchments.

8.2. Evaluation of commercial Bismuth-based electrodes for Pb (II) detection

Bismuth electrodes were provided by Gwent Electronic Materials Ltd (United Kingdom). As a substrate, a thermoplastic polyester (Valox) was used. Carbon-bismuth paste (C2130610D1) was used to print working electrode, while pure carbon (C2030519P4) for counter electrode. Ag/AgCl ink (C2130809D5, 60/40 ratio) was employed for reference electrode. The diameter of the working electrode was 3.8 mm. Example of a sheet with 6 electrodes is shown in Figure 2.
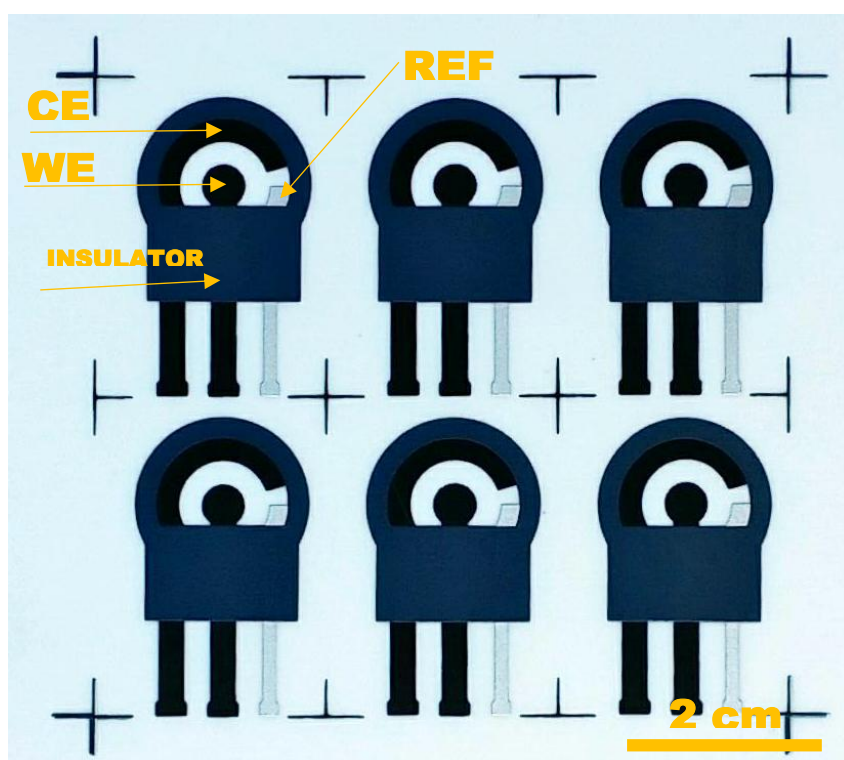
Figure 2 Screen-printed electrodes with carbon-bismuth paste printed on Valox. CE – counter electrode; WE – working electrode; REF – reference electrode.

All measurements were repeated 3 times, using different electrode in each case. Detection was performed by placing 150 μL of the sample onto the electrode. Electrochemical measurements were carried out using computer-controlled Autolab PGSTAT-12 (302 N-High performance) (potentiostat/galvanostat) with general-purposes electrochemical

software operating system (GPES version 4.9.007, from Eco Chemie B.V., Utrecht, The Netherlands).

8.2.1. Optimization of the key parameters

An exhaustive optimization was performed in order to match the best detection performance (Fig. 3). The most important parameter is the deposition potential (Fig. 3A). It can be generally assumed, that the more negative potential applied, the more analyte can be detected. However, this parameter defines also the specificity. Thus, if the potential is too negative, any interference are more likely to occur, including hydrogen reduction leading to bubbles generation (H_2). -1.2 V was found as the best deposition potential, giving a high signal for the control sample of 125 ppb of Pb(II). In the case of deposition time (Fig. 3B), 230 s was chosen, as further increase of the time did not cause an improvement regarding assay sensitivity.

Detection buffer is another important issue when detection of heavy metals is performed. HCl was used as a cheap and easy to prepare reagent (Fig. 3C). The role of the buffer is to maintain a low pH as well as support electrochemical redox reactions. Although the highest signal was obtained using 1M HCl, we definitely rejected this approach as it causes huge deviations between each measurement. This happened due to too high H^+ concentration, so some gas bubbles are generated during the deposition step. As in this approach there is no flow or stirring provided (just a drop of sample onto the electrode) there is no possibility to remove the excess of gas with the flow, so it is seriously affects the quality of the measurement, mainly by the increase of a background current. Finally, a 0.1 M HCl was chosen. Samples diluted in this buffer have a pH <2 and no bubbles are observed during detection.

Those electrodes are dedicated to being a disposable sensor. Nevertheless, an electrochemical response of the same electrode in repeated measurements was checked (Fig. 3D). It can be observed that there is no clear and reproducible behavior. This results from electrodes morphology, as they contain carbon-bismuth paste, Bi is oxidized and reduced during each measurement. Some of the Bi layers is probably removed, some are

still maintained onto the surface. This process seems to be quite random so it is not recommended to use a single electrode for more than one measurement. Fortunately, there is good intra-electrode reproducibility. A standard deviation does not usually exceed 7-9% what is a very good result in the field of screen-printed electrodes.
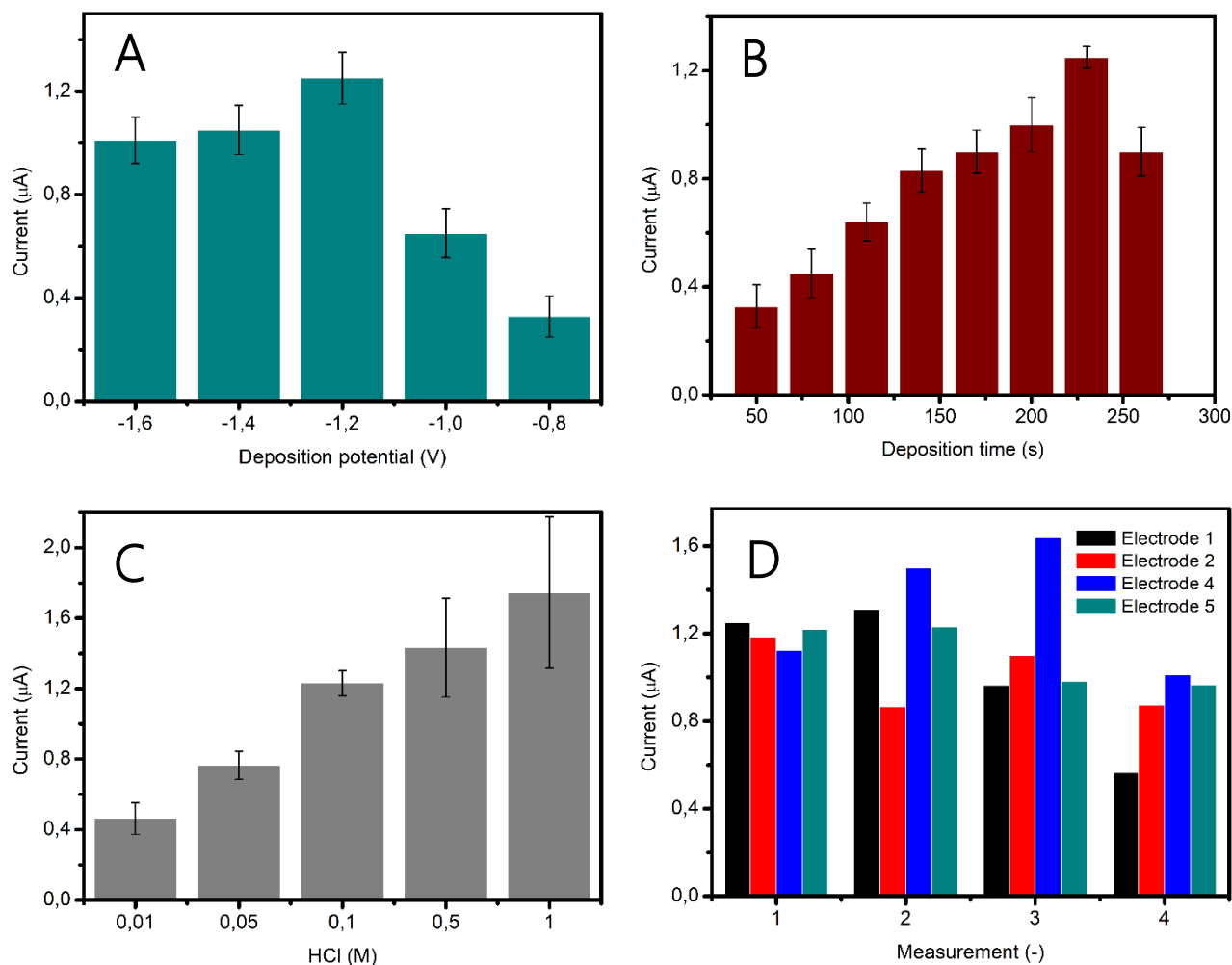
Figure 3 Optimization of the key parameters. **A.** Deposition potential (V); **B.** Deposition time (s); **C.** buffer (HCl) concentration (M); **D.** inter- and intra-electrode reproducibility.

8.2.2. Calibration curve in standard solution using Bi electrodes

Final measurements are shown in Fig. 4. Using optimized protocol Pb(II) was detected with the LOD of 0.40 ppb and LOQ of 1.34 ppb. These results can be considered as a satisfactory, taking into account that the measurement is performed in static mode, not in the flow. It can be expected that the same approach, working in flow, would bring even higher sensitivity (due to a renewal of the sample and improved contact between the liquid and the electrode).

Nonetheless, this method can be considered as reproducible, sensitive and trustful, regarding detection of Pb(II) in water.
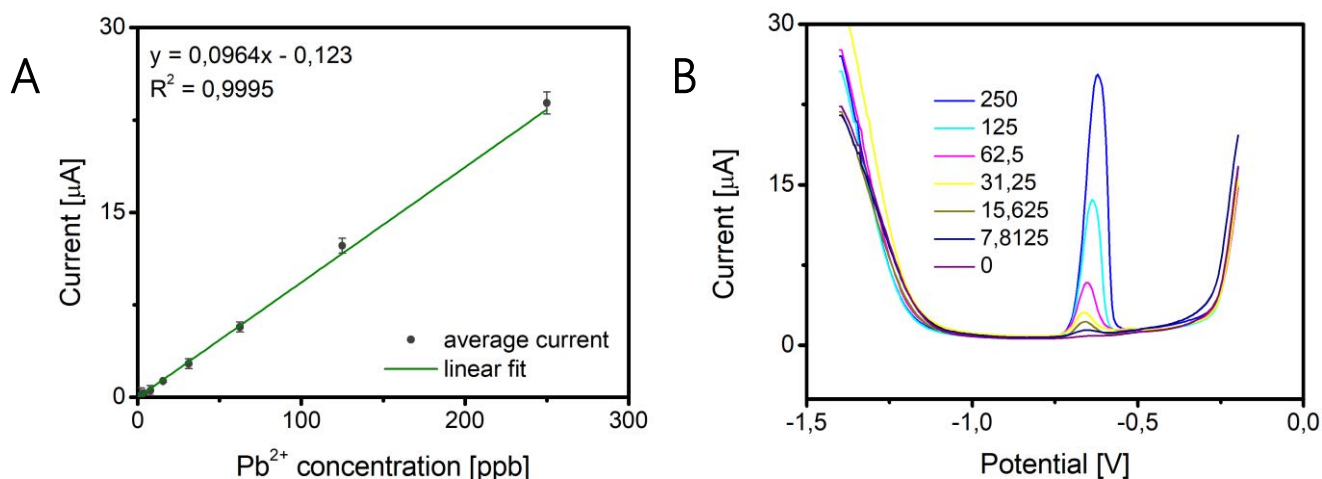
Figure 4 A. Calibration curve of Pb(II) detection in 0.1 M HCl using optimized protocol; **B.** Voltammograms of different concentrations (ppb) of Pb(II).

8.2.3. Calibration curve in standard solution using home-made screen-printed electrodes in flow-mode

As the device described in Chapter 4 is based on microfluidic, electrochemical measurements are performed in the flow. As Bi electrodes are dedicated for a single use, they are not practical for this application. Thus, the home-made screen-printed carbon electrodes were employed. Optimization of the electrochemical factors is described in points 3.2-3.3 of this Annex.

Final detection of Pb in flow was performed using 0.1 M HCl as a buffer, -1.2 V as a deposition potential and 120 s as a deposition time. Comparing with Bi electrodes, where

detection was in static mode, an equilibration step was extended up to 25 s. This is due to possible noises visible on the voltammogram if the liquid is still moving.

The LOD (obtained as 3x standard deviation of the lowest concentration divided by the slope of the calibration curve) obtained was 0.50 ppb, while LOQ (obtained as 10x standard deviation of the lowest concentration divided by the slope of the calibration curve) 1.68 ppb (Figure 5). These numbers are pretty similar to the results obtained with the Bi electrodes. Although the performance of bare carbon electrode is generally worse (the lack of Bi layer enhancing the electrochemical response) the use of the flow compensates this drawback. Moreover, this approach facilitates re-usability. We have observed that by flushing 0.1 M HCl and performing a blank measurement, all the metal traces can be removed from the electrode and a new measurement can be obtained.
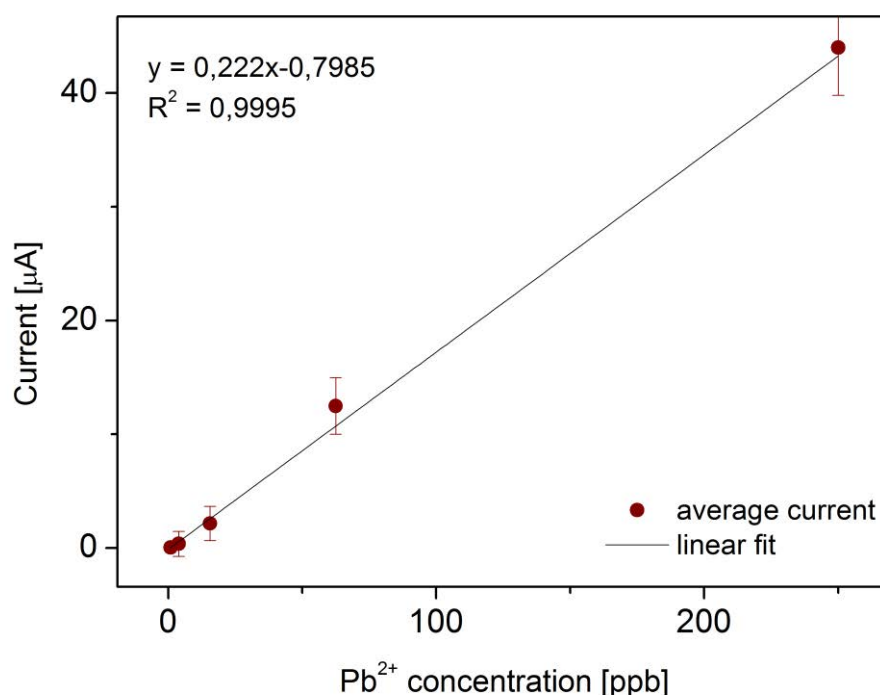
Figure 5 Calibration curve of Pb(II) detection in microfluidic chip in 0.1 M HCl with the flow rate 1.2 mL/min.

8.3. Evaluation of the home-made screen-printed carbon electrodes towards heavy metal detection

8.3.1. SPCE fabrication

Screen-printed electrodes were fabricated using standard, already reported protocol [1, 6]. The design of the electrodes is shown in Figure 6.
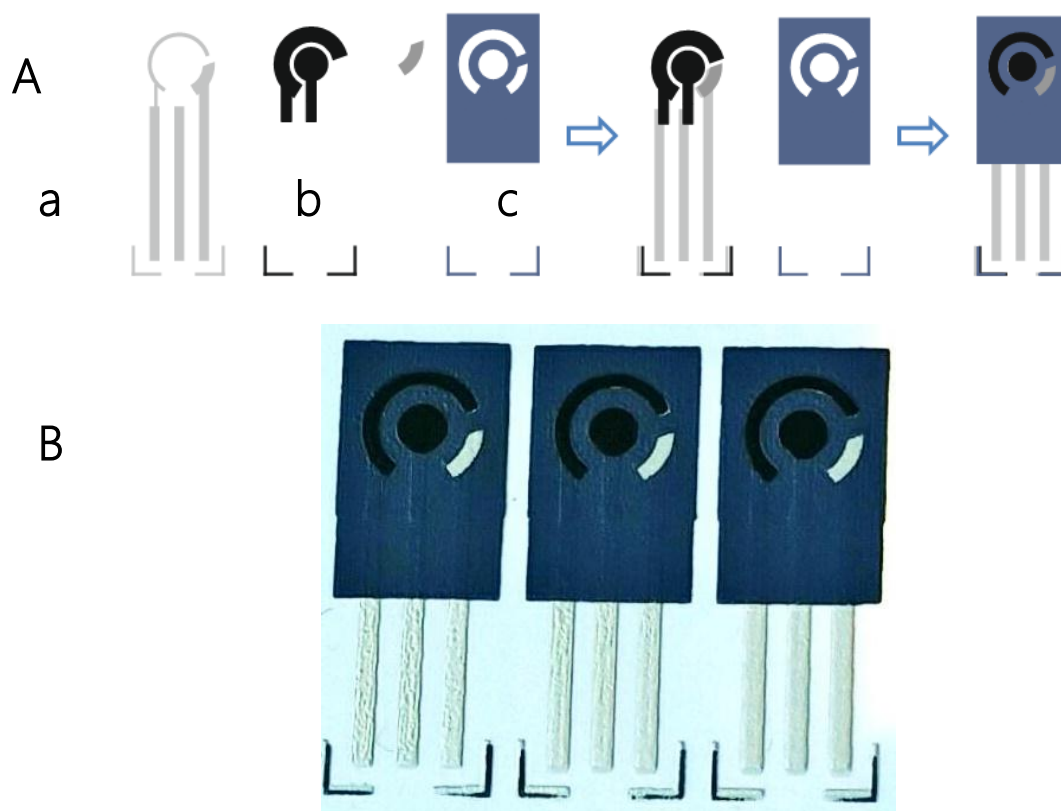
Figure 6 Screen-printed carbon electrodes **A.** The order of printing electrodes´ layers; **B.** 3 SPCE electrodes printed on polyester sheet.

8.3.2. Flow system

The detection system consists of a PMMA cell, where the screen-printed electrode is placed. There are one inlet and one outlet allowing connecting polymeric tubes. One of them is connected to the peristaltic pump (Perimax), used as a driving unit for the system. The electrode is connected directly to the portable potentiostat (EmStat Blue, Palmsens, Netherlands). The detection setup is presented in Figure 7.
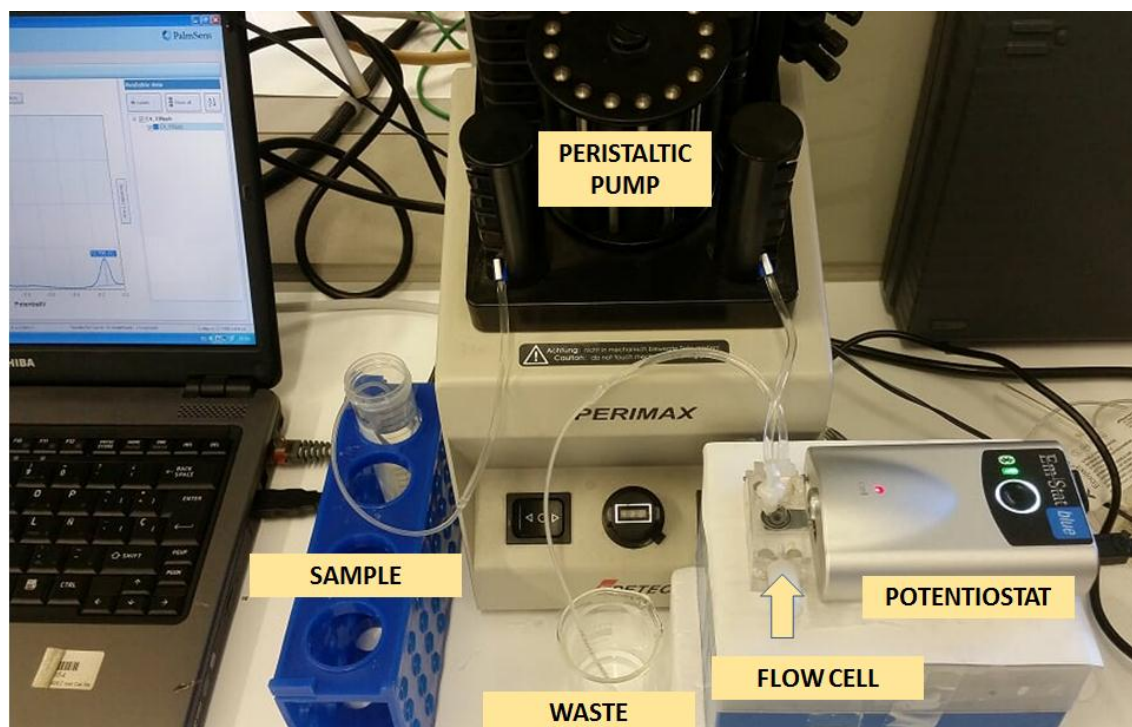
Figure 7 Setup for flow-based electrochemical detection of heavy metals.

8.3.3. Optimization of the key parameters

As a reference metals, Zn and Cu were evaluated. Those metals are present in water not only due to human activities but also occur naturally at low levels. Thus, their detection was interesting from the point of view of the INTCATCH project.

As the detection was performed in flow, that was the first factor to be evaluated. A general agreement between an increase of the flow rate and the increase of the current was observed (data not shown). Finally, a 3 mL/min flow rate was chosen giving a sufficiently high signal. In this case, about 8 mL of sample is used to perform detection.

Another factor similarly affecting measurements is the deposition time. As it can be expected the longer it is, the higher current is measured. A 120 s was chosen as an

optimal one. Although the longer time would provide a higher signal, this would lead to a large usage of the sample (>10 mL).

One of the most important parameters to be considered in heavy metals detection is the deposition potential. As it was mentioned in the introduction, depending on its value, certain metals are or are not deposited onto electrode's surface.

We have observed that Cu and Zn behaves opposite in presence of different potential values (Figure 8A). In the case of Cu, there is a very broad spectrum of deposition potential allowing to detect this metal. In the case of Zn, it works slightly different, only for the deposition potential lower than -1.4 V any signal can be obtained. This is a natural consequence of standard reduction potential values.

Figure 8B shows the reproducibility of a single screen-printed electrode. It can be observed that many measurements can be performed using the same electrode, without any loss of the activity. Obviously, an error of about >9% can be observed, however that is always happening for the home made electrodes.
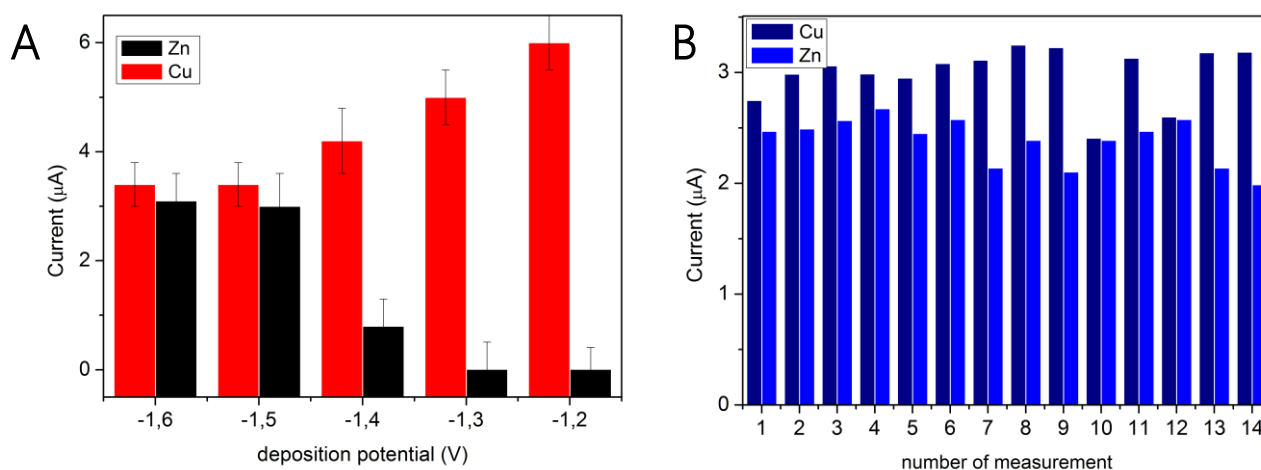
Figure 8 A. Effect of deposition potential (V) on Zn and Cu detection; **B.** Reproducibility of a single SPCE electrode used for Zn and Cu detection (50 ppb).

Another crucial factor influencing detection is the buffer. At the beginning, 0.1 M HCl was used but it was observed that when the deposition potential applied is -1.4 V or lower, a significant number of hydrogen bubbles appear sometimes causing even electrode's

destruction. Thus, in the case of Zn detection, where -1.4 V was chosen as an optimal deposition potential, a diluted buffer of 0.01 M HCl was used. In the case of Cu, if -1.2 V is applied, there is no issue with bubbles generation so 0.1 M HCl can be used.

8.3.4. Calibration curve in standard solution

Calibration curves (Figure 9) for Zn and Cu were obtained using optimal conditions for each metal. In the case of Cu: -1.2 V deposition potential, deposition time 120 s, 50 s pretreatment time, 20 s equilibration time, 3 mL/min flow rate, 0.1 M HCl as a buffer. For Zn: -1.4 V deposition potential, deposition time 120 s, 50 s pretreatment time, 20 s equilibration time, 3 mL/min flow rate, 0.01 M HCl as a buffer.

Linear detection of metals was observed in the range of 3.125-100 ppb and 12.5-400 ppb for Cu and Zn respectively. The sensitivity for Zn (slope of the calibration curve) and, as a consequence, the limit of detection is significantly lower compared to Cu. This is due to deposition potential which is less specific.
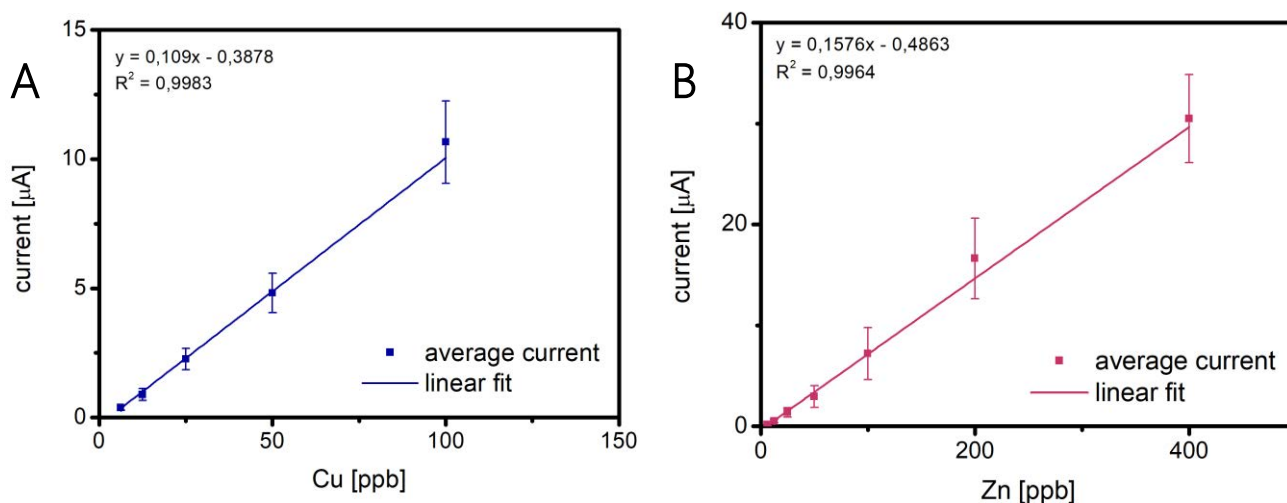
Figure 9 Calibration curves of **A.** Cu and **B.** Zn. Experimental conditions as explained in the text.

8.3.5. Simultaneous detection and interferences

As this technique is supposed to be employed for real samples detection, it was necessary to study possible interference between metals so as to know how the presence of a given element affects the ability to detect the other.

Samples of Cu and Zn having fixed concentration (100 ppb) were spiked with metals such as Pb, Cd, Ni, Cu and Zn in the concentration range of 0-100 ppb. Measurements were performed using a deposition potential -1.4 V and 0.01 M HCl as a buffer. Conditions for Zn were used as using conditions for Cu none of the Zn could be detected.

Results are shown in Table 1 and Table 2. It can be observed that detection of Cu is not significantly affected in presence of other metals. A slight increase of signal can be observed as well as the shift of peak. In the case of Zn, even the lowest concentration of metals (1.75 ppb) reduces the Zn signal by more or less 50%. In this condition, differentiation of other metals is hard, as peaks move significantly and background currently is relatively high.

These observations are related to two factors. The deposition potential of -1.4 V is not that specific as -1.2 V and generates a higher background current affecting sensitivity as well as the limit of detections. Apart from electrochemistry, metals have their own affinity to carbon materials. According to literature, Pb and Cu are reported to have the highest affinity while Zn, the lowest[7].

Table 1 Interferences between Cu and other metals

		current (µA)				average	standard dev.	RSD [%]
		1	2	3	4			
100 ppb	Cu	8.421	11.282	8.220	8.700	**9.156**	1.431	15.63%
0 ppb	Zn	0.000	0.000	0.000	0.000	**0.000**		
0 ppb	Cd	0.000	0.000	0.000	0.000	**0.000**		
0 ppb	Pb	0.000	0.000	0.000	0.000	**0.000**		
0 ppb	Ni	0.000	0.000	0.000	0.000	**0.000**		
100 ppb	Cu	9.907	11.162	7.541	10.174	**9.696**	1.535	15.83%
1.75 ppb	Zn	0.000	0.000	0.000	0.000	**0.000**		
1.75 ppb	Cd	0.000	0.000	0.000	0.000	**0.000**		

1.75 ppb	Pb	0.000	0.000	0.000	0.000	**0.000**		
1.75 ppb	Ni	0.000	0.000	0.000	0.000	**0.000**		
100 ppb	Cu	12.850	13.566	10.854	11.075	**12.086**	1.331	11.01%
6.25 ppb	Zn	0.000	0.000	0.000	0.000	**0.000**		
6.25 ppb	Cd	0.592	0.277	0.000	0.000	**0.217**	0.282	129.76%
6.25 ppb	Pb	1.051	1.152	2.204	2.794	**1.800**	0.843	46.83%
6.25 ppb	Ni	0.000	0.000	0.000	0.000	**0.000**		
100ppb	Cu	12.876	12.881	12.672	11.000	**12.357**	0.910	7.36%
25 ppb	Zn	0.000	0.000	0.000	0.000	**0.000**		
25 ppb	Cd	0.000	0.000	0.000	0.000	**0.000**		
25 ppb	Pb	4.732	5.436	5.023	4.087	**4.820**	0.567	11.77%
25 ppb	Ni	0.000	0.000	0.000	0.000	**0.000**		
100 ppb	Cu	13.276	14.162	16.189	14.984	**14.653**	1.239	8.46%
100 ppb	Zn	0.000	0.000	0.000	0.000	**0.000**		
100 ppb	Cd	0.000	0.000	0.000	0.000	**0.000**		
100 ppb	Pb	8.276	8.523	8.317	8.849	**8.491**	0.262	3.08%
100 ppb	Ni	0.000	0.000	0.000	0.000	**0.000**		

Table 2 Interferences between Zn and other metals

		current (µA)					standard dev.	RSD [%]
		1	2	3	4	**average**		
100 ppb	Zn	6.590	6.147	6.061	5.430	**6.057**	0.478	7.89%
0 ppb	Cu	0.000	0.000	0.000	0.000	**0.000**	0.000	
0 ppb	Cd	0.000	0.000	0.000	0.000	**0.000**	0.000	
0 ppb	Pb	0.000	0.000	0.000	0.000	**0.000**	0.000	
0 ppb	Ni	0.000	0.000	0.000	0.000	**0.000**	0.000	
100 ppb	Zn	3.011	4.713	2.008	3.130	**3.216**	1.118	34.77%
1.75 ppb	Cu	0.000	0.000	0.000	0.000	**0.000**	0.000	
1.75 ppb	Cd	0.000	0.000	0.000	0.000	**0.000**	0.000	
1.75 ppb	Pb	0.276	0.282	0.190	0.131	**0.220**	0.073	33.03%
1.75 ppb	Ni	0.000	0.000	0.000	0.000	**0.000**	0.000	
100 ppb	Zn	3.376	3.506	2.620	2.677	**3.045**	0.461	15.15%
6.25 ppb	Cu	0.280	0.289	0.232	0.230	**0.258**	0.031	12.07%
6.25 ppb	Cd	0.000	0.000	0.000	0.000	**0.000**	0.000	
6.25 ppb	Pb	0.673	0.707	0.475	0.510	**0.591**	0.116	19.58%
6.25 ppb	Ni	0.000	0.000	0.000	0.000	**0.000**	0.000	
100 ppb	Zn	3.145	3.342	2.694	2.902	**3.021**	0.283	9.35%
25 ppb	Cu	1.740	1.172	1.172	1.278	**1.340**	0.271	20.22%
25 ppb	Cd	0.337	0.304	0.156	0.160	**0.239**	0.095	39.62%
25 ppb	Pb	1.846	1.597	1.643	2.040	**1.782**	0.203	11.42%
25 ppb	Ni	0.000	0.000	0.000	0.000	**0.000**	0.000	

100 ppb	Zn	0.722	0.547	0.130	0.511	**0.478**	0.249	52.21%
100 ppb	Cu	8.554	8.662	12.920	11.721	**10.464**	2.199	21.01%
100 ppb	Cd	5.575	5.634	3.020	2.993	**4.306**	1.500	34.84%
100 ppb	Pb	3.822	3.750	2.744	2.941	**3.314**	0.551	16.64%
100 ppb	Ni	0.722	0.547	0.103	0.511	**0.471**	0.262	55.64%

8.4.   Conclusions

It can be concluded that square wave anodic stripping voltammetry is a sensitive technique allowing the detection of various heavy metals in a ppb range. The detection performance depends mainly on the deposition potential as well as the unique composition of the working electrode (in our case carbon and carbon-bismuth were tested). In the case of Pb, using Bismuth electrodes in static mode (drop measurements), a LOD of 0.4 ppb was obtained, while using screen-printed carbon electrodes in flow mode 0.5 ppb respectively.

Flow-based detection of Cu and Zn was evaluated as well. Cu was detected with the LOD of 3 ppb and Zn was detected with the LOD of 12 ppb. Cu, similarly as Pb is relatively easy to detect and its determination is hardly affected by the presence of other metals in the sample. In the case of Zn, a presence of any other metals significantly affects the detection performance. This happens due to a very negative potential applied (-1.4 V) that reduces nearly all metals (as well as impurities) onto a screen-printed electrode surface.

8.5. References

1.   Medina-Sanchez, M., et al., *On-chip electrochemical detection of CdS quantum dots using normal and multiple recycling flow through modes*. Lab on a Chip, 2012. **12**(11): p. 2000-2005.

2.   Medina-Sanchez, M., S. Miserere, and A. Merkoci, *Nanomaterials and lab-on-a-chip technologies*. Lab on a Chip, 2012. **12**(11): p. 1932-1943.

3.   March, G., T.D. Nguyen, and B. Piro, *Modified Electrodes Used for Electrochemical Detection of Metal Ions in Environmental Analysis*. Biosensors 2015, **5**(2), 241-275.

4.   Barton, J., et al., *Screen-printed electrodes for environmental monitoring of heavy metal ions: a review*. Microchimica Acta, 2016. **183**(2): p. 503-517.

5.   Mayorga-Martinez, C.C., et al., *Bismuth nanoparticles for phenolic compounds biosensing application*. Biosensors & Bioelectronics, 2013. **40**(1): p. 57-62.

6.   Chałupniak, A. and A. Merkoçi, *Toward integrated detection and graphene-based removal of contaminants in a lab-on-a-chip platform*. Nano Research, 2017: p. 1-15.

7.   Sitko, R., et al., *Adsorption of divalent metal ions from aqueous solutions using graphene oxide*. Dalton Transactions, 2013. **42**(16): p. 5682-5689.

8.   Cadevall, M., J. Ros, and A. Merkoci, *Bismuth nanoparticles integration into heavy metal electrochemical stripping sensor*. Electrophoresis, 2015. **36**(16): p. 1872-1879.

ANNEX IV

Accepted manuscripts

18

Recent Trends in Nanomaterials Integration into Simple Biosensing Platforms

Andrzej Chałupniak and Arben Merkoçi

CONTENTS

18.1 Introduction

Since more than five decades when the first biosensor was implemented, research and development in this field have continuously progressed taking advantages of discoveries of new technologies and materials. Currently, due to the strategic importance of nanotechnology in modern science and industry, nanomaterials are increasingly being used in various applications with particular interest in various areas. There is no difference in the case of biosensors, where nanomaterials have found a versatile role as substrates for nanodevices fabrication, as signal transducers and labels.

The development of biosensors runs two ways at the same time. One of them relates to the complex and high-throughput analysis systems for certain compounds. Such biosensing systems can be used in modern analytical laboratories, clinical, and industrial applications. The second group consists of biosensing devices suitable for rapid analysis, which do not require the use of sophisticated equipment and trained personnel. This group is

particularly promising because it allows the creation of versatile products, available for everyone and easy to use, which are important, for example, in the diagnosis of disease markers, environmental monitoring out of the laboratory (infield), in places with low recourses and developing countries, where access to specialized laboratories is limited.

Access to technological innovations always affects the level of advancement of societies. For example, the widespread use of simple biosensors such as glucometers, pregnancy tests, and portable devices, can help in further creation of awareness in healthcare prevention. Thus, biosensors can play an important role in education [1].

In this chapter, different biosensing techniques are discussed, from easy paper-based biosensors to more complex Lab-on-a-Chip (LOC) devices. All of them combine the use of novel nanomaterials.

18.2 Nanomaterials Improve Biosensing

Nanomaterials play a major role in biosensing, due to the versatile functions that they can play in biosensors. Used as labels, they can produce signals that are easy to measure and quantify (that is, fluorescence emitted by Quantum dots (QDs); as signal amplifiers, they can enhance the response of the sensor (i.e., Iridium Oxide (IrOX) nanoparticles with their electrocatalytic activity). The unique electrical, chemical, and mechanical properties allow using nanomaterials as substrates for biosensing devices, that is, electrodes covered by graphene oxide (GO). Simultaneously, some nano/microparticles due to their porous structure can be used as carriers for bioreceptors molecules or demonstrate the ability to adsorb selected compounds, providing the ability to use them not only for sensing but also for removal of contaminants. Most of the nanomaterials can be easily conjugated with proteins, enzymes, antibodies, and DNA, what makes possible to obtain specific and sensitive biosensing systems. In this section, some interesting and efficient nanomaterials will be described regarding their application in biosensors.

18.2.1 N ano- and Microparticles

According to IUPAC definition, nanoparticles are particles of any shape with dimensions in the range of 1–100 nm, while microparticles are bigger with size in the range of 100– 100 μm [2,3]. Since there are a lot of micro/nanoparticles already reported as useful for biosensors, only some of them, particularly those more promising, will be described.

Gold Nanoparticles (AuNP) are one of the most commonly used nanoparticles. Depending of their size, which can be controlled during the synthesis process, they show different parameters both electrochemical and optical. This makes them very versatile and useful for various detection strategies, where AuNPs can work as labels and signal transducers. The conjugation of AuNP with proteins and other biomolecules is very easy and can be obtained without using specific linkers and chemical modification. This feature encourages scientists to use AuNP in biosensing. Due to their intensive color, AuNPs also can be used as labels in colorimetric test like paper-based immunoassay as well as in various electrochemical techniques as is explained below.

AuNPs are mainly employed as electrochemical labels in biosensors. In principle, there are two ways to detect them. The first method is Differential Pulse Voltammetry (DPV), where potential is applied to initiate the reaction of reducing tetrachloroaurate

ions to gold metal after (prior oxidation) and measured current used as analytical signal. This approach was reported, that is, for magnetoimmunoassay for Salmonella detection [4]. Another strategy for electrochemical detection with AuNP is taking advantage of Hydrogen Evolution Reaction (HER). In this case, AuNP presents catalytic activity (toward hydrogen ions reduction) when they are deposited onto the electrode in the presence of an acid (HCl). After applying a fixed potential, the current signal from the reducing hydrogen is measured and used as analytical signal. This reaction is easy to be followed making this approach very convenient and possible to be employed for various detection strategies like cancer cells [5,6], viruses, DNA, and protein detection. Another interesting example is immobilization of casein peptides to AuNP surface so as to obtain nanocarriers for electrochemical study of the adhesion of casein peptides to pathogen bacteria [7].

For more specific approaches, or detection improvements, AuNPs can be easily modified. For example, when AuNPs are modified with ferrocene derivative (FcD): 1,1′-ferrocenyl bis(methylene lipoic acid ester), such complex can work as an efficient transducing system due to shifting of the ferrocene oxidation potential. This approach was employed by Mars et al. for human IgG detection representing a novel potential shift-based transducing system for sensitive immunosensing [8].

Another interesting example is IrOx nanoparticles, with the size around 12 nm, which are synthesized from potassium hexachloroiridate (IV) (K_2IrCl_6) and sodium hydrogen citrate sesquihydrate ($Na_2C_6H_6O_7 \cdot 1.5H_2O$). Thanks to conductivity and electronic switching properties their possible application in biosensors is varied. IrOx nanoparticles are already reported as a conductivity enhancer for pesticides and phenol detection as well as an electrochemical label for ApoE immunoassay, where the antibodies are labeled with IrOx. They are able to enhance Water Oxidation Reaction (WOR). These nanoparticles electrocatalyze water splitting, which is followed by chronoamperometry by measurements of the current generated during the corresponding reaction [9].

One of the important expectations for the novel materials is to be environmentally friendly and biocompatible. Calcium carbonate microparticles ($CaCO_3MP$) meet these demands. The work of Lopez-Marzo et al. comprehensively describes the possibility of formation of $CaCO_3$-poly(ethyleneimine) (PEI). Such complex shows high potential for biosensing applications due to the possibility to conjugate it with proteins, nucleic acids, and other biomolecules [10]. These particles found applications also in microfluidic systems, working for both sensing and removal of phenol compounds. Biosensing ability was possible due to cross linking of $CaCO_3MPs$ with tyrosinase by glutaraldehyde, while the removal ability is connected with porous structure and capacity of microparticles to adsorb phenolic compounds [11].

18.2.2 Quantum Dots (QDs)

QDs, fluorescent semiconductors, have recently become increasingly popular tags for molecular imaging and biosensing. Their optical properties like narrow and size-tunable emission spectra (what leads to multicolor detection), various and broad absorption profiles and chemical stability, make them competitive with respect to organic fluorophores, which are commonly used as fluorescent labels [12, 13]. Depending on the type of QDs, their fluorescence lifetime can be 10 times longer comparing to organic fluorophores. However, QDs have some disadvantages like potential toxicity due to the presence of heavy metals, which is not well known yet, but also bigger size (from 2 to 15 nm) than organic fluorophores, what can be a drawback in some approaches [14].

An important advantage is the possibility of QD to be optically and electrochemically detected. Electrochemical method is related to detection of Cd contained in CdS QD (or any other metal depending on the QD). Such detection can be performed on screen-printed electrodes using Square Wave Anodic Stripping Voltammetry. While the potential is applied, in the presence of proper buffer, cadmium (Cd^{2+} ion onto the QD surface) is reduced to the working electrode surface and oxidized (electrochemical stripping). The specific peak, at the characteristic red-ox potential of cadmium can be observed [15]. This technique is faster, cheaper, and easier to be performed in comparison with optical detection. Electrochemical detection of QDs can be implemented to high-throughput, automated detection systems. Furthermore, electrochemical detection of QD is really sensitive. In the work reported by Medina-Sánchez et al., QD detection in microfluidic chip was possible in the range between 50 and 8000 ng mL^{-1} with a sensitivity of 0.0009 µA/(ng mL^{-1}) [16]. Since QDs usually contain thiol (-SH) and carboxyl (-COOH) on their surface reactive group, it is possible to easily conjugate them with biomolecules with sensing abilities (i.e., antibodies, aptamers) as well as with proteins like streptavidin, biotin, so as to obtain QDs labels that are able to perform analytical signal enhancement. To make it feasible, it is necessary to use a proper biolinker like primary amines, thioglycolic acid, peptides, or chitosan polymer [17]. QDs were already employed for electrochemical screening of apoptosis of mammalian cells. QDs conjugated with Annexin-V can effectively bind to phosphatidylserine, a phospholipid expressed in the outer membrane of apoptotic cells. Electrochemical detection, comparing to optical one was characterized by shorter time and possibility to perform versatile quantified analysis [18].

In the following parts, application of nanomaterials in biosensing techniques like LOC and microarray will be described.

18.2.3 Carbon Nanomaterials

Carbon is characterized by the presence in various allotropic forms. Physical and chemical properties of a given carbon allotrope depend on hybridization. Carbon materials that are found to be used in biosensing usually have sp2 hybridization. These are, for example, graphite, carbon nanotubes, and graphene.

Carbon nanomaterials, due to their surface properties, conductivity, and biocompatibility, are good candidates for application in electrochemical biosensors. For example, multiwalled carbon nanotubes (MWCNTs) were reported by Perez Lopez et al. as a material raising the signal intensity of tyrosinase biosensor for catechol detection by 90% [19]. This phenomenon was caused due to improved electronic transference between enzyme and MWCNTs layer. At the same time, surface properties of carbon nanotubes (CNTs) make them useful for enzyme and other biomolecules immobilization. The versatility of this material was also proofed in the work, where MWCNTs was immobilized onto magnetic particles for catechol detection and shown to be very useful and easy for manipulation in ON-OFF response biosensing platform [20].

Carbon nanomaterials also show interesting optical properties. In the work of MoralesNarvaez et al., the Förster Resonance Energy Transfer (FRET) was measured between QD and various carbon nanomaterials: graphite, CNTs, carbon nanofibers (CNFs), and GO. The highest quenching was observed for GO (97 ± 1%), which is what makes this material very useful for future applications employing the phenomena of FRET with interest for biosensing approach (Figure 18.1a) [21]. Moreover, Graphene Quantum Dots (GQD) can be used for small molecules detection (Figure 18.1b) due to the ability of convenient **385**
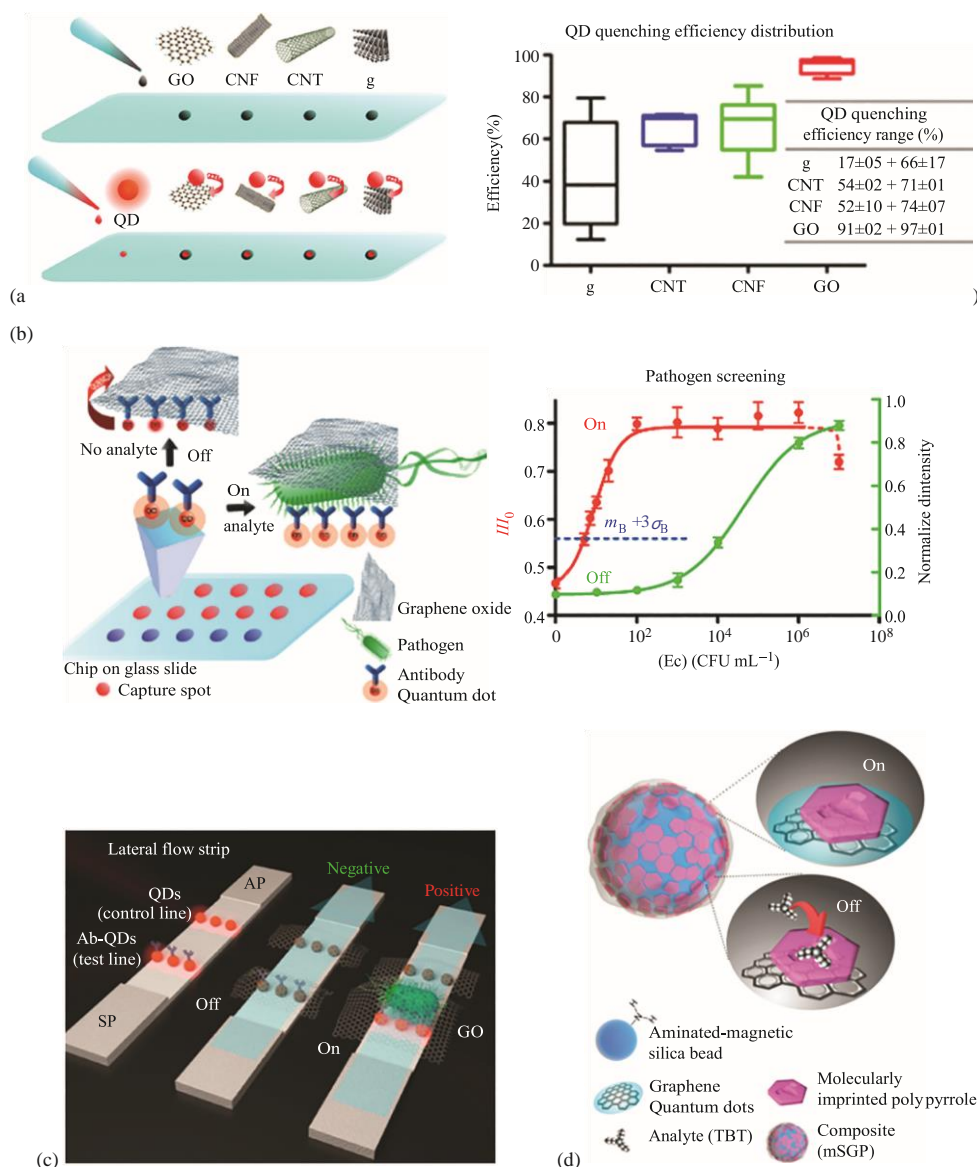
FIGURE 18.1
Carbon nanomaterials in optical biosensing. (a) Comparison of QD quenching caused by various carbon nanomaterials (GO—Graphene Oxide, CNT—Carbon nanotubes, CNF—Carbon nanofibers, g—graphite). (Reprinted from *Carbon*, 50(8), Morales-Narvaez, E. et al., Simple Forster resonance energy transfer evidence for the ultrahigh quantum dot quenching efficiency by graphene oxide compared to other carbon structures, 2987–2993, Copyright 2012, with permission from Elsevier.); (b) Pathogen detection in microarray format using
GO as a revealing agent. (Modified with permission from, John Wiley & Sons, Copy Right 2013, MoralesNarvaez, E. et al. 2013. *Angewandte Chemie-International Edition* 52(51), 13779–13783.); (c) Pathogen detection in lateral-flow format using GO as a revealing agent. (Reprinted with permission from Morales-Narvaez, E. et al. 2015. Photoluminescent Lateral-flow immunoassay revealed by graphene oxide: Highly Sensitive paper-based pathogen detection. *Anal. Chem.* 87(16), 8573–8577. Copyright 2015 American Chemical Society.); (d) Smallmolecule detection based on molecularly imprinted polymer (MIP) and GO. (Reprinted with permission from Zor, E. et al. 2015. Graphene quantum dots-based photoluminescent sensor: A multifunctionalcomposite for pesticide detection. *ACS Appl. Mat. Interfaces*. Copyright 2015 American Chemical Society.)

conjugation with magnetic silica beads (used as a carrier) and molecular imprinted polymer (recognition of the analyte) [22].

Carbon nanomaterials can play varied roles in biosensors. For further studies we recommend the following reviews that comprehensively describe them [13, 23]. Some examples of application of carbon materials in optical biosensors are presented in Figure 18.1.

18.2.4 Micro- and Nanomotors

Just as the name suggests, micro- and nanomotors are supposed to perform various mechanical movements like, for example, shuttling, rolling, and rotation on others, due to inducing them by a specific factor. We can distinguish nano/micromotors driven by light, magnetic field, acoustic wave (physical control), as well as by energy resulting from various chemical reactions, where selected compounds act as fuels for motors [26]. Nano/micromotors movement behavior opens a lot of opportunities to take as advantage in biosensing systems. They can support mixing process in microscale, what improves mass transport and increases the intensity of sensors response; for example, in microarray. Acting as carriers, nano/micromotors can be conjugated with biomolecules such as antibodies working as moving sensing or capturing probe, which can be applied in microfluidic systems [27]. Nano/micromotors are promising tools not only in biodetection but also removal. A good example is the work of Guix et al. where alkanethiol-coated Au/Ni/PEDOT/Pt shows ability to capture, transport, and remove oil droplets [28]. Another interesting example is bacteria detection made through Concanavalin A (ConA) immobilized onto the nanomotors surface [29].

18.2.5 Micromotors Support Mass Transport

Usability and versatility of different assays performed in liquid phase (such as immunoassays) can be limited by mass transport, which depends on chemical and physical properties of the molecules working as a bioreceptor and target. The induction of any kind of micromixing can be helpful for improving the efficiency of the assay. One of the promising approaches is using self-propelling micromotors. In that work, protein detection (ApoE) based on immunoassay, with fluorophore as a label, was improved 3.5-folds (signal intensity) due to application of Polianyline (PANI)-platinum micromotors. Amplification of the signal at the same time can significantly reduce the limit of detection (LOD). The only potential drawback in this study is using hydrogen peroxide as a fuel for micromotors, which in some cases can be a way to degrade the proteins used in a given assay [30].

18.2.6 Nanochannels

Another approach in the application of nanomaterials is using them as filters, which selectively allowed analyte (e.g., protein biomarkers) passing through them. This is the example of biomimetic approach, because in live organisms, cell metabolism is driven by proteins located in cell membranes which are selectively permeable for various ions, nutrients, and other biomolecules [31].

Nanochannels support high sensitivity and selectivity in biosensing. Due to determined size of pores, sample is filtered (interfering big size analytes remain on top of the channel) when it reaches the inner surface of nanochannels where the bioreception occurs. Such behavior reduces the risk of unspecific bonding and introduction of any interference from impurities. Nanochannels can be functionalized inside the membranes; so it

is possible to stop the analyte inside them. The nanochannel blocking can be followed by electrochemical techniques [31]. One of the example is voltammetric detection of trombine, where anodized alumina oxide filter (AAO) membrane was used as a nanochannel, with internal diameter of porous 200 nm. As a bioreceptor, antitrombin IgG labeled with AuNP was used. When the channel is blocked due to immunocomplex formation, diffusion of $[Fe(CN)_6]^{4-}$ is decreased serving such a phenomena (DPV signal decrease) as a source of analytical signal. This system showed very low LOD (LOD 1.8 ng mL^{-1}), even when the analysis was performed in spiked blood samples [32]. Nanochannels can be effectively used for cancer biomarkers sensing from the blood thanks to nanochannel-based filtration of the whole blood. In that case, it was possible to detect 52 U mL^{-1} of CA15-3 breast cancer marker [33]. Another approach for cancer biomarkers was studied using Prussian blue nanoparticles (PBNPs) working as a redox indicator in immunoassay. Application of PBNPs instead of $[Fe(CN)_6]^4$ led to lower detection limit (from 200 µg mL^{-1} to 34 pg human IgG mL^{-1}) (Figure 18.2b and c) [34].

Various materials can be employed for nanochannels preparation. One of the recently published examples is the use of carboxylated polystyrene nanospheres (PS, 500 and 200 nm-sized) coating the working area of flexible screen-printed indium tin oxide/ polyethylene terephthalate (ITO/PET) electrode. Similarly as an example mentioned above, this platform was used for IgG detection as a model protein. Unlike AAO membranes, this approach overcomes many of the limitations in terms of integration and sensitivity, and represents a really disposable biosensing device for a one-step assays (Figure 18.2a) [35].

18.3 Paper NanoBiosensors

The launch of the first pregnancy test in the mid-1970s started the popularity of paperbased biosensors. It was proof that biosensors can be simple devices, possible to be used by everyone, relatively cheap and accessible. Nowadays, when all innovations are also assessed for their impact on the environment, paper-based biosensors positively stand out for their biodegradability and safety for the user and the environment. The portability of paper-based biosensors allows using them in any place on earth, regardless of the availability of specialized laboratories and personnel. This opens the way to improve medical diagnostics and environmental monitoring in developing countries. Paper-based biosensors can also be used in food and pharmaceutical industry to perform preliminary analyses related to quality control, which precede further in-depth test in dedicated laboratories. Furthermore, these biosensors can be both qualitative and quantitative, depending on the needs. Optical detection, possible even with the naked eye, is easy and fast [36, 37].

Paper-based biosensors are already used for proteins, DNA, and other compounds sensing. Like in most biosensors, detection is based on affinity of the specific antibodies or DNA sequences (or aptamers) to target compounds [36]. Although most of the articles present paper-based biosensors for biomarkers detection, these devices also represent an interesting solution for environmental screening. One of the examples is heavy metal detection (cadmium) in paper device reported by López-Marzo et al. [38, 39].

Lateral flow assays (LFA) are one of the most popular paper-based sensors, and their main advantages is versatility and different detection possibilities (optical, electrochemical).
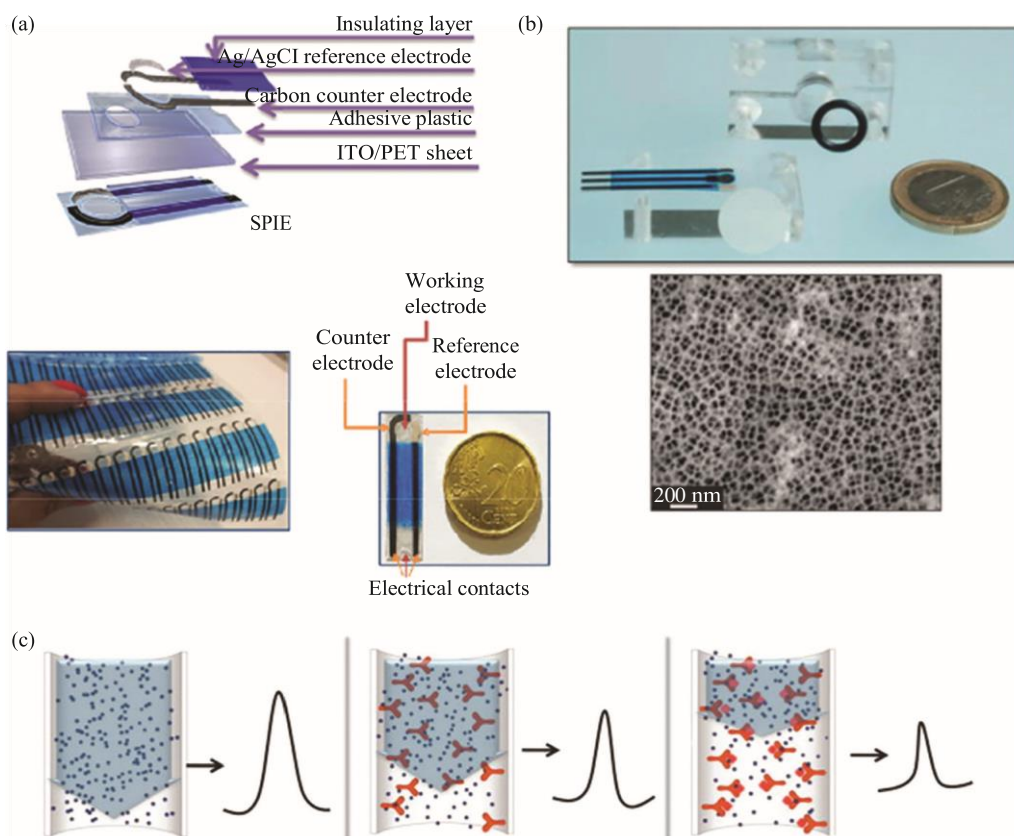
FIGURE 18.2
Application of nanochannels in biosensing. (a) Schematic representation of the different materials and layers, which form the SPIE (screen-printed ITO/PET electrodes). (With kind permission from Springer Science+Business Media: *Nano Res.*, Nanoparticles-based nanochannels assembled on a plastic flexible substrate for label-free immunosensing, 8(4), 2015, 1180–1188, de la Escosura-Muniz, A. et al.); (b) Schematic representation of the process occurring on the nanochannels modified electrode. (Reprinted from *Biosens. Bioelectron.,* 67, Espinoza-Castaneda, M. et al., Nanochannel array device operating through Prussian blue nanoparticles for sensitive label-free immunodetection of a cancer biomarker, 107–114, Copyright 2015, with permission from Elsevier.); (c) Schematic representation of the sensing principle: the voltammetric signal of the PBNPs decrease with the subsequent AAO membranes modification. (Reprinted from *Biosens. Bioelectron.,* 67, EspinozaCastaneda, M. et al., Nanochannel array device operating through Prussian blue nanoparticles for sensitive label-free immunodetection of a cancer biomarker, 107–114, Copyright 2015, with permission from Elsevier.)

They consist of detection pad, conjugation pad, sample pad, and absorption pad. Detection pad is made of nitrocellulose and its role is capturing the analyte since capturing bioreceptors (i.e., antibodies) are printed onto it. Glass fiber is used for conjugation pad, where conjugate with the color label (e.g., AuNP) is stored. Sample and absorption pads are made of cellulose; those pads support the flow of the liquid and purify the sample [36, 37, 39].

Although paper-based biosensors offer many opportunities it is still necessary to overcome some drawbacks like improving the limit of detection, sensitivity, and enabling parallel detection of different targets. Application of nanoparticles, through working both as a carrier or label can increase the usability of this type of biosensors.

One of the promising tools in paper-based biosensors is AuNP nanoparticles, due to strong red color, which facilitates optical detection and properties useful for electrochemical

sensing. Applications of AuNP for sensing various protein, DNA, and cancer cells in paper biosensors are already reported. To improve detection, different types of particles can be used, that is, QDs or magnetic particles [36].

A very interesting solution to enhance the signal for optical detection in paper-based biosensor is using enzymes able to perform reaction resulting in appearance of color. Such approach was proposed by Parolo et al. where AuNP was conjugated with antibodies previously labeled with HRP. Increase of the color on the strip (by the use of various HRP substrates; in that case TMB, AEC, and DAB) increased the sensitivity of the assay up to 1 order of magnitude in comparison with nonmodified AuNPs [40].

Seeing that paper-based biosensors operation is based on liquid flow, optimization of this parameter can provide interesting results. Changing the geometry characteristics of the pads like width, shape, and length affect flow speed and distribution of the liquid (Figure 18.2). In the work of Parolo et al., the increase of the sensitivity was up to eightfold due to increasing the size of conjugation and sample pad (Figure 18.2b) [41]. Referring to the idea of liquid flow manipulation to enhance the sensitivity of paper-based device, Rivas et al. proposed the use of delay hydrophobic barriers fabricated by wax printing. For this purpose, wax pillar patterns were printed onto the nitrocellulose membrane to generate delays as well as pseudoturbulence in the microcapillary flow. Biosensing performed for model protein (HigG) showed threefold improvement of the sensitivity (Figure 18.2c) [42].

Another approach increasing sensitivity is triple-line lateral flow sensor reported by Rivas et al. for *Leishmania infantum* DNA detection. Beside control line, two test lines are printed onto the LF strip in order to detect double-labeled (FITC/biotin) amplified *Leishmania* DNA (TL1) and 18S rNA gene (endogenous control) (TL2) [43].

All of the examples mentioned above were focused on colorimetric detection of analytes. However, it is possible also to design photoluminescent LF biosensor, where QD-Ab complex is printed on the substrate and GO is used as a quenching agent. Morales-Narvaez et al. reported photoluminescent detection of *E. Coli* and *S. Typhimurium* with a LOD of 10 CFU mL^{-1} in standard buffer and 100 CFU mL^{-1} in bottled water and milk [25].

Mechanical strength and chemical neutrality allow fabricating electrochemical paperbased biosensors, where electrodes are printed directly on the various paper material in the same way such as commonly used screen-printed electrodes. An example of this approach was shown by Parolo et al. The nitrocellulose membrane HF240 was used to fabricate screen-printed carbon electrodes (SPCE), which was tested for AuNP and QD electrochemical detection. Such electrodes, compared with SPCE-based on polyester show significantly higher hydrophilicity of the surface and better electrochemical response. Those properties are linked to 3D structure of the membrane, which enhance the performance of the device [44].

Future development for paper-based devices seems to be so potent because of the need for readily available and inexpensive biosensors. The main challenge is to increase the level of specificity, sensitivity, and improve fabrication process, which would help in attaining better reproducibility of assays performed in paper-based biosensors.

One of the critical points in development of paper-based nanobiosensors is finding the novel type of paper substrates, which are easy to fabricate, biocompatible, and suitable for performing various chemical/biological reactions. One of the promising material is nanopaper. Bacterial cellulose nanopaper is a multifunctional material known for numerous properties such as biocompatibility, optical transparency, sustainability, biodegradability, thermal properties, high mechanical strength, flexibility, hydrophilicity, **390**

broad chemical-modification capabilities, high porosity, and high surface area. Its interaction with QD, GO, AuNP, and AgNP were already studied by Morales-Narvaez et al. showing a very good suitability of nanopaper for further biosensing applications (Figure 18.2a) [45].

18.4 Microarray Technology

High-throughput technologies are of interest to both scientists and entrepreneurs. Microarrays due to their versatility are currently used for sensing different compounds and molecules such as DNA, RNA, peptides, proteins (including antibodies), and also cells or tissues. Microarray revolutionized genomic studies due to the possibility to measure expressions of various genes in a short time or to perform genotyping. Nowadays, microarrays have gained recognition as a promising tool for biosensing [46]. These platforms are really flexible. As a substrate for spotting, different types of glass (or other materials), with various chemical modifications, that is, silanization can be used, so as to fit it to the type of spotted molecule. Depending on the willingness of the user/researcher, targets or capture agent can be spotted (i.e., antibodies). In this case, microarray sensing can act as a direct, indirect, or competitive assay—similar to ELISA. In this section, the main lines of development for this biosensing technology including another way to improve their versatility are described [47, 48].

18.4.1 Q Ds as a Fluorescence Enhancer

Many researchers are looking for new compounds that will be successfully used as fluorescence markers in biodetection systems. QDs can effectively replace organic fluorophores in microarray biosensing. It is worth mentioning that QDs comparing with organic fluorophores have broader and stronger absorption spectra and their emission is characterized by narrow and symmetric spectrum [14]. Depending on the type of QDs, their fluorescence lifetime can be 10 times longer comparing to organic fluorophores. In the work of Morales Narvaez et al., cadmium-selenide/zinc sulfide (CdSe/ZnS) QDs were tested versus fluorescent dye Alexa 647 as reporters in protein immunoassay (ApoE was used as a model protein). Authors observed that QDs are highly effective reporters in microarray, but their properties strongly depend on excitation wavelength. For 532 nm excitation wavelength, using QDs provided five times lower LOD. Those studies open the way for further use of QDs in microarray [14].

18.4.2 GO as a Fluorescence Quenching Factor in Microarray

Due to the ability of GO to quench the fluorescence, described earlier, it is possible to take advantage of this phenomena in biosensing strategy. The properties of fluorescence quenching depend on the distance between donor and acceptor (according to FRET phenomena). Therefore, it can be assumed that increasing the distance between QDs (donor) and GO (acceptor) measurable changes in fluorescence can be observed [12,49]. This approach has been used for bacteria detection (*E. coli* O157:H7). QDs c onjugated with antibodies against bacteria were spotted on the glass slide. The slides were incubated with samples with or without (blank) bacteria and subsequently GO was **391**
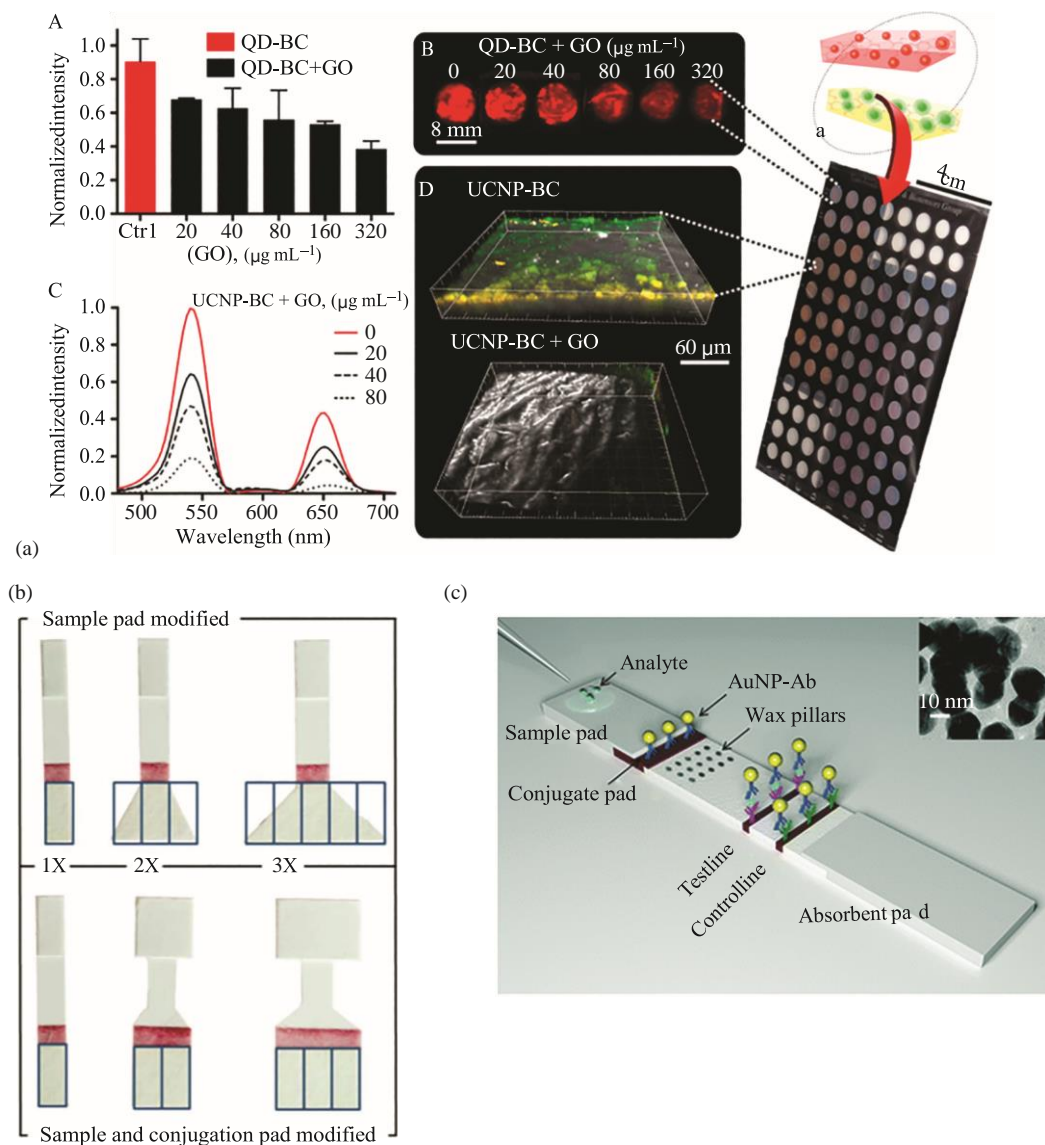
FIGURE 18.3

Novelties in the field of paper biosensors. (a) Nanopaper (BC) multiwell plate for photoluminescent tests. (Reprinted with permission from Morales-Narvaez, E. et al. 2015. Nanopaper as an optical sensing platform. *Acs Nano*. 9(7), 7296–7305. Copyright 2015 American Chemical Society.); (b) Modification of lateral flow test geometry in order to improve sensitivity. (Parolo, C. et al. 2013. Simple paper architecture modifications lead to enhanced sensitivity in nanoparticle based lateral flow immunoassays. *Lab Chip* 13(3), 386–390. Reproduced by permission of The Royal Society of Chemistry.); (c) Application of wax pillars as a hydrophobic barriers in lateral flow test. (Rivas, L. et al. 2014. Improving sensitivity of gold nanoparticle-based lateral flow assays by using wax-printed pillars as delay barriers of microfluidics. *Lab Chip* 14(22), 4406–4414. Reproduced by permission of The Royal Society of Chemistry.)

added. The biggest quenching was observed in blanks, while spots with bacteria showed reduced quenching (increase of fluorescence) (Figure 18.1b). However, this response that was found to be as a digital-like test very versatile and efficient for bacteria detection (LOD: 5 CFU mL^{-1}) cannot be used for sensing proteins or small molecules due to their size, which is not sufficient to affect the level of quenching [24, 50].

18.5 Lab-on-a-Chip (LOC)

Microfluidic LOC devices are characterized by small size of sensing platforms, small volume of reagents (μL, nL, pL, fL) used for performing assay, and low energy consumption. Microfluidic systems can be well automated and used either for preconcentration, isolation, and detection of interesting analytes. One of the most interesting applications is microfluidic chips for electrochemical and optical biosensing, which can be applied for detection of various biomarkers, organic compounds, etc. Versatility of LOC devices makes possible to integrate various sensing materials and strategies [51].

LOC microfluidic devices usually consist of microfluidic chip and driving units. Samples and reagents are introduced into the channel. Flow can be driven by different kinds of syringe pumps or dedicated flow control systems. Newest solutions also allow manipulating of liquids by surface acoustic wave and micropumps. Small diameter of microfluidic channel causes relatively low usage of reagents. Thanks to external driving units, parameters of reaction can be well controlled. Environment of microfluidic channel is permanently isolated from outside (unlike most assays performed in microplates, test tubes, etc.), which protects reactions and facilitates reproducible results. Depending on the purpose, different designs of microfluidic chips can be used for mixing, incubation, and preconcentration of the sample. Channels can also work as incubators for cell culturing and carrying out specific chemical reactions. For biosensing applications, chips with incorporated electrodes are particularly interesting to obtain electrochemical sensors. The surface of the channel can be treated by different reagents for further modification by biomolecules (i.e., proteins). In addition, devices equipped with magnets are useful for performing magnetoimmunoassay utilizing magnetic beads (MB) [51,52]. Researchers are focused on miniaturization detection platforms as well as all driving units, which assist them. Recently, LOC devices with all integrated electronic driving units were obtained by using printed circuit board (PCB) as a substrate for microfluidic chip [53, 54].

18.5.1 Unlimited Possibilities of Microfluidic Devices Designs

One of the common techniques for efficient prototyping of microfluidic devices is softphotolithography, where polydimethylsiloxane (PDMS) chip is fabricated with hollowed microfluidic channel and substrate capable for permanent bonding with PDMS [54]. Apart from glass, one of the most widespread materials used for this purpose is polycarbonate (PC). PC is especially interesting as a substrate in electrochemical microfluidic devices due to the possibility of using electrodes directly printed on its surface. This is possible thanks to well-developed screen-printed technology, however, it can be fabricated using different techniques, for example, ink-jet printing and photolithography. The flexibility of screen-printing technology allows their application in microfluidic **393**

platforms obtaining various platforms with customized electrodes. On the other hand, transparency of PDMS enables for visual control of the process either in macro- and microscale (using optical

microscopes). More sophisticated microfluidic chips consist of channel layer where all reaction occurs and control layer, also made of PDMS but responsible for controlling of the flow of liquid by operating the valves built in the chip and driven by air pressure. This strategy can be used for increasing the sensitivity of assay by recirculation of the compounds that can be detected [16]. Another important feature of PDMS is oxygen permeability; thanks to this, PDMS chips are widely used for cell culturing [51].

18.5.2 Detection and Removal of Hazardous Compounds in Microfluidic Systems

A large number of dangerous compounds such as toxins, pesticides, chemicals, and biocidal compounds require continuous and rapid monitoring of their concentrations. Microfluidic systems due to their automation and small volume of sample needed for analysis can be a promising approach especially for analysis of such kinds of compounds. Microfluidic platforms can combine in one device all analysis steps such as cleaning, preconcentration, detection, and further removal of a given analyte. This also leads to the possibility of creating portable devices, which could work without necessarily using sophisticated professional laboratory equipments. Smart systems for different pollutants detection, where sensing strategy is based on inhibition of enzymatic reactions are already reported. For example, a simple LOC device is based on biocompatible and biodegradable $CaCO_3$-PEI nanostructured microparticles (MPs) used to detect and remove phenolic wastes. The detection of phenol using a hybrid PDMS/glass chronoimpedimetric microchip and its removal in the same LOC system through the use of an extra $CaCO_3$-PEI MPs microcolumn was achieved (with LOD 4.64 nM) [11, 55].

Due to the easy fabrication process and flexibility, LOC devices can integrate novel material for electrochemical detection. One of the examples is the work reported by Medina-Sanchez et al. where boron-doped diamond (BDD) electrodes are employed for electrochemical detection and degradation of the pesticide atrazine (Atz). Chronoamperometry revealed a very low LOD of 3.5 pM for Atz [56].

18.5.3 E ffective Sensing of Biomarkers

Common biological interactions usually used for biomarkers detection like antigen–antibody (immunoassays), enzyme–substrate, and aptamer–target can be easily implemented to microfluidic platforms. Thanks to this, it is possible to obtain better LOD, faster response of sensor, and moreover prototyping of multifunctional devices able to analyze a number of biomarkers from one sample in one device. Similarly, just as in microfluidic systems for environment monitoring, it is possible to perform in one chip all necessary steps for sample pretreatment. This is very important taking into account that clinical samples usually consist of blood, serum, etc. In our group, we have already proposed microfluidic devices for different biomarkers (i.e., IgG [57], ApoE) working as an electrochemical sensors. Most of obtained solutions are based on sandwich immunoassay, where specific antibodies against given target. Furthermore, secondary antibodies were used and functionalized with QDs, which allowed for sensitive electrochemical detection (Square Wave Anodic Stripping Voltammetry) of interesting biomarkers [52].
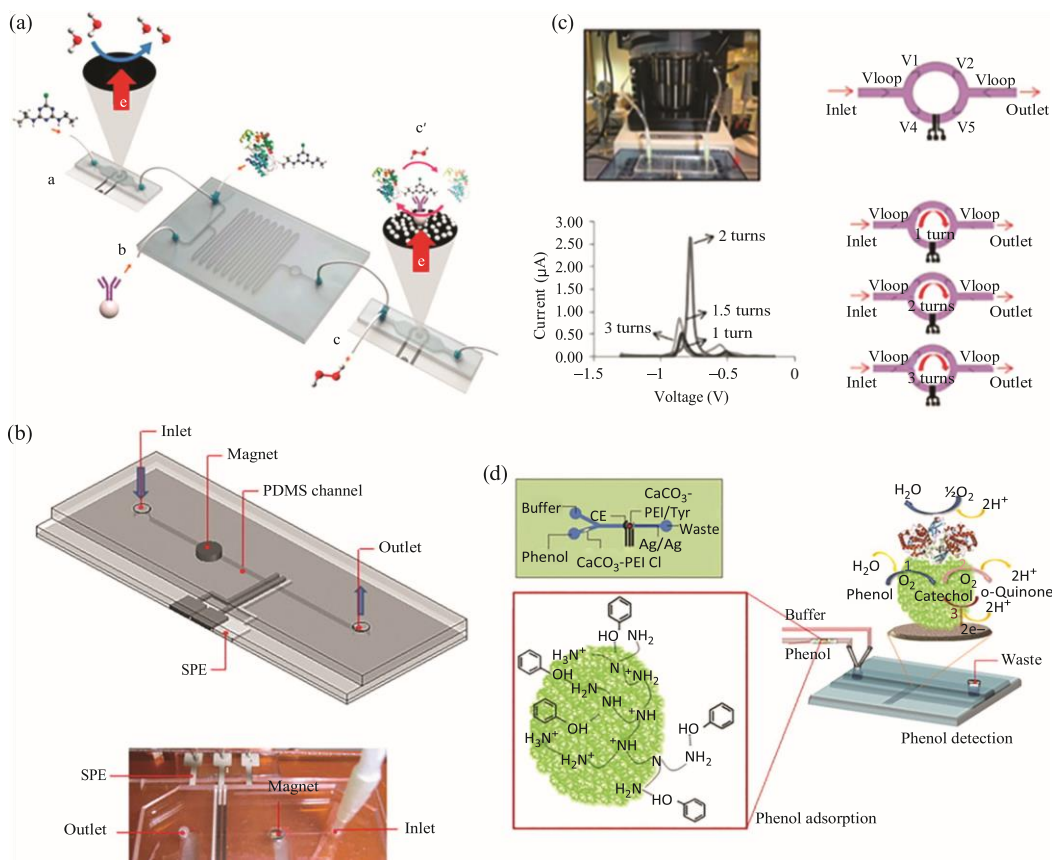
FIGURE 18.4

Lab-on-a-chip platforms for biosensing application. (a) Atrazine detection and degradation in LOC device. (Reprinted from *Biosens. Bioelectron*, Medina-Sánchez et al., Microfluidic platform for environmental contaminants sensing and degradation based on boron-doped diamond electrodes, Copyright 2015, with permission from Elsevier.); (b) Electrochemical detection of ApoE in LOC device using QDs as labels. (Reprinted from *Biosens. Bioelectron.*, 54, Medina-Sanchez, M. et al., On-chip magneto-immunoassay for Alzheimer's biomarker electrochemical detection by using quantum dots as labels, 279–284, Copyright 2014, with permission from Elsevier.); (c) Improved electrochemical QDs detection in recycling flow through mode LOC device. (MedinaSanchez, M. et al. 2012. On-chip electrochemical detection of CdS quantum dots using normal and multiple recycling flow through modes. *Lab Chip*. 12(11), 2000–2005. Reproduced by permission of The Royal Society of Chemistry.); (d) Phenol detection and removal in LOC device with CaCO₃ microparticles as an adsorbent. (Reprinted from *Biosens. Bioelectron*, 55, Mayorga-Martinez, C. C. et al., An integrated phenol "sensoremoval" microfluidic nanostructured platform, 355–359, Copyright 2014, with permission from Elsevier.)

18.6 Conclusions

In this chapter, nanomaterials as flexible building blocks of biosensing devices have been presented. Due to the use of nanomaterials, we can observe progressive change in the field of biosensing devices.

Electrochemical biosensors achieved increased sensitivity and LOD due to the application of various nanoparticles such as AuNP, IrO2, QD, as well as carbon materials. All those materials play a role of effective label, as the chemical reaction they catalyze/perform is

related to the quantity of a given analyte. Similarly, optical biosensing became more potent by using QDs in microarray assays compared to commonly known organic fluorophores. Most of the nanomaterials are suitable to be used in various conditions. Because of this property they can be employed for paper-based nanobiosensors as well as LOC devices. Another possible function of nanomaterials is intermediation in (bio)chemical reactions, one of the good examples is nanomotors, which motion support the mass transport of bio-molecules improving the sensitivity of immunoassays performed in microarray format. Moreover, nanomaterials can be used as a substrate for biosensing platform and/or environment of reaction. Nanopaper (bacterial cellulose) is a very promising material in various optical-sensing techniques due to its physical and chemical properties. Nanochannels made of different materials can work as effective filters and separate analyte from the solution.

One of the factors facilitating popularization of nanomaterials is its ease of synthesis. Another crucial factor is that even though nanomaterials may be expensive, the quantity used for biosensing assay is sufficiently low (this is especially seen in microfluidic biosensors) to make the final biosensing device relatively cost-effective, which is essential from the point of view of possible commercialization of such novelties.

However, novel nanomaterials present interesting chemical and physical properties and their interaction with humans, animals, and environment is not well known yet. For this reason, implementation of any new nanomaterial in biosensors should be always preceded by a thorough risk analysis.

References

1. Naik, P. P. et al. 2015. Android integrated urea biosensor for public health awareness. *Sens. Biosens. Res.* 3, 12–17.
2. Aleman, J. et al. 2007. Definitions of terms relating to the structure and processing of sols, gels, networks, and inorganic-organic hybrid materials (IUPAC recommendations 2007). *Pure Appl. Chem.* 79(10), 1801–1827.
3. Vert, M. et al. 2012. Terminology for biorelated polymers and applications (IUPAC Recommendations 2012). *Pure Appl. Chem.* 84(2), 377–408. 4. Afonso, A. S. et al. 2013. Electrochemical detection of Salmonella using gold nanoparticles. *Biosens. Bioelectron.* 40(1), 121–126.
5. de la Escosura-Muniz, A. et al. 2009. Rapid Identification and quantification of tumor cells using an electrocatalytic method based on gold nanoparticles *Anal. Chem.* 81, 10268.

6. Maltez-da Costa, M. et al. 2012. Detection of Circulating cancer cells using electrocatalytic gold nanoparticles. *Small* 8(23), 3605–3612.
7. Espinoza-Castaneda, M. et al. 2013. Casein modified gold nanoparticles for future theranostic applications. *Biosens. Bioelectron.* 40(1), 271–276.
8. Mars, A. et al. 2013. Gold nanoparticles decorated with a ferrocene derivative as a potential shift-based transducing system of interest for sensitive immunosensing. *J. Mat. Chem. B.* 1(23), 2951–2955.
9. Mayorga-Martinez, C. C. et al. 2014. Iridium oxide nanoparticle induced dual catalytic/ inhibition based detection of phenol and pesticide compounds. *J. Mat. Chem. B.* 2(16), 2233–2239.
10. Lopez-Marzo, A., Pons, J., and Merkoci, A. 2012. Controlled formation of nanostructured $CaCO_3$-PEI microparticles with high biofunctionalizing capacity. *J. Mat. Chem. B.* 22(30), 15326–15335.

11. Mayorga-Martinez, C. C. et al. 2013. Nanostructured CaCO$_3$-poly(ethyleneimine) microparticles for phenol sensing in fluidic microsystem. *Electrophoresis* 34(14), 2011–2016.
12. Marin, S. et al. 2011. Electrochemical Investigation of cellular uptake of Quantum Dots decorated with a proline-rich cell penetrating peptide. *Bioconjugate Chem.* 22(2), 180–185.
13. Marin, S., and Merkoci, A. 2012. Nanomaterials Based electrochemical sensing applications for safety and security. *Electroanalysis* 24(3), 459–469.
14. Morales-Narvaez, E. et al. 2012. Signal Enhancement in antibody microarrays using quantum dots nanocrystals: Application to potential Alzheimer's disease biomarker screening. *Anal. Chem.* 84(15), 6821–6827.
15. Marin, S., and Merkoci, A. 2009. Direct electrochemical stripping detection of cystic-fibrosis related DNA linked through cadmium sulfide quantum dots. *Nanotechnology* 20(5), 055101. 16. Medina-Sanchez, M. et al. 2012. On-chip electrochemical detection of CdS quantum dots using normal and multiple recycling flow through modes. *Lab Chip.* 12(11), 2000–2005.
17.   Mazumder, S. et al. 2009. Review: Biofunctionalized quantum dots in biology and medicine. *J. Nanomat.*

18. Monton, H. et al. 2015. Annexin-V/quantum dot probes for multimodal apoptosis monitoring in living cells: Improving bioanalysis using electrochemistry. *Nanoscale* 7(9), 4097–4104.
19. Perez Lopez, B., and Merkoci A. 2009. Improvement of the electrochemical detection of catechol by the use of a carbon nanotube based biosensor. *Analyst* 134(1), 60–64.
20. Perez-Lopez, B., and Merkoci, A. 2011. Magnetic nanoparticles modified with carbon nanotubes for electrocatalytic magnetoswitchable biosensing applications. *Adv. Funct. Mat.* 21(2), 255–260.
21. Morales-Narvaez, E. et al. 2012. Simple Forster resonance energy transfer evidence for the ultrahigh quantum dot quenching efficiency by graphene oxide compared to other carbon structures. *Carbon* 50(8), 2987–2993.
22. Zor, E. et al. 2015. Graphene quantum dots-based photoluminescent sensor: A multifunctional composite for pesticide detection. *ACS Appl. Mat. Interfaces.*
23. Perez-Lopez, B., and Merkoci, A. 2012. Carbon nanotubes and graphene in analytical sciences. *Microchimica Acta* 179(1–2), 1–16.
24. Morales-Narvaez, E., Hassan, A.-R., and Merkoci, A. 2013. Graphene oxide as a pathogenrevealing agent: Sensing with a digital-like response. *Angewandte Chemie-International Edition* 52(51), 13779–13783.
25. Morales-Narvaez, E. et al. 2015. Photoluminescent Lateral-flow immunoassay revealed by graphene oxide: Highly Sensitive paper-based pathogen detection. *Anal. Chem.* 87(16), 8573–8577.
26. Guix, M., Mayorga-Martinez, C. C., and Merkoci, A. 2014. Nano/micromotors in (bio)chemical science applications. *Chem. Rev.* 114(12), 6285–6322.
27. Garcia, M. et al. 2013. Micromotor-based lab-on-chip immunoassays. *Nanoscale*, 5(4), 1325–1331.
28. Guix, M. et al. 2012. Superhydrophobic alkanethiol-coated microsubmarines for effective removal of oil. *Acs Nano* 6(5), 4445–4451.
29. Campuzano, S. et al. 2012. Bacterial isolation by lectin-modified microengines. *Nano Lett.* 12(1), 396–401.
30. Morales-Narvaez, E. et al. 2014. Micromotor enhanced microarray technology for protein detection. *Small* 10(13), 2542–2548.
31. de la Escosura-Muniz, A., and Merkoci, A. 2012. Nanochannels preparation and application in biosensing. *Acs Nano* 6(9), 7556–7583.
32. de la Escosura-Muniz, A. et al. 2013. Nanochannels for diagnostic of thrombin-related diseases in human blood. *Biosens. Bioelectron.* 40(1), 24–31.
33. de la Escosura-Muniz, A., and Merkoci, A. 2011. A nanochannel/nanoparticle-based filtering and sensing platform for direct detection of a cancer biomarker in blood. *Small* 7(5), 675–682.
34. Espinoza-Castaneda, M. et al. 2015. Nanochannel array device operating through Prussian blue nanoparticles for sensitive label-free immunodetection of a cancer biomarker. *Biosens. Bioelectron.* 67, 107–114.

35. de la Escosura-Muniz, A. et al. 2015. Nanoparticles-based nanochannels assembled on a plastic flexible substrate for label-free immunosensing. *Nano Res.* 8(4), 1180–1188.
36. Parolo, C., and Merkoci, A. 2013. Paper-based nanobiosensors for diagnostics. *Chem. Soc. Rev.* 42(2), 450–457.
37. Quesada-Gonzalez, D., and Merkoci, A. 2015. Nanoparticle-based lateral flow biosensors. *Biosens. Bioelectron.* 73, 47–63.
38. Lopez Marzo, A. M. et al. 2013. All-integrated and highly sensitive paper based device with sample treatment platform for Cd^{2+} immunodetection in drinking/tap waters. *Anal. Chem.* 85(7), 3532–3538.
39. Lopez-Marzo, A. M. et al. 2013. High sensitive gold-nanoparticle based lateral flow Immunodevice for Cd^{2+} detection in drinking waters. *Biosens. Bioelectron.* 47, 190–198.
40. Parolo, C., de la Escosura-Muniz, A., and Merkoci, A. 2013. Enhanced lateral flow immunoassay using gold nanoparticles loaded with enzymes. *Biosens. Bioelectron* 40(1), 412–416.
41. Parolo, C. et al. 2013. Simple paper architecture modifications lead to enhanced sensitivity in nanoparticle based lateral flow immunoassays. *Lab Chip* 13(3), 386–390.
42. Rivas, L. et al. 2014. Improving sensitivity of gold nanoparticle-based lateral flow assays by using wax-printed pillars as delay barriers of microfluidics. *Lab Chip* 14(22), 4406–4414.
43. Rivas, L. et al. 2015. Triple lines gold nanoparticle-based lateral flow for enhanced and simultaneous *Leishmania* DNA detection and endogenous control. *Nano Res.*
44. Parolo, C. et al. 2013. Paper-based electrodes for nanoparticle detection. *Part. Part. Sys. Characteri.* 30(8), 662–666.
45. Morales-Narvaez, E. et al. 2015. Nanopaper as an optical sensing platform. *Acs Nano.* 9(7), 7296–7305.
46. Goldsmith, Z. G., and Dhanasekaran, N. 2004. The microrevolution: Applications and impacts of microarray technology on molecular biology and medicine (review). *Int. J. Mol. Med.* 13(4), 483–495.
47. Tu, S. et al. 2014. Protein microarrays for studies of drug mechanisms and biomarker discovery in the era of systems biology. *Curr. Pharm. Des.* 20(1), 49–55.
48. Dufva, M. 2005. Fabrication of high quality microarrays. *Biomol. Eng.* 22(5–6), 173–184.
49. Monton, H. et al. 2012. The use of quantum dots for immunochemistry applications. *Methods mol. Biol. (Clifton, N. J.)*, 906, 185–192.
50. Morales-Narvaez, E., and Merkoci A. 2012. Graphene oxide as an optical biosensing platform. *Adv. Mat.* 24(25), 3298–3308.
51. Medina-Sanchez, M., Miserere, S., and Merkoci, A. 2012. Nanomaterials and lab-on-a-chip technologies. *Lab Chip* 12(11), 1932–1943.
52. Medina-Sanchez, M. et al. 2014. On-chip magneto-immunoassay for Alzheimer's biomarker electrochemical detection by using quantum dots as labels. *Biosens. Bioelectron.* 54, 279–284.
53. Chee, P. S. et al. 2013. Micropump pattern replication using printed circuit board (PCB) technology. *Mat. Manufac. Processes* 28(6), 702–706.
54. Duffy, D. C. et al. 1998. Rapid prototyping of microfluidic systems in poly(dimethylsiloxane). *Anal. Chem.* 70(23), 4974–4984.
55. Mayorga-Martinez, C. C. et al. 2014. An integrated phenol "sensoremoval" microfluidic nanostructured platform. *Biosens. Bioelectron* 55, 355–359.
56. Medina-Sánchez et al. 2015. Microfluidic platform for environmental contaminants sensing and degradation based on boron-doped diamond electrodes. *Biosens. Bioelectron.*
57. Ambrosi, A., Guix, M., and Merkoci, A. 2011. Magnetic and electrokinetic manipulations on a microchip device for bead-based immunosensing applications. *Electrophor.* 32(8), 861–869.

Micro and nanomotors in diagnostics ☆

Andrzej Chałupniak [a], Eden Morales-Narváez [a], Arben Merkoçi [a,b,*]

[a] ICN2 — Nanobioelectronics & Biosensors Group, Institut Català de Nanociència i Nanotecnologia, Campus UAB, Bellaterra (Barcelona) 08193, Spain
[b] ICREA — Institucio Catalana de Recerca i Estudis Avançats, Barcelona 08010, Spain

ARTICLE INFO

ABSTRACT

Synthetic micro/nanomotors are tiny devices than can be self-propelled or externally powered in the liquid phase by different types of energy source including but not limited to: catalytic, magnetic or acoustic. Showing a myriad of mechanical movements, building block materials, sizes, shapes and propulsion mechanisms micro/ nanomotors are amenable to diagnostics and therapeutics. Herein we describe the most relevant micro/ nanomotors, their fabrication pathways, propulsion strategies as well as in vivo and in vitro applications related with oligonucleotides, proteins, cells and tissues. We also discuss the main challenges in these applications such as the influence of complex media and toxicity issues as well as future perspectives.

© 2015 Elsevier B.V. All rights reserved.

Contents

1. Introduction

Artificial micro/nanomotors are diminutive devices (microscaled or nanoscaled, respectively) than can be self-propelled or externally powered in the liquid phase by different types of energy source such as catalytic, electro/magnetic or acoustic. Being a relatively new branch

of research, the first devices were reported in 2004 by Paxton et al. and Fournier et al. [1,2]. Both of them presented nanoscale rods able to perform autonomous movement. Since that time scientists are focused on developing novel micro/nanomotors with various size, properties and propulsion mechanisms. Micro/nanomotors exhibit a variety of features such as: (a) mechanical movements (e.g., rotation, rolling, shuttling, delivery, contraction and collective motion), (b) compositions / building block materials (e.g. they are commonly made of silicon-based materials, polymers or noble and other metals), (c) sizes (ranging from the nanoscale to the microscale), (d) shapes (e.g., in the form of wires, rods, spheres and tubes/rockets) and (e) propulsion mechanisms (including bubble propulsion, self-electrophoresis, self-diffusiophoresis and self-acustophoresis) [3]. Due to such peculiarities, micro/nanomotors are amenable to nanobiotechnological tools. In fact, the international scientific community is devoting substantial effort to research and develop advantageous diagnostic and therapeutic applications based on micro/nanomotors [3–5]. Herein we introduce an overview of the state-of-the-art in micro/nanomotors for diagnostic applications. In particular, we describe the most relevant micro/nanomotors in the diagnostics context, their fabrication routes, propulsion strategies, interactions with oligonucleotides, proteins, immunoassays, cells and tissues. We also discuss the main challenges in these applications such as the influence of complex media and toxicity-related issues as well as future perspectives.

2. Micro and nanomotors

Micro/nanomotors bear various structures, properties and applications. An inspiration to obtain synthetic micro/nanomotors comes from nature as there is a myriad of examples of motion performed in live organisms. For instance, cytoskeletal proteins are responsible for intracellular transport of organelles, molecules, etc. Their movement is possible thanks to ATP hydrolysis. Similarly to synthetic motors they represent nanoscale size headed by 70 nm length Kinesin [6]. Because of their biocompatibility (they exploit ATP as fuel), biological motors may be interesting for in vivo applications, however control, manipulation and further modifications of them are thoroughly challenging and above all may lead to loss of their essential function. As a result, scientific community has been focused on artificial micro/nanomotors whose fabrication, control and manipulation are amenable to their motion. On the other hand, isolation of specific proteins from live organisms or its biosynthesis is not required. Moreover, synthetic micro/nanomotors can be easily integrated with various nanomaterials playing different roles in such kind of devices [3].

Micro/nanomotors may provide a huge step in the field of miniaturized devices. Depending on the intended application, different fabrication strategies must be kept in mind since each specific shape requires a specialized fabrication technique as well as determines their motion mechanism besides other properties. As a result, surface properties determine the possible mechanism of propulsion. Thus, preparation of useful motors requires integration of several crucial factors. In this section, we will focus on fabrication strategies of micro/nanomotors that are relevant to diagnostic applications such as nanowires, spherical and tubular micro/nanomotors as well as their propulsion mechanisms.

2.1. Fabrication strategies

2.1.1. Nanowires

Nanowires are the simplest 1D structures used as nano and micromotors. The most convenient method to fabricate them is based on metal electroplating inside a template. Commonly, anodic aluminum oxide (AAO) or polycarbonate membrane (PC) can be used as a template structure. In a standard experiment: a membrane is coated with a conductive metal, such as gold or silver, so as to create a working electrode. An electrode made of Ag/AgCl operates as a reference electrode

and a Pt wire, as a counter electrode. Afterwards, a metallic layer is electrodeposited. More than one layer of different metals can be used aiming at synthesizing bimetallic nanowires. Several metals such as Ag, Au, Pd, Pt, Zn, Sn, Cu and Pb are commonly used for nanowires fabrication. Releasing of nanowires from the membranes occurs after treatment with acid or base solutions [7,8].

2.1.2. Spherical micro- and nanomotors

Janus, one of the Roman's mythology gods of beginnings and transitions is usually depicted with two faces that represent future and past. This character became the inspiration for the naming of spherical particles having each hemisphere with different chemical or physical properties. It means that Janus micro- and nanomotors consist of two hemisphere playing different roles, one of them is usually related with propulsion ability (react with fuel or some external stimuli) while the second can be modified depending on the targeted application (for example functionalized metal surface with a proper receptor for biosensing applications) [8,9].

Various techniques can be employed to obtain Janus micro- and nanomotors. In principle, the fabrication process is based on metallic thin films deposition onto the surface of microbeads. Generally, such microbeads are made of silica (SiO_2) [10] or polystyrene [11–13] and the fabrication process involves a monolayer of beads that is uniformly distributed on glass slides or silicon wafers. Under electron-beam evaporation or sputtering processes, the top part of the microspheres is covered by a catalytic metal such as Ir, Au, Pt or Ti. Tuning of the area and thickness of metallic layer can be achieved by titling the angle of the substrate where the monolayer of microbeads is deposited and controlling the intensity of sputtering process (of metallic material to be deposited) (see Fig. 1). The metallic hemisphere usually provides the redox ability that plays a key role in Janus nano/micromotors propulsion [8,9]. Propulsion strategies are explained in Section 2.2.

Depending on their fabrication process, Janus particles show a broad range in size, ranging from nanoparticles; e.g., 30 nm [16], 75 nm [19], up to microparticles such as polystyrene (1–5 μm) [11], Mg–Pt (20–30 μm) [20,21] or SiO_2 (10–50 μm) [22]. Janus nanomotors fabrication processes are various. For example, Fisher et al. used Pt nanoparticles produced by block copolymer micelle lithography and deposited Au by glancing angle deposition. This process is briefly shown in Fig. 1C. Since only nano-sized motors can be potentially exploited in in vivo applications, where the issue of size is not irrelevant, an overall tendency of Janus nanoparticles size reduction can be observed. On the other hand, as discussed in Section 2.4.1., reducing the size affects motion ability, thus specific strategies to obtain efficient propulsion mechanisms are crucial [8,9].

2.1.3. Tubular micro- and nanomotors

Tubular micro- and nanomotors, similarly as nanowires, have a longitude shape but are distinguished by having tubular structure with specific inner and outer part, which can be modified in a versatile way to obtain specific properties.

Most of the tubular micromotors are obtained by a rolling-up process developed by Mei et al. in 2008 [23]. Briefly, this process is based on a patterning of a photoresist on a substrate (e.g., Si wafer) bearing a sacrificial layer. Metals are evaporated at glanced angle creating a window that determines the process of rolling (which occurs after etching the substrate), see Fig. 2D. By changing different parameters such as angle, temperature and thickness, it is possible to obtain microtubes with different diameters varying from 1 to about 30 μm. The main disadvantage of this technique is a relatively big size of microtubes and the need of a clean room, which increases the fabrication cost significantly [8,9].

Probably, for those who are just starting the work with tubular micromotors (called also microjets), the most interesting fabrication technique is electroplating. Similar to nanowires fabrication, this approach exploits porous membranes as a template (such as PC or AAO
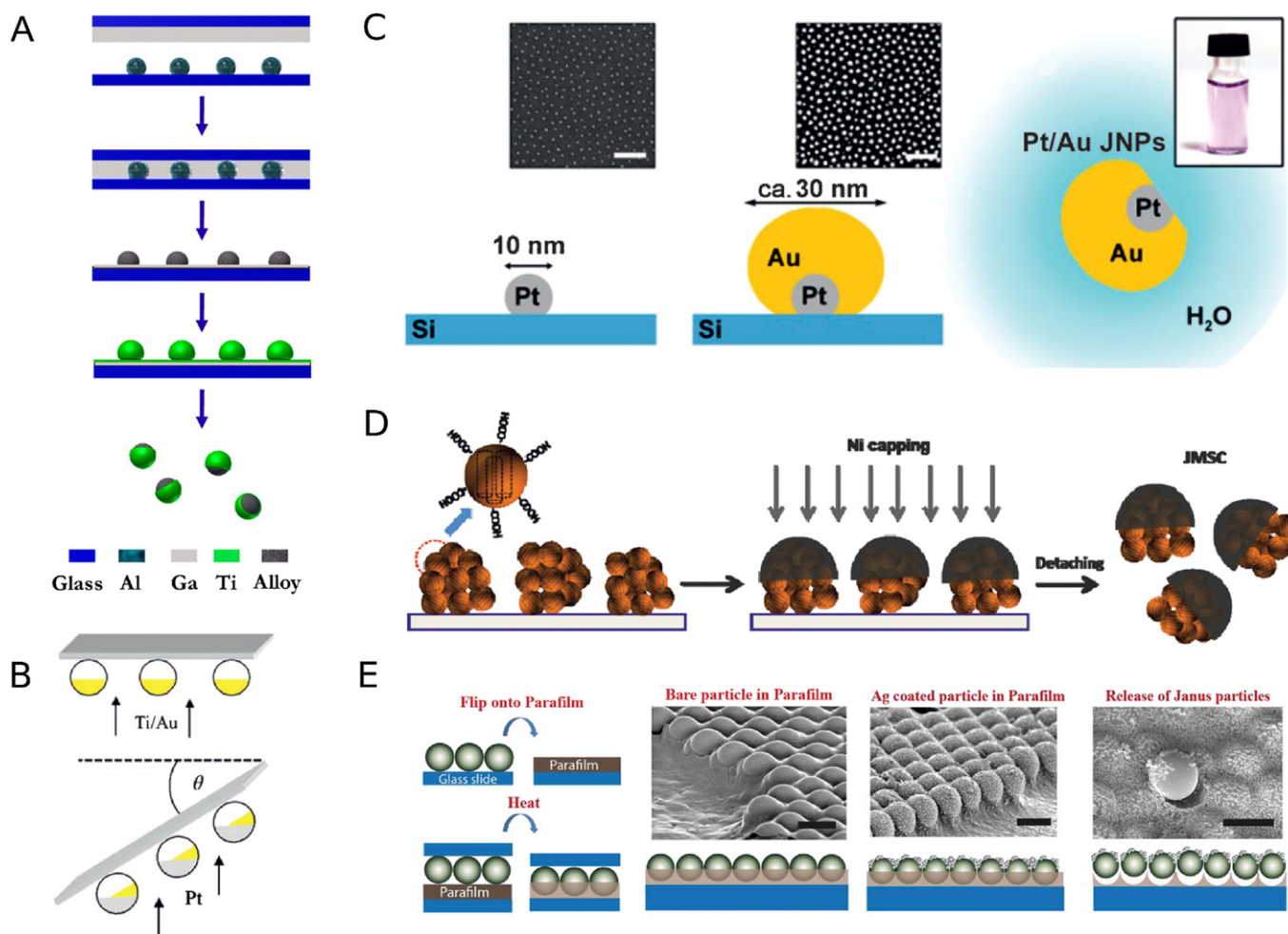
Fig. 1. Janus nano/micromotors fabrication strategies. A. Fabrication of water-driven Al-Ga/Ti micromotors, modified with permission from American Chemical Society, Copy Right (2012) [14]. B. Fabrication of Pt/Au Janus nanomotors by asymmetric coating, modified with permission from American Institute of Physics, Copy Right (2010) [15]. C. Fabrication of Au/Pt Janus nanomotors by block copolymer micelle lithography on silicon wafer, modified with permission from American Chemical Society, Copy Right (2014) [16]. D. Janus mesoporous silica cluster fabrication, modified with permission from Royal Society of Chemistry, Copy Right (2015) [17]. E. Synthesis of Janus particles by embedding SiO$_2$ particles in Parafilm, modified with permission from John Wiley and Sons, Copy Right (2014) [18].

membranes) to perform electrodeposition of a given metal or chemical compound. This process can be performed step by step depositing different compounds onto the same membrane obtaining different layers. After dissolving the electrodeposited membrane, the released tubes keep the shape of the membrane pores and may be used for further modifications. As it can be seen, the main advantage of this technique is that it is easy-to-use, as only simple equipment (potentiostat) is required to perform the electrodeposition. This process does not demand a clean room, which reduces the fabrication cost and time significantly. Membranes used for electrodeposition, usually with pores of 2 μm diameter, are cheap and commercially available. They just need to be conductive to act as electrode, which can be achieved by gold sputtering before fabrication process.

One of the most relevant examples of micromotors obtained by templateted electrosynthesis is PANI/Pt microtubes developed by Gao et al. They are only 8 μm long and require low concentration of hydrogen peroxide as fuel (0.2%), see Fig. 2A [24].

It is worth mentioning that various chemical groups and compounds can be electrodeposited facilitating further modifications, for example bioconjugation (see Fig. 2B–C). The fabrication of microjets-containing molecularly imprinted polymers (MIP) [25], polyaniline (PANI) [24], poly(3,4-ethylenedioxythiophene) (PEDOT) [26], polypyrrole (PPy) [27] are already reported. However, easy and versatile fabrication methods are still requested. For instance, a surprising nature-inspired

approach has been developed by Pumera et al., where Platinum microengines were synthesized using banana or apple tissues. Fruit tissues are used as a support on which a thin platinum film is deposited by means of physical vapor deposition. Upon sonication of the cells/Pt-coated substrate in water, microscrolls of highly uniform sizes are spontaneously formed [28].

2.2. Propulsion strategies

Nano- and micromotors, similar to other nano/microscopic objects, can move as a result of various chemical reactions and physical phenomena. One of the most popular areas of nano- and micromotors are those chemically-driven, which require a specific fuel and specific composition of their surface. Besides chemical processes, motion of nano- and micromotors can be induced by physical energy such as magnetic fields, ultrasounds, light or electric fields. Taking into account the current progress in this field and its possible applications in diagnosis and biosensing, this review will be focused on catalytic, magnetic and ultrasounds nanomotors.

2.2.1. Catalytically powered nanomotors

The catalytic nanomotors approach is based on a chemical reaction that occurs between the motors surface and the fuel in the medium where the motors operate. Thus, how nano- and micromotors
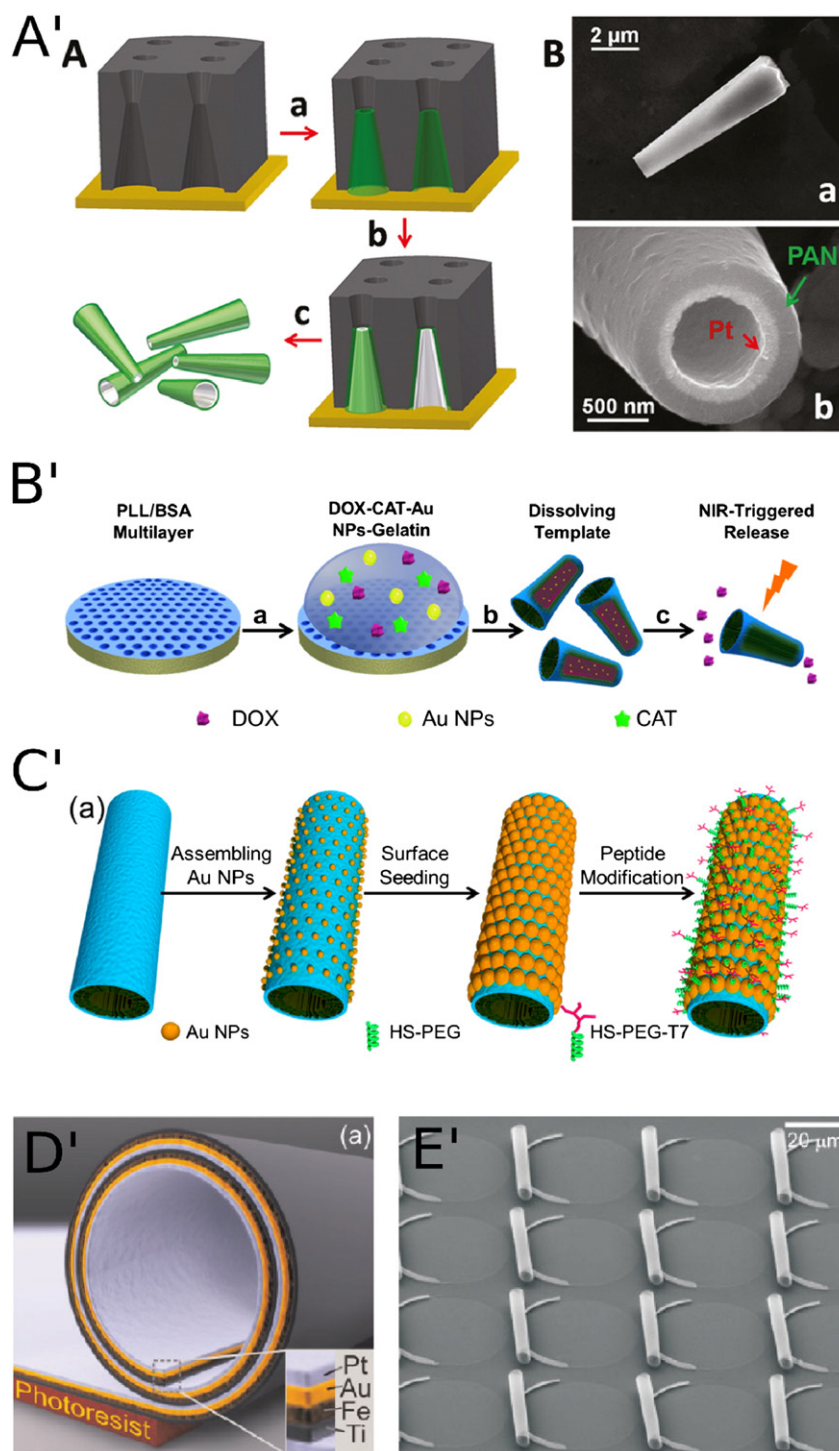
Fig. 2. Fabrication of tubular micro- and nanomotors. A′. Fabrication of template-based Pt/Polyaniline microtubes, modified with permission from American Chemical Society, Copy Right (2011) [24]. B′. Fabrication and light-triggered drug release process of (PLL/BSA)10-DOX-CAT-AuNPs-gelatin rockets, modified with permission from American Chemical Society, Copy Right (2014) [29]. C′. Fabrication process of the AuNP-modified polyelectrolyte multilayer microengines coated with a thin AuNP and a tumor-targeted peptide, modified with permission from American Chemical Society, Copy Right (2014) [30]. D′. Schematic diagram of a rolled-up microtube consisting of Pt/Au/Fe/Ti multilayers on a photoresist sacrificial layer, modified with permission from Royal Society of Chemistry, Copy Right (2012) [31]. E′. SEM image of an array of rolled-up SiO/SiO$_2$ nanomembranes layer, modified with permission from Royal Society of Chemistry, Copy Right (2012) [32].

will behave depends on type of fuel, its concentration, as well as motor physical properties such as dimensions, surface to volume ratio, etc. [3].

Depending on the type of motors and fuel, the propulsion mechanism is still not well explained and it is a subject of debate among scientists. Nonetheless, we can point out three main mechanisms: bubble propulsion, self-electrophoresis and self-diffusiophoresis. Bubble propulsion is typical for tubular micro- and nanomotors. After wetting the catalytic material, bubbles are created due to a reaction occurring onto its surface. As a consequence, bubbles accumulation and release leads to a motion toward microtube opening, which triggers the movement of the microtubes. The microtubes speed depends on the tube

dimensions, fuel concentration as well as liquid (medium) properties (e.g. viscosity) [9].

In case of the nanowires motion one of the most possible action mechanisms is self-electrophoresis. The motion mechanism is based on the changes of the nanowire electric field, which is created due to asymmetric distribution of ions. Thus, when nanowires consists of 2 different metal layers, one of them preferably catalyzes the oxidation of hydrogen peroxide creating an excess of hydrogen ions on one of the nanowires sites [9].

Motion mechanism of spherical particles depends on chemical composition of its surface. Bubble propulsion occurs owing to Mg–water or Al–water reaction [11,33], while driving by hydrogen peroxide decomposition is probably due to self-electrophoresis [9].

Catalytic micro/nanomotors are able to perform several types of motion that are limited by the access of the fuel in the medium. Thus, the micro/nanomotors trajectory is quite chaotic and it cannot be easily guided. Consequently, combining 2 different types of propulsion aiming at guiding the explored micro/nanomotors may be advantageous. For instance, second propulsion could be magnetic — this requires depositing a layer of ferromagnetic metal such as Nickel. Then, in presence of an external magnetic field in synergy with fuel in the medium, the explored micro/nanomotors will move toward magnetic guidance making also propulsion resulting from chemical reaction on its surface. Most of the researches concerning catalytic nanomotors exploit hydrogen peroxide as fuel. However in order to develop versatile, biocompatible and environmental friendly nanodevices it is necessary to develop

other types of propulsion chemistry. For instance, Zn layer of micro/nanomotor in acidic environment is digested and as a result gaseous hydrogen is produced leading to bubbles generation (Fig. 3A). Hydrolysis of metals is another way to generate hydrogen bubbles, this approach was used for propulsion of Al–Ga Janus micromotors (Fig. 3B). It is also possible to perform double catalytic reaction, where the final product is a gas (Fig. 3F). More examples reported in the literature are shown in Fig. 3.

2.2.2. Magnetic nanomotors

Nano- and micromotors driven by magnetic fields are one of the most promising approaches compared to other propulsion mechanisms. Since the movement of micro/nanomotors is induced by external magnetic fields, the presence of any fuel in the micro/nanomotors environment is not particularly necessary. Such micro/nanomotors are interesting to be used in vivo due to their potential biocompatibility and independence of the chemical composition in the medium where they operate. However, physical, especially, rheological properties of certain liquids are not indifferent to propulsion efficiency. It is worth mentioning that a magnetic field source (e.g. a simple magnet) is relatively cheap and can be easily integrated into more sophisticated devices. That opens a lot of possibilities to use magnetically-driven nanomotors also in biosensing since other magnetic particles such as magnetic beads are commonly used in biodetection (e.g. magnetoimmunoassays), separation, pre-concentration, and
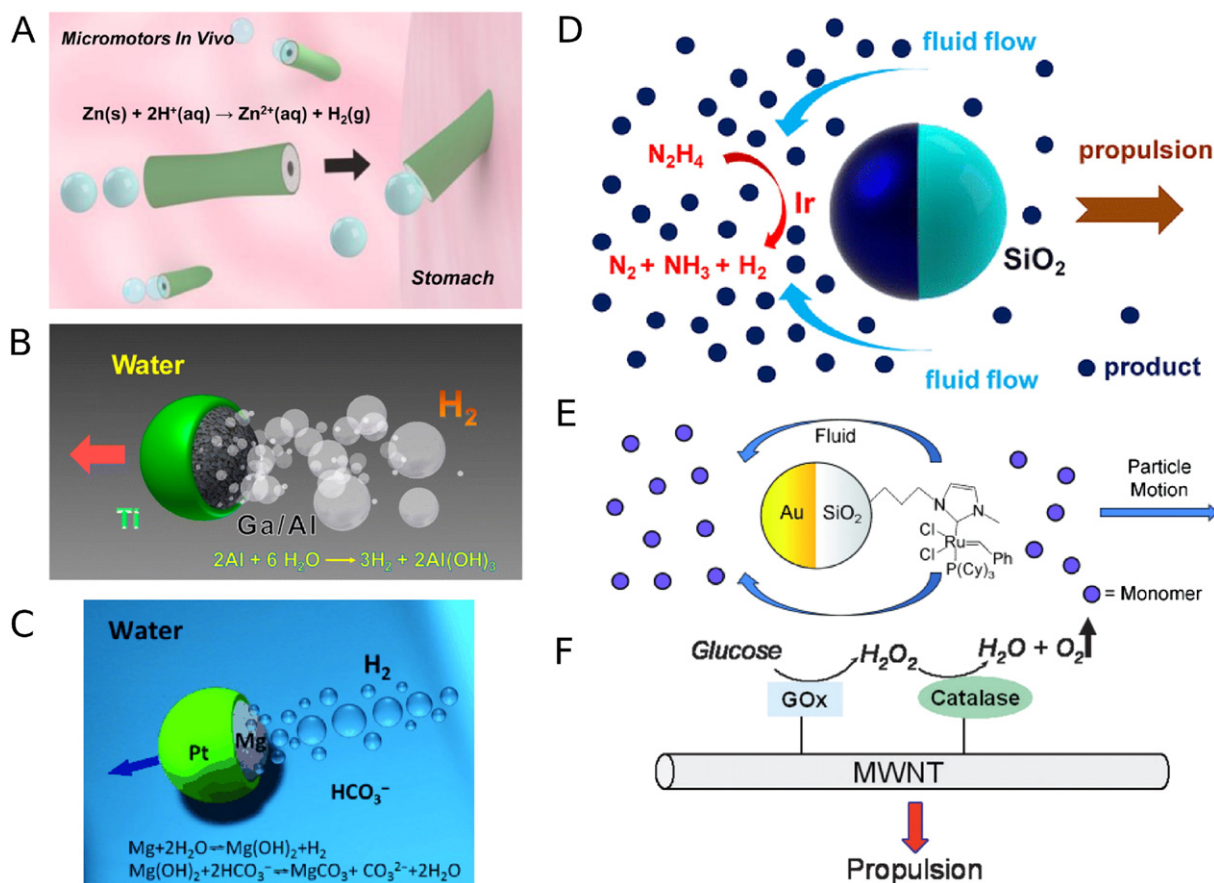
Fig. 3. Different reported strategies for catalytical propulsion of micro/nanomotors. A. Propulsion of Zn microtubes by gastric acid (HCl) as fuel, modified with permission from American Chemical Society, Copy Right (2014) [34]. B. Propulsion of Al–Ga Janus micromotors based on water–aluminum reaction, modified with permission from American Chemical Society, Copy Right (2012) [14]. C. Propulsion of Mg/Pt Janus micromotors by Magnesium–Water reaction, modified with permission from John Wiley and Sons, Copy Right 2013 [21]. D. Propulsion of Iridium-Based Janus Micromotors by Hydrazine–Iridium reaction, modified with permission from American Chemical Society, Copy Right (2014) [35]. E. Propulsion of Au/SiO₂ Janus micromotors by polymerization, modified with permission from WILEY-VCH Verlag GmbH & Co. KGaA, Copy Right (2011) [36]. F. Propulsion of multi-walled carbon nanotube based on catalysis of glucose, modified with permission from Royal Society of Chemistry, Copy Right (2008) [37].

purification. Combining magnetic properties with the propulsion ability may be a source of significant improvement in various analytical techniques.

There are different types of magnetically-driven micro/nanomotors. We can distinguish flexible micromotors that are a kind of nanowires, polymer-based structures (for example combining PDMS and magnetite) and rigid structures. Rigid structures due to screw-like shape are especially interesting for micro/nanomotors applications as such shape facilitates efficient motion in low Reynolds number liquids. Another example of rigid structures is the corkscrew-shaped motors. Magnetic motors motion depends on the level of magnetic force and its direction. It is also possible to combine magnetic domains with catalytic properties, creating micro/nanomotors that are guided by magnetic fields and execute bubble-propelled motion at the same time [3]. This approach has been exploited in a lab-on-a-chip (LOC) application. Due to external magnetic guidance, motors can move through desired channels performing semi-automated operations. Hence, such devices do not require any external pumps and driving units as the motion of micro/nanomotors is autonomous. A good example was reported by Garcia et al. [26] where catalytic polymer/Ni/Pt microtube engine is able to perform an immunoassay by transporting molecules from different channels of LOC platform when guided by magnetic field.

2.2.3. Ultrasound nanomotors

Similar to magnetically-driven micro/nanomotors, ultrasound propulsion does not require any kind of chemical fuel. As ultrasounds operate in the range of frequency above 20 kHz, they are not audible for humans. Even so, ultrasounds can be used in different medical applications safely, for instance in diagnosis (e.g. ultrasonography), therapy (e.g. targeted ultrasound drug delivery) or other treatments such as teeth cleaning or liposuction assisted by ultrasound [38]. Thus, in vivo applications of micro/nanomotors driven by ultrasounds are very promising due to their potential biocompatibility.

One of the most significant examples of acoustically-driven micromotors has been reported by Wang et al. MHz frequency acoustic waves demonstrated the ability to rotate, align, propel and assemble metallic microrods either in water and high ionic strength solution. A systematic comparison of the microrods structure with other types of particles (metal spheres and polymer particles) proved that strategic factors influencing the ability of motion are the size and material used to obtain micromotors. The mechanism proposed by the authors is self-acoustophoresis, which shows a desired direction due to shape asymmetry and microrods curvature [39].

Suitability of ultrasound propelled micromotors for biological applications has been proved by Garcia-Gradilla et al. Three segment nanowires Au–Ni–Au were functionalized with lectin and antibody against Protein A. Guidance was performed using either external magnet (magnetic field) or piezoelectric transducer (ultrasounds). As a proof-of-concept nanowires were used for bacteria (Escherichia coli) detection as well as for drug delivery (due to pH-sensitive drug-loaded polymeric segment) [40]. Similar nanowires consisting of Au–Au–Ni–Au with porosity (to extend the capacity of drug loading) also showed great ability of propulsion by ultrasounds [41]. Ultrasounds can be used not only for directional movement of one motor into given direction, but also to study interaction between them. Xu et al. proposed the use of acoustic waves to induce: reversible assembly of Pt–Au catalytic nanomotors, controlled swarm movement and separation of various motors. The mechanism of swarming results from interaction between individual motors and acoustic waves. The process of assembling is very fast and reversible (see Fig. 4A). Such possibilities of well-controlled movement and assembling of motors open the way to a wide portfolio of implementations of nanomotors, including biosensing / diagnosis [42].

The process of reversible swarming was also studied by Mallouk et al. Bimetallic gold–ruthenium microrods were propelled in opposite directions in water by ultrasound and by catalytic decomposition of hydrogen peroxide, see Fig. 4B [43].

2.3. Micro- and nanomotors for diagnostic and biosensing applications

(Bio)functionalized micro/nanomotors are paving the path to novel and advantageous biodetection systems. In fact, micro/nanomotors not only can be functionalized with biological receptors including oligonucleotides or antibodies, they can also be functionalized with artificial receptors such as molecularly imprinted polymers so as to capture and isolate biomolecules, as demonstrated by Orozco et al. [25]. Since biomarkers screening is clinically relevant, [44] e.g. in cancer and neuro-diseases detection and monitoring, biomarker molecules such as specific oligonucleotides and different proteins have been targeted for biosensing using micro/nanomotors. Due to their size and vortex effect associated to their motion, bubble-propelled micromotors have been exploited in advantageous analytical tasks. However, motion-driven DNA-sensing based on Au–Pt nanomotors have led to highly sensitive platforms. Here we introduce an overview of this endeavor, discussing different micro/nanomotors-based approaches for oligonucleotide and protein detection.

2.3.1. Interaction of micro/nanomotors with oligonucleotides

Wu et al. (2010) reported a pioneer approach on synthetic nanomotors aiming at transducing biorecognition events into motion [45]. This novel biodetection platform was engineered to detect DNA and E. coli 16S rRNA. However, it can also be extended to protein biomarkers detection using antibodies or other kind of biorecognition probes. The motion-driven DNA-sensing approach is based on speed and distance as analytical signals. In fact, such motion parameters of non-modified catalytic Au–Pt nanomotors were directly correlated with the dissolution of silver nanoparticle labels (in the peroxide fuel) reporting a sandwich DNA hybridization complex as the produced Ag^+-enriched fuel improves the nanomotors speed (see Fig. 5A). Since the sensing mechanism is highly sensitive, the authors proved this technology to exhibit a limit of detection of 40 amol [45].

Recently, Nguyen and Minteer (2015) developed a motion-driven DNA biosensor from PEDOT–Au microtubes. The inner surface of the tubular microengines is decorated with DNA probes to capture selectively the target to be reported by Pt nanoparticles complexed with complementary DNA strands. As a consequence, upon fuel addition, the motion of the microengine is modulated by the catalytic activity of the amount of Pt nanoparticles at the inner surface labeling the target, see Fig. 5B. This motion-based biosensing platform exhibits a limit of detection around 1 pmol [46].

Interestingly, according to the literature, when the outer surface of the microrockets is functionalized with biorecognition probes, the fast motion and bubble release trigger local vortexes that promote the mass transfer of the target toward the functionalized microjet surface. In this context, the DNA hybridization occurring "on-the-fly" is more efficient than the DNA hybridization occurring without motion. In fact, Kagan et al. (2011) reported a 13-fold enhancement of DNA capture when compared with static or externally shaken microrockets. Importantly, such "on-the-fly" hybridization can be efficiently carried out even in complex samples (e.g. serum, urine, cell lysate and saliva) in order to perform nucleic acid isolation without any sample treatment [47].

2.3.2. Interaction of micromotors with proteins/immunoassays

García et al. (2013) reported the first antibody-decorated tubular microengines designed to capture and transport target proteins between microfluidic chambers. Catalytic polymer/Ni/Pt microengines were biofunctionalized with antibodies targeting IgG protein, as a model protein, in order to achieve a micromotor-based immunoassay offering "on-the-fly" capture and isolation/sorting capabilities, see Fig. 6A′. The immunocomplex can be easily visualized through optical microscopy by using an antigen/antibody labeled with a polymeric-sphere tracer. This novel assay is highly selective and eliminates time-
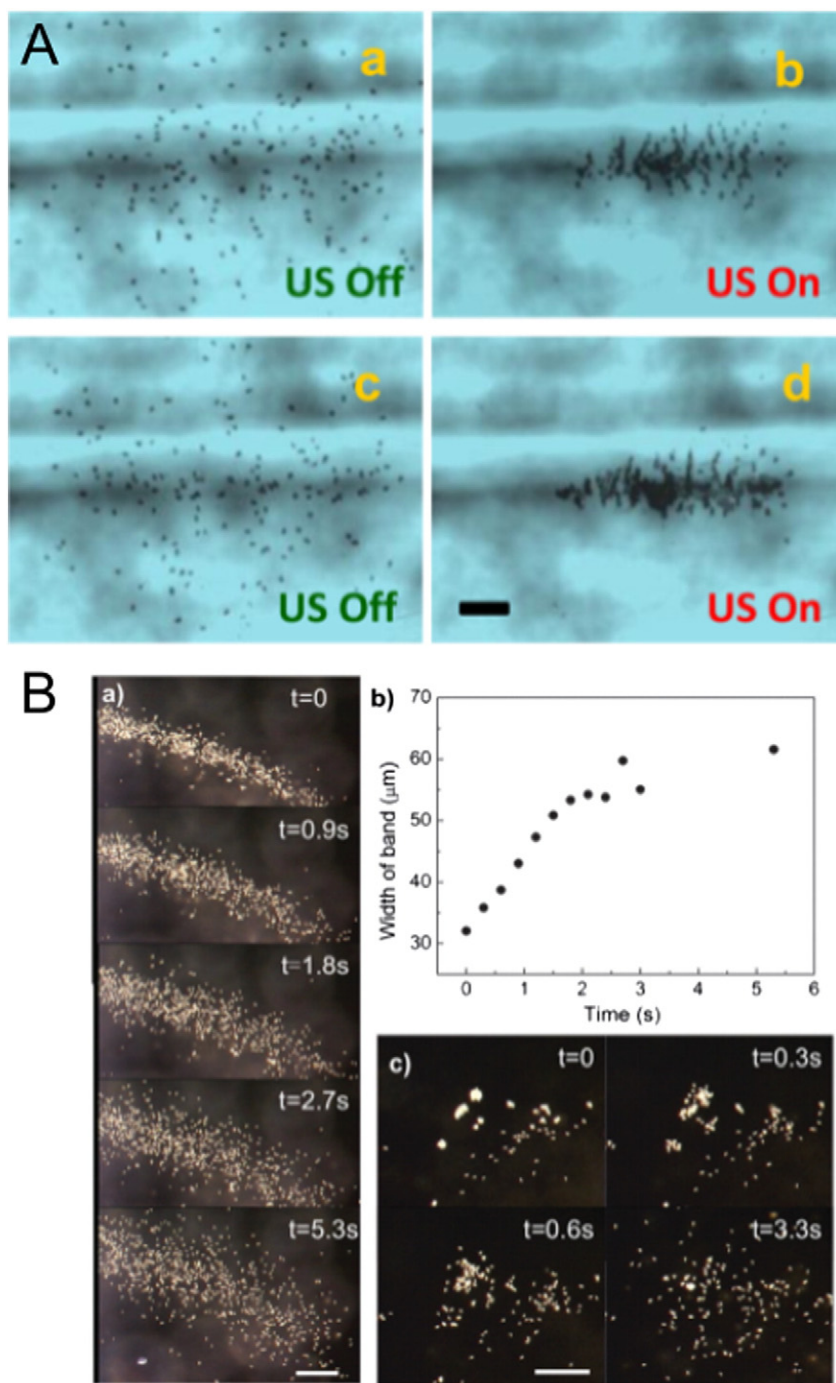
Fig. 4. Reversible swarming and separation of nano- and micromotors propelled by ultrasounds. A. Ultrasound-triggered reversible swarming and dispersion of Pt–Au nanowire motors. (a, c) Catalytic nanomotors swimming autonomously by the decomposition of hydrogen peroxide fuel. (b, d) Rapid ultrasound-triggered assembly of nanomotors into a swarm. Scale bar, 10 μm; concentration of nanomotors, ~200/μL, modified with permission from Royal Society of Chemistry, Copy Right (2014) [42]. B. Transition between aggregated and dispersed states of a group of Au–Ru microrods at the acoustic cell bottom. (a) Snapshots of the disintegration of a loose band of Au–Ru microrods at different times (ultrasound was turned off at t = 0); (b) the width of the band in (a) as a function of time; (c) snapshots of the disintegration of a tight cluster of Au–Ru microrods at different times (ultrasound was turned off at t = 0). Scale bar: 50 mm, modified with permission from American Chemical Society, Copy Right (2014) [43].

consuming washing steps, simplifying and accelerating the overall immunoassay procedure [26]. Taking advantage of these features, Yu et al. (2014) exploited antibody-functionalized AuNP/PANI/Pt micromotors to perform rapid "on-the-fly" sandwich immuno-complexes targeting carcinoembryonic antigen. The assay takes 5 min and operates in a range of 1–1000 ng mL^{-1} [48]. In addition, labeling

the captured proteins with microscopic particles showing different sizes and shapes facilitates multiplexed analysis of proteins, as proved by Vilela et al. (see Fig. 6B′) [49].

On the other hand, the aforementioned vortex effect triggered by the micromotors motion not only promotes the mass transfer of the target toward the functionalized microjet surface (i.e. "on-the-fly"), but also

Fig. 5. Micro/nanomotors for oligonucleotide sensing. A. Motion-based biosensing using nanomotors, modified with permission from Nature Publishing Group, Copy Right (2010) [45]. B. Motion-based biosensing using micromotors, modified with permission from Royal Society of Chemistry, Copy Right (2015) [46]. C. Microjet decorated with DNA, modified with permission from American Chemical Society, Copy Right (2011) [47].
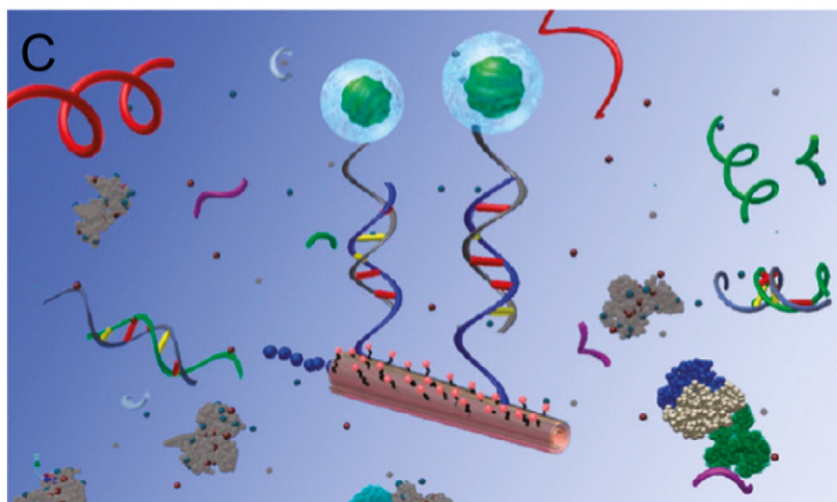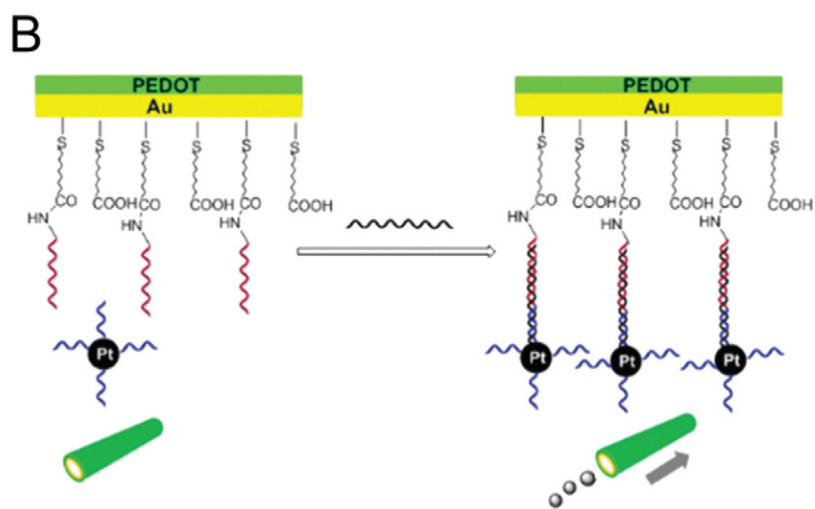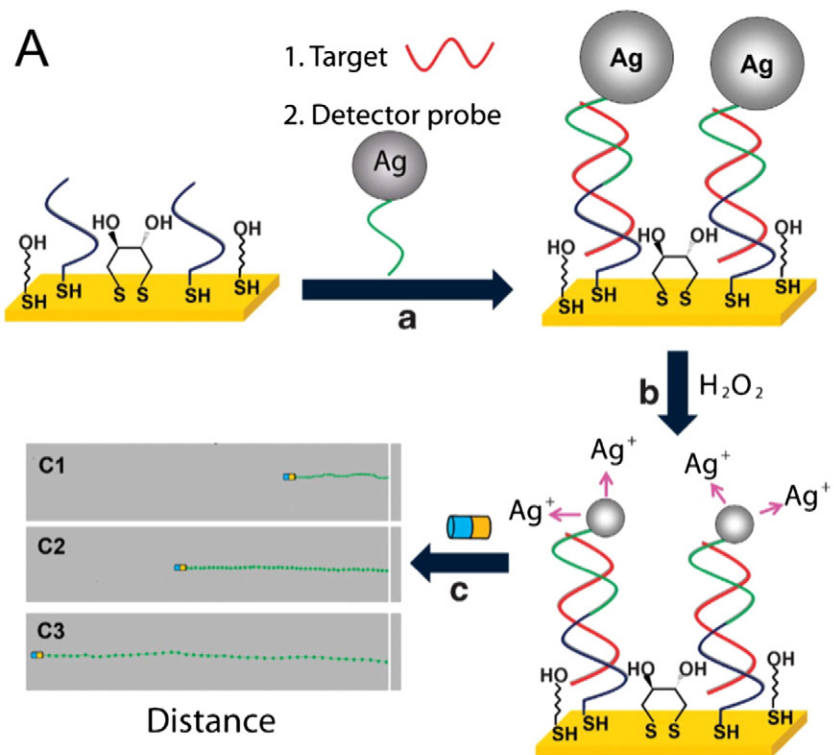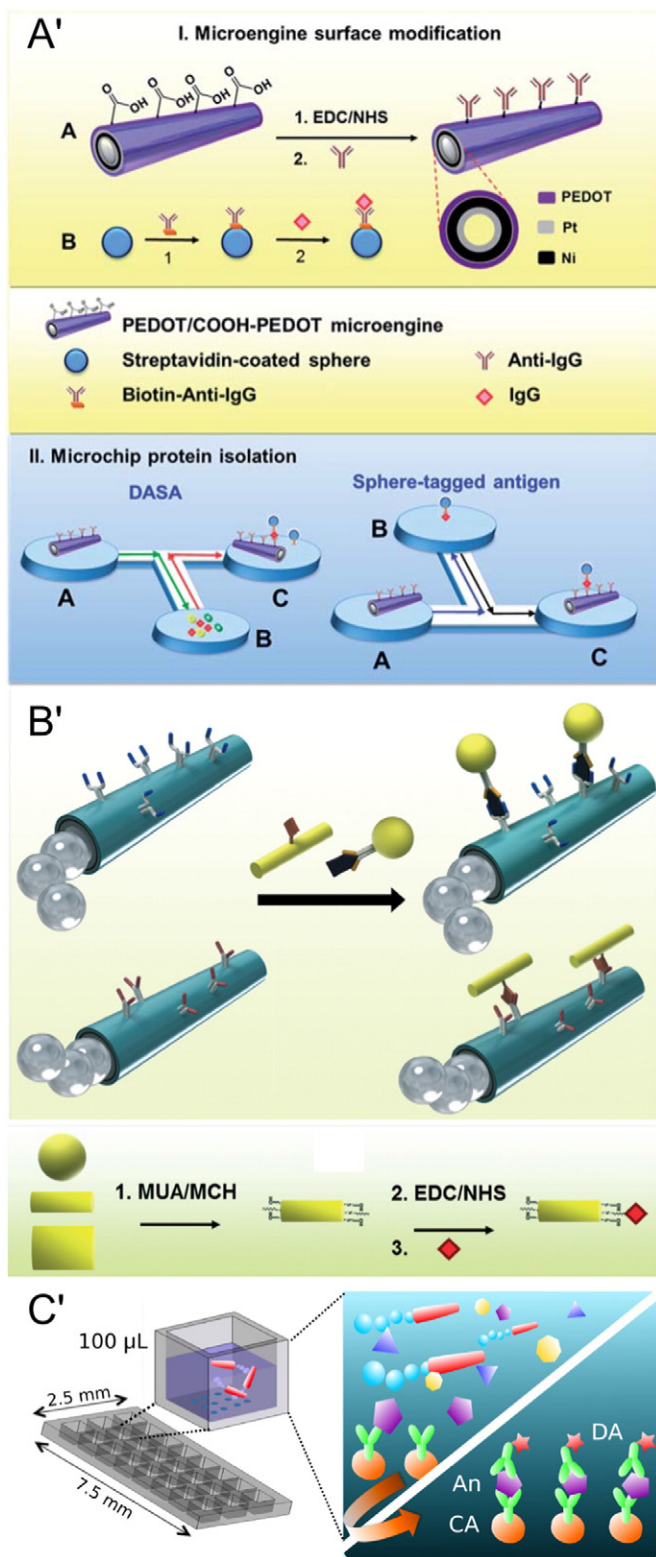
Fig. 6. Micromotors for protein sensing. A′. Antibody-decorated micromotor for protein detection, modified with permission from Royal Society of Chemistry, Copy Right (2012) [26]. B′. Micromotor-based multiplexed immunoassay via different microscopic tracers. Modified with permission from Royal Society of Chemistry, Copy Right (2014) [49]. C′. Microarray immunoassay assisted by microengines, modified with permission from John Wiley and Sons, Copy Right (2014) [50].

may assists the mass transfer of the target molecule within the matrix of a sample solution toward a sensing surface, where the bioreceptor is located and the target is expected to be selectively attached, see Fig. 6C′. In

fact, Morales-Narváez et al. demonstrated that a microarray-based immunoassay, targeting a potential Alzheimer biomarker (apolipoprotein E), assisted by PANI/Pt microengines outperforms the signal intensity of a non-assisted microarray up to 3.5 times. It suggests that the mass transport toward the microarray sensing surface was dramatically modulated by the vortex effect resulting from the microengines motion [50].

2.3.3. Interactions with cells and tissues

Nano and micromotors operating in live organisms and cells open the way to novel applications in the field of nanomedicine and nanodiagnostics. In particular, in vivo applications might involve nanosurgery, cell sorting, biopsy and versatile biosensing and diagnosis [4,51]. Currently, several works concerning interaction of micro/nanomotors with cells and tissues are already reported. However, more involvement in this field is required to provide versatile nanodevices offering safe and promising applications. Serious concerns and challenges about in vivo applications in the future are also discussed in Section 2.4.

Different types of micro/nanomotors have been reported as suitable engines to work in cell culture environment. A list of interesting examples is itemized in Table 1. Most of the available reports are related to nanomotors as drug delivery tools [4]. Surface functionalization enables researchers to load specific drugs on micro/nanomotors surface (one of the most commonly tested is DOX–Doxorubicin). Micro/nanomotors motion leads to drug delivery targeting specific cells, such as cancer cells. Specificity is a crucial issue since it ensures that the explored drug will treat the target cells, whereas non-target cells (healthy cells) will not be affected by the drug. Drug releasing takes place when specific factors are modulated — i.e., temperature, ionic strength, pH etc. [52]. Another important concern is that such micro/nanomotors should not be toxic so as not to create a risk affecting healthy cells. However, as displayed in Table 1, the biggest challenge occurs when catalytic micro/nanomotors are used, since their motion is generally based on hydrogen peroxide as fuel, which shows cytotoxicity even at low concentrations in cell culture. As a consequence, a major effort should be devoted to bio-friendly fuels (like water) or motors propelled by external stimulation such as those guided by magnetic fields or ultrasounds. Perhaps one of the most interesting and promising approaches is combining biological elements with synthetic motors so as to obtain biocompatible and versatile nanodevices. Recently, Wang and colleagues reported human erythrocytes with iron oxide incorporated. This strategy facilitates performing propulsion either by magnetic field or by ultrasounds. Since erythrocytes keep their structure and properties, they are totally biocompatible, which was confirmed by adding them to macrophage cell culture. The process of red blood cells uptake was not observed [53].

To the best of our knowledge, until now, the application of nanomotors in cell/tissue detection has been scarcely explored. Taking into account the progress in the field of drug delivery (compatibility with cells, ability to recognize target cells) we might assume that such research should attract attention in the near future. We hope that implementation of nanomotors in diagnosis, in vivo biosensing (e.g. in cell cultures) may provide rapid progress in effective biosensing techniques and medical analysis.

The first in vivo application was recently published by Gao et al. [34] Catalytic PEDOT/Zn nanomotors were fabricated using template-directed electrodeposition (See Fig. 7). The propulsion mechanism is based on hydrogen evolution as a result of zinc dissolution in acidic environment. These micromotors were applied in live mouse stomach. Owing to their loading with AuNP, it was possible to monitor the micromotors behavior, their retention in stomach tissue, and the time necessary to unload AuNP. Cytotoxicity studies confirmed good biocompatibility of the studied micromotors, which was facilitated by their composition. In fact, the product of such micromotors reaction (Zn^{2+}) is commonly found in whole organism, whereas PEDOT polymer has been reported to be non-
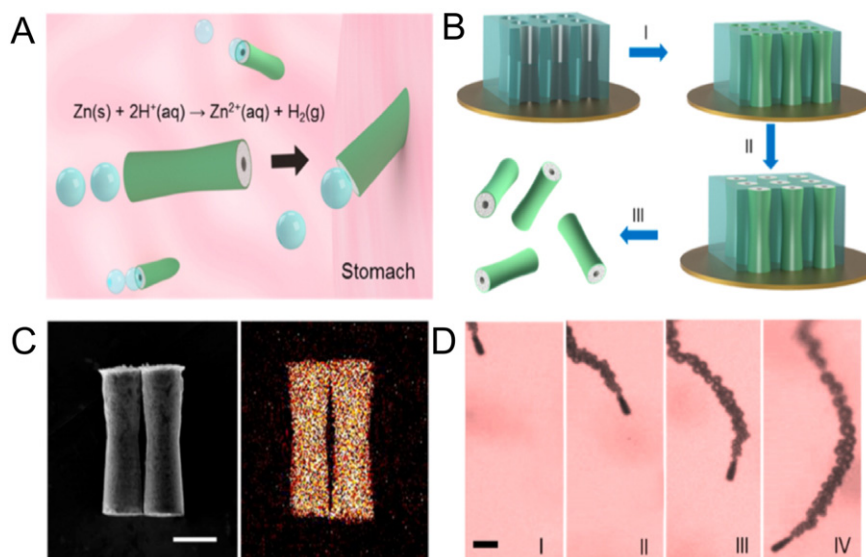
Fig. 7. Preparation and characterization of PEDOT/Zn micromotors. (a) Schematic of the in vivo propulsion and tissue penetration of the zinc-based micromotors in mouse stomach. (b) Preparation of PEDOT/Zn micromotors using polycarbonate membrane templates: I) deposition of the PEDOT microtube, (II) deposition of the inner zinc layer, and (III) dissolution of the membrane and release of the micromotors. (c) Scanning electron microscopy (SEM) image (left) of the PEDOT/Zn micromotors and the corresponding energy-dispersive X-ray spectroscopy (EDX) data (right) of elemental Zn in the micromotors. Scale bar, 5 μm. (d) Time lapse images of the propulsion of PEDOT/Zn micromotors in gastric acid under physiological temperature (37 °C). Scale bar, 20 μm, modified with permission from American Chemical Society, Copy Right (2014) [34].

toxic in live organisms [54]. Apoptosis test (TUNEL, Terminal deoxynucleotidyl transferase dUTP nick end labeling) of gastric cells from stomach due to micromotors ingestion did not show any increase of apoptotic cells. These findings prove the possibility of in vivo applications of micro/nanomotors [34].

2.4. Main challenges and future perspectives

"The Fantastic Voyage" — the movie from 1966 unambiguously became an inspiration and headed scientists' imagination toward miniaturized devices for therapy and diagnostics. Although last decades brought a huge improvement in the field of micro/nanomotors, there are still some issues requiring special attention in order to realize easy and safe in vivo applications. The main challenges will be briefly described in this section.

2.4.1. Micro/nanomotors in vivo — the influence of complex media

The micro/nanomotors field is progressing very quickly and intensively. Probably, one of the main problems is finding a new path to take advantage of the emerging novelties in this field toward practical and commercial applications. Unfortunately, most of the micro/nanomotors that have been developed exhibit scarce ability to be used for example in real sample biosensing, diagnosis or drug delivery. Unlike macroscopic objects, the ability of motion in micro and nanoscale is predominantly dependent on liquids viscosity and Brownian diffusion. Random direction of Brownian motion and low Reynold's number of microscopic objects (due to their size) makes proper motion harder and require suitable strategies of propulsion [9,64]. Regardless of the application (in vitro, in vivo), the environment in which micro/nanomotors work is characterized by specific pH, ionic strength and presence of various biomolecules such as proteins, nucleic acids and lipids. However, in in vitro applications, such as immunoassays, it is possible to control the properties of the involved buffers, which is actually impossible in in vivo applications (for example, blood is very complex and varies in each organism). One of the main strategies to improve micro/nanomotors motion is by increasing the fuel concentration. However, this effect is limited taking into account micro/nanomotors properties and the influence of fuel into the reaction environment (as discussed below). Consequently, another common strategy is reaction buffers supplementing

through surfactants, which facilitate propulsion by reducing the solution viscosity. Depending on the targeted application and micro/nanomotor type, such surfactants can be concentrated at different levels, for instance: 10% (v/v) soap [57,65], 0.3–2.0% (w/v) sodium cholate [24,66], 0.1–5.0% Triton X-100 [14,67,68] or 1% sodium cholate [69]. It is not insignificant which type of surfactant will be used: anionic surfactants support micro/nanomotors motion better than those which are cationic [69].

In biosensing and drug delivery applications, one of the most challenging media is blood. Finding a suitable pathway to cope with micro/nanomotors propulsion in human blood will lead to unprecedented applications, for example rapid blood testing or nutrients/drug delivery, etc. via vascular system. Since blood plays an important role in metabolism, it contains various biomolecules including crucial proteins such as albumins, immunoglobulins and clotting factors. Oxygen and nutrients transport makes blood full of electrolytes and gases [70,71]. Therefore, it is easy to predict that this environment is not neutral for micro/nanomotors. First of all, physical properties of blood affect motion ability. Secondly, biomolecules presenting in blood can react with micro/nanomotors if they contain compounds showing unspecific affinity. Zhao et al. reported interesting results that confirm these concerns. They performed motion studies of microjets in PBS and artificial blood solution. In presence of 3% H_2O_2 as fuel and 1% SDS as surfactant, there was no motion in blood, whereas in PBS the micromotors behavior was correct. Even serial dilution of blood shows that inhibition of motion is significant. Bubble ejection was observed in a sample diluted at least 100 times while motion required a 1000-dilution. The authors of this research suggested that for high blood concentration the major factor linked to motion inhibition is the microtube blockage by red blood cells, whereas in highly diluted samples the viscosity decrease is correlated with the velocity increase [70]. Further studies are necessary to discover advantageous approaches with a view to overcoming this current challenge.

2.4.2. Toxicity of micro/nanomotors and their fuels

As discussed above, future applications of micro/nanomotors are limited by the motion challenge concerning in vivo/biological environments. Another crucial challenge of these micro/nanodevices is their biocompatibility. Some of them are fabricated using toxic reagents giving rise to a serious limitation in real in vivo applications, for example in diagnosis or drug delivery. As Pumera et al. discussed, it is actually quite

Table 1
Micro/nanomotors tested on cell culture.

Type of micro/nanomotors	Propulsion mechanism	Type of cell culture	Applications/observations	Reference
Au–Pt bimetallic nanotubes	Catalytic — (hydrogen peroxide as fuel)	Human lung epithelial cells (A549)	24 h and 48 h post exposure study did not show toxicity of motors toward cells (verified using MTT and WST-8 test)	[55]
Self-assembled polymer multilayer nanorockets loaded with anticancer drug	Catalytic — (hydrogen peroxide as fuel) and magnetic	HeLa	HeLa cells survived 3% of H_2O_2 used as a fuel for 30 min. This time can be extended when H_2O_2 is lower but the temperature is 37 °C. Motors have the ability to attach to cells, partially penetrate them and deliver a loaded drug (Doxorubicin)	[56]
Janus mesoporous silica nanoparticles (MSN) with DOX loaded in mesoporous pore channels	Catalytic — (hydrogen peroxide as fuel)	HeLa	MSN motors are able to deliver DOX to cells and they are not toxic, unlike their fuel — H_2O_2.	[19]
Nanoporous gold nanowires loaded with DOX	Ultrasounds	HeLa	Successful delivery of drug to HeLa cells using ultrasounds.	[41]
InGaAs/GaAs/(Cr)Pt	Catalytic — (hydrogen peroxide as fuel)	Yeast cells	Ability to load yeast cells was observed. In presence of 3 cells loaded, the motors velocity decrease from 125 to 25 μm/s	[57]
		HeLa	Drilling in HeLa cells	
AuNP (PAH/PSS)20 PtNP micromotors	Catalytic — (hydrogen peroxide as fuel)	HeLa, RBC	Micromotors showed ability of specific binding to RBC via peptide modification. By photothermal (NIR) treatment, micromotors cause the apoptosis of HeLa cells (cancer therapy).	[30]
Mg/Pt-Poly(N-isopropylacrylamid) (PNIPAM) Janus micromotors	Catalytic — (water as fuel)	RBC	High hemocompatibility of micromotors was proved: ability of motion, non-toxic, bubbles size that not exceed RBC size.	[58]
Ferrite coated magnetic nanomotors	Magnetic	C2C12 mouse myoblast cells	Biocompatibility and proper movement in different bio-fluids. Non-toxic effect on C2C12 mouse myoblast cells after a 3-day experiment.	[59]
Flexible magnetic nickel–silver nanoswimmers	Magnetic	HeLa	Successful delivery of DOX to HeLa cells	[60]
Liposome functionalized with artificial bacterial flagella	Magnetic	C2C12 mouse myoblast cells	Successful delivery of Calcein to cells but the problem of clearance by RES was observed	[61]
Rod-shaped gold nanomotors	Acoustic wave	HeLa	Nanomotors propulsion inside HeLa cells does not affect their viability	[62]
autonomous DNA nanorobot	Non-guided move toward target	NK leukemia cells, T cells	As a proof of principle, nanorobots loaded with combinations of antibody fragments were used in two different types of cell-signaling stimulation in tissue culture.	[63]
Bovine serum albumin/poly-l-lysine (PLL/BSA) multilayer rocket	Catalytic — (hydrogen peroxide as fuel) and magnetic	HeLa	Motion toward cells and drug delivery. The drug (DOX) was observed. under biological conditions. The studied motors are biodegradable (enzymatic treatment)	[29]
Magnetic particles encapsulated in RBC	Magnetic	J774 murine macrophage cells	Propulsion is possible in whole (non-diluted) blood. The inhibited macrophage uptake confirms the biocompatibility of the RBC motors.	[53]

surprising how researchers put much effort into obtaining novel micro/nanomotors while forgetting about the issue of biocompatibility [55]. Even if nano/micromotors were biocompatible and suitable for live organisms, the challenge is still the propulsion mechanism, particularly those catalytically powered. H_2O_2 is one of the most common fuels that produce oxygen bubbles triggering a propulsion mechanism. Unfortunately, H_2O_2 is highly toxic and even a concentration below 1% is not particularly suitable to perform any reaction in vivo or even in vitro. Long exposure to small amount of hydrogen peroxide leads to reduction of cells viability. On the other hand, literature suggest that high concentrations of H_2O_2 (e.g. >1%, v/v) impact the overall immunoassay performance negatively, probably due to proteins denaturation [50].

In order to assess the suitability of micro/nanomotors for in vivo applications, it is necessary to check their potential toxicity; for example, using mammalian cells as a model. Some of the most commonly known assays are MTT (3-(4,5-dimethylthiazol-2-yl)-2,5-diphenyltetrazolium bromide) and WST-8 (2-(2-methoxy-4-nitrophenyl)-3-(4-nitrophenyl)-5-(2,4-disulfophenyl)-2H-tetrazolium). Both tests are based on analysis of the cell membrane integrity since they measure the level of mitochondrial dehydrogenase that catalyzes the conversion of tetrazolium salt to purple, insoluble formazan. If the explored cells are destroyed or present reduced viability, the level of mitochondrial enzyme is lower [72].

Catalytic micro/nanomotors can be successfully used in vivo if the propulsion mechanisms exploit a non-toxic fuel such as water or glucose. Gao et al. proposed water-driven micromotors which are environmentally friendly and biocompatible. They are composed of an Al-Ga binary alloy microsphere. Hydrogen bubbles are produced upon contact with water, which is based on a simple reaction:

$$2Al + 6H_2O \rightarrow 3H_2 + 2Al(OH)_3.$$
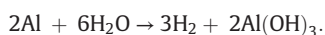
However this reaction depends on specific parameters such as ionic strength and pH. Interestingly, the investigators proved that water-driven motors move efficiently even in biological media such as human serum [14].

Another approach exploiting a biocompatible fuel was proposed by Kumar and colleagues, who utilized glucose and glucose oxidase functionalized nanomotors. The mechanism of propulsion is based on catalysis of glucose conversion to D-1,5-gluconolactone with hydrogen peroxide as a byproduct [73]. Similar idea was proposed by Pantarotto et al., where carbon nanotubes were modified with glucose oxidase and catalase so as to perform tandem catalytic conversion of glucose and hydrogen oxide [37]. Although this approach is interesting, the main drawback is that the required concentration of glucose is very high (above 1 M), which practically limits the possibility to use them in vivo where glucose is naturally present. For example, in blood the glucose concentration ranges at the mmol L^{-1} range. Probably, in in vivo applications the more promising micro/nanomotors are those that do not require chemical fuel and their motion is driven by external stimulus. Literature reports some examples of magnetic nanomotors for drug delivery, particularly loaded with DOX [60], Calcein [61] and

Rhodamine B [74]. In addition, nanowires composed of Au/Ni/Au/PPy and Au–Au–Ni–Au were propelled by ultrasounds [40,41].

3. Conclusions

Micro/nanomotors can be tailored in terms of size, shape, composition and propulsion mechanism according to the targeted application. Although micro/nanomotors are reported to transport biomolecules, sense biomarkers, perform drug delivery tasks and interact with tissues, their exploitation in diagnostics is still in its early stage and represents a major challenge due to the influence of complex media (matrix) in their motion and their potential toxicity associated with their composition and fuel. As new generations of micro/nanomotors become more operative in a biologically friendly fashion, these diminutive machines are likely to perform more advanced tasks in diagnostics and they will be an asset in therapeutics.

Acknowledgments

References

[1] S. Fournier-Bidoz, A.C. Arsenault, I. Manners, G.A. Ozin, Synthetic self-propelled nanorotors, Chem. Commun. (2005) 441–443.

[2] W.F. Paxton, K.C. Kistler, C.C. Olmeda, A. Sen, S.K.St. Angelo, Y. Cao, T.E. Mallouk, P.E. Lammert, V.H. Crespi, Catalytic nanomotors: autonomous movement of striped nanorods, J. Am. Chem. Soc. 126 (2004) 13424–13431.

[3] M. Guix, C.C. Mayorga-Martinez, A. Merkoçi, Nano/micromotors in (bio)chemical science applications, Chem. Rev. 114 (2014) 6285–6322.

[4] W. Gao, J. Wang, Synthetic micro/nanomotors in drug delivery, Nanoscale 6 (2014) 10486–10494.

[5] S. Sánchez, L. Soler, J. Katuri, Chemically powered micro- and nanomotors, Angew. Chem. Int. Ed. 54 (2015) 1414–1444.

[6] R.D. Vale, R.A. Milligan, The way things move: looking under the hood of molecular motor proteins, Science 288 (2000) 88–95.

[7] J. Fu, S. Cherevko, C.-H. Chung, Electroplating of metal nanotubes and nanowires in a high aspect-ratio nanotemplate, Electrochem. Commun. 10 (2008) 514–518.

[8] J. Parmar, X. Ma, J. Katuri, J. Simmchen, M.M. Stanton, C. Trichet-Paredes, L. Soler, S. Sanchez, Nano and micro architectures for self-propelled motors, Sci. Technol. Adv. Mater. 16 (2015).

[9] S. Sanchez, L. Soler, J. Katuri, Chemically powered micro- and nanomotors, Angew. Chem. Int. Ed. 54 (2015) 1414–1444.

[10] L.F. Valadares, Y.-G. Tao, N.S. Zacharia, V. Kitaev, F. Galembeck, R. Kapral, G.A. Ozin, Catalytic nanomotors: self-propelled sphere dimers, Small 6 (2010) 565–572.

[11] J.R. Howse, R.A.L. Jones, A.J. Ryan, T. Gough, R. Vafabakhsh, R. Golestanian, Self-motile colloidal particles: from directed propulsion to random walk, Phys. Rev. Lett. 99 (2007).

[12] J.R. Howse, R.A.L. Jones, A.J. Ryan, R. Golestanian, Self-motile colloidal particles: from random walks to directed propulsion and chemotaxis, Abstr. Pap. Am. Chem. Soc. 237 (2009).

[13] A. Brown, W. Poon, Ionic effects in self-propelled Pt-coated Janus swimmers, Soft Matter 10 (2014) 4016–4027.

[14] W. Gao, A. Pei, J. Wang, Water-driven micromotors, ACS Nano 6 (2012) 8432–8438.

[15] J.G. Gibbs, N.A. Fragnito, Y. Zhao, Asymmetric Pt/Au coated catalytic micromotors fabricated by dynamic shadowing growth, Appl. Phys. Lett. 97 (2010).

[16] T.-C. Lee, M. Alarcon-Correa, C. Miksch, K. Hahn, J.G. Gibbs, P. Fischer, Self-propelling nanomotors in the presence of strong Brownian forces, Nano Lett. 14 (2014) 2407–2412.

[17] X. Ma, S. Sanchez, A bio-catalytically driven Janus mesoporous silica cluster motor with magnetic guidance, Chem. Commun. 51 (2015) 5467–5470.

[18] B.-E. Pinchasik, H. Moehwald, A.G. Skirtach, Mimicking bubble use in nature: propulsion of Janus particles due to hydrophobic–hydrophilic interactions, Small 10 (2014) 2670–2677.

[19] M. Xuan, J. Shao, X. Lin, L. Dai, Q. He, Self-propelled Janus mesoporous silica nanomotors with sub-100 nm diameters for drug encapsulation and delivery, ChemPhysChem 15 (2014) 2255–2260.

[20] W. Gao, X. Feng, A. Pei, Y. Gu, J. Li, J. Wang, Seawater-driven magnesium based Janus micromotors for environmental remediation, Nanoscale 5 (2013) 4696–4700.

[21] F. Mou, C. Chen, H. Ma, Y. Yin, Q. Wu, J. Guan, Self-propelled micromotors driven by the magnesium–water reaction and their hemolytic properties, Angew. Chem. Int. Ed. 52 (2013) 7208–7212.

[22] M. Manjare, Y. BoZhao, Bubble driven quasioscillatory translational motion of catalytic micromotors, Phys. Rev. Lett. 109 (2012) 128305.

[23] Y. Mei, G. Huang, A.A. Solovev, E.B. Urena, I. Moench, F. Ding, T. Reindl, R.K.Y. Fu, P.K. Chu, O.G. Schmidt, Versatile approach for integrative and functionalized tubes by strain engineering of nanomembranes on polymers, Adv. Mater. 20 (2008) 4085.

[24] W. Gao, S. Sattayasamitsathit, J. Orozco, J. Wang, Highly efficient catalytic microengines: template electrosynthesis of polyaniline/platinum microtubes, J. Am. Chem. Soc. 133 (2011) 11862–11864.

[25] J. Orozco, A. Cortés, G. Cheng, S. Sattayasamitsathit, W. Gao, X. Feng, Y. Shen, J. Wang, Molecularly imprinted polymer-based catalytic micromotors for selective protein transport, J. Am. Chem. Soc. 135 (2013) 5336–5339.

[26] M. Garcia, J. Orozco, M. Guix, W. Gao, S. Sattayasamitsathit, A. Escarpa, A. Merkoçi, J. Wang, Micromotor-based lab-on-chip immunoassays, Nanoscale 5 (2013) 1325–1331.

[27] W. Gao, S. Sattayasamitsathit, A. Uygun, A. Pei, A. Ponedal, J. Wang, Polymer-based tubular microbots: role of composition and preparation, Nanoscale 4 (2012) 2447–2453.

[28] H. Wang, J.G.S. Moo, M. Pumera, Tissue cell assisted fabrication of tubular catalytic platinum microengines, Nanoscale 6 (2014) 11359–11363.

[29] Z. Wu, X. Lin, X. Zou, J. Sun, Q. He, Biodegradable protein-based rockets for drug transportation and light-triggered release, ACS Appl. Mater. Interfaces 7 (2015) 250–255.

[30] Z. Wu, X. Lin, Y. Wu, T. Si, J. Sun, Q. He, Near-infrared light-triggered "on/off" motion of polymer multi layer rockets, ACS Nano 8 (2014) 6097–6105.

[31] A.A. Solovev, Y. Mei, E.B. Urena, G. Huang, O.G. Schmidt, Catalytic microtubular jet engines self-propelled by accumulated gas bubbles, Small 5 (2009) 1688–1692.

[32] S.M. Harazim, W. Xi, C.K. Schmidt, S. Sanchez, O.G. Schmidt, Fabrication and applications of large arrays of multifunctional rolled-up SiO/SiO_2 microtubes, J. Mater. Chem. 22 (2012) 2878–2884.

[33] R. Golestanian, T.B. Liverpool, A. Ajdari, Propulsion of a molecular machine by asymmetric distribution of reaction products, Phys. Rev. Lett. 94 (2005).

[34] W. Gao, R. Dong, S. Thamphiwatana, J. Li, W. Gao, L. Zhang, J. Wang, Artificial micromotors in the mouse's stomach: a step toward in vivo use of synthetic motors, ACS Nano 9 (2015) 117–123.

[35] W. Gao, A. Pei, R. Dong, J. Wang, Catalytic iridium-based janus micromotors powered by ultralow levels of chemical fuels, J. Am. Chem. Soc. 136 (2014) 2276–2279.

[36] R.A. Pavlick, S. Sengupta, T. McFadden, H. Zhang, A. Sen, A polymerization-powered motor, Angew. Chem. Int. Ed. 50 (2011) 9374–9377.

[37] D. Pantarotto, W.R. Browne, B.L. Feringa, Autonomous propulsion of carbon nanotubes powered by a multienzyme ensemble, Chem. Commun. (2008) 1533–1535.

[38] A. Carovac, F. Smajlovic, D. Junuzovic, Application of ultrasound in medicine, Acta inform. med.: AIM : j. Soc. Med. Inform. Bosn. Herzegovina: casopis Drustva za medicinsku informatiku BiH 19 (2011) 168–171.

[39] W. Wang, L.A. Castro, M. Hoyos, T.E. Mallouk, Autonomous motion of metallic microrods propelled by ultrasound, ACS Nano 6 (2012) 6122–6132.

[40] V. Garcia-Gradilla, J. Orozco, S. Sattayasamitsathit, F. Soto, F. Kuralay, A. Pourazary, A. Katzenberg, W. Gao, Y. Shen, J. Wang, Functionalized ultrasound-propelled magnetically guided nanomotors: toward practical biomedical applications, ACS Nano 7 (2013) 9232–9240.

[41] V. Garcia-Gradilla, S. Sattayasamitsathit, F. Soto, F. Kuralay, C. Yardimci, D. Wiitala, M. Galarnyk, J. Wang, Ultrasound-propelled nanoporous gold wire for efficient drug loading and release, Small 10 (2014) 4154–4159.

[42] T. Xu, F. Soto, W. Gao, R. Dong, V. Garcia-Gradilla, E. Magana, X. Zhang, J. Wang, Reversible swarming and separation of self-propelled chemically powered nanomotors under acoustic fields, J. Am. Chem. Soc. 137 (2015) 2163–2166.

[43] W. Wang, W. Duan, Z. Zhang, M. Sun, A. Sen, T.E. Mallouk, A tale of two forces: simultaneous chemical and acoustic propulsion of bimetallic micromotors, Chem. Commun. 51 (2015) 1020–1023.

[44] A. de Gramont, S. Watson, L.M. Ellis, J. Rodon, J. Tabernero, A. de Gramont, S.R. Hamilton, Pragmatic issues in biomarker evaluation for targeted therapies in cancer, Nat. Rev. Clin. Oncol. 12 (2015) 197–212.

[45] J. Wu, S. Balasubramanian, D. Kagan, K.M. Manesh, S. Campuzano, J. Wang, Motion-based DNA detection using catalytic nanomotors, Nat. Commun. 1 (2010) 36.

[46] K. Van Nguyen, S.D. Minteer, DNA-functionalized Pt nanoparticles as catalysts for chemically powered micromotors: toward signal-on motion-based DNA biosensor, Chem. Commun. 51 (2015) 4782–4784.

[47] D. Kagan, S. Campuzano, S. Balasubramanian, F. Kuralay, G.-U. Flechsig, J. Wang, Functionalized micromachines for selective and rapid isolation of nucleic acid targets from complex samples, Nano Lett. 11 (2011) 2083–2087.

[48] X. Yu, Y. Li, J. Wu, H. Ju, Motor-based autonomous microsensor for motion and counting immunoassay of cancer biomarker, Anal. Chem. 86 (2014) 4501–4507.

[49] D. Vilela, J. Orozco, G. Cheng, S. Sattayasamitsathit, M. Galarnyk, C. Kan, J. Wang, A. Escarpa, Multiplexed immunoassay based on micromotors and microscale tags, Lab Chip 14 (2014) 3505–3509.

[50] E. Morales-Narváez, M. Guix, M. Medina-Sánchez, C.C. Mayorga-Martinez, A. Merkoçi, Micromotor enhanced microarray technology for protein detection, Small 10 (2014) 2542–2548.

[51] M.E. Davis, Z. Chen, D.M. Shin, Nanoparticle therapeutics: an emerging treatment modality for cancer, Nat. Rev. Drug Discov. 7 (2008) 771–782.

[52] G. Tiwari, R. Tiwari, B. Sriwastawa, L. Bhati, S. Pandey, P. Pandey, S.K. Bannerjee, Drug delivery systems: an updated review, Int. j. pharm. invest. 2 (2012) 2–11.

[53] Z. Wu, T. Li, J. Li, W. Gao, T. Xu, C. Christianson, W. Gao, M. Galarnyk, Q. He, L. Zhang, J. Wang, Turning erythrocytes into functional micromotors, ACS Nano 8 (2014) 12041–12048.

[54] M. Asplund, E. Thaning, J. Lundberg, A.C. Sandberg-Nordqvist, B. Kostyszyn, O. Inganas, H. von Holst, Toxicity evaluation of PEDOT/biomolecular composites intended for neural communication electrodes, Biomed. Mater. 4 (2009).

[55] E.L.K. Chng, G. Zhao, M. Pumera, Towards biocompatible nano/microscale machines: self-propelled catalytic nanomotors not exhibiting acute toxicity, Nanoscale 6 (2014) 2119–2124.

[56] Z. Wu, Y. Wu, W. He, X. Lin, J. Sun, Q. He, Self-propelled polymer-based multilayer nanorockets for transportation and drug release, Angew. Chem. Int. Ed. 52 (2013) 7000–7003.

[57] A.A. Solovev, W. Xi, D.H. Gracias, S.M. Harazim, C. Deneke, S. Sanchez, O.G. Schmidt, Self-propelled nanotools, ACS Nano 6 (2012) 1751–1756.

[58] F. Mou, C. Chen, Q. Zhong, Y. Yin, H. Ma, J. Guan, Autonomous motion and temperature-controlled drug delivery of Mg/Pt-Poly(N-isopropylacrylamide) Janus micromotors driven by simulated body fluid and blood plasma, ACS Appl. Mater. Interfaces 6 (2014) 9897–9903.

[59] P.L. Venugopalan, R. Sai, Y. Chandorkar, B. Basu, S. Shivashankar, A. Ghosh, Conformal cytocompatible ferrite coatings facilitate the realization of a nanovoyager in human blood, Nano Lett. 14 (2014) 1968–1975.

[60] W. Gao, D. Kagan, O.S. Pak, C. Clawson, S. Campuzano, E. Chuluun-Erdene, E. Shipton, E.E. Fullerton, L. Zhang, E. Lauga, J. Wang, Cargo-towing fuel-free magnetic nanoswimmers for targeted drug delivery, Small 8 (2012) 460–467.

[61] R. Mhanna, F. Qiu, L. Zhang, Y. Ding, K. Sugihara, M. Zenobi-Wong, B.J. Nelson, Artificial bacterial flagella for remote-controlled targeted single-cell drug delivery, Small 10 (2014) 1953–1957.

[62] W. Wang, S. Li, L. Mair, S. Ahmed, T.J. Huang, T.E. Mallouk, Acoustic propulsion of nanorod motors inside living cells, Angew. Chem. Int. Ed. 53 (2014) 3201–3204.

[63] S.M. Douglas, I. Bachelet, G.M. Church, A logic-gated nanorobot for targeted transport of molecular payloads, Science 335 (2012) 831–834.

[64] E.M. Purcell, Life at low Reynolds-number, Am. J. Phys. 45 (1977) 3–11.

[65] S. Sanchez, A.A. Solovev, S.M. Harazim, O.G. Schmidt, Microbots swimming in the flowing streams of microfluidic channels, J. Am. Chem. Soc. 133 (2011) 701–703.

[66] J. Orozco, S. Campuzano, D. Kagan, M. Zhou, W. Gao, J. Wang, Dynamic isolation and unloading of target proteins by aptamer-modified microtransporters, Anal. Chem. 83 (2011) 7962–7969.

[67] W. Gao, M. D'Agostino, V. Garcia-Gradilla, J. Orozco, J. Wang, Multi-fuel driven Janus micromotors, Small 9 (2013) 467–471.

[68] S. Campuzano, J. Orozco, D. Kagan, M. Guix, W. Gao, S. Sattayasamitsathit, J.C. Claussen, A. Merkoçi, J. Wang, Bacterial isolation by lectin-modified microengines, Nano Lett. 12 (2012) 396–401.

[69] H. Wang, G. Zhao, M. Pumera, Crucial role of surfactants in bubble-propelled microengines, J. Phys. Chem. C 118 (2014) 5268–5274.

[70] G. Zhao, M. Viehrig, M. Pumera, Challenges of the movement of catalytic micromotors in blood, Lab Chip 13 (2013) 1930–1936.

[71] M.M. Mueller, E. Seifried, Blood transfusion in Europe: basic principles for initial and continuous training in transfusion medicine: an approach to an European harmonisation, Trans. Clin. Et Biol. 13 (2006) 282–289.

[72] T. Mosmann, Rapid colorimetric assay for cellular growth and survival — application to proliferation and cyto-toxicity assays, J. Immunol. Methods 65 (1983) 55–63.

[73] A. Kumar, T. Hideyo, K.C. Chang, S. Ayusman, B. Eric, Glucose driven catalytic nanomotor to create motion at microscale, J. Biotech Res 5 (2013) 35–39.

[74] F. Qiu, R. Mhanna, L. Zhang, Y. Ding, S. Fujita, B.J. Nelson, Artificial bacterial flagella functionalized with temperature-sensitive liposomes for controlled release, Sensors Actuators B Chem. 196 (2014) 676–681.

Toward integrated detection and graphene-based removal of contaminants in a lab-on-a-chip platform

Andrzej Chałupniak[1] and Arben Merkoçi[1,2] (✉)

[1] *Catalan Institute of Nanoscience and Nanotechnology (ICN2), CSIC and The Barcelona Institute of Science and Technology, Campus UAB, Bellaterra, 08193 Barcelona, Spain*

[2] *ICREA, Pg. Lluís Companys 23, 08010 Barcelona, Spain*

ABSTRACT

A novel, miniaturized microfluidic platform was developed for the simultaneous detection and removal of polybrominated diphenyl ethers (PBDEs). The platform consists of a polydimethylsiloxane (PDMS) microfluidic chip for an immunoreaction step, a PDMS chip with an integrated screen-printed electrode (SPCE) for detection, and a PDMS-reduced graphene oxide (rGO) chip for physical adsorption and subsequent removal of PBDE residues. The detection was based on competitive immunoassay-linked binding between PBDE and PBDE modified with horseradish peroxidase (HRP-PBDE) followed by the monitoring of enzymatic oxidation of o-aminophenol (o-AP) using square wave anodic stripping voltammetry (SW-ASV). PBDE was detected with good sensitivity and a limit of detection similar to that obtained with a commercial colorimetric test (0.018 ppb), but with the advantage of using lower reagent volumes and a reduced analysis time. The use of microfluidic chips also provides improved linearity and a better reproducibility in comparison to those obtained with batch-based measurements using screen-printed electrodes. In order to design a detection system suitable for toxic compounds such as PBDEs, a reduced graphene oxide–PDMS composite was developed and optimized to obtain increased adsorption (based on both the hydrophobicity and π–π stacking between rGO and PBDE molecules) compared to those of non-modified PDMS. To the best of our knowledge, this is the first demonstration of electrochemical detection of flame retardants and a novel application of the rGO-PDMS composite in a biosensing system. This system can be easily applied to detect any analyte using the appropriate immunoassay and it supports operation in complex matrices such as seawater.

1 Introduction

Lab-on-a-chip (LOC) platforms are being intensively developed since the last decade due to their versatility, ease of fabrication, and a multitude of applications in biosensing and analysis. So far, LOC devices have

---

Address correspondence to arben.merkoci@icn2.cat

been reported for the detection of protein [1], nucleic acids [2, 3], drugs [4, 5], hormones [6, 7], and many different organic compounds. Thus, LOC devices are very promising for health diagnostics, environmental screening, and ensuring safety and security.

Various methodologies of LOC fabrication have recently been developed involving materials such as paper [8], glass [9, 10], polymers [11, 12], or even proteins (e.g., gelatin [13, 14]). The use of a certain material depends on the desired application, physicochemical properties of the analyte to be detected, the need for biocompatibility, and possibly integration with other devices and materials [11].

One of the most common approaches in LOC development is polydimethylsiloxane-based (PDMS) technology (soft-lithography), where a polymeric elastomer is used to fabricate chips of different shapes, patterns, and properties [15].

Development of low-volume (in the range of micro- and nano-liters) and portable devices is especially interesting for environmental screening of potentially hazardous compounds. The monitoring of various pollutants present in air, soil, or water requires regular monitoring, and the use of an LOC device can allow efficient in-field detection; access to sophisticated laboratories is limited, expensive, and time consuming.

LOC devices have been reported for electrochemical detection of phenolic compounds [16, 17] and atrazine [18], optical platforms for pesticides [19], and heavy metal detection [20]. An LOC can be applied not only for the analysis of pollutants derived from industry and urban areas, but also for toxins originating from the natural environment such as those produced from marine microalgae [21–23].

The detection of polybrominated diphenyl ethers (PBDEs), a class of halogenated compounds, similar to polychlorinated diphenyls (PCBs) and commonly used as flame retardants, needs to be improved. PBDEs were introduced into the market in the 1960s and used for many years in domestic electronics, toys, furniture, polyurethane foams, and building materials [24, 25]. Over time, however, the negative effects of long-term exposure to PBDEs have been demonstrated, although many examples are not well investigated. As a result, commercial mixtures of PBDEs were banned from all applications in 2004 (penta-brominated

diphenyl ether (BDE) and octa-BDE) and 2013 (deca-BDE) in USA, European Union, and elsewhere [26, 27].

Due to their hydrophobicity, PBDEs can accumulate in various tissues and organs, especially in adipose tissue and their exposure is correlated with liver dysfunction [28]. PBDEs can also be found in breast milk, and many investigations have demonstrated dependence between the persisting contact with materials containing PBDE (by dermal absorption, consumption of contaminated food or inhalation) and their further accumulation in the body. Besides the small size and hydrophobicity, the biphenyl chemical structure of PBDEs is similar to that of the thyroid hormones (3,5-diiodothyronine (T2), 3,3,5-triiodothyronine (T3), and 3,3,5,5-tetraiodothyronine (T4)), and it has been confirmed that PBDEs bind with alpha- and beta-thyroid hormone receptors. PBDEs are also linked to neurodevelopment toxicity and various types of tumors [28, 29].

Despite the need for monitoring PBDE levels, only a few methods have been reported so far for their detection. Standard determination of PBDE is based on gas chromatography (GC) separation combined with electrode capture detection (GC-ECD) or mass spectrometry (GC-MS). The use of these methods is still limited by high equipment cost, the need for a qualified workforce, and high time consumption [30–32]. One of the alternatives is a competitive immunoassay for PBDE detection that is based on competition between PBDE molecules and PBDE modified with horseradish peroxidase (HRP-PBDE) in binding to anti-PBDE antibodies that are coupled to magnetic beads (MB-Ab). The signal is revealed using a well-known enzymatic reaction that catalyzes 3,3',5,5'-tetramethylbenzidine (TMB) oxidation, resulting in a colored product that can be easily measured by spectrophotometry. This method is relatively simple and offers an attractive range of detection (0.025–1.0 ppb of PBDE), both in standard solutions and environmental samples like soil or seawater.

Taking advantage of well-developed antibodies and a competitive reaction, we modified the colorimetric kit by performing electrochemical detection of HRP-PBDE and replacing TMB with o-aminophenol (o-AP) as a substrate for the electrochemical reaction. We

believe that the electrochemical reaction will provide an opportunity to assay PBDEs with better sensitivity and may lead to improved automation by integration into an LOC device. The LOC system and the detection approach are shown in Fig. 1.

The role of nanomaterials in LOC and other devices has grown significantly in recent years for both sensing and environmental removal of contaminants. In this context, we take advantage of the adsorption and removal capabilities of reduced graphene oxide (rGO) toward certain contaminants. As a proof of concept,

a composite of PDMS and rGO (rGO-PDMS) was developed and used to fabricate a microfluidic chip, where post-measurement samples are injected and organic traces, including excess PBDE, are immobilized and adsorbed onto the channel walls to improve the safety of the whole system. Such non-covalent interactions between PBDEs and carbon materials (based on π–π stacking) were previously used for novel extraction methods [33, 34] and micromotor-based removal of PBDEs [35]. Various composites of PDMS with carbon materials have also been developed, but
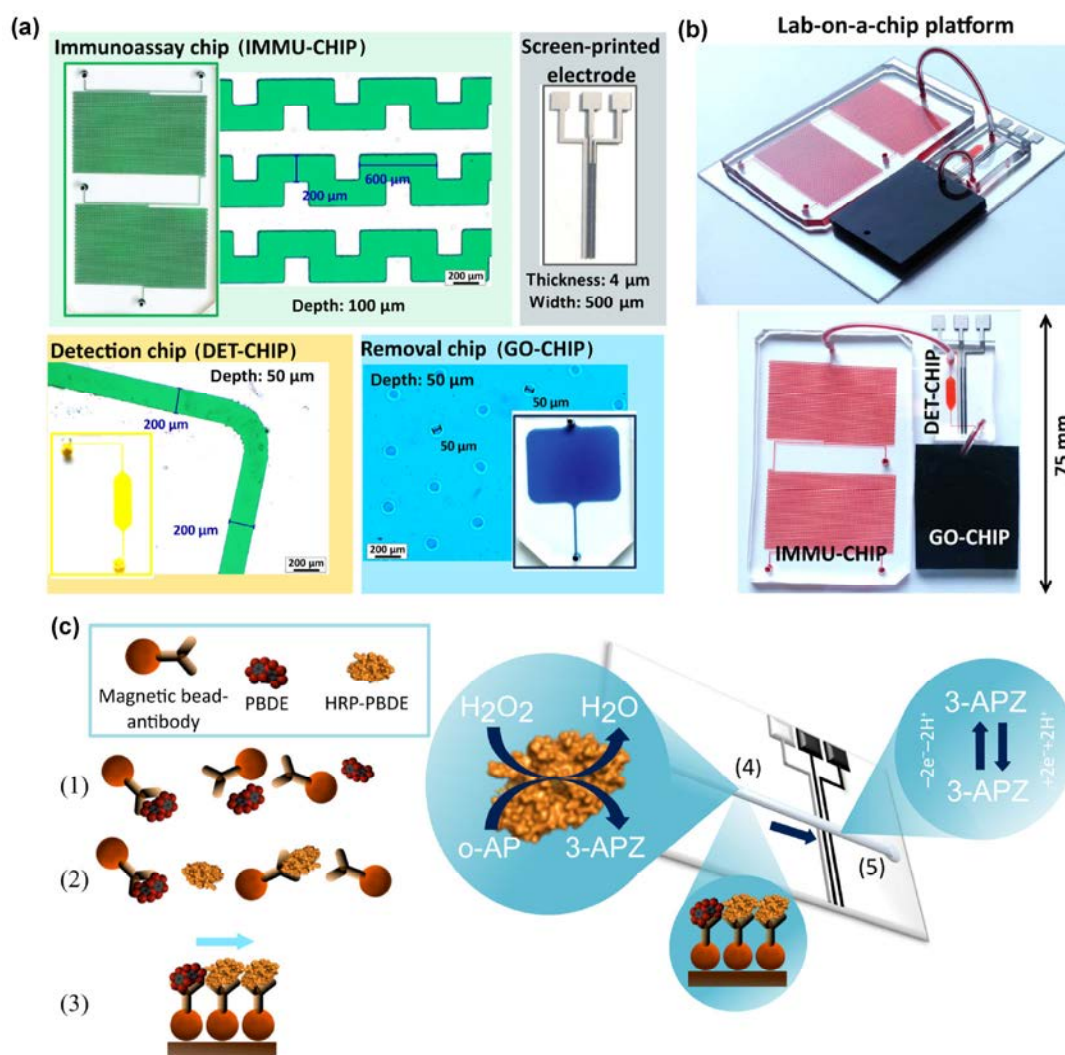
Figure 1 LOC system for detection and removal of PBDEs. (a) Components of the LOC device with visualization of the microfluidic structures (10× magnification objective); (b) side and top view of the assembled LOC device on a polycarbonate substrate with a screen-printed carbon electrode (SPCE); (c) assay procedure: (1) on-chip mixing and incubation of magnetic beads coupled to anti-PBDE antibodies (MB-Ab) with samples containing PBDE, (2) on-chip mixing and incubation of MB-Ab with HRP-PBDE, (3) immobilization of the immunocomplex in chip using an external magnet and washing of unbound molecules, (4) incubation with substrate solution (o-AP + H_2O_2), and (5) electrochemical detection of the product of enzymatic reaction (3-aminophenoxazone (3-APZ)).

most of them are based on sophisticated protocols that have been optimized to obtain conductive rather than highly adsorptive materials [36, 37].

To the best of our knowledge, this is the first approach showing an LOC device with an electrochemical approach for PBDE detection. Herein, a novel rGO-PDMS composite is used for the first time in an LOC device for biosensing and removal purposes.

2   Experimental

2.1   Reagents

PBDE colorimetric immunoassay kit was purchased from Abraxis (Pennsylvania, USA). PBDE stock solution was purchased from AccuStandard Inc. The screen-printed inks (carbon sensor paste C2030519P4 and silver–silver chloride paste C2130809D5) were purchased from Gwent Group, UK. Polycarbonate sheets were purchased from Vink Plastics S.L.U., Spain. PDMS (Sylgard® 184 Elastomer kit) was purchased from Ellsworth Adhesives Iberica, Spain. Graphene oxide stock solution (5 mg/mL) was purchased from Angstron Materials (Dayton, USA). A negative photoresist (SU8-50) and an appropriate developer were purchased from Microchem, USA. Flexible photolithography masks were provided by Microlitho, UK. Four-inch silicon wafers were purchased from NOVA Electronic Materials. Hydrogen peroxide, o-aminophenol, HPLC grade methanol, phosphate buffered saline (PBS), 3-aminopropyltriethoxylane (APTES), L-ascorbic acid (L-AA), and microscopic glass slides were purchased from Sigma. Britton–Robinson (BR) buffer (0.04 M, pH 5.7) was prepared as described elsewhere [38]. All commercial reagents were of analytical grade and handled according to the material safety data sheets suggested by the suppliers.

2.2   Instruments

Screen-printed carbon electrodes (SPCE) were fabricated by screen-printing technology using a screen-printer (DEK 248, UK). Electrochemical measurements were carried out using computer-controlled Autolab PGSTAT-12 (302 N-High performance, potentiostat/galvanostat) with a general-purpose electrochemical software operating system (GPES version 4.9.007,

from Eco Chemie B.V., Utrecht, the Netherlands). Microfluidic chips with an integrated SPCE electrode were connected to the Autolab PGSTAT-12 with a specially adapted electrical edge connector. A syringe pump (Pump 11 Elite; Harvard Apparatus, USA) was used as a driving unit for microfluidic system. The syringe pump was equipped with 0.5 mL glass syringes (Gastight®, Hamilton, USA). Centrifuge SIGMA 2-16PK was used for rGO purification and a magnetic stirrer (IKA lab disc white) was used during the reduction process. Plasma cleaner PDC-002 was used as a source of oxygen plasma for chip fabrication. Microfluidic chip operation was optimized using an optical microscope (Olympus IX71, Germany) coupled with a CCD camera (Olympus DP72, Germany) with the bright field mode, 10× magnification.

2.3   Experimental methodology

Unless otherwise stated, all optimization experiments regarding microfluidic chips were carried out on five independent chips. Optimization of electrochemical measurements was carried out using five independent screen-printed electrodes. Final calibration curves were obtained based on three repetitions. When the colorimetric method was used, each sample was run in duplicate according to the manufacturer's procedure. All errors of the results obtained were expressed as a relative standard deviation (RSD).

2.4   Fabrication and operation of LOC devices

Fabrication of screen-printed electrodes was based on already reported design and procedures, using polycarbonate sheets as the substrate [39]. The microfluidic mold was prepared using a previously reported methodology of photolithography process [15, 39], where a 4-inch silicon wafer was spin coated with a negative photoresist SU8-50 and patterned by photolithography using a flexible mask.

PDMS was mixed with its curing agent in the mass ratio 10:1. After intensive stirring for 5 min, an excess of air bubbles was removed using vacuum. Afterward, PDMS was poured onto the silicon wafer with a given design of the microfluidic chip and kept on the hotplate at 70 °C for 4–5 h until completely polymerized. After polymerization, proper shapes of PDMS were cut out

from the template, washed in miliQ water, followed by isopropanol and dried on the hotplate at 70 ℃ for 10 min. In order to modify the surface, oxygen plasma treatment was performed. Meanwhile, polycarbonate sheets (either with or without screen-printed electrodes) were washed with miliQ water, followed by isopropanol, ethanol, plasma treatment, and incubated in 2% APTES solution in order to silanize the surface (1 h). Afterward, both parts (PDMS and polycarbonate) were simply attached to each other, forming a permanent bonding that was strengthened by incubation on the hotplate at 70 ℃ for 1 h. Prior to the assay, the chips were connected with each other using polymeric tubes.

A general scheme of the system as well as dimensions of microfluidic channels are shown in Fig. 1. The system consists of three microfluidic chips: immunoassay chip (IMMU-CHIP), detection chip (DET-CHIP), and removal chip (GO-CHIP).

IMMU-CHIP consisted of channels with repeatable curvatures and three inlets (MB-Ab, PBDE, and HRP-PBDE). The role of curvatures was to support the diffusion between mixed reagents. In this chip, an immunoreaction between PBDE/HRP-PBDE and MB-Ab occurred. The PDMS layer was attached either to glass or polycarbonate.

DET-CHIP consisted of a single channel and the chamber (10 mm length, 3 mm width, and approximate volume of 15 μL) where the immunocomplex (MB-Ab-PBDE/HRP-PBDE) was immobilized by an external magnet placed underneath the chip. This chip was bonded to polycarbonate with SPCE. The DET-CHIP could be employed as a part of the LOC system as well as a separate chip just for various electrochemical measurements.

GO-CHIP was fabricated using the rGO-PDMS composite. The design used to fabricate this chip was based on a broad channel with pillars along its surface so as to increase surface-area-to-volume ratio and improve the adsorption performance through the microfluidic channel. The fabrication process was based on the patterning of the SU-8 photoresist.

2.5 Optical evaluation of the on-chip immunoreaction performance

The motivation for using a microfluidic chip for mixing (IMMU-CHIP) is the possibility that the process can

be automated by simply passing the sample through the channel, where mixing supports both (1) PBDE binding to MB-Ab and (2) HRP-PBDE binding. The design of IMMU-CHIP was previously used and its effectiveness (not reported here) in biochemical reactions was confirmed.

Using an optical microscope, the process of mixing was observed, so as to match the best parameters and make sure that all chemicals used in the assay are compatible with the materials used for the LOC device. As all the reagents seemed to be transparent for microscopy, Trypan blue (10%) was used to facilitate the distinction between two different solutions during mixing. The washing step was also assessed in order to identify an optimum flow rate and buffer volume (Fig. S1 in the Electronic Supplementary Material (ESM)).

2.6 Optimization of the on-chip magneto-immunoassay

IMMU-CHIP was fabricated as described in section 2.4, and it was washed by priming with 1 mL of washing buffer (water + 0.05% Tween-20) prior to use. A dedicated inlet was connected with a syringe containing reagents of magneto-immunoassay for PBDE detection.

Two types of optimization experiments were performed. The first experiment checked the occurrence of non-specific adsorption of PBDE to PDMS and changes in non-specific adsorption in relation to the flow rate. A solution of 1.0 ppb PBDE was flushed through the whole chip and collected in a microcentrifuge (Eppendorf tube) at the outlet. A colorimetric test was then performed following the standard procedure (S1 in the ESM). Results were expressed as a% of signal relative to the control sample of 1.0 ppb of PBDE.

The second experiment checked the possible adsorption of magnetic beads and HRP-PBDE onto the microchannel. The first inlet was connected to a PBDE blank solution (0.0 ppb), the second to MB-Ab, and the third to HRP-PBDE. The solutions were injected and mixed in a chip with each other at different flow rates, collected in an Eppendorf tube, and proceeded as in standard procedure for colorimetric detection of PBDE. Results were expressed as a% of signal obtained by using a control sample containing MB-Ab, HRP-

PBDE, and 0.0 ppb of PBDE.

2.7 Preparation of rGO-PDMS composite

An already reported approach for GO reduction using L-AA was employed [40]. L-AA was added to 200 mL GO solution to reach the concentration of 50 mg/mL. Samples were adjusted to desired pH using NaOH solution and incubated for 48 h with continuous magnetic stirring (600 rpm). After reduction, solution was transferred to 15 mL centrifugal tubes and centrifuged for 1 h, 12,000 rpm, and 4 °C. The supernatant was discarded, while pellets were washed with miliQ water. This step was repeated twice using miliQ and twice using 96% (v/v) ethanol. Purified solution of rGO was immediately used for further experiments.

Two components of the PDMS kit (elastomer and curing agent) were mixed in a volume ratio of 10:2. After stirring, a desired amount of rGO was added and vigorous stirring was continued for about 10 min. Afterward, rGO-PDMS was poured onto a silicon wafer with the design of a given chip. The wafer with rGO-PDMS was kept for 1 h at room temperature (RT) in order to remove air bubbles entrapped within the polymer before polymerization. Then, the wafer was kept on a hotplate and incubated at 70 °C for 4–5 h when the rGO-PDMS was completely polymerized. Microfluidic chips were fabricated using the same procedure.

Analysis of the rGO-PDMS composite (the effect of the pH, flow rate, and rGO concentration) was performed to determine the ability to adsorb a standard solution of PBDE (1.0 ppb). All parameters were optimized to maximize the adsorption yield. Experiments were based on passing the PBDE sample through the rGO-PDMS chip (with a single channel of 5 cm length, 500 μm width, and 100 μm depth) and then determining the concentration of PBDE using the colorimetric kit. As this kit is a competitive assay, the relative adsorption was determined using the following formula (Eq. (1))

$$\text{ADS} = A1_{(1.0\text{ppb})} - A0_{(1.0\text{ppb})}/B0_{(0,0\text{ppb})} \qquad (1)$$

where $A1_{(1.0\text{ppb})}$ is the absorbance of sample used in chip, with the initial concentration of 1.0 ppb; $A0_{(1.0\text{ppb})}$

is the absorbance of control sample with the initial concentration of 1.0 ppb; and $B0_{(0,0\text{ppb})}$ is the absorbance of the blank control sample containing 0.0 ppb solution.

2.8 Electrochemical detection

Electrochemical detection of HRP is inspired by already reported works [38, 41]. The competitive immunoassay results show that the level of HRP is inversely proportional to the level of PBDE. HRP catalyzes the redox reaction where hydrogen peroxide is converted to water molecules, while a given substrate is oxidized. In this approach (Fig. 1(c)), o-AP was chosen as the substrate for the enzymatic reaction due to its compatibility with other assay reagents and suitable electrochemical properties. Oxidation of o-AP leads to the formation of 3-aminophenoxazone (3-APZ) that can be reduced on the SPCE surface and detected in several electrochemical techniques such as cyclic voltammetry (CV), differential pulse voltammetry (DPV), chronoamperometry (AMP), and square wave anodic stripping voltammetry (SW-ASV). As the PBDE detection kit based on the HRP-PBDE molecule is optimized for a relatively narrow PBDE concentration range, SW-ASV was chosen because this technique is reportedly much more sensitive than others. Nevertheless, some examples of PBDE detection using CV and DPV are shown in Fig. S2 in the ESM. The following parameters were applied: deposition potential (–0.6 V); deposition time 20 s; equilibration time 15 s; potential range from 0.0 to –0.6 V; step potential 4 mV; amplitude 25 mV; and frequency 25 Hz.

Detection using the microfluidic chip was preceded by measurements based on bare SPCE so as to determine the optimal detection protocol. Briefly, the immunoassay was performed as usual; after washing an immunocomplex, samples were reconstituted in 10 μL of PBS buffer and 100 μL of substrate solution (o-AP + H_2O_2 in BR buffer) and incubated for 30 min. After incubation, 50 μL of the sample was pipetted onto the SPCE surface and electrochemical measurements were performed. Following this procedure, incubation time, o-AP concentration, H_2O_2 concentration, and deposition time in SW-ASV were optimized.

Then, electrochemical detection was performed using DET-CHIP. Parameters for detection were chosen based on optimization in static measurements. In this

case, when the substrate solution is injected into the microfluidic channel, it passes through the chamber where magnetic beads with the immunocomplex are immobilized; therefore, the enzymatic reaction was performed in flow and the product passed further along the channel up to the electrode surface where it was electrochemically deposited and detected. In addition, the optimum flow rate was analyzed in order to determine the best sensitivity and limit of detection.

3   Results and discussion

3.1   rGO-PDMS composite

Graphene oxide and other carbon derivatives are already reported as effective adsorbents of a range of molecules. In this work, we tried to combine the ability of rGO to adsorb PBDE with the convenient properties of PDMS chips by using an LOC device with increased adsorption performance (Fig. 2). Similar approaches are already reported, where graphene materials and PDMS were used as the composite, but they are used for its electrical properties and none was applied for the adsorption and removal applications in LOC devices [36, 42]. As presented, the rGO-PDMS composite does not need to be conductive; therefore, a much simpler fabrication protocol can be used that utilizes the adsorption property of rGO, which is attractive for lab-on-a-chip applications.

Furthermore, as the adsorption mechanism is based on π–π stacking, the rGO-PDMS composite can be
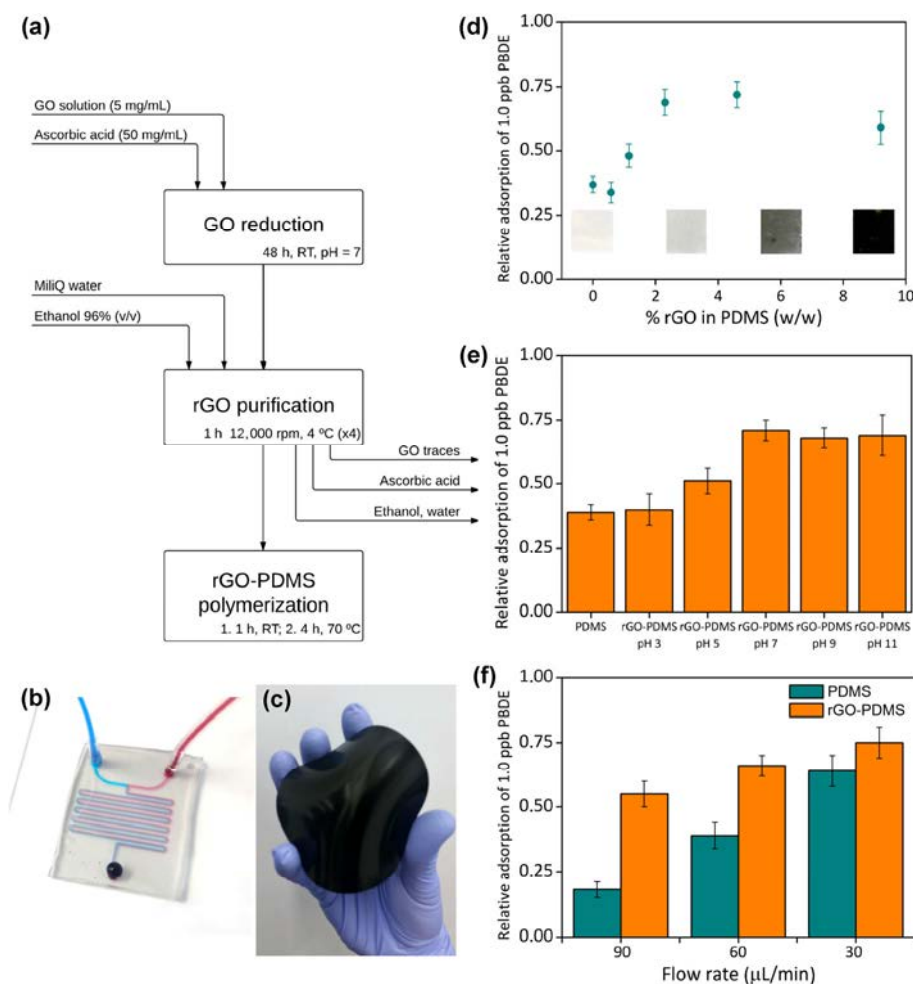
Figure 2   rGO-PDMS composite (a) fabrication process; (b) example of rGO-PDMS-glass chip filled with color inks; (c) example of flexible solid piece of rGO-PDMS; (d) the effect of rGO concentration (w/w) on PBDE adsorption; (e) the effect of pH during reduction process on PBDE adsorption; (f) the effect of flow rate on PBDE adsorption using rGO-PDMS and bare PDMS.

employed for various biomolecules such as DNA or proteins as both structures contain abundant aromatic rings. As a proof of concept, we performed the analogous test as for PBDEs but measured the adsorption of a model protein (HRP) and the effect of rGO adsorption can be clearly observed (Fig. S3 in the ESM).

We identified pH as an important factor facilitating rGO reduction and thus the efficiency of PDMS adsorption. Experiments based on PBDE adsorption onto the rGO-PDMS channel (Fig. 2(e)) showed that an increase of pH leads to an increase in adsorption; this effect peaks at pH 7. Above pH 7, there is no significant improvement in absorption.

It is not surprising that an increase in the rGO concentration in the PDMS will make adsorption stronger as more rGO will be exposed to the channel surface. However, any compound added to PDMS may affect its ability to polymerize. We found (Fig. 2(d)) that when the rGO concentration is lower than 1% (w/w), there is no improvement in adsorption and probably a slight decrease compared to that obtained with bare PDMS. A concentration of 4.5% (w/w) is optimal as it results in the highest adsorption of PBDE (around 70%). When the concentration is higher than 4.5% but lower than 10%, the adsorption capacity significantly decreases and the composite keeps its physical properties such as durability and hardness. If the concentration of rGO is higher than 10% (v/v), polymerization proceeds and the gas bubbles that are always slowly released during the polymerization of PDMS prevent the formation of a flat, homogenous layer of rGO-PDMS. Such a high concentration of rGO-PDMS also changes some physical properties as the polymer is too flexible and spongy. This effect may be related to the presence of rGO, but our opinion is that it is due to the presence of excessive solvent (water from the rGO suspension) in PDMS, which evaporates during polymerization and affects the structure of the polymer. Taking into account these observations, we decided to perform the last steps of rGO purification in ethanol solution, as it is compatible with PDMS and can evaporate very quickly without affecting the polymerization.

Flow rate is a major factor that influences microfluidic processes. We proved (Fig. 2(f)) that an increase of flow rate will decrease the adsorption yield. However, comparison of PDMS to rGO-PDMS shows that in a higher flow rate (90 μL/min), the effect of rGO is distinct (with a significant increase of adsorption) compared to that achieved at lower flow rates (30 μL/min).

Final measurements in the LOC system were completed with the rGO-PDMS chip fabricated using the design shown in Fig. 1 (GO-CHIP) and under the optimal conditions mentioned above. Due to a significantly increased contact surface area between the liquid and the rGO-PDMS channel, its adsorption capacity is higher than that of a single-channel chip.

We tested PBDE in the concentration range 1–1,000 ppb and identified that the total adsorption capacity is between 100 and 1,000 ppb, both in the standard buffer solution and seawater (Fig. S4 in the ESM). We believe that this is sufficient for real sample treatment as the usual level of PBDE in seawater is significantly lower than 10 ppb [43–45]. Moreover, a decrease in the flow rate may further improve the adsorption capability. In this work, as all of the operations are performed simultaneously, the flow rate value is determined by the other steps performed in the IMMU-CHIP and DET-CHIP.

Apart from the adsorption capability, the possible reuse of the platform was tested. We found that solvents introduced to the GO-CHIP channel can extract the previously adsorbed PBDE. Acetone was the most suitable solvent, as this solvent enabled desorption of PBDE in four subsequent cycles and recovery of nearly 100% PBDE (Fig. S5 in the ESM). The ease of fabrication indicates that this platform is more feasible when considered as disposable, rather than reusable platform.

3.2 Electrochemical detection of PBDE (bare SPE)

Development of a lab-on-a-chip platform for electro-chemical detection was preceded by experiments involving just screen-printed electrodes. Figure 3 shows parameters that were optimized in order to find the best conditions for PBDE determination. The most crucial parameter is the concentration of o-AP (Fig. 3(a)). If it is higher than 0.12 mM, it contributes to non-enzymatic oxidation and reduces the signal-to-noise ratio, similarly as reported elsewhere [38]. For this reason, 0.6 mM
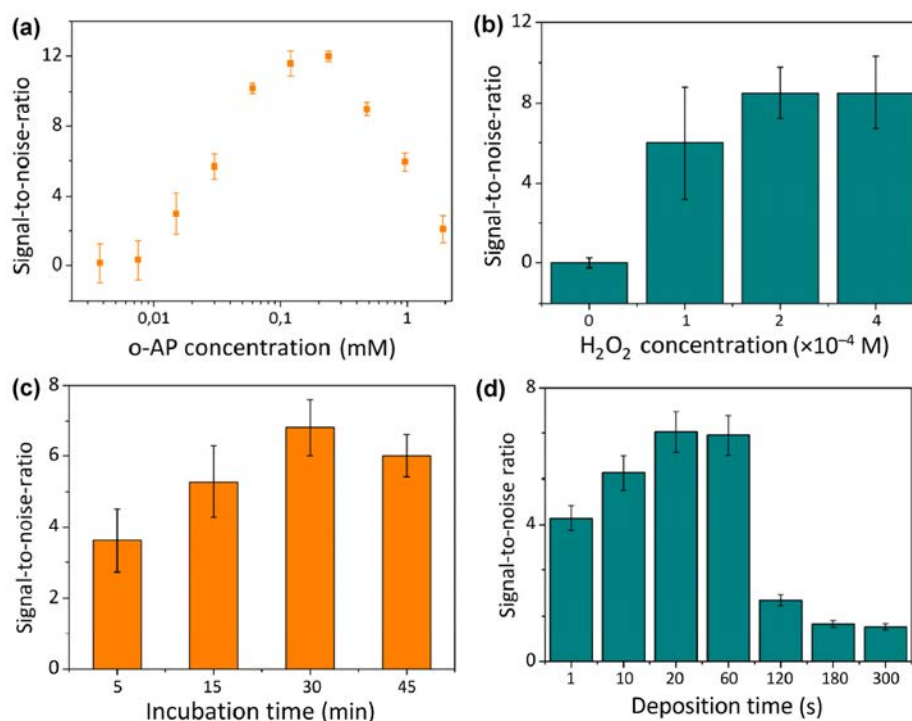
Figure 3 Optimization of electrochemical detection in static conditions using bare SPCE: (a) optimization of substrate (o-AP) concentration, (b) optimization of hydrogen peroxide concentration, (c) optimization of incubation time (enzymatic reaction), and (d) optimization of deposition time in square wave anodic stripping voltammetry. All results expressed as signal-to-noise ratio calculated as a ratio between the signal represented by control sample (0.0 ppb of PBDE) and substrate solution.

o-AP was chosen for further experiments, providing satisfactory sensitivity. The effect of the other component, the substrate solution (hydrogen peroxide), upon reaction sensitivity (Fig. 3(b)) was also studied; thus, the concentration of 2×10^{-4} M was used, as reported elsewhere [38].

Incubation time is the time when redox reaction is catalyzed by HRP. The time providing the highest SNR (Fig. 3(c)), 30 min, is quite similar to the time of reaction in a commercial colorimetric method (20 min). Further time extension does not lead to any sensitivity improvement.

An increase in the deposition time (Fig. 3(d)) leads to a proportional increase of SNR. However, if the deposition time exceeded 60 s, an enormous decrease of SNR is observed due to electrochemical oxidation of the substrate (o-AP), which prevails over the effect of the enzymatic reaction (HRP catalysis). Thus, 20 s was chosen as the optimum deposition time, which provides good sensitivity and reduces the risk of false-positive results.

3.3 Lab-on-a-chip optimization

The next step in the LOC platform development was evaluation of the IMMU-CHIP performance. Figure 4(a) shows the process of mixing between the solution of PBDE and MB-Ab suspension. It can be seen that when solutions meet each other in the microfluidic channel, they do not mix and flow separately. However, due to the curvature of the channel, the solution is further conveyed from laminar into turbulent flow; as a result, the diffusion between them occurs quite efficiently and facilitates the immunoreaction. Figure 4(a)(3) shows the ending section of the mixer chip, where the color of the solution is already uniform; hence, a reaction between PBDE and MB-Ab is likely.

Figure 4(b) presents the results of flow rate optimization, where a colorimetric kit was used as a reference technique. Regarding PBDE adsorption, an increase of flow rate is linked with an increase of PBDE recovery, which means that no analyte is lost during the assay. For the flow rate equal or higher than
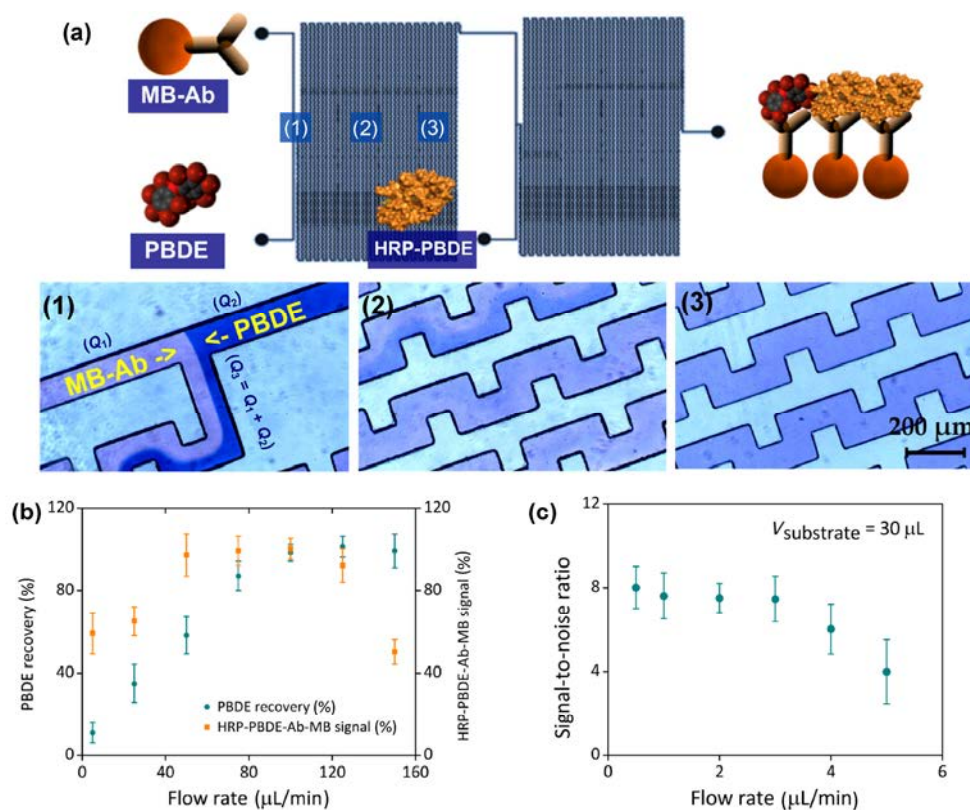
Figure 4 Optimization of LOC operation. (a) Visualization of mixing in IMMU-CHIP between reagents in the (1) intersection where MB-Ab meet PBDE, (2) middle part of the chip where mixing process partially occurred, and (3) terminal section of the channel where samples are fully mixed. Trypan-blue (10%) was used to visualize PBDE solution; pictures were taken using an optical microscope with 20× magnification; (b) optimization of the flow rate in the IMMU-CHIP was based on a colorimetric test regarding the PBDE recovery and immunocomplex (HRP-PBDE-Ab-MB) signal when passing the microfluidic channel; and (c) optimization of the flow rate during enzymatic reaction in electrochemical detection of HRP-PBDE (DET-CHIP). All results are expressed as the signal-to-noise ratio calculated as a ratio between the signal represented by substrate solution without PBDE as a control sample.

100 µL/min, PBDE adsorption is no longer observed. Regarding the on-chip immunoreaction, the efficiency of the reaction is not very high when the low flow rate is applied (60% of control signal for the flow rate of 5 µL/min), which is probably related to protein adsorption or the physical loss of magnetic beads. On the other hand, when very high flow rates are applied, the efficiency of the reaction is also not satisfactory, probably due to the reduced time that limits the occurrence of the immunoreaction. Thus, analysis of both curves shows that the flow rate of about 100 µL/min offers a compromise, as PBDE adsorption is not observed and the reaction between HRP-PBDE and MB-Ab works with the maximum efficiency.

Compared to electrochemical measurements performed just by drop casting (batch/static measurements), in chip detection (DET-CHIP) requires a high level of attention to the flow rate, as the main factor affecting sensitivity and limit of detection. The flow of the sample particularly supports the enzymatic reaction, where substrate solution is mixed with the immunocomplex and 3-APZ is obtained, as well as the deposition process, where 3-APZ is accumulated onto the electrode surface. In electrochemical stripping (the detection step), the flow is stopped and this step is performed in static conditions.

In order to find the optimal conditions, some measurements of different flow rates (defined by taking into account the constant volume of the injected o-AP/H_2O_2/PBS solution, 30 µL) as well as the desired time of the enzymatic reaction were carried out. Figure 4(c) shows that an increase in the flow rate

correlates with a decrease in the signal-to-noise ratio. This is obviously caused by the reduced time that is a key factor in enzymatic reactions. Flow rates between 0.5 and 3 µL/min allowed to perform reaction with a relatively high signal-to-noise ratio, similar to the optimal condition (30 min) of static measurements. The final experiments were performed using the flow rate of 2 µL/min, where the reaction time is only 15 min.

Similar to static measurements, the time of 20 s was found to be optimal for the deposition step (data not shown). The process of deposition was performed with a flow rate of 90 µL/min in order to transfer all of the solution from the chip, where an enzymatic reaction occurred. We have observed that such a relatively high flow rate supports the sensitivity of the assay as the background current is much lower than that in static measurements. This results from the amount of molecules adsorbed onto the electrode during the deposition step that is lower at the higher flow rate.

3.4 Complete detection of PBDE using the lab-on-a-chip platform

Figure 5 presents the final results of all methods compared. As it can be seen in Fig. 5(a), the signal of SW-ASV is represented by curves in which negative current is inversely proportional to the PBDE concentration. Each peak is characterized by a specific potential of about –0.35 V that shifts slightly toward –0.3 V when the concentration of HRP-PBDE increases. We have also observed that the presence of salts (e.g., PBS) influences the potential value by shifting it toward –0.4 V, without affecting the signal intensity (data not shown). All measurements were performed in the presence of PBS (o-AP + H_2O_2 and PBS in a ratio 10:1) so as to keep a reproducible value of potential. In order to validate the developed technique, we simultaneously performed the commercial colorimetric test (Fig. 5(b)). The limit of detection (LOD) of this technique is about 0.019 ppb PBDE and is in accordance with the results obtained by electrochemical measurement, where the LOD is about 0.018 ppb, both for the whole assay performed in a chip and only for the detection step performed in a chip. This is not surprising as the LOD of this method is limited by the immunoassay performance, rather than HRP detection as the concentration of the labeling protein is sufficient, in both samples with the highest and lowest concentrations of PBDE. Such a limit of detection seems sufficient for all possible applications, taking
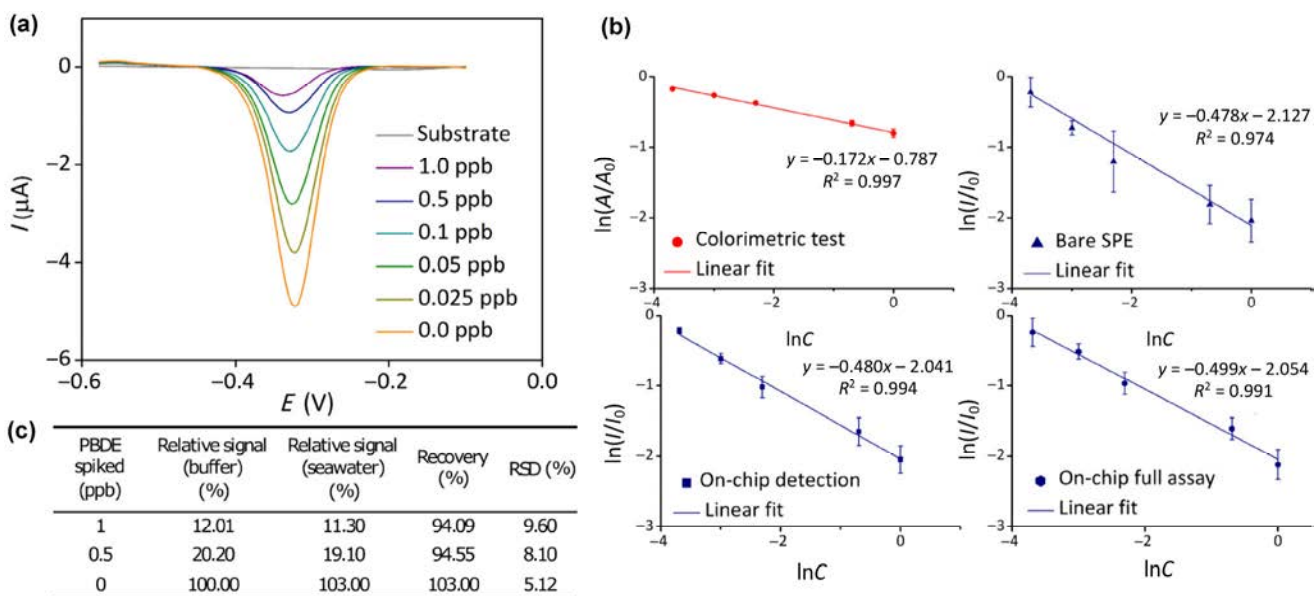
Figure 5 Comparison of optical and electrochemical detection of PBDE. (a) Example of SW-ASV measurements of different concentrations of PBDE (0.0–1.0 ppb) using the LOC system; (b) calibration curves showing the detection of PBDE using a colorimetric test as well as different modes of electrochemical detection; and (c) electrochemical detection in seawater samples spiked with PBDE standard solutions.

into account the amount of PBDEs found globally; for instance, seawater in Jiaozhou Bay in China (6.59 ppb) [43], coastal water of the Aegean Sea (0.03–0.05 ppb) [44], or various indoor environments in Barcelona, Spain (7.3–13.9 ppb) [45].

Compared to the optical detection method, the electrochemical approach has higher method sensitivity and is clearly seen by the slope of the calibration curves (Fig. 5(b)). Furthermore, a major difference regarding linearity and reproducibility can be observed by comparing measurements performed on a bare electrode with those in a microfluidic chip (either just detection or the whole assay). Detection based just on bare electrodes was linked with a much worse coefficient of determination (R^2 = 0.974 compared to R^2 = 0.994) and higher errors amongst all repetitions of the experiment in the microfluidic chip. This is probably related to the nature of square wave anodic stripping voltammetry, as good performance of this technique depends on the diffusion and contact between the electrode surface and the sample. Apparently, this works better in microfluidics where the deposition process is performed under flow and the presence of the microfluidic channel keeps a constant volume of liquid in contact with the working electrode and prevents the evaporation of the sample by limiting any influences from the external environment. This confirms the already reported statements on improved performance of the SW-ASV in microfluidics compared to that of the bare screen-printed electrodes. It is especially meaningful taking into account the use of home-made electrodes fabricated using more eco-friendly materials (carbon, silver/silver-chloride) than electrodes containing toxic mercury [39].

3.5 Validation of the lab-on-a-chip device in seawater samples

In order to justify the practical application of the presented LOCs device, we evaluated seawater samples spiked with the PBDE standard solution, as described in S2 in the ESM. Results are shown in Fig. 5(c), and as there is clear evidence of good recovery yield (94.1%–103.0%), it can be assumed that this method is fully compatible with seawater samples. This is possible due to washing steps where all the trace chemicals

are removed so there is minimal influence on electrochemical detection. As already mentioned, the presence of salts (ionic strength) does not affect the signal intensity. As the system is based on magneto-immunoassay, the use of magnetic beads in a chip also supports an efficient method of capturing analytes from a complex matrix such as seawater.

3.6 Comparison with other methods and future perspectives

Comparison between the colorimetric and electro-chemical methods regarding the use of reagents is shown in Table S1 in the ESM. Owing to the use of microfluidics, less reagents are consumed and a significant amount of time is saved. By using a syringe pump as a driving unit, automation of the system is obtained. Moreover, instead of a syringe pump, programmable microfluidic flow controllers might be applied for this platform, providing full automation of the process and eliminating the need of a highly qualified workforce. This is crucial, as PBDE is a small molecule, which can be detected mainly in the competitive immunoassay format. This kind of assay is generally more sophisticated than that for label-free methods; thus, more time and attention are usually required to perform the analysis. Although simple and sensitive label-free methods for PBDE detection based on pattern recognition are reported, the risk of cross-reactivity and the need of data separation limit the practical application of these methods [46]. Another example of label-free detection of PBDE is electro-chemical impedance spectroscopy, which although specific, provides much higher LOD (1.3 ppb) compared to that reported in our work [47].

Another possible future improvement of the presented platform is its high-throughput applications. By miniaturizing all of the chips and multiplying them, it would be possible to run several assays in parallel without an extension of the total size of the sensing system.

4 Conclusions

This work describes the synthesis of a novel, integrated microfluidic platform for simultaneous capture,

detection, and removal of polybrominated diphenyl ethers. The presented system consists of three microfluidic chips: the IMMU-CHIP, where the analyte is captured and immunoreaction occurred; the DET-CHIP, where the level of HRP-PBDE is quantified using SW-ASV; and the GO-CHIP, which is responsible for the removal of potentially toxic PBDEs.

The LOD achieved was 0.018 ppb, which is in accordance with that of the currently available methods for PBDE detection. Electrochemical detection performed in the microfluidic chip showed better sensitivity compared to that of the commercial colorimetric method and better reproducibility and linearity than those of electrochemical measurements performed simply using a bare screen-printed electrode.

The practical impact of this work is twofold: Firstly, the proof that electrochemical detection of PBDEs can be performed, and secondly, that the rGO-PDMS composite in microfluidic devices can be employed as an efficient adsorbent of various compounds. To the best of our knowledge, both of the issues mentioned above are not yet reported.

Furthermore, the small size, durability, and suitability for operation with seawater samples suggest that the presented platform can be employed in marine environmental analysis; for example, as an integrated component of buoys. Combining this with commercially available miniaturized potentiostats (electrochemical detection) and microfluidic driving units will result in a small and fully automated detection platform.

Acknowledgements

Electronic Supplementary Material: Supplementary material (protocol of colorimetric detection of PBDE, data treatment, measurements in seawater, alternative electrochemical methods, protein adsorption to rGO-PDMS composite, comparison of electrochemical and optical methods) is available in the online version of this article at http://dx.doi.org/10.1007/s12274-016-1420-3.

References

[1] Medina-Sánchez, M.; Miserere, S.; Morales-Narváez, E.; Merkoçi, A. On-chip magneto-immunoassay for Alzheimer's biomarker electrochemical detection by using quantum dots as labels. *Biosens. Bioelectron.* **2014**, *54*, 279–284.

[2] Marasso, S. L.; Giuri, E.; Canavese, G.; Castagna, R.; Quaglio, M.; Ferrante, I.; Perrone, D.; Cocuzza, M. A multilevel lab on chip platform for DNA analysis. *Biomed. Microdevices* **2011**, *13*, 19–27.

[3] Lee, H. H.; Yager, P. Microfluidic lab-on-a-chip for microbial identification on a DNA microarray. *Biotechnol. Bioprocess Eng.* **2007**, *12*, 634–639.

[4] Kurbanoglu, S.; Mayorga-Martinez, C. C.; Medina-Sánchez, M.; Rivas, L.; Ozkan, S. A.; Merkoçi, A. Antithyroid drug detection using an enzyme cascade blocking in a nanoparticle-based lab-on-a-chip system. *Biosens. Bioelectron.* **2015**, *67*, 670–676.

[5] Kimura, H.; Ikeda, T.; Nakayama, H.; Sakai, Y.; Fujii, T. An on-chip small intestine-liver model for pharmacokinetic studies. *J. Lab. Autom.* **2015**, *20*, 265–273.

[6] Ozhikandathil, J.; Badilescu, S.; Packirisamy, M. Detection of bovine growth hormone using conventional and lab-on-a-chip technologies: A review. *Int. J. Adv. Eng. Sci. Appl. Math.* **2015**, *7*, 177–190.

[7] Ozhikandathil, J.; Packirisamy, M. Nano-islands integrated evanescence-based lab-on-a-chip on silica-on-silicon and polydimethylsiloxane hybrid platform for detection of recombinant growth hormone. *Biomicrofluidics* **2012**, *6*, 46501.

[8] Medina-Sánchez, M.; Cadevall, M.; Ros, J.; Merkoçi, A. Eco-friendly electrochemical lab-on-paper for heavy metal detection. *Anal. Bioanal. Chem.* **2015**, *407*, 8445–8449.

[9] da Costa, E. T.; Santos, M. F. S.; Jiao, H.; do Lago, C. L.; Gutz, I. G. R.; Garcia, C. D. Fast production of microfluidic devices by CO_2 laser engraving of wax-coated glass slides. *Electrophoresis* **2016**, *37*, 1691–1695.

[10] Ambrosi, A.; Guix, M.; Merkoçi, A. Magnetic and electrokinetic manipulations on a microchip device for bead-based immunosensing applications. *Electrophoresis* **2011**, *32*, 861–869.

[11] Medina-Sánchez, M.; Miserere, S.; Merkoçi, A. Nanomaterials and lab-on-a-chip technologies. *Lab Chip* **2012**, *12*, 1932–1943.

[12] Li, S. G.; Xu, Z. G.; Mazzeo, A.; Burns, D. J.; Fu, G.; Dirckx, M.; Shilpiekandula, V.; Chen, X.; Nayak, N. C.; Wong, E. et al. Review of production of microfluidic devices: Material, manufacturing and metrology. In *Proceedings of the SPIE 6993, MEMS, MOEMS and Micromachining III*, Strasbourg, France, 2008.

[13] Bhise, N. S.; Manoharan, V.; Massa, S.; Tamayol, A.; Ghaderi, M.; Miscuglio, M.; Lang, Q.; Zhang, Y. S.; Shin, S. R.; Calzone, G. et al. A liver-on-a-chip platform with bioprinted hepatic spheroids. *Biofabrication* **2016**, *8*, 014101.

[14] He, J. K.; Chen, R. M.; Lu, Y. J.; Zhan, L.; Liu, Y. X.; Li, D. C.; Jin, Z. M. Fabrication of circular microfluidic network in enzymatically-crosslinked gelatin hydrogel. *Mater. Sci. Eng. C-Mater. Biol. Appl.* **2016**, *59*, 53–60.

[15] Xia, Y. N.; Whitesides, G. M. Soft lithography. *Ann. Rev. Mater. Sci.* **1998**, *28*, 153–184.

[16] Mayorga-Martinez, C. C.; Hlavata, L.; Miserere, S.; López-Marzo, A.; Labuda, J.; Pons, J.; Merkoçi, A. An integrated phenol "sensoremoval" microfluidic nanostructured platform. *Biosens. Bioelectron.* **2014**, *55*, 355–359.

[17] Mayorga-Martinez, C. C.; Hlavata, L.; Miserere, S.; López-Marzo, A.; Labuda, J.; Pons, J.; Merkoçi, A. Nanostructured $CaCO_3$-poly(ethyleneimine) microparticles for phenol sensing in fluidic microsystem. *Electrophoresis* **2013**, *34*, 2011–2016.

[18] Medina-Sánchez, M.; Mayorga-Martinez, C.; Watanabe, T.; Ivandini, T.; Honda, Y.; Pino, F.; Nakata, K.; Fujishima, A.; Einaga, Y.; Merkoçi, A. Microfluidic platform for environmental contaminants sensing and degradation based on boron-doped diamond electrodes. *Biosens. Bioelectron.* **2016**, *75*, 365–374.

[19] Tan, H. Y.; Loke, W. K.; Nguyen, N. T.; Tan, S. N.; Tay, N. B.; Wang, W.; Ng, S. H. Lab-on-a-chip for rapid electrochemical detection of nerve agent Sarin. *Biomed. Microdevices* **2014**, *16*, 269–275.

[20] Ibarlucea, B.; Díez-Gil, C.; Ratera, I.; Veciana, J.; Caballero, A.; Zapata, F.; Tárraga, A.; Molina, P.; Demming, S.; Büttgenbach, S. et al. PDMS based photonic lab-on-a-chip for the selective optical detection of heavy metal ions. *Analyst* **2013**, *138*, 839–844.

[21] Feng, C. Y.; Wei, J. F.; Li, Y. J.; Yang, Y. S.; Wang, Y. H.; Lu, L.; Zheng, G. X. An on-chip pollutant toxicity determination based on marine microalgal swimming inhibition. *Analyst* **2016**, *141*, 1761–1771.

[22] Zheng, G. X.; Li, Y. J.; Qi, L. L.; Liu, X. M.; Wang, H.; Yu, S. P.; Wang, Y. H. Marine phytoplankton motility sensor integrated into a microfluidic chip for high-throughput pollutant toxicity assessment. *Mar. Pollut. Bull.* **2014**, *84*, 147–154.

[23] Zheng, G. X.; Wang, Y. H.; Wang, Z. M.; Zhong, W. L.; Wang, H.; Li, Y. J. An integrated microfluidic device in marine microalgae culture for toxicity screening application. *Mar. Pollut. Bull.* **2013**, *72*, 231–243.

[24] Hooper, K.; McDonald, T. A. The PBDEs: An emerging environmental challenge and another reason for breast-milk monitoring programs. *Environ. Health Perspect.* **2000**, *108*, 387–392.

[25] Andrade, N. A.; McConnell, L. L.; Torrents, A.; Ramirez, M. Persistence of polybrominated diphenyl ethers in agricultural soils after biosolids applications. *J. Agric. Food Chem.* **2010**, *58*, 3077–3084.

[26] Guo, W. H.; Holden, A.; Smith, S. C.; Gephart, R.; Petreas, M.; Park, J. S. PBDE levels in breast milk are decreasing in California. *Chemosphere* **2016**, *150*, 505–513.

[27] Ward, J.; Mohapatra, S. P.; Mitchell, A. An overview of policies for managing polybrominated diphenyl ethers (PBDEs) in the Great Lakes Basin. *Environ. Int.* **2008**, *34*, 1148–1156.

[28] Darnerud, P. O.; Eriksen, G. S.; Jóhannesson, T.; Larsen, P. B.; Viluksela, M. Polybrominated diphenyl ethers: Occurrence, dietary exposure, and toxicology. *Environ. Health Perspect.* **2001**, *109*, 49–68.

[29] Porterfield, S. P. Vulnerability of the developing brain to thyroid abnormalities: Environmental insults to the thyroid system. *Environ. Health Perspect.* **1994**, *102*, 125–130.

[30] Ahn, K. C.; Gee, S. J.; Tsai, H. J.; Bennett, D.; Nishioka, M. G.; Blum, A.; Fishman, E.; Hammock, B. D. Immunoassay for monitoring environmental and human exposure to the polybrominated diphenyl ether BDE-47. *Environ. Sci. Technol.* **2009**, *43*, 7784–7790.

[31] Butryn, D. M.; Gross, M. S.; Chi, L. H.; Schecter, A.; Olson, J. R.; Aga, D. S. "One-shot" analysis of polybrominated diphenyl ethers and their hydroxylated and methoxylated analogs in human breast milk and serum using gas chromatography-tandem mass spectrometry. *Anal. Chim. Acta* **2015**, *892*, 140–147.

[32] Li, Z.; Li, C.; Lin, D.; Kang, W. J.; Pan, D. Y.; Wu, M. H. GC/MS analysis of polybrominated diphenyl ethers in vegetables collected from Shanghai, China. In *Proceedings of the 2013 International Conference on Material Science and Environmental Engineering (MSEE 2013)*, 2013, pp 292–296.

[33] Liu, Q.; Shi, J. B.; Sun, J. T.; Wang, T.; Zeng, L. X.; Zhu, N. L.; Jiang, G. B. Graphene-assisted matrix solid-phase dispersion for extraction of polybrominated diphenyl ethers and their methoxylated and hydroxylated analogs from environmental samples. *Anal. Chim. Acta* **2011**, *708*, 61–68.

[34] Zhang, H.; Lee, H. K. Plunger-in-needle solid-phase microextraction with graphene-based sol–gel coating as sorbent for determination of polybrominated diphenyl ethers. *J. Chromatogr. A* **2011**, *1218*, 4509–4516.

[35] Orozco, J.; Mercante, L. A.; Pol, R.; Merkoçi, A. Graphene-based Janus micromotors for the dynamic removal of pollutants. *J. Mater. Chem. A* **2016**, *4*, 3371–3378.

[36] Chen, M. T.; Tao, T.; Zhang, L.; Gao, W.; Li, C. Z. Highly conductive and stretchable polymer composites based on graphene/MWCNT network. *Chem. Commun.* **2013**, *49*, 1612–1614.

[37] Shahzad, M. I.; Giorcelli, M.; Shahzad, N.; Guastella, S.; Castellino, M.; Jagdale, P.; Tagliaferro, A. Study of carbon nanotubes based polydimethylsiloxane composite films. In *Proceedings of the 6th Vacuum and Surface Sciences Conference of Asia and Australia (VASSCAA-6)*, Islamabad, Pakistan, 2013.

[38] Lee, A. C.; Liu, G. D.; Heng, C. K.; Tan, S. N.; Lim, T. M.; Lin, Y. H. Sensitive electrochemical detection of horseradish peroxidase at disposable screen-printed carbon electrode. *Electroanalysis* **2008**, *20*, 2040–2046.

[39] Medina-Sánchez, M.; Miserere, S.; Marín, S.; Aragay, G.; Merkoçi, A. On-chip electrochemical detection of CdS quantum dots using normal and multiple recycling flow through modes. *Lab Chip* **2012**, *12*, 2000–2005.

[40] Zhang, J. L.; Yang, H. J.; Shen, G. X.; Cheng, P.; Zhang, J. Y.; Guo, S. W. Reduction of graphene oxide via L-ascorbic acid. *Chem. Commun.* **2010**, *46*, 1112–1114.

[41] Nourani, S.; Ghourchian, H.; Boutorabi, S. M. Magnetic nanoparticle-based immunosensor for electrochemical detection of hepatitis B surface antigen. *Anal. Biochem.* **2013**, *441*, 1–7.

[42] Xu, R. Q.; Lu, Y. Q.; Jiang, C. H.; Chen, J.; Mao, P.; Gao, G. H.; Zhang, L. B.; Wu, S. Facile fabrication of three-dimensional graphene foam/poly(dimethylsiloxane) composites and their potential application as strain sensor. *ACS Appl. Mater. Interfaces* **2014**, *6*, 13455–13460.

[43] Ju, T.; Ge, W.; Jiang, T.; Chai, C. Polybrominated diphenyl ethers in dissolved and suspended phases of seawater and in surface sediment from Jiaozhou Bay, North China. *Sci. Total Environ.* **2016**, *557–558*, 571–578.

[44] Lammel, G.; Audy, O.; Besis, A.; Efstathiou, C.; Eleftheriadis, K.; Kohoutek, J.; Kukučka, P.; Mulder, M. D.; Přibylová, P.; Prokeš, R. et al. Air and seawater pollution and air-sea gas exchange of persistent toxic substances in the Aegean Sea: Spatial trends of PAHs, PCBs, OCPs and PBDEs. *Environ. Sci. Pollut. Res.* **2015**, *22*, 11301–11313.

[45] Cristale, J.; Hurtado, A.; Gómez-Canela, C.; Lacorte, S. Occurrence and sources of brominated and organophosphorus flame retardants in dust from different indoor environments in Barcelona, Spain. *Environ. Res.* **2016**, *149*, 66–76.

[46] Xu, D.; Zhu, W.; Wang, C.; Tian, T.; Li, J.; Lan, Y.; Zhang, G. X.; Zhang, D. Q.; Li, G. T. Label-free detection and discrimination of poly-brominated diphenylethers using molecularly imprinted photonic cross-reactive sensor arrays. *Chem. Commun.* **2014**, *50*, 14133–14136.

[47] Radhakrishnan, R.; Suni, I. I.; Bever, C. S.; Hammock, B. D. Impedance biosensors: Applications to sustainability and remaining technical challenges. *ACS Sustainable Chem. Eng.* **2014**, *2*, 1649–1655.

Electronic Supplementary Material

Toward integrated detection and graphene-based removal of contaminants in a lab-on-a-chip platform

Andrzej Chałupniak[1] and Arben Merkoçi[1,2] (✉)

[1] *Catalan Institute of Nanoscience and Nanotechnology (ICN2), CSIC and The Barcelona Institute of Science and Technology, Campus UAB, Bellaterra, 08193 Barcelona, Spain*
[2] *ICREA, Pg. Lluís Companys 23, 08010 Barcelona, Spain*

S1   Colorimetric detection of PBDE

Colorimetric test as a well-established and reproducible method was used as a reference technique regarding electrochemical measurements and optimization of flow operation in microfluidic chips. All steps were performed as follows, according to manufacturer's manual. Magnetic beads, antibodies, HRP-PBDE and PBDE standard were used for development of on-chip electrochemical assay.

S2   Procedure of colorimetric test

1. Add 250 μL of the appropriate standard, control, or sample.
2. Mix the PBDE antibody coupled paramagnetic particles thoroughly and add 500 μL to each tube.
3. Vortex for 1 to 2 s minimizing foaming.
4. Incubate for 20 min at room temperature.
5. Add 250 μL of PBDE enzyme conjugate to each tube.
6. Vortex for 1 to 2 s minimizing foaming.
7. Incubate for 20 min at room temperature.
8. Separate in the magnetic separation rack for 2 min.
9. Decant and gently blot all tubes briefly in a consistent manner.
10. Add 1 mL of washing solution T to each tube and vortex tubes for 1–2 s. Return tubes and allow to remain in the magnetic separation unit for 2 min.
11. Decant and gently blot all tubes briefly in a consistent manner.
12. Repeat steps 10 and 11 an additional time.
13. Remove the rack from the separator and add 500 μL of color solution to each tube.
14. Vortex for 1 to 2 s minimizing foaming.
15. Incubate for 20 min at room temperature.
16. Add 500 μL of stopping solution to each tube.

Address correspondence to arben.merkoci@icn2.cat

17. Add 1 mL washing solution to a clean test tube. Use as blank in step 17.

18. Read results at 450 nm within 15 min after adding the stopping solution.

S3　Data treatment

The mean absorbance of each sample (or standard solution) is normalized towards control sample containing 0.0 ppb of PBDE as follow

$A = A_x/A_0$ (%)

Where A_x is the mean absorbance of a given sample and A_0 is the mean absorbance of standard without PBDE standard. Calibration curve is obtained by plotting the $\ln(A)$ on Y axis versus $\ln(C)$ (concentration) of X axis.

S4　Limit of detection

Limit of detection of the colorimetric method is expressed as a concentration that represents 90% of signal of control sample 0.0 ppb PBDE. It´s estimated by manufacturer at around 0.017 ppb, however in our case the limit of 0.019 ppb was obtained. Same approach was applied to determine the LOD of electrochemical measurements.

S5　Seawater samples

Preparation of seawater sample was in accordance with the protocol for PBDE detection provided by Abraxis. Briefly, seawater sample (Barcelona, Spain) was collected in sterile glass vessel and diluted immediately (1:1) with methanol. In order to get rid of macroscopic impurities, seawater sample was filtrated through 20 μm syringe filter. Such prepared seawater samples were tested for the presence of PBDE following the same procedures as for commercial standard solutions both in optical and electrochemical experiments.

S6　Optimization of the on-chip washing step

In order to check the optimum conditions for washing step, MB-Ab-HRP-PBDE complex was mixed with 10% (v/v) Trypan blue solution and IMMU-CHIP was primed with it. Using optical microscope the removal of ink
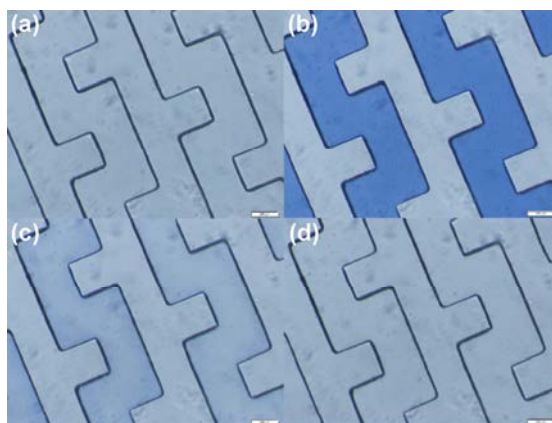

Figure S1　Visualization of the washing step using optical microscope and MB-Ab-HRP-PBDE samples mixed with 10% trypan blue. (a) Microfluidic channel before priming the solution, (b) microfluidic channel after priming the solution, (c) microfluidic channel after 2 min of washing step with the flow rate 150 μL/min, (d) microfluidic channel after 5 min of washing step with the flow rate 150 μL/min, no more ink is visible.

was observed under the proper washing. It was found that that the flow of 150 μL/min provides the optimum washing performance taking into account the time of this step as well as buffer usage.

S7 Cyclic voltammetry and differential pulse voltammetry for PBDE detection

Besides square wave anodic stripping voltammetry, other electrochemical techniques such as CV or DPV might be used. However, comparing to SW-ASV they show lower sensitivity. Figure S2 shows examples of curved for positive control (1.0 ppb PBDE), negative control (0.0 ppb PBDE) and substrate solution (o-AP + H_2O_2).
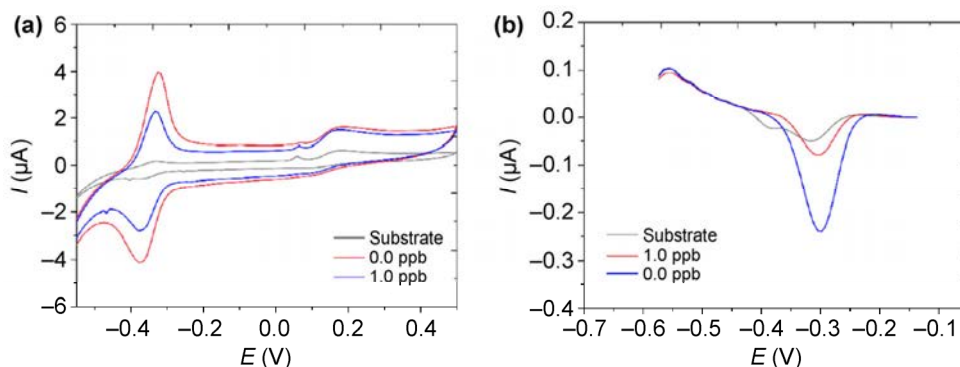
Figure S2 Alternative techniques for PBDE detection: (a) cyclic voltammetry, (b) differential pulse voltammetry. All curves obtained in static measurements according to the same protocol as in section 3.3.
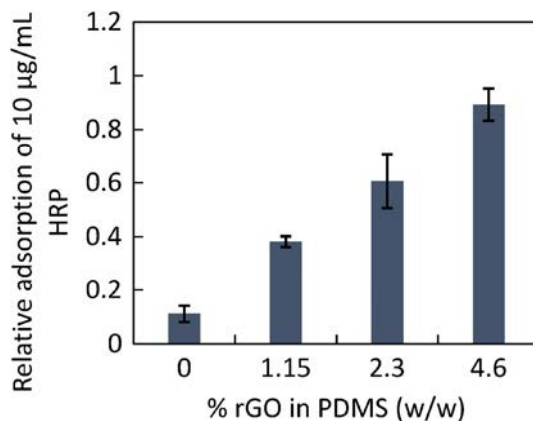
Figure S3 Adsorption of protein (HRP) to rGO-PDMS surface.

**Table S1** Comparison of reagents usage (in μL) in different systems

|	Colorimetric	Electrochemical (SPE)	Electrochemical (LOC)
MB-Ab		500	250
PBDE/sample		250	125
HRP-PBDE		250	125
Washing buffer		1,000	400
Colour solution	500	—	—
Stopping solution	500	—	—
o-AP+H_2O_2	—	100	27
PBS		10	3

S8   Adsorption capability of GO-CHIP

The aim of this experiment was to measure the maximum concentration of PBDE that can be adsorbed by GO-CHIP using constant flow rate. Samples of PBDE (500 μL) dissolved in buffer (10% methanol in water) or seawater (pre-treatment as mentioned in S5) were injected to GO-CHIP with the flow rate of 90 μL/min. Samples were collected at the outlet of the chip and diluted accordingly prior to colorimetric test. The level of adsorbed PBDE was determined following the same procedure as in section 2.7.
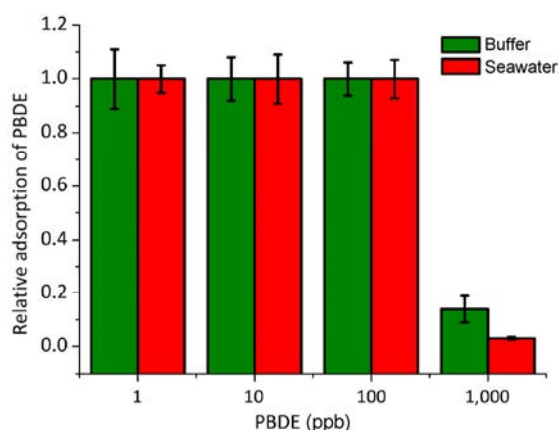
Figure S4   Adsorption of PBDE (1, 10, 100, 1,000 ppb) to GO-CHIP in buffer and seawater. Results obtained from 3 repetitions using a new GO-CHIP in each case.

S9   Reusability of GO-CHIP

10 ppb PBDE (500 μL) standard solution was injected to GO-CHIP similarly as in other experiments. Samples were collected at the outlet of the chip and diluted accordingly prior to colorimetric test, in order to proof that all PBDE is adsorbed by GO-CHIP. Afterwards, GO-CHIP was dried by injecting nitrogen. Solvent (500 μL) was injected to GO-CHIP with the flow rate of 40 μL/min and samples were treated as in previous step (collection, dilution, colorimetric test). Results were normalized towards the signal from non-treated 10 ppb PBDE standard solution. Each GO-CHIP was evaluated 4 times by repeating the same procedure. After each cycle, the channel of GO-CHIP was rinsed with miliQ water.
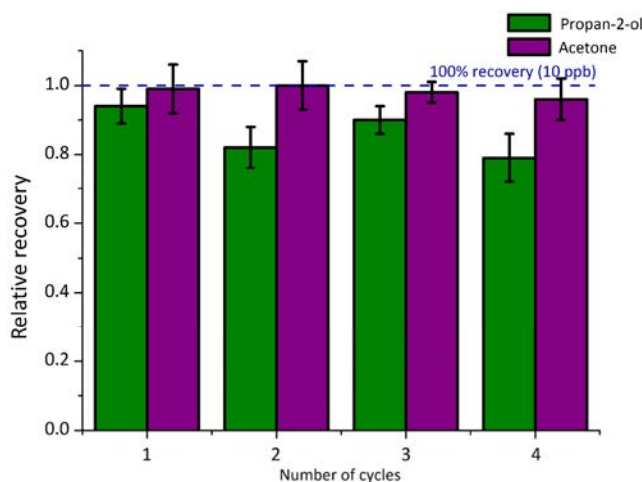
Figure S5   Recovery of PBDE (10 ppb) adsorbed by GO-CHIP using propan-2-ol and acetone as solvents for extraction. Results obtained from 3 repetitions using a new GO-CHIP in each case.

Rapid on-chip apoptosis assay on human carcinoma cells based on annexin-V/quantum dot probes

Helena Montón[a,b,1], Mariana Medina-Sánchez[a,1], Joan Antoni Soler[a], Andrzej Chałupniak[a], Carme Nogués[b], Arben Merkoçi[a,c,*]

[a] Catalan Institute of Nanoscience and Nanotechnology (ICN2), CSIC and The Barcelona Institute of Science and Technology, Campus UAB, Bellaterra, 08193 Barcelona, Spain
[b] Departament de Biologia Cel·lular, Fisiologia i Immunologia, Universitat Autònoma de Barcelona, Campus UAB-Facultat de Biociències, Bellaterra, 08193 Barcelona, Spain
[c] ICREA, Pg. Lluís Companys 23, 08010 Barcelona, Spain

ARTICLE INFO

ABSTRACT

Despite all the efforts made over years to study the cancer expression and the metastasis event, there is not a clear understanding of its origins and effective treatment. Therefore, more specialized and rapid techniques are required for studying cell behaviour under different drug-based treatments. Here we present a quantum dot signalling-based cell assay carried out in a segmental microfluidic device that allows studying the effect of anti-cancer drugs in cultured cell lines by monitoring phosphatidylserine translocation that occurs in early apoptosis. The developed platform combines the automatic generation of a drug gradient concentration, allowing exposure of cancer cells to different doses, and the immunolabeling of the apoptotic cells using quantum dot reporters. Thereby a complete cell-based assay for efficient drug screening is performed showing a clear correlation between drug dose and amount of cells undergoing apoptosis.

1. Introduction

Drug discovery is a field of research in constant development due to the need of new and improved drugs to treat different kinds of disorders, diseases or illnesses. Up to date, several methods for drug development have been reported (Koel and Kaljurand, 2006). The development of new strategies to study the effect of specific drugs on biological samples are of crucial importance to verify the drug function on human cell lines before conducting the clinical trials (Lledo-Fernandez and Banks, 2011; Peng and Chiou, 1990).

One of the most important fields in drug development research is related to cancer treatment (Rodwell, 2013; Suggitt and Bibby, 2005; Lieberman et al., 2001). Most anticancer drugs such as Camptothecin (CAMPT) induce apoptosis (Lin et al., 2013; Han et al., 2009), with some common characteristics (endonucleolytic cleavage of DNA, chromatin condensation, caspases activity, phospholipids transloca-tion, etc.), which can be used to develop different methods for cell apoptosis detection by the recognition of a specific apoptotic marker (Sellers and Fisher, 1999). Several strategies to detect apoptotic cells have been reported being the detection of phosphatidylserine (PS), a

phospholipid located in the inner leaflet of the plasma membrane (PM) that translocates to the outer one at early stages of apoptosis, one of the most common methods currently in use.

Detection of PS through the specific phospholipid-binding protein Annexin V (AnnV) has been widely used for diagnosis (Schutters and Reutelingsperger, 2010; Van Tilborg et al., 2010) and as an imaging tool to monitor the apoptotic cell death progression when AnnV is conjugated to a fluorescent dye (Andree et al., 1990; Vermes et al., 1995). This non-invasive technique for the cell is a good alternative for drug screening assays. However, one of the main problems of AnnV-based fluorescent probes is the limited photostability of the organic dyes conjugated to it and the scarce diversity of commercially available AnnV-conjugated dyes, to avoid spectral overlapping. These problems can be solved using Quantum Dots (QDs) as fluorescent reporters instead of standard organic dyes (Resch-Genger et al., 2008).

QDs are already commercially available due to their high demand given their unique optical properties and great potential in diagnostic imaging with particular interest in cancer diagnosis (Algar and Krull, 2010). We have already reported the advantages of QDs over organic dyes for labelling intracellular structures through double or triple

* Corresponding author at: Catalan Institute of Nanoscience and Nanotechnology (ICN2), CSIC and The Barcelona Institute of Science and Technology, Campus UAB, Bellaterra, 08193 Barcelona, Spain.
E-mail addresses: carme.nogues@uab.cat (C. Nogués), arben.merkoci@icn2.cat (A. Merkoçi).
[1] These authors contributed equally.

immunocytochemistries, showing higher fluorescence intensity, narrower bandwidth and higher photostability (Montón et al., 2009) and we have as well demonstrated the efficient employment of QDs as labels in microarray technology for either protein (Morales-Narváez et al., 2012) (Alzheimer's disease biomarker screening) or bacteria (Morales-Narváez et al., 2013) detection (E. coli sensing in a digital like response via fluorescence quenching with graphene oxide). Thereby, the use of QDs conjugated to AnnV provides a unique candidate to monitor apoptosis in time-lapse imaging due to their high photostability (Le Gac et al., 2006).

QD-based labelling strategies can improve conventional technologies but, modifications in the assay platform such as the use of microfluidics would allow the development of a cheaper and more efficient method (Vannoy et al., 2011) by down-scaling the cell environment, making biological interactions more dynamic (microflows), and decreasing sample, reagents and time of analysis (Janasek et al., 2006).

Microfluidic devices are basically known as integrative platforms to carry out diverse and complex experiments (Whitesides, 2006). Although many researchers are proposing highly integrated and sophisticated platforms (Du et al., 2013; Jang et al., 2011), the complexity of the experiments for non-experienced personnel can be a drawback due to their multiple components. However, the use of modular configurations, also called "building blocks" (Hill et al., 2016), brings the opportunity to couple different kinds of chips depending on the requirements of each experiment in a versatile and simple way, resulting in a large number of combinations (Yuen, 2008; Yuen et al., 2009). The main idea is that several microfluidic components can be connected in a motherboard to perform a larger integrated system (Skafte-Pedersen et al., 2013), or to mimic organs on a chip for drug screening under different physiological conditions (Loskill et al., 2015).

DNA detection (Hsieh et al., 2012; Yazdi et al., 2013), protein immunoassays (Diercks et al., 2009; Tekin and Gijs, 2013), and cell-based experiments (Hajba and Guttman, 2014), based on microfluidic platforms have been widely reported in the literature. Focusing on cell studies using microfluidics, several platforms for cytotoxicity evaluation and drug discovery have also been described (El-Ali et al., 2006; Jedrych et al., 2011). However, the above mentioned platforms have been used to study drug toxicity in cells by analysing their morphology or viability ex-situ mainly using organic dyes, which are not stable and not sensitive enough for long-term studies (Kim et al., 2011; Wang et al., 2015).

Here, we present a more specialized assay in which the translocation of PS to the outer leaflet of the plasma membrane in apoptotic cells is specifically labelled by an AnnV-QD conjugate, all done within microfluidic modules, giving more insight on the apoptotic process. The anticancer drug CAMPT is used as model to induce apoptosis and QDs conjugated to AnnV to reveal the PS translocation in cells undergoing apoptosis upon exposition to CAMPT. To achieve the drug test in human carcinoma cells we carry out the assay in a segmental microfluidic device in two phases: i) we culture the cells into the chip intended for apoptotic cell detection (CELL chip) and then we connect it with the concentration gradient generator chip (CGG), previously reported by Jeon et al. (2000) to expose the cells to different CAMPT doses; ii) the cells previously exposed to different CAMPT doses are incubated with the AnnV-QD conjugates prepared using a mixer chip (MIX). The AnnV-QD labelling performed in a microfluidic platform proves to be an effective method to quantify cell apoptosis through specific recognition of PS.

2. Results

2.1. Optimisation of the CELL chip

We established a sterilisation method for the CELL chip, made of glass and polydimethylsiloxane (PDMS), and an appropriate number of

cells to seed in it to obtain optimal results. On the one hand, we checked different methods of sterilisation: i) chips filled with 70% ethanol, emptied immediately after and followed by UV light exposure for 1 h after removing the ethanol, ii) chips filled with 70% ethanol and exposed to UV light for 1 h, and iii) chips filled with 70% ethanol until use (no UV light exposure). According to our experiments, the sterilisation methods involving UV light exposure resulted in low cell attachment and growing, probably due to the creation of free radicals produced by the UV-cleavage of the polymer backbone in the PDMS. The presence of free radicals might affect the cell growth due to oxidative stress which can modify both cells and cell products leading to cell apoptosis, protein modification, cross-linking and precipitation. (Lobo et al., 2010). Therefore the most suitable method in terms of cell culture growth 24 h post-seeding was a single-step of filling it with ethanol 70% until use (Supporting information Fig. S1). On the other hand, we analysed the number of cells growing in each chamber of the sterilised chip (1, 2, or 3 in Fig. 1A, i) to ensure that the cells were uniformly distributed in the CELL chip. We designed the CELL chip with oval-shaped chambers and channel ramifications to obtain a uniform distribution of cells and to avoid a possible cell detachment caused by high flow, which is very important for obtaining reproducible results during microscope image acquisition (Fig. S2). With this design, we found no differences in cell number among the chambers (Fig. 1A, ii), therefore each chamber is considered a replicate in the final assay. In addition, we seeded different number of cells in different chips to find the optimal concentration of cells after 24 h incubation (data not shown). We chose to seed 120,000 cells per chip to almost reach a cell monolayer in the chambers at the moment of inducing the apoptosis (24 h post seeding).

2.2. Optimisation of the CGG chip

To optimise the performance of the CGG chip we evaluated the flow rate and duration of the reagent injection. We simulated the real composition of the solutions to be used in the final assay: supplemented cell culture medium (Minimum Essential Medium, MEM) was introduced by one of the inlets and a combination of MEM, dimethyl sulfoxide (DMSO, CAMPT diluent) and trypan blue (to simulate CAMPT drug and to visualize the mixture) was introduced through the other one. To evaluate the gradient of concentrations obtained with the CGG chip, we took microscope images in the outlets (Fig. 1B, i) and we further processed them with ImageJ software to obtain the relative intensities of colour (Supporting information Fig. S3) which would be related to a specific solution concentration introduced in the inlets. According to theoretical predictions for such design (Supporting information Fig. S4), the relative concentrations in the outlets should be 0, 0.125, 0.5, 0.875 and 1, corresponding to 0, 2.5, 10, 17.5 and 20 µM of CAMPT. We compared the experimental values obtained at different flow rates and times (Supporting information Table 1) with the predicted theoretical values (Fig. 1B, ii) and we found that a 10 µL/min flow rate during 3 min resulted in the closest to theoretical given concentrations at the end of each outlet. The experimental concentrations corresponded to 0, 4, 11, 16 and 20 µM respectively. Considering that range a good start point for gradual doses of CAMPT we used this setup to test the platform performance for a full drug screening assay. We as well carried out repeatability and reproducibility studies by repeating measurements in the same chip and in three different chips, respectively (Supporting information Fig. S5) and we found negligible differences between measures, thus demonstrating the functionality of the CGG chip in generating a gradient of concentrations.

2.3. Optimisation of the MIX chip

Conjugation of AnnV-biotin with Streptavidin-QDs is performed in the first section of the chip (C sector -conjugation-, Fig. 1C, i) whereas AnnV-QD is mixed with the Ca^{2+} enriched medium for cell incubation
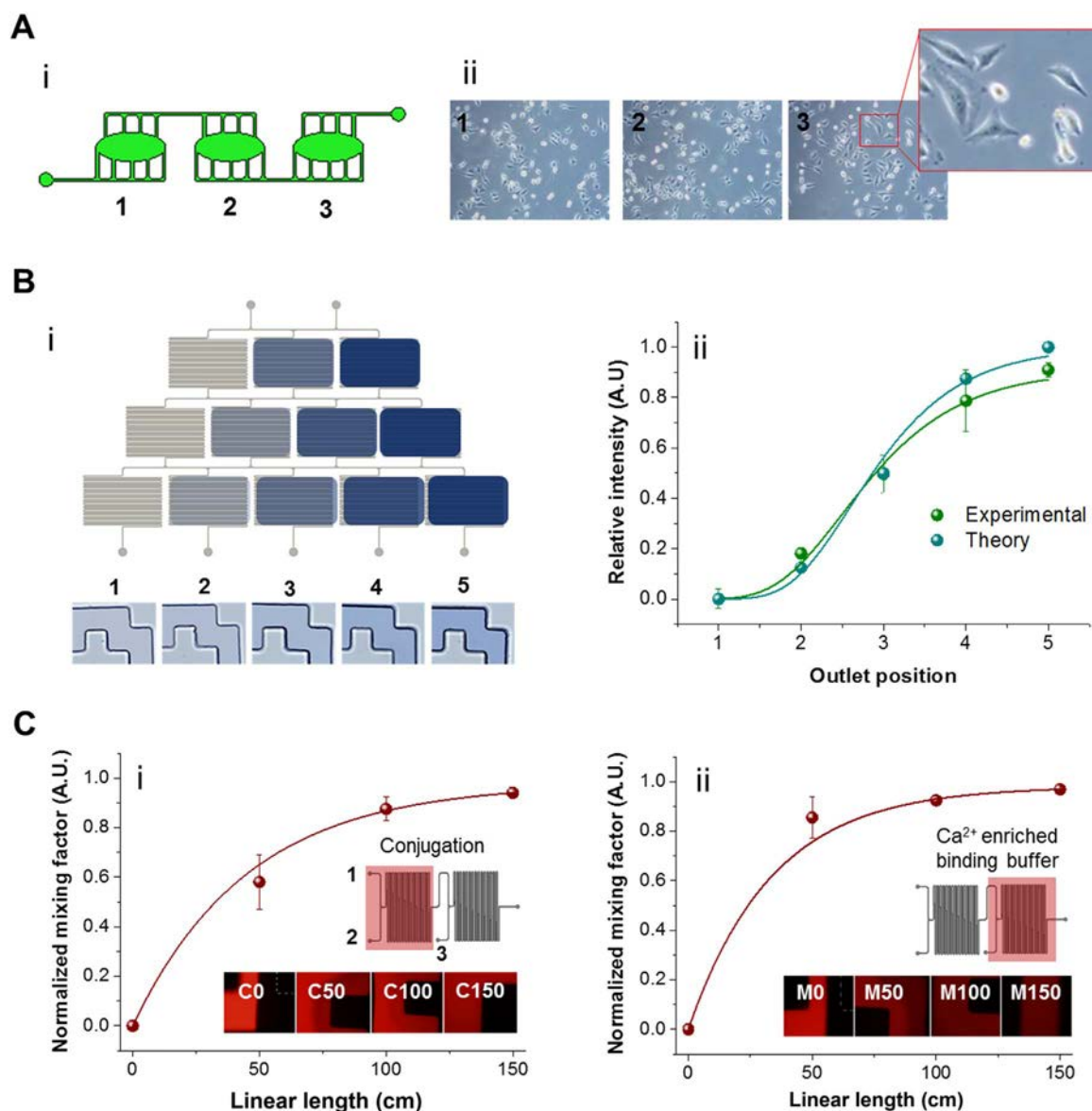
Fig. 1. Segmental chips optimisation. (A) CELL chip optimisation: i) schematic of the CELL chip with the three chambers where cells are seeded for analysis, and ii) cells uniformly distributed in the three chambers of the same chip 24 h post-seeding. (B) Optimisation of concentration gradient generator: i) schematic of the CGG chip with the corresponding outlet images (optical images of the trypan blue dilutions at the end of the channel of each outlet), and ii) comparison between theoretical and optimal experimental concentration data resulted from the obtained solutions at the outlets (0, 2.5, 10, 17.5, 20 μM and 0, 4, 11, 16, 20 μM, respectively), and (C) optimisation of the MIX chip: i) graph of mixing factors obtained from images taken at C0, C50, C100 and C150 cm of the channel path in the C sector (conjugation of AnnV and QDs), and ii) Graph of mixing factors calculated along the M sector of the chip from images taken at M0, M50, M100 and M150 cm, where conjugated AnnV-QDs are mixed with the Ca^{2+} enriched binding buffer. (For interpretation of the references to color in this figure legend, the reader is referred to the web version of this article).

in the second section (M sector -mixing-, Fig. 1C, ii). To optimise the performance of the MIX chip we first evaluated the C sector by introducing streptavidin-QDs at a concentration of 120 nM through inlet 1 (Fig. 1C) and AnnV-biotin through inlet 2 (Fig. S6, Supporting information). Fluorescence images were taken at certain points (C0, C50, C100 and C150 cm) from the beginning of the inlet path of C sector in order to evaluate the fluorescence intensity in several Regions of Interest (ROIs) with the aim to calculate the mixing factor, which reflects the homogeneity of the solution and thus the best conditions to perform the AnnV-QD conjugation. We tested several flow rates and injection times (Supporting information Table 2). We found that a flow rate of 5 μL/min during 12 min were the optimal parameters to obtain a mixing factor value of almost 1 at the end of the C sector of the chip (Fig. 1C, i). We also carried out repeatability and reproducibility studies for the C sector and we observed negligible differences between measurements or chips (Supporting information Fig. S7a).

We proceeded similarly to evaluate the M sector of the MIX chip (Fig. 1C, ii); we introduced AnnV binding buffer through inlet 3. We acquired fluorescence images along the channel path in M sector (M0, M50, M100 and M150 cm: see, inset images in Fig. 1C, ii) and we determined the mixing factors at each of these points. We found the best compromise between the duration of the assay (6 min) and the obtaining of appropriate mixing factors at a flow rate of 20 μL/min (Fig. 1C, ii). As for the C sector, we evaluated repeatability and reproducibility for M sector of the chips and we found no significant differences between repeated measurements neither in a same chip nor in different ones (See Supporting information Fig. S7b).

2.4. Screening the apoptotic effect of CAMPT on human adenocarcinoma cells

Once the three modules were separately optimised, the suitability of
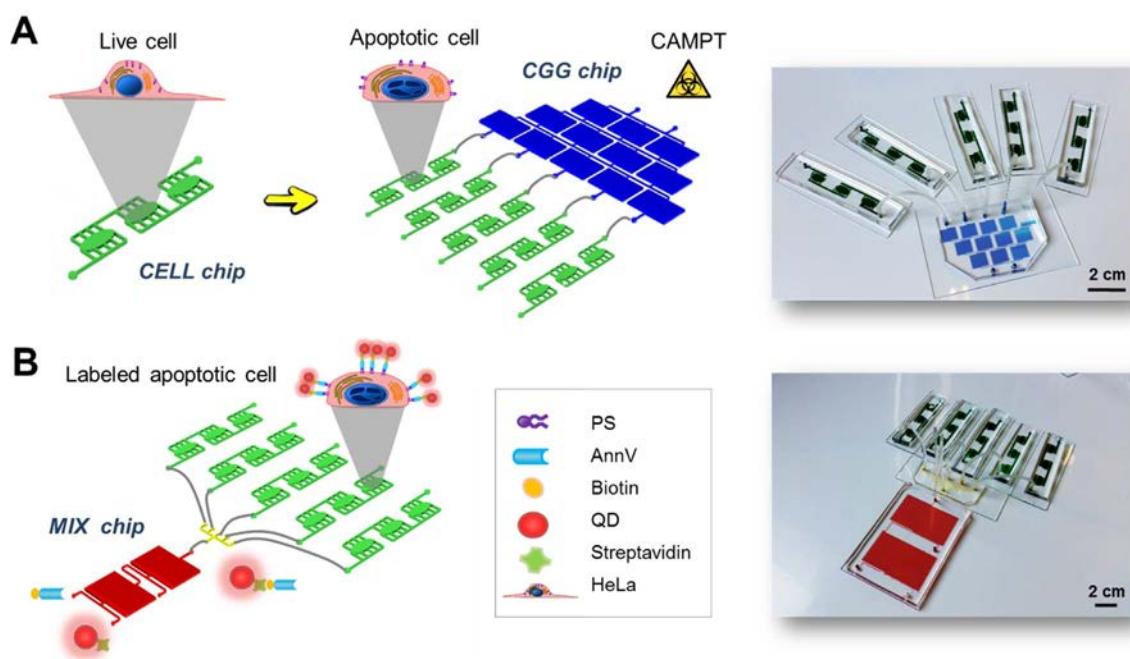
Fig. 2. Modular microfluidic platform for apoptosis monitoring. (A) Human carcinoma cells (HeLa) are cultured in the CELL chip composed by three identical chambers. Cells growing in the CELL chip are exposed to different CAMPT doses obtained through the concentration gradient generator chip (CGG). In this stage, cells will start translocation the PS to the outer leaflet of the plasma membrane. (B) In a second step a mixer chip (MIX) with two identical areas is in charge, first, of the conjugation of biotinylated AnnV with streptavidin-QD and, second, the mixture of AnnV-QD conjugates with the binding buffer containing the Ca^{2+} required for the specific binding with the translocated PS. The MIX chip is then connected to the CELL chip in order to incubate cells with the probe and to label the apoptotic cells. Photographs of the set of chips used in the two-stage assay are shown next to the schematics: (A) fluidic interconnection between the CGG chip where the CAMPT doses are generated and the respective CELL chips where cells are grown, (B) fluidic interconnection of the MIX chip, where the AnnV-QD conjugation takes place, with the CELL chips exposed, in the previous step (A), to different doses of CAMPT. Labelling is done in this step.

the modular platform to carry out a real cell-based assay was demonstrated by performing three sequential steps. First, the cells were seeded in 5 different CELL chips and incubated overnight to proliferate in a CO_2 incubator. Second, after incubation each of the 5 CELL chips was connected to an outlet of the CGG chip followed by introduction of 20 µM CAMPT (diluted in DMSO) and 1X MEM through the two different inlets of the CGG chip (Fig. 2A). As a result, each CELL chip was exposed to a different dose of CAMPT ranging from 0 to 20 µM using optimal flow rates and times (Table 1) (Fig. 2A).

Then CELL chips were disconnected from the CGG chip and placed in the incubator for 4 h in order to allow the induction of apoptosis in the cell cultures. The third step of the assay was to label positive-apoptosis cells with AnnV-QD probes (Fig. 2B). To achieve this, biotinylated AnnV and streptavidin-QD were introduced through the two inlets (1 and 2) of the C sector of the MIX chip followed by the introduction of AnnV binding buffer through the third inlet (3) located in the M sector of the MIX chip in order to dilute the AnnV-QD probe in the appropriate binding buffer. We sequentially connected the MIX chip to each of the CELL chips in order to let the probe interact with the

cells. We incubated the CELL chips with the AnnV-QD probe solution for 30 min in order to label the translocated PS in apoptotic cells, followed by a washing step of supplemented MEM for 7 min at a flow rate of 4 µL/min to remove unbound AnnV-QD. Each CELL chip exposed to a different dose of CAMPT was analysed by fluorescence microscopy in order to determine the percentage of apoptotic cells. Three areas per chamber for each chip were selected to acquire bright field images (Fig. 3A, i) and fluorescence images (Fig. 3A, ii) for further analysis.

The images were processed to establish the apoptosis ratio for each CAMPT dose exposure (0, 4, 11, 16 and 20 µM). As expected, the higher the concentration of CAMPT used to induce apoptosis the higher the number of cells labelled with AnnV-QD (apoptotic cells). In order to determine the number of apoptotic cells upon different drug concentrations, we calculated the ratio between the number of positive cells (apoptotic cells labelled with AnnV-QD) upon the total number of cells (apoptotic and non-apoptotic cells). Fig. 3B shows the dose-response curve of cell cultures exposed to specific doses of CAMPT (0; 4; 11; 16; and 20 µM) obtained from the image analysis. Each point represents the mean value obtained from the quantification of three different chambers and the error bars show the standard deviation between those measurements. A certain amount of apoptosis (10–20%) was found for chips incubated with 0 µM CAMPT corresponding to the basal level of apoptosis within the cell culture. Two replicates of this experiment were carried out in different days and results obtained were similar (Supporting information Fig. S8) showing the good reproducibility of the method.

3. Discussion

The results shown here indicate an appropriate correlation between the dose of CAMPT and the relative number of apoptotic cells labelled with AnnV-QD probes. As a proof-of-concept, we have demonstrated the applicability of the platform to carry out cell-based assays for drug

Table 1
Flow rate and time settings to perform the full assay.

	CGG chip[a]	MIX chip (C sector)[b]	MIX chip (M sector)[c]	CELL chip[d]
Flow rate (µL/min)	10	5 (inlet 1) 5 (inlet 2)	10 (outlet C sector) 10 (inlet 3)	4
Time of injection (min)	3	8	4	5

[a] Generation of CAMPT concentration.
[b] Conjugation of AnnV and QD.
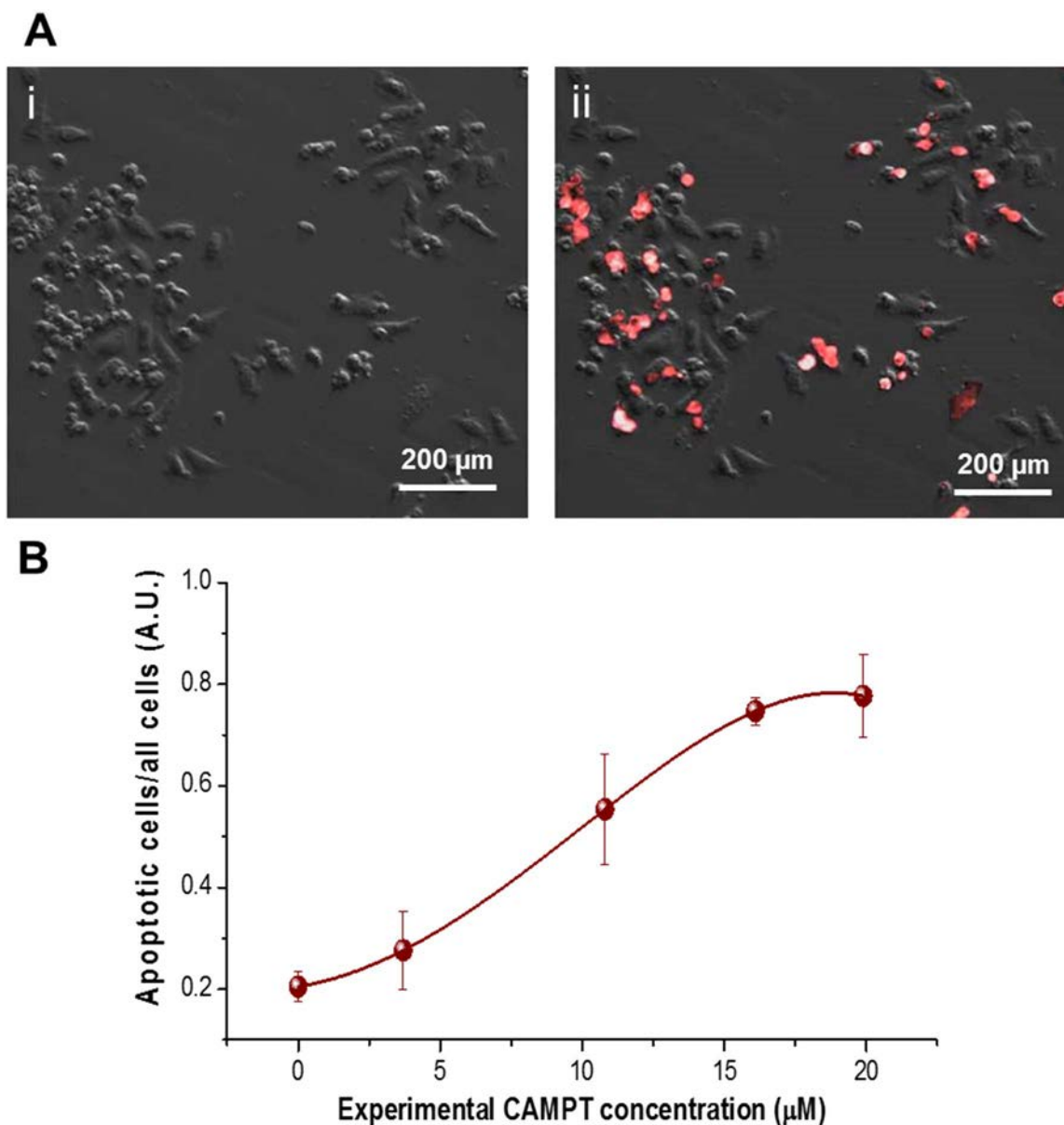[c] Mixing with AnnV binding buffer.
[d] Injection of AnnV-QD labelling into CELL chips.

Fig. 3. Apoptosis induction by different CAMPT doses. (A) Example of images obtained from the chips after incubation with CAMPT and labelling with AnnV-QD: i) typical bright field image of a selected area of the chamber, ii) fluorescence image of the same selected area overlapped with the bright field image. (B) Graph showing the dose-response curve corresponding to the ratio of apoptotic cells/total cells (QD-labelled cells/total number of cells) in relation to the CAMPT concentration they were incubated with. Standard deviation bars show the repeatability results between the three different chambers of a CELL chip.

screening with a low standard deviation (from 3% to 8%). Considering the factors that a cell based assay for drug development should feature, such as sensitivity of detection and reagent stability (Riss, 2005), an important advantage of the developed system is the use of QD instead of fluorescent dyes to reveal apoptosis. QDs are one of the most robust bioassay labels to carry out long optimisations and quantifications which require high sensitivity and stability of signal that other labels such as dyes cannot provide. Their compatibility in biological media, long-term stability and resistance to photobleaching make them ideal tools to monitor real time events, as we have shown, obtaining sensitive and reliable measures of apoptosis. Moreover, the versatility of QDs offers the possibility to evolve this work in different ways to fulfil a specific goal depending on the bioanalytical/bioassay scenario. For instance, CELL chips can be fabricated with integrated electrodes and electrochemical assays can be performed using the same QD-based probes thanks to the use of redox properties of QDs (Medina-Sánchez et al., 2015). Proof of that is the electrochemical-based microfluidic platform we have reported as an efficient alternative to detect very low

levels of a relevant biomarker for diagnostics (Medina-Sánchez et al., 2014). Therefore, an important advantage of the presented QD mediated monitoring is the possibility to be also used in a dual optical/electrical detection (given the QD properties) that may allow a fast quantitative monitoring of the apoptosis process induced by a chemical stimulus. In this way the effect of certain doses of an anticancer drug would be detected electrochemically in-chip as it has been recently demonstrated in batch mode (Montón et al., 2015).

The developed platform combines the versatility of QDs with the advantages of modular microfluidics: each chip can be modified, replaced by another one or removed to obtain a suitable system for each new application. The obtained results demonstrate that the combination of QDs with a modular microfluidic platform gives rise to a robust and sensitive cell assay for drug discovery applications. In addition this leads to significant both time and reagent saving due to the in-chip preparation of the reagents (drug doses, labelling probe conjugation) and due to the small volumes required to perform the assay. For example, experiments performed in the presented modular

microfluidic system use 4 times less volume of CAMPT stock solution (1 μL of stock solution is sufficient to prepare all working solutions in CGG chip) comparing with common techniques based on multiple well plates. Similarly, smaller volumes of QDs, cells suspensions and buffers are used in microfluidic chips than in plate-based assays. Moreover, this cell-based assay performed in microfluidic chips is characterized by a shorter duration of the experiment (at least 40% using our platform) and by fewer manual steps that may introduce variability in the system. For instance, if a multiple well plate is necessary to carry out the same or a similar assay several additional steps can be applied. For example, the conjugation protocol would include various washing and separation steps, while in microfluidics this step is reduced and simplified by flowing a buffer through the channel, reducing time and avoiding possible damage of the cell culture. Regarding the preparation of CAMPT doses, these should be manually and individually prepared in the case of a multiple well plate based assay. The use of the proposed microfluidic chip drastically reduces errors in manipulation and cell contamination in addition of offering a robust and easy to use system even for use out of a specialized laboratory and even by non-professional users.

The novelty of this work relies not only on the use of an optimised modular platform to carry out a full drug screening assay without manual steps (from drug doses and labelling to apoptosis detection) but also on the high accuracy of the assay as shown in the reproducibility of the results. The functionalities of the chips we used in this work have been already described and similar geometries have been used separately for different purposes. However their combination to carry out a complex assay in a simple, fast and cost-effective manner has not been reported until now. So far, reported lab-on-chip platforms for drug screening or imaging purposes have been used in disconnected steps so either drug concentration preparation, labelling or both of them have been done manually (Kim et al., 2011; Zhao et al., 2013). Moreover, the versatility of the modular platform we presented will allow a number of different types of assays to be performed, other than drug screening, opening the doors to many other applications.

4. Conclusions

In this work, we presented a versatile modular microfluidic platform that performs optical drug screening assays. As test bed, we focused on the detection of apoptosis in cancer cells, induced by the presence of the pro-apoptotic drug Camptothecin. In particular, we combined geometrically different chips to achieve three main functionalities: the generation of a drug gradient concentration, the functionalisation of QDs with AnnV, and the optical detection of apoptotic HeLa cells. Our platform successfully showed a clear correlation between drug dose and amount of cells undergoing apoptosis. Compared to traditional methods used for drug screening, our platform offers improved ease of use (decreasing the number of manual steps), speed (reducing the overall assay time by 40%), miniaturization/portability and versatility. Considering that this QDs/modular microfluidic bioassay platform can be easily adapted to specific requirements by redesigning the geometries of the chips, the probes or the target cells, we believe that our system can meet the needs of laboratories looking for a versatile methodology to evaluate new drugs during preclinical stages.

Notes

The authors declare no competing financial interest.

Acknowledgements

Appendix A. Supplementary material

Supplementary data associated with this article can be found in the online version at doi:10.1016/j.bios.2017.03.034.

References

Algar, W.R., Krull, U.J., 2010. New opportunities in multiplexed optical bioanalyses using quantum dots and donor-acceptor interactions. Anal. Bioanal. Chem. 398, 2439–2449. http://dx.doi.org/10.1007/s00216-010-3837-y.

Andree, H.A., Reutelingsperger, C.P., Hauptmann, R., Hemker, H.C., Hermens, W.T., Willems, G.M., 1990. Binding of vascular anticoagulant alpha (VAC alpha) to planar phospholipid bilayers. J. Biol. Chem. 265, 4923–4928.

Diercks, A.H., Ozinsky, A., Hansen, C.L., Spotts, J.M., Rodriguez, D.J., Aderem, A., 2009. A microfluidic device for multiplexed protein detection in nano-liter volumes. Anal. Biochem. 386, 30–35. http://dx.doi.org/10.1016/j.ab.2008.12.012.

Du, G.S., Pan, J.Z., Zhao, S.P., Zhu, Y., Den Toonder, J.M.J., Fang, Q., 2013. Cell-based drug combination screening with a microfluidic droplet array system. Anal. Chem. 85, 6740–6747. http://dx.doi.org/10.1021/ac400688f.

El-Ali, J., Sorger, P.K., Jensen, K.F., 2006. Cells on chips. Nature 442, 403–411. http://dx.doi.org/10.1038/nature05063.

Hajba, L., Guttman, A., 2014. Circulating tumor-cell detection and capture using microfluidic devices. TrAC – Trends Anal. Chem. 59, 9–16. http://dx.doi.org/10.1016/j.trac.2014.02.017.

Han, J., Talorete, T.P.N., Yamada, P., Isoda, H., 2009. Anti-proliferative and apoptotic effects of oleuropein and hydroxytyrosol on human breast cancer MCF-7 cells. Cytotechnology 59, 45–53. http://dx.doi.org/10.1007/s10616-009-9191-2.

Hill, D.A., Anderson, L.E., Hill, C.J., Mostaghim, A., Rodgers, V.G.J., Grover, W.H., 2016. MECs: "building blocks" for creating biological and chemical instruments. PLoS One, 11. http://dx.doi.org/10.1371/journal.pone.0158706.

Hsieh, K., Patterson, A.S., Ferguson, B.S., Plaxco, K.W., Soh, H.T., 2012. Rapid, sensitive, and quantitative detection of pathogenic DNA at the point of care through microfluidic electrochemical quantitative loop-mediated isothermal amplification. Angew. Chem. – Int. Ed. 51, 4896–4900. http://dx.doi.org/10.1002/anie.201109115.

Janasek, D., Franzke, J., Manz, A., 2006. Scaling and the design of miniaturized chemical-analysis systems. Nature 442, 374–380. http://dx.doi.org/10.1038/nature05059.

Jang, Y.-H., Hancock, M.J., Kim, S.B., Selimović, S., Sim, W.Y., Bae, H., Khademhosseini, A., 2011. An integrated microfluidic device for two-dimensional combinatorial dilution. Lab Chip 11, 3277–3286. http://dx.doi.org/10.1039/c1lc20449a.

Jedrych, E., Flis, S., Sofinska, K., Jastrzebski, Z., Chudy, M., Dybko, A., Brzozka, Z., 2011. Evaluation of cytotoxic effect of 5-fluorouracil on human carcinoma cells in microfluidic system. Sens. Actuators, B Chem. 160, 1544–1551. http://dx.doi.org/10.1016/j.snb.2011.08.071.

Jeon, N.L., Dertinger, S.K.W., Chiu, D.T., Choi, I.S., Stroock, A.D., Whitesides, G.M., 2000. Generation of solution and surface gradients using microfluidic systems. Langmuir 16, 8311–8316. http://dx.doi.org/10.1021/la000600b.

Kim, M.J., Lee, S.C., Pal, S., Han, E., Song, J.M., 2011. High-content screening of drug-induced cardiotoxicity using quantitative single cell imaging cytometry on microfluidic device. Lab Chip 11, 104–114. http://dx.doi.org/10.1039/c0lc00110d.

Koel, M., Kaljurand, M., 2006. Application of the principles of green chemistry in analytical chemistry. Pure Appl. Chem. 78, 1993–2002. http://dx.doi.org/10.1351/pac200678111993.

Le Gac, S., Vermes, I., Van Den Berg, A. Den, 2006. Quantum dots based probes conjugated to Annexin V for photostable apoptosis detection and imaging. Nano Lett. 6, 1863–1869. http://dx.doi.org/10.1021/nl060694v.

Lieberman, M.M., Patterson, G.M., Moore, R.E., 2001. In vitro bioassays for anticancer drug screening: effects of cell concentration and other assay parameters on growth inhibitory activity. Cancer Lett. 173, 21–29. http://dx.doi.org/10.1016/S0304-3835(01)00681-4.

Lin, R.K., Ho, C.W., Liu, L.F., Lyu, Y.L., 2013. Topoisomerase II? deficiency enhances camptothecin-induced apoptosis. J. Biol. Chem. 288, 7182–7192. http://dx.doi.org/10.1074/jbc.M112.415471.

Lledo-Fernandez, C., Banks, C.E., 2011. An overview of quantifying and screening drugs of abuse in biological samples: past and present. Anal. Methods 3, 1227–1245. http://dx.doi.org/10.1039/c1ay05057e.

Lobo, V., Patil, A., Phatak, A., N.C., 2010. Free radicals, antioxidants and functional foods: impact on human health. Pharm. Rev. 118–126 (4), 118–126. http://dx.doi.org/10.4103/0973-7847.70902.

Loskill, P., Marcus, S.G., Mathur, A., Reese, W.M., Healy, K.E., 2015. μorgano: A Lego®-like plug & play system for modular multi-organ-chips. PLoS One 10, 1–13. http://dx.doi.org/10.1371/journal.pone.0139587.

Medina-Sánchez, M., Miserere, S., Morales-Narváez, E., Merkoçi, A., 2014. On-chip magneto-immunoassay for Alzheimer's biomarker electrochemical detection by using quantum dots as labels. Biosens. Bioelectron. 54, 279–284. http://dx.doi.org/10.1016/j.bios.2013.10.069.

Medina-Sánchez, M., Miserere, S., Marín, S., Aragay, G., Merkoçi, A., 2015. On-chip electrochemical detection of CdS quantum dots using normal and multiple recycling flow through modes. Biosens. Bioelectron. 70, 194–201. http://dx.doi.org/10.1039/c2lc00007e.

Montón, H., Nogués, C., Rossinyol, E., Castell, O., Roldán, M., 2009. QDs versus Alexa: reality of promising tools for immunocytochemistry. J. Nanobiotechnol. 7, 1–10. http://dx.doi.org/10.1186/1477-3155-7-4.

Montón, H., Parolo, C., Aranda-Ramos, A., Merkoçi, A., Nogués, C., 2015. Annexin-V/quantum dot probes for multimodal apoptosis monitoring in living cells: improving bioanalysis using electrochemistry. Nanoscale 7, 4097–4104. http://dx.doi.org/10.1039/C4NR07191C.

Morales-Narváez, E., Hassan, A.R., Merkoçi, A., 2013. Graphene oxide as a pathogen-revealing agent: sensing with a digital-like response. Angew. Chem. – Int. Ed. 52, 13779–13783. http://dx.doi.org/10.1002/anie.201307740.

Morales-Narváez, E., Montón, H., Fomicheva, A., Merkoçi, A., 2012. Signal enhancement in antibody microarrays using quantum dots nanocrystals: application to potential Alzheimer's disease biomarker screening. Anal. Chem. 84, 6821–6827. http://dx.doi.org/10.1021/ac301369e.

Peng, G.W., Chiou, W.L., 1990. Analysis of drugs and other toxic substances in biological samples for pharmacokinetic studies. J. Chromatogr. B Biomed. Sci. Appl.. http://dx.doi.org/10.1016/S0378-4347(00)82279-3.

Resch-Genger, U., Grabolle, M., Cavaliere-Jaricot, S., Nitschke, R., Nann, T., 2008. Quantum dots versus organic dyes as fluorescent labels. Nat. Methods 5, 763–775. http://dx.doi.org/10.1038/nmeth.1248.

Riss, T., 2005. Selecting cell – based assays for drug discovery screening. Cell Note, 16–21, (Issue).

Rodwell, C., 2013. Drug trials: in a spin. Nat. Rev. Cancer 13, 78. http://dx.doi.org/10.1038/nrc3463.

Schutters, K., Reutelingsperger, C., 2010. Phosphatidylserine targeting for diagnosis and treatment of human diseases. Apoptosis 15, 1072–1082. http://dx.doi.org/10.1007/s10495-010-0503-y.

Sellers, W.R., Fisher, D.E., 1999. Apoptosis and cancer drug targeting. J. Clin. Investig. 104, 1655–1661. http://dx.doi.org/10.1172/JCI9053.

Skafte-Pedersen, P., Sip, C.G., Folch, A., Dufva, M., 2013. Modular microfluidic systems using reversibly attached PDMS fluid control modules. J. Micromech. Microeng. 23, 055011. http://dx.doi.org/10.1088/0960-1317/23/5/055011.

Suggitt, M., Bibby, M.C., 2005. 50 Years of preclinical anticancer drug screening: empirical to target-driven approaches. Clin. Cancer Res.. http://dx.doi.org/10.1073/pnas.69.4.1042.

Tekin, H.C., Gijs, M. A.M., 2013. Ultrasensitive protein detection: a case for microfluidic magnetic bead-based assays. Lab Chip 13, 4711–4739. http://dx.doi.org/10.1039/c3lc50477h.

Van Tilborg, G.A.F., Vucic, E., Strijkers, G.J., Cormode, D.P., Mani, V., Skajaa, T., Reutelingsperger, C.P.M., Fayad, Z.A., Mulder, W.J.M., Nicolay, K., 2010. Annexin A5-functionalized bimodal nanoparticles for MRI and fluorescence imaging of atherosclerotic plaques. Bioconjugate Chem. 21, 1794–1803. http://dx.doi.org/10.1021/bc100091q.

Vannoy, C.H., Tavares, A.J., Omair Noor, M., Uddayasankar, U., Krull, U.J., 2011. Biosensing with quantum dots: a microfluidic approach. Sensors 11, 9732–9763. http://dx.doi.org/10.3390/s111009732.

Vermes, I., Haanen, C., Steffens-Nakken, H., Reutelingsperger, C., 1995. A novel assay for apoptosis. flow cytometric detection of phosphatidylserine expression on early apoptotic cells using fluorescein labelled Annexin V. J. Immunol. Methods 184, 39–51. http://dx.doi.org/10.1016/0022-1759(95)00072-I.

Wang, Y., Tang, X., Feng, X., Liu, C., Chen, P., Chen, D., Liu, B.F., 2015. A microfluidic digital single-cell assay for the evaluation of anticancer drugs. Anal. Bioanal. Chem. 407, 1139–1148. http://dx.doi.org/10.1007/s00216-014-8325-3.

Whitesides, G.M., 2006. The origins and the future of microfluidics. Nature 442, 368–373. http://dx.doi.org/10.1038/nature05058.

Yazdi, S.H., Giles, K.L., White, I.M., 2013. Multiplexed detection of DNA sequences using a competitive displacement assay in a microfluidic SERRS-based device. Anal. Chem. 85, 10605–10611. http://dx.doi.org/10.1021/ac402744z.

Yuen, P.K., 2008. Smartbuild-a truly plug-n-play modular microfluidic system. Lab Chip 8, 1374–1378. http://dx.doi.org/10.1039/b805086d.

Yuen, P.K., Bliss, J.T., Thompson, C.C., Peterson, R.C., 2009. Multidimensional modular microfluidic system. Lab Chip 9, 3303–3305. http://dx.doi.org/10.1039/b912295h.

Zhao, L., Caot, J.-T., Wu, Z.-Q., Li, J.-X., Zhu, J.-J., 2013. Lab-on-a-chip for anticancer drug screening using quantum dots probe based apoptosis assay. J. Biomed. Nanotechnol..

Supporting Information

Rapid on-chip apoptosis assay on human

carcinoma cells based on annexin-V / quantum

dot probes

Helena Montón[1,2†], Mariana Medina-Sánchez[1†], Joan Antoni Soler[1], Andrzej Chałupniak[1], Carme Nogués[2]* and Arben Merkoçi[1,2]*

[1] Catalan Institute of Nanoscience and Nanotechnology (ICN2), CSIC and The Barcelona Institute of Science and Technology, Campus UAB, Bellaterra, 08193 Barcelona, Spain

[2] Departament de Biologia Cel·lular, Fisiologia i Immunologia, Universitat Autònoma de Barcelona, Campus UAB-Facultat de Biociències, 08193 Bellaterra (Barcelona), Spain.

[3] ICREA, Pg. Lluís Companys 23, 08010 Barcelona, Spain.

*E-mail: arben.merkoci@icn2.cat, carme.nogues@uab.cat

† These authors contributed equally

Methods

Design and chip features

The design of each module (CGG, MIX and CELL) was done taking into account the required functionality (concentration gradient generation, mixing and immunoassay performance and cell seeding and analysis) in terms of modularity, versatility, easy assembly, among others, as reported previously (Tang and Lee, 2010).

CGG and MIX chips were designed with long paths through serpentine shapes. Each serpentine sector of the CGG chip was 100 µm depth, 125 µm width and 172 mm of path length whereas each serpentine sector of the MIX chip was 100 µm depth, 200 µm width and 1,500 mm of path length. The CELL chip had three chambers of 9 mm length and 5 mm width, a main channel of 1 mm width with ramifications (that connected each chamber with the main channel) of 0.5 mm width (Figure S2). These ramifications were included in each chamber in order to minimize the stress that the flow can produce in the cells growing inside the chips (Ziolkowska et al., 2010).

Fabrication of PDMS/glass chips

All chips were fabricated by soft-lithography as previously described (McDonald et al., 2000). Briefly, a 4-inch silicon wafer was spin coated with a negative photoresist (SU8-50, from Microchem, USA) and patterned by photolithography by using a flexible mask (Microlitho, UK). Poly-dimethylsiloxane (PDMS, from Ellsworth, Spain) was poured onto the resulting mould and cured at 65 ºC for 2 h. After this, the PDMS channel and glass substrate were assembled; both surfaces, glass and PDMS, were activated for 1 min by air plasma 30 W (Harrick Plasma, USA) and put into contact to achieve irreversible bonding. PDMS was chosen as material for fabricating channels that will be in contact with cells,

specifically due to its transparency and gas permeability as well as easy prototyping and low cost (Halldorsson et al., 2015).

Hydrodynamic optimisation of CGG chips

Design of the CGG chip was based on previous work (Jedrych et al., 2011). The fabricated chip consists on sequential mixers to be used for producing a gradient of concentration in the corresponding outlets. Experimental data with our CGG chip were obtained to compare the relative concentrations with the theoretical ones. Quantification of relative concentrations at the outlets was performed by introducing through inlet 1 cell culture medium MEM (Minimum Essential Medium, Gibco) supplemented with 10 % Foetal Bovine Serum (FBS, Gibco) and with a 25 % dimethyl sulfoxide (DMSO, Sigma), which is the Camptothecin (CAMPT) solvent in stock solutions. Through the inlet 2, MEM supplemented with 10% FBS and with a 10% of Trypan blue (Fluka by Sigma Aldrich, Spain) was introduced. Trypan blue was used during the optimisation experiments to allow measurements of colour intensity because although MEM has phenol red in its composition it is transparent at small volumes. For filling-up the chips, 1 mL syringes (Hamilton, USA) and syringe pumps (Harvard Apparatus USA) were used. To determine optimal flow rate and time of infusion different settings were tested in order to find the less time-consuming configuration allowing the obtaining of desired values of relative concentrations.

Image processing and determination of relative concentrations generated in CGG chips

Images at the outlets of CGG chips were captured with an optical microscope (Olympus IX71, Germany) coupled with a CCD camera (Olympus DP72, Germany) using the bright field mode, 4x magnification objective.

Image J (U. S. National Institutes of Health, Maryland, USA) was used for the image post-processing in order to determine the relative concentrations at the outlets. Two regions of interest (ROIs) inside (X, X') and outside (Y, Y') the channel were selected for quantification. First of all a division between the intensities of the paired areas X/Y and X'/Y' was done respectively in order to avoid errors due to differences attributed to imaging itself such as a change of environmental light. Then the mean of the two obtained values was calculated and, in order to normalize the results, the colour intensity in the outlets was compared with intensities in the intersection of the two inlets. Two ROIs in inlet 1 (α, inside, and β, outside the channel) and two ROIs in inlet 2 (α', inside, and β', outside the channel) were considered. Considering all parameters the following equation (Eq. 1) was established to obtain normalized intensities at the outlets:

$$\text{Normalized relative intensity} = \frac{Mean\left(\dfrac{X}{X'};\dfrac{Y}{Y'}\right)-\dfrac{\alpha'}{\beta'}}{\dfrac{\alpha}{\beta}-\dfrac{\alpha'}{\beta'}} \qquad \text{(Eq. 1)}$$

Hydrodynamic optimisation of MIX chips

Optimisations for the MIX chip were carried out in order to determine convenient mixing factors inside the channels which would later allow the formation of AnnV-QD conjugate and the mixing with the appropriate buffer. Different solutions were introduced through the inlets to establish mixing factors at different points along the channel path (0; 50; 100 and 150 mm approximately): streptavidin QD655 (Life Technologies, Spain) at a 120 nM from a stock solution prepared in QD incubation buffer (Borate buffer pH 9.2, Life Technologies, Spain) were introduced through one of the inlets, whereas QD incubation buffer and Ca^{2+} containing AnnV binding buffer were introduced through the second and third inlet

respectively. To determine optimal flow rate and time of infusion different settings were tested in order to find the less time-consuming configuration allowing the obtaining of the best mixing factor.

Image processing and determination of mixing factors

Images at different points along the channel path were captured using an optical microscope (Olympus IX71, Germany) coupled with a CCD camera (Olympus DP72, Germany) using the fluorescence mode, 4x magnification objective. An HBO mercury lamp was used as UV-light excitation source and a TRITC filter cube was set to select convenient emission wavelength coming from QDs.

The mixing factor at each selected point was calculated by measuring the mean fluorescence intensity of two ROIs per side of the channel (See Figure S5A for more details), the so-called I_{max} (X and X') and I_{min} (Y and Y'), due to maximum and minimum fluorescence observed at the origin in the inlet cross where solutions have not yet been mixed. First the mean intensity between X and X', and between Y and Y' were calculated separately then the mixing factor was obtained as follows:

$$\text{Mixing factor} \quad = \frac{I_{min}}{I_{max}} \qquad \text{(Eq. 2)}$$

The closer to 1 the better was the resulting mixture. Mixing factors were normalized after calculating I_{min} (mean α, α') and I_{max} (mean β, β') at the inlet cross (See Figure S5 B for more details) allowing to obtain the mixing factor at this point as reference, the so-called Normalized Mixing Factor (NMF) in the inlet. Then, normalized values of mixing factors at each selected point were calculated as follows:

$$NMF = \frac{Mixing\ factor - Mixing\ Factor\ in\ the\ inlet}{1 - Mixing\ Factor\ in\ the\ inlet} \qquad (Eq.3)$$

Cell culture

Human adenocarcinoma HeLa cell line (ATCC®) was used as a model of adherent cell culture to carry out cell-based assays. Cells were maintained as a monolayer of cells in 25 cm^2 flasks in MEM medium supplemented with 2 mM L-Glutamine and 10% FBS in standard conditions (5% CO_2 at 37 ºC).

Cells in exponential phase of growth were used in the assays. Cells were detached by trypsinization, that is, MEM was removed and flasks were washed twice with 2 mL of 1X Hank's Balanced Saline Solution (HBSS, Gibco) without Ca^{2+} and Mg^{2+}. Then 1 mL of 1X trypsin/EDTA solution (Gibco) was added and incubated at standard conditions for 3 min. Once cells were detached and could be seen individualized under an optical microscope 4 mL of fresh supplemented MEM was added to neutralize the effect of trypsin. Cells were quantified using a Neubauer chamber.

Optimisation of CELL chip sterilisation

Chips must be sterilised before cell seeding to avoid contaminations. Sterilisation method was optimised in CELL chips and the optimal method was implemented to sterilise the rest of the chips. Different sterilisation procedures were evaluated: i) chips were filled in with 70 % ethanol, ethanol was removed and then chips exposed to UV light for 1h, ii) chips were filled in with 70 % ethanol and exposed to UV light for 1h (no ethanol removal), and iii) chips were filled in with 70 % ethanol until use (no UV light exposure). In all cases, after

sterilisation, MEM was introduced in the chips to replace ethanol which is toxic for the cells. Then, cells growing in flasks were counted as described previously and seeded into the chips manually using 1 mL plastic syringes (Sigma Aldrich, Spain). To optimise the sterilisation method three different chips were used and 60,000 cells per chip were seeded and incubated in standard conditions. Images of each of the three chambers of the chips were taken at 4 h and 24 h after cells were seeded in the chips to evaluate cell adhesion and proliferation.

On-chip apoptosis induction by CAMPT in cell-based assays

All material required to carry out this step (syringes, syringe pumps, connector tubes, etc) was introduced to the safety cabinet in order to be sterilised for 15 min under UV light. Then, CGG chip was sterilised, as mentioned in the main text, by introducing 70 % ethanol first and replacing it by fresh MEM until use. Each of the outlets of the CGG chip was connected with a plastic connector tube to one CELL chip so finally 5 CELL chips were connected to the CGG chip. Then, supplemented MEM was introduced in one of the inlets and a 20 μM CAMPT solution in the other one at a flow rate of 10μL/min during 15 min. A range of CAMPT concentrations (0; 2.5; 10; 17.5 and 20 μM) was produced and automatically distributed to different CELL chips.

Cell labeling with AnnV-QD conjugates in cell-based assays

Before connecting MIX and CELL chips, AnnV-QD conjugation in an appropriate buffer was formed in the MIX chip and then CELL chips were filled in with the already created label, one by one. To fulfill this, biotinilated AnnV (diluted half with QD incubation buffer) and streptavidin QDs at 120 nM were introduced through the first and second inlets with a flow rate of 5 μL/min during 12 min whereas 2X AnnV binding b (diluted in MEM) was

7

introduced through the third inlet with a flow rate of 10 µL/min during 12 min. After 12 min, the MIX chip was completely filled. Flow rate and time of infusion was changed to 4 µL/min and 7 min in order to fill in each of CELL chips previously incubated with CAMPT. CELL chips were incubated during 30 min in the CO_2 incubator at 37ºC to ensure the binding of the AnnV-QDs conjugate with the PS expressed in apoptotic cells. After that time, the unbound QDs were removed from inside the CELL chips by introducing supplemented MEM at a flow rate of 4 µL/min during 7 min.

Cell apoptosis detection using Fluorescence Microscopy

Optical detection of AnnV-QD labelled apoptotic cells was performed using an inverted microscope. CELL chips were placed in the stage of the microscope and 3 ROIs per chamber (9 ROIs per chip) were selected in order to obtain images for the analysis. A 10x objective coupled with a phase contrast lens was used to obtain bright field images of all cells and UV light in combination with a TRITC filter cube were used to obtain fluorescence images of apoptotic cells due to the maximum emission wavelength at 655 nm of QDs used.

Quantification of apoptosis level

To determine the level of apoptosis present in each chip bright field and fluorescence images were analysed. A total number of cells was obtained by counting individual cells in bright field images whereas the number of apoptotic cells was established counting cells in fluorescence images, where they can be easily identified for their red colour due to the QD emission at 655 nm.

The ratio between apoptotic cells and total number of cells was established for each chamber of the chip dividing the number of AnnV-QD labelled cells (in red) and the number of total

cells. The closer to 1 the value was the higher percentage of apoptosis found. Mean values per chip were determined considering the values obtained in the three chambers of a CELL chip. The level of apoptosis found in each CELL chip was related graphically with the concentration of CAMPT to which it was exposed previously.

References

Halldorsson, S., Lucumi, E., Gómez-Sjöberg, R., Fleming, R.M.T., 2015. Advantages and challenges of microfluidic cell culture in polydimethylsiloxane devices. Biosens. Bioelectron. 63, 218–231. doi:10.1016/j.bios.2014.07.029

Jedrych, E., Chudy, M., Dybko, A., Brzozka, Z., 2011. The microfluidic system for studies of carcinoma and normal cells interactions after photodynamic therapy (PDT) procedures. Biomicrofluidics 5, 1–6. doi:10.1063/1.3658842

McDonald, J.C., Duffy, D.C., Anderson, J.R., Chiu, D.T., Wu, H., Schueller, O.J., Whitesides, G.M., 2000. Fabrication of microfluidic systems in poly(dimethylsiloxane). Electrophoresis 21, 27–40. doi:10.1002/(SICI)1522-2683(20000101)21:1<27::AID-ELPS27>3.0.CO;2-C

Tang, L., Lee, N.Y., 2010. A facile route for irreversible bonding of plastic-PDMS hybrid microdevices at room temperature. Lab Chip 10, 1274–1280. doi:10.1039/b924753j

Ziolkowska, K., Jedrych, E., Kwapiszewski, R., Lopacinska, J., Skolimowski, M., Chudy, M., 2010. PDMS/glass microfluidic cell culture system for cytotoxicity tests and cells passage. Sensors Actuators, B Chem. 145, 533–542. doi:10.1016/j.snb.2009.11.010

Supporting Figures
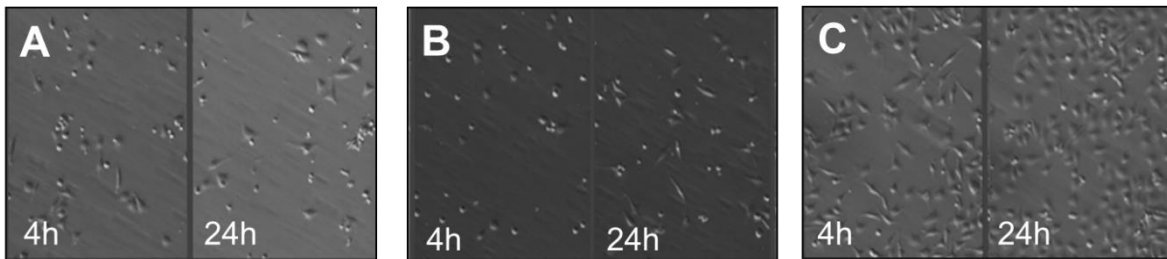
Figure S1. Comparison between sterilisation methods. (A) Chips were filled in with 70 % ethanol, ethanol was removed and then chips exposed to UV light for 1h, **(B)** Chips were filled in with 70 % ethanol and exposed to UV light for 1h (no ethanol removal), and **(C)** Chips were filled in with 70 % ethanol until use (no UV light exposure).
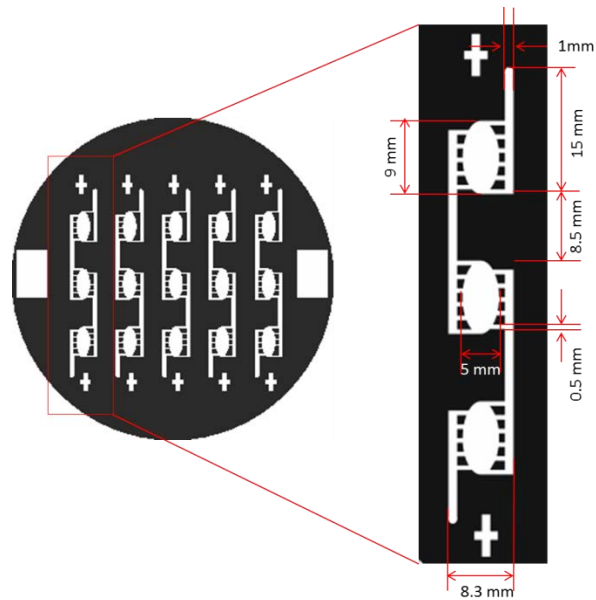

Figure S2. CELL chip mask dimensions. The design of the CELL chip mask with a zoom corresponding to a single chip is shown for a more detailed description of its specific dimensions.
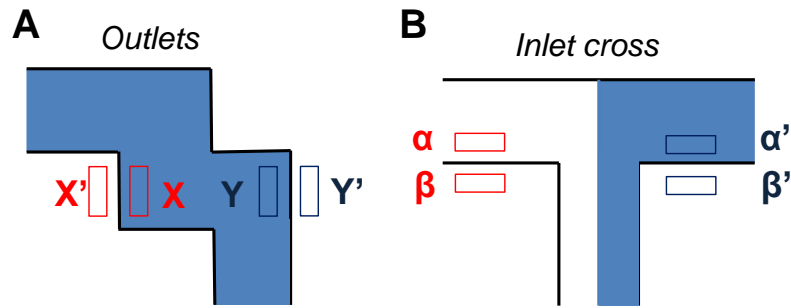
Figure S3. Quantification of relative concentrations in CGG chip. In order to evaluate the performance of the CGG chip, relative concentrations at the outlets were calculated. **(A)** Two regions of interest (ROIs) inside (X, X') and outside (Y, Y') the channel were selected in each outlet for quantification, and **(B)** In order to obtain normalized data, colour intensity at the outlets was compared with two ROIs of inlet 1 (α, inside, and β, outside the channel) and two ROIs in inlet 2 (α', inside, and β', outside the channel).
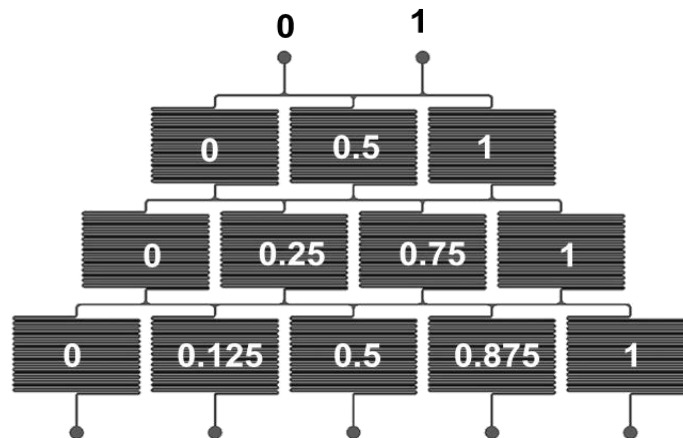
Figure S4. Calculation of theoretical concentrations within the CGG chip. According to the distribution of mixers in the CGG chip, considering 0 and 1 the values of relative concentrations at the inlets, the relative concentrations at the outlets will be: 0; 0.125; 0.5; 0.875 and 1.
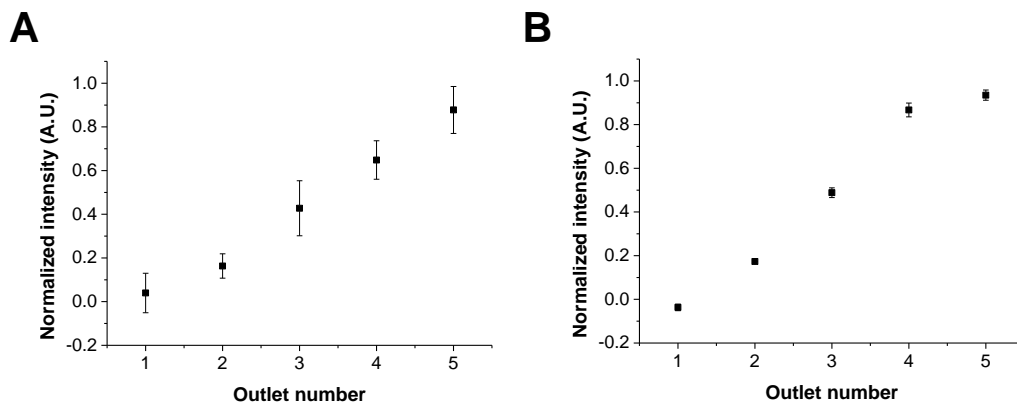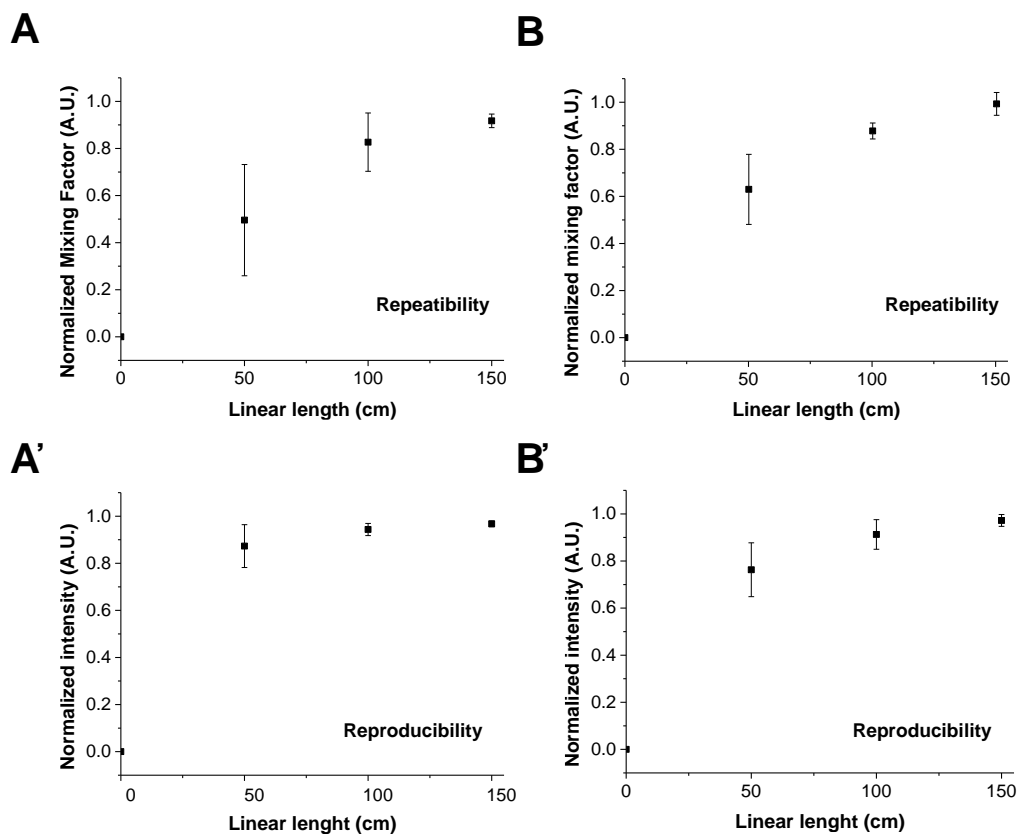
Figure S5. Reproducibility and repeatability studies in CGG chips. (A) Graphics corresponding to the assays performed in three different (CGG) chips. The values of the graphics represent the relative intensity obtained in each of the outlets and the error bars the standard deviation obtained by doing the evaluation three times, and **(B)** Reproducibility results for the (CGG) chip. The error bars correspond to the standard deviation obtained from the results of the evaluations done in three different chips.
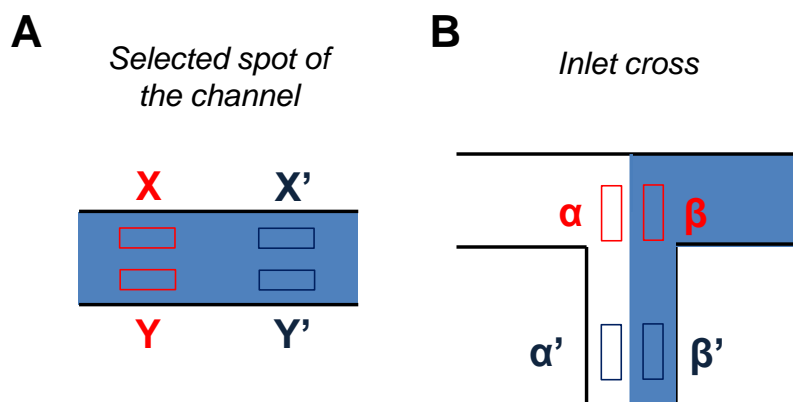
Figure S6. Fluorescence Intensity quantification of MIX chip. The mixing factor at each selected spot of the channel was calculated by measuring the mean fluorescence intensity of two ROIs selected in each side of the channel **(A)**, the so-called I_{max} (mean: X, X') and I_{min} (mean: Y, Y') due to maximum and minimum fluorescence observed at the inlet cross, where solutions have not yet been

mixed , and **(B)** I_{min} (mean α, α') and I_{max} (mean β, β') in the inlet cross were also calculated and further used in order to normalize the mixing factors obtained in each selected spot of the channel.

Figure S7. Reproducibility and repeatability in MIX chips. (A) Graphics corresponding to three different repeatability assays performed in three different MIX chips. The values of the graphic correspond to the normalized mixing factor obtained at different positions of the chip and the error bars to the standard deviation obtained by doing the evaluation three times, and **(B)** Reproducibility results for the (MIX) chip. The error bars correspond to the standard deviation obtained from the results of the evaluations done in three different chips.
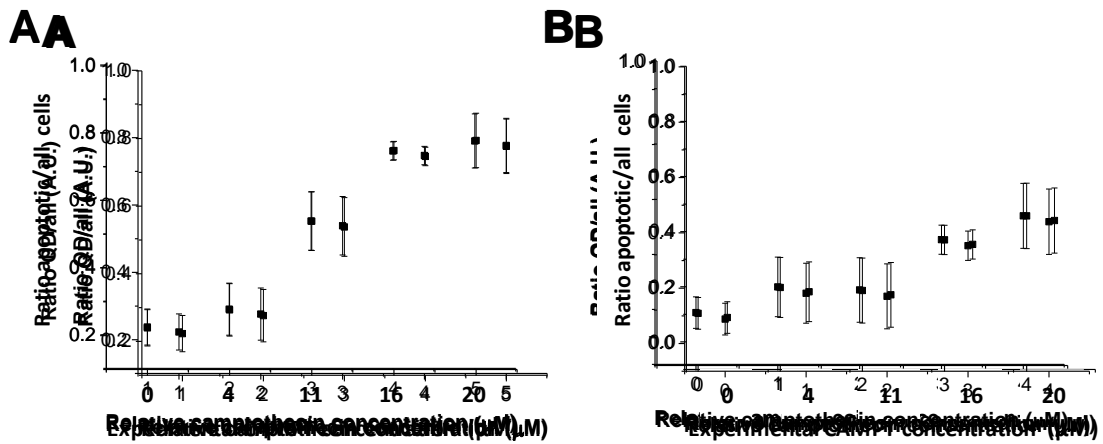
Figure S8. Full assay comparison carried out in different days. Full assays of cell apoptosis monitoring were carried out several times in order to evaluate the variability of the experiment. Incubations of 4h with CAMPT were carried out and the ratio of apoptotic cells/all cells (QD-labelled cells/all cells) from the total number of cells was established. Graphs obtained from data of a first assay **(A)** and a second assay, and **(B)** show the same trend although the number of apoptotic cells varies from one day to another. The error bars correspond to the standard deviations.

Tables

Table 1. Flow rate and time settings to optimise the performance of the CGG chip

	Flow rate (µl/min)	Time (min)	Experimental concentration*	Theoretical concentration*
Setting 1	10 Both inlets	3	0; 0.18; 0.5; 0.79 and 0.91	0; 0.125; 0.5; 0.875 and 1
Setting 2	5 Both inlets	6	0; 0.41; 0.7; 0.84 and 0.93	

Experimental and theoretical concentration values are given as arbitrary units (A.U.)

Table 2. Flow rate and time settings to optimise the MIX chip performance

Flow rates: (µl/min)	Inlet 1: 1 Inlet 2: 1 Inlet 3: 2	Inlet 1: 5 Inlet 2: 5 Inlet 3: 10	Inlet 1: 10 Inlet 2: 10 Inlet 3: 20
C sector time (min)	40	8	4
M sector time (min)	20	4	2
Total time (min)	60	12	6